HARMONIC AND ANHARMONIC
VIBRATIONS IN RUBIDIUM METAL

HARMONIC AND ANHARMONIC VIBRATIONS IN RUBIDIUM METAL

by

JOHN RICHARD DAWN COPLEY, B.A.

A Thesis
Submitted to the Faculty of Graduate Studies
in Partial Fulfilment of the Requirements
for the Degree
Doctor of Philosophy

McMaster University
October 1970

DOCTOR OF PHILOSOPHY (1970)
(Physics)

McMASTER UNIVERSITY
Hamilton, Ontario

TITLE: Harmonic and Anharmonic Vibrations in Rubidium Metal

AUTHOR: John Richard Dawn Copley, B.A. (Oxford University)

SUPERVISOR: Professor B. N. Brockhouse

NUMBER OF PAGES: xv, 274

SCOPE AND CONTENTS:

The atomic vibrations in rubidium have been studied by the method of slow neutron spectrometry. The results have been analysed to yield atomic force constants which are used to compute the phonon frequency distribution. An interesting effect in the $[00\zeta]L$ branch has been examined, and an explanation of the observations is offered.

Anharmonic calculations of frequency shifts and widths are presented, as well as a calculation of the anharmonic heat capacity. The third and fourth derivatives of the real space interatomic potential, which are required for these computations, are estimated in various ways.

A determination of the lattice spacing of rubidium by neutron diffraction is described.

ACKNOWLEDGEMENTS

I am particularly grateful to my research supervisor, Professor B. N. Brockhouse, F.R.S., for his interest and encouragement at all stages of this work. He has been able to share with me both his feeling and his enthusiasm for the field of solid state physics.

I have benefited from many discussions with my colleagues in the neutron scattering group at McMaster: Mr. J. D. Couper, Mr. D. H. Dutton, Mr. R. R. Dymond, Dr. E. D. Hallman, Mr. W. A. Kamitakahara, Mr. A. Larose, Dr. A. P. Miiller, Dr. S. C. Ng, Dr. A. P. Roy, and Mr. H. C. Teh. I am also grateful to members of the group for their assistance with the experiments described in this thesis.

The neutron scattering group at Atomic Energy of Canada Ltd., Chalk River, have been most helpful and encouraging, and I appreciate their interest in this work. In particular Dr. R. A. Cowley, Dr. G. Dolling, Dr. W. J. L. Buyers, and Mr. E. A. Glaser have assisted me on several occasions. I am grateful to the staff of AECL, Chalk River, for the use of experimental and computational facilities.

It is a pleasure to thank Dr. E. R. Cowley for the long hours he has spent discussing many aspects of this work, and for critically reading a large part of the manuscript; Dr. J. A. Morrison for his interest and encouragement in the later stages of this project: Dr. T. Timusk and Dr. R. W.

MacPherson for their collaboration in the work on potassium chloride; Dr. D. W. Taylor and Dr. J. P. Carbotte for their advice and instruction; and Mr. W. Scott and Mr. S. Kocsis for their invaluable assistance with the experimental apparatus.

I am indebted to Dr. S.H. Chen, who originally obtained the large rubidium crystal, and who kindly lent the helium cryostat. I must also thank Dr. G. A. de Wit, who suggested the experiments on potassium chloride, and collaborated in the early stages of that experiment.

I am grateful to the National Research Council of Canada and to McMaster University, for their financial support in the form of research grants and scholarships.

The excellent figures in this thesis were drawn by Mrs. S. Duke, to whom I offer my heartfelt thanks.

I am sincerely grateful to Mrs. H. Kennelly for her fine and accurate typing of this thesis, and for her patience with me and my handwriting.

Lastly I thank my dear wife, Diane, for her continued patience and forbearance, for her encouragement, and for her assistance in typing a draft and proofreading the final version.

TABLE OF CONTENTS

LIST OF FIGURES

Page

LIST OF TABLES

CHAPTER I

CRYSTAL DYNAMICS AND NEUTRON SCATTERING

A. INTRODUCTION

Crystals have been known to man for thousands of years. The word crystal, which originally referred to quartz alone, was later applied to materials which exhibited marked regularities in their external appearance. Such regularities are now known to result because the atoms which compose such solids are arranged in an ordered fashion throughout the crystal.

Many solids, including metals, minerals and salts, are polycrystalline. They consist of many very small crystals, known as crystallites, arranged in different orientations and separated by various types of imperfection. In recent times methods have been developed for growing large single crystals of many of these materials, in which the ordered arrangement of atoms exists throughout the specimen. This has stimulated a large amount of experimental research into the properties of these materials.

The arrangement of the atoms in a crystal is most commonly determined by x-ray diffraction techniques. The first materials to be studied were the alkali halides KCl, NaCl, KBr, and KI, whose structures were reported by W. L. Bragg (1913). More recently both neutron and electron diffraction techniques have been utilized to probe the atomic structure of matter.

At all temperatures the atoms in a material are moving. In a simple solid they execute small oscillatory motions about their equilibrium positions: the study of atomic motions is known as crystal dynamics, or lattice dynamics. The kinetic energy of an atom increases with increasing temperature, and the heat capacity of a material may be defined as the energy required to raise its temperature by one degree. Dulong and Petit (1819) observed that the product of the heat capacity per unit weight, and the atomic weight, was roughly a constant, independent of the material. This result was explained by Richarz (1893) by analogy with the kinetic theory of gases.

By the turn of the century there was considerable evidence that the Dulong and Petit law was incorrect at low temperatures. Einstein (1907) proposed that a solid containing N atoms be represented by a set of 3N independent oscillators of identical frequency ν. Using Boltzmann's statistics he obtained the result

$$C_V = 3Nk_B\left(\frac{h\nu}{k_BT}\right) \frac{\exp(h\nu/k_BT)}{[\exp(h\nu/k_BT)-1]^2} , \qquad \text{(I-A1)}$$

where C_V is the heat capacity (at constant volume), k_B and h are Boltzmann's and Planck's constants, and T is the temperature.

Debye (1912) generalized Einstein's theory by assuming a distribution of frequencies for the atomic oscillators. Regarding a solid as a continuum, he obtained the result

$$C_V = 9Nk_B(\frac{T}{\theta_D})^3 \int_0^{x_D} \frac{x^4e^x dx}{[e^x-1]^2} \qquad \text{(I-A2)}$$

where $x = h\nu/k_BT$ and $x_D = h\nu_D/k_BT = \theta_D/T$. In this expression ν_D is the maximum frequency in the material, and θ_D is known as the Debye temperature. The Debye theory predicts that $C_V \propto T^3$ at very low temperatures. This is in agreement with experiment, since only long wavelength vibrations are excited at such temperatures, and the discrete nature of the material may therefore be disregarded. The Einstein model is incorrect at low temperatures. At high temperatures both the Einstein and the Debye theory predict the Dulong and Petit value which is simply $3Nk_B$.

Born (1965) has described how he and von Kármán (1912) came to develop an atomic theory of lattice vibrations. Their paper appeared only "a few weeks" after that of Debye. It is now known that this theory is superior to the Debye theory, but for many years the Born-von Kármán theory lay dormant because there was no direct information about the individual vibrational frequencies in a solid.

Born and von Kármán postulated a system of atoms which move as though connected by Hookeian springs. The motions of the individual atoms are complicated in this picture, but the system may be regarded instead as a collection of independent oscillators having frequencies given by the dispersion relation,

$$\nu = \nu(\underset{\sim}{q}j) = \omega(\underset{\sim}{q}j)/2\pi \qquad \text{(I-A3)}$$

where $\underset{\sim}{q}$ is the wave vector of the mode, and j is a "branch index". The energy levels of a harmonic oscillator of frequency ν are separated by an amount $h\nu$: this quantum of energy is generally called a "phonon" by analogy with the word photon*.

The first experimental determination of phonon frequencies was that of Olmer (1948), who measured the intensity of diffuse scattering of x-rays by a crystal of aluminium. Several other metals were examined in the fifties, and these measurements collectively served to demonstrate that the Born-von Kármán model is basically correct. The x-ray technique has now been very largely superseded by the method of slow neutron inelastic scattering.

Since the mass of a neutron is comparable with atomic masses, it is not unreasonable that thermal neutrons have energies comparable with phonon energies in a crystal ($\approx$ 0.025 eV). In addition the de Broglie wavelength of a thermal neutron ($\approx$ 1.8 Å) is comparable with interatomic distances. For this reason both the energy and the wave vector of a thermal neutron are changed substantially when it is scattered by a phonon, and in consequence these changes may be measured fairly easily to within a few per cent. Such is not the case with

---

*The term "phonon" is attributed to Tamm, by Maradudin and Fein (1962), who give a reference to Seitz (1952). Ziman (1960) quotes Frenkel (1932) as the originator of the word.

electromagnetic radiation. X-rays have wavelengths of the right order, but their energies are $\approx 10^4$ ev. The energy change on scattering by a phonon is too small to be measured: instead the phonon energy is deduced from the intensity of the diffuse scattering, a complicated and somewhat indirect procedure. On the other hand, infrared photons have energies comparable with phonon energies, but because of their long wavelength ($\approx 10^5$ Å), they can only interact with single phonons if they have very small wave vector.

Measurements of phonon frequencies in aluminium by the neutron scattering method were first made by Brockhouse and Stewart (1955) and by Carter et al. (1957). Since that time the field has expanded rapidly. Several types of spectrometer have been developed, and methods of automatic operation are steadily being improved and diversified. A wide variety of systems has been examined and the spectra of excitations other than phonons are now measured. In the last few years considerable attention has been paid to improving the accuracy of the measurements through a better understanding of the various factors, such as instrumental resolution and the choice of instrumental parameters, which determine the possible errors in the measurements. General References 1-4, and 7 give some idea of the past and present scope of the field.

Substantial advances have also been made in the theory of crystal dynamics. Ludwig (1967) describes developments in the theories of molecular crystals, anharmonicity and thermodynamics, and the interaction between phonons and various types of radiation. Clearly both the theorists and the experimentalists in this field are very active at the present time.

B. OUTLINE OF THE THESIS

The remainder of this chapter contains a description of the theory of lattice dynamics in the harmonic approximation, and a review of the theory and practice of slow neutron scattering. None of this work is original; it is included in order to provide a useful background for the discussion which follows.

Measurements of normal mode frequencies in rubidium are described in Chapter II. The results are analysed in several ways, and phonon frequency distributions are presented.

Chapter III contains a brief account of the anharmonic theory of vibrations in crystals and their effect on the neutron scattering cross section. Calculations of the effects of anharmonicity on individual vibrational modes, and on the heat capacity in rubidium, are described and discussed.

A measurement of the lattice spacing in rubidium metal, and the characterization of the single crystal used in the phonon measurements, are described in Appendix I. Appendices II and III contain discussions of "spurious" scattering processes, and of the effects of instrumental resolution. Some of the algebra involved in simplifying various anharmonic expressions is described in Appendices IV and V, and the last two appendices (VI and VII) supplement the reprints at the end of the thesis, which describe a measurement of the scattering amplitude of rubidium, and work on the crystal dynamics of potassium chloride.

C. LATTICE DYNAMICS IN THE HARMONIC APPROXIMATION

(i) The Potential Energy

The dynamical behaviour of a crystalline solid is determined by the form and relative strength of the interactions between its constituent atoms. Solids are generally classified according to their properties into such categories as metals, inert-gas solids and ionic crystals. The various microscopic theories of lattice dynamics may be classifed in a similar way. These theories differ with respect to their assumptions about the predominant forces in the material, but they are all based on a very general formulation of the potential energy due to Born and von Kármán (1912). This formulation is based on two assumptions.

In the adiabatic approximation it is assumed that the electrons in the solid instantaneously take up a configuration appropriate to that of the displaced nuclei, and that their energy may therefore be effectively included in the potential energy of the nuclei. The degree of validity of this approximation has been discussed by several authors. Peierls (1955) (p.6) states that in metals the approximation is not justified, but this view is not generally held. Born and Huang (1954) discuss the approximation, and conclude that it is valid for "all important crystal properties".

Secondly we make the realistic assumption that the nuclear displacements are small compared with interatomic distances. We therefore write the potential energy of the system, $\Phi(\underline{R})$ where $\underline{R}$ denotes the nuclear positions, as a Taylor's series in the displacements:

$$\Phi(\underline{R}) = \Phi(\underline{R})\Big|_o + \sum_{\ell\alpha} \phi_\alpha(\ell)u_\alpha(\ell) + \frac{1}{2!}\sum_{\substack{\ell\ \alpha\\ \ell'\beta}} \phi_{\alpha\beta}(\ell\ell')u_\alpha(\ell)u_\beta(\ell')$$

$$+ \frac{1}{3!}\sum_{\substack{\ell\ \alpha\\ \ell'\beta\\ \ell''\gamma}} \phi_{\alpha\beta\gamma}(\ell\ell'\ell'')u_\alpha(\ell)u_\beta(\ell')u_\gamma(\ell'')$$

$$+ \frac{1}{4!}\sum_{\substack{\ell\ \alpha,\ell''\gamma\\ \ell'\beta,\ell'''\sigma}} \phi_{\alpha\beta\gamma\sigma}(\ell\ell'\ell''\ell''')u_\alpha(\ell)u_\beta(\ell')u_\gamma(\ell'')u_\sigma(\ell''')$$

$$+ \dots \qquad \text{(I-C1)}$$

Here $u_\alpha(\ell)$ is the α component of the displacement of atom ℓ, and

$$\phi_\alpha(\ell) = \frac{\partial\Phi(\underline{R})}{\partial u_\alpha(\ell)}\Big|_o$$

$$\phi_{\alpha\beta}(\ell\ell') = \frac{\partial^2\Phi(\underline{R})}{\partial u_\alpha(\ell)\partial u_\beta(\ell')}\Big|_o$$

$$\phi_{\alpha\beta\gamma}(\ell\ell'\ell'') = \frac{\partial^3\Phi(\underline{R})}{\partial u_\alpha(\ell)\partial u_\beta(\ell')\partial u_\gamma(\ell'')}\Big|_o$$

$$\phi_{\alpha\beta\gamma\sigma}(\ell\ell'\ell''\ell''') = \frac{\partial^4\Phi(\underline{R})}{\partial u_\alpha(\ell)\partial u_\beta(\ell')\partial u_\gamma(\ell'')\partial u_\sigma(\ell''')}\Big|_o \qquad \text{(I-C2)}$$

The subscript o indicates that the expressions are evaluated with the nuclei in their equilibrium positions.

In most theories of lattice dynamics a further approximation, the harmonic approximation, is made: terms in Eq. (I-C1) containing three or more displacements are neglected. In this way the equations of motion decouple, and the atomic motions may be represented as a system of independent simple harmonic oscillators. The harmonic approximation is an excellent starting point for treating many properties of the crystal lattice.

In the remainder of this section and in Chapter II we shall stay within this approximation. The consequences of retaining higher order terms in the potential energy will be discussed in Chapter III. The general Born-von Kármán theory, which is presented in the following pages, is not restricted to systems with two body forces. In particular we note that "atomic force constants" (introduced in the following subsection) which are often extracted from the measured dispersion curves of metals, include the effect of many-body forces. On the other hand the majority of theoretical treatments of lattice vibrations assume a two-body potential, but again parameters of these models which are fitted to experiment will incorporate the effects of many-body forces if they are present.

(ii) Equations of Motion, and the Dynamical Matrix

To simplify the discussion we shall consider a perfect crystal with no defects or impurities, and we shall neglect surface effects. These topics have been discussed by Elliott (1966) and by Wallis and Gazis (1965) respectively. The following treatment is further specialized to the case of one atom per primitive unit cell.

The Hamiltonian for the crystal, H, contains a kinetic energy term,

$$T = \frac{m}{2} \sum_{\ell\alpha} \dot{u}_\alpha^{\,2}(\ell)$$

where m is the mass of an atom, and the dot denotes differentiation with respect to time. The potential energy is written (in the harmonic approximation) as

$$\Phi(\underline{R}) = \Phi(\underline{R})\Big|_o + \sum_{\ell\alpha} \phi_\alpha(\ell) u_\alpha(\ell) + \frac{1}{2} \sum_{\substack{\ell\ \alpha \\ \ell'\beta}} \phi_{\alpha\beta}(\ell\ell') u_\alpha(\ell) u_\beta(\ell') \qquad \text{(I-C3)}$$

Using Hamilton's equation,

$$\frac{\partial H}{\partial u_\alpha(\ell)} = -\frac{\partial p_\alpha(\ell)}{\partial t} = -\frac{m\partial^2 u_\alpha(\ell)}{\partial t^2},$$

we obtain

$$-m\ddot{u}_\alpha(\ell) = \phi_\alpha(\ell) + \sum_{\ell'\beta} \phi_{\alpha\beta}(\ell\ell') u_\beta(\ell')$$

We immediately note that $-\phi_\alpha(\ell)$ is a component of the force on atom ℓ in the equilibrium configuration, which therefore vanishes. The equation of motion is then

$$m\ddot{u}_\alpha(\ell) = -\sum_{\ell'\beta} \phi_{\alpha\beta}(\ell\ell') u_\beta(\ell'). \qquad \text{(I-C4)}$$

The "atomic force constant" (AFC), $\phi_{\alpha\beta}(\ell\ell')$, is the negative of the α component of the force on atom ℓ, when atom ℓ' is displaced unit distance in the β direction. It only depends on the relative positions of atoms ℓ and ℓ'. Furthermore the number of independent AFC's for a particular shell of neighbours is very considerably reduced by symmetry. For example there are only 3 independent nearest neighbour AFC's in the face centred cubic (f.c.c.) lattice. (See also Brockhouse et al. 1968b).

If the AFC's for a particular shell of neighbours are derivable from a potential V(r) which depends only on scalar r, then they may be expressed in terms of radial and tangential force constants as follows:

$$-\phi_{\alpha\beta}(\ell\ell') = \frac{\delta_{\alpha\beta}}{r}\frac{dV}{dr} + \frac{r_\alpha r_\beta}{r^2}\left(\frac{d^2V}{dr^2} - \frac{1}{r}\frac{dV}{dr}\right)\Bigg|_{r=|\underline{r}(\ell)-\underline{r}(\ell')|} \qquad \text{(I-C5)}$$

Under these "axially symmetric" conditions, there are only two independent AFC's per shell of neighbours.

If the constant term $\Phi\ (\underline{R})\big|_0$, in Eq. (I-C3), is taken to be independent of volume, then an extra (equilibrium) condition exists linking the AFC's. For the b.c.c. case this condition is (Brockhouse et al. 1968b):

$$(1XX)-(1XY)+(2YY)+4(3ZZ)+11(4YY)-11(4YZ)+4(5XX)-4(5XY)+\ \ldots\ = 0$$

Here the number inside the brackets denotes the shell of neighbours and the letters denote the element of the 3×3 force constant matrix for this shell. In metals the constant term is sometimes taken to be volume dependent, in which case the equilibrium condition, as stated above, no longer holds. Following Brockhouse et al. (1968b) we shall take "central forces" to mean axially symmetric forces which satisfy the equilibrium condition.

We write a trial solution to Eq. (I-C4) as

$$u_\alpha(\ell) = C(\underset{\sim}{q}j)e_\alpha(\underset{\sim}{q}j)\exp\{i[\underset{\sim}{q}\cdot\underline{r}(\ell)-\omega(\underset{\sim}{q}j)t]\}. \qquad \text{(I-C6)}$$

This solution satisfies the Bloch condition, and represents a periodic vibration of frequency ω. For a particular wave-vector $\underset{\sim}{q}$ there are 3 modes of vibration, labelled $j = 1,2,3$: $e_\alpha(\underset{\sim}{q}j)$ is a component of a unit eigenvector, or polarization vector, and $C(\underset{\sim}{q}j)$ is an amplitude factor. The general solution is obtained by summing Eq. (I-C6) over $\underset{\sim}{q}$ and j. Substituting Eq. (I-C6) into Eq. (I-C4), we obtain a set of 3 equations

$$m\omega^2(\underset{\sim}{q}j)e_\alpha(\underset{\sim}{q}j) = \sum_\beta D_{\alpha\beta}(\underset{\sim}{q})e_\beta(\underset{\sim}{q}j) \qquad \text{(IC-7)}$$

where

$$D_{\alpha\beta}(\underset{\sim}{q}) = \sum_{\ell'} \phi_{\alpha\beta}(\ell\ell')\exp\{i\underset{\sim}{q}\cdot[\underline{r}(\ell)-\underline{r}(\ell')]\} \qquad \text{(IC-8)}$$

is an element of the dynamical matrix $\underline{\underline{D}}$, which is seen to be independent of ℓ, since terms in the summand only depend on relative displacements.

An infinitesimal uniform translation of the crystal in the x-direction may be represented by $u_\alpha(\ell) = \delta_{\alpha x}$ for all ℓ. Since no internal forces act, $\ddot{u}_\alpha(\ell) = 0$. Substituting into Eq. (I-C4), we obtain the important result:

$$\sum_{\ell'} \phi_{\alpha\beta}(\ell\ell') = 0, \quad \text{or}$$

$$\phi_{\alpha\beta}(\ell\ell) = - \sum_{\ell'}{}' \phi_{\alpha\beta}(\ell\ell') \tag{IC-9}$$

where the prime indicates exclusion of the term $\ell = \ell'$. We may therefore write

$$D_{\alpha\beta}(\underline{q}) = \sum_{\ell'}{}' \phi_{\alpha\beta}(\ell\ell')[\exp\{i\underline{q}\cdot\underline{r}(\ell'\ell)\}-1] \tag{IC-10}$$

where $\underline{r}(\ell'\ell) = \underline{r}(\ell') - \underline{r}(\ell)$.

Multiplying both sides of Eq. (IC-7) by $e_\alpha(\underline{q}j)$, summing over α, and using the fact that $\underline{e}(\underline{q}j)$ is a unit vector, we have

$$m\omega^2(\underline{q}j) = \sum_{\alpha\beta} e_\alpha(\underline{q}j) D_{\alpha\beta}(\underline{q}) e_\beta(\underline{q}j) \tag{I-C11}$$

Thus solutions to Eq. (I-C4) are obtained by diagonalizing the dynamical matrix.

It remains to determine the allowed values of $\underline{q}$. The "cyclic boundary condition" (see Born and Huang (1954), p.45) is normally employed. We simply state the result.

For a crystal with N primitive cells there are N states uniformly distributed within the first Brillouin zone of the reciprocal lattice. The reciprocal lattice is defined by the set of vectors $\underline{b}$ such that $e^{i\underline{a}\cdot\underline{b}} = 1$, where $\underline{a}$ is a vector of the direct lattice. The first Brillouin zone is usually defined such that every point within the zone is closer to the origin than to any other reciprocal lattice point.

In the case of a crystal with n atoms per primitive unit cell, a particular atom is labelled (ℓk), where ℓ designates the cell, and k the atom within the cell. The equations of motion become

$$m_k \ddot{u}_\alpha(\ell k) = - \sum_{\ell' k' \beta} \phi_{\alpha\beta}(\ell k \ell' k') u_\beta(\ell' k')$$

in an obvious extension of the notation, and we now obtain

$$m_k \omega^2(\underline{q}j) = \sum_{\substack{\alpha\beta \\ kk'}} e_\alpha(\underline{q}jk) D_{\alpha\beta}(\underline{q}kk') e_\beta(\underline{q}jk') \qquad \text{(I-C12)}$$

with

$$D_{\alpha\beta}(\underline{q}kk') = \sum_{\ell' k'}{}' \phi_{\alpha\beta}(\ell k \ell' k')[\exp\{i\underline{q}\cdot\underline{r}(\ell' k', \ell k)\} - 1]. \qquad \text{(I-C13)}$$

The branch index j takes on 3n values.

If the interatomic potential $\phi(r)$ is only a function of $|\underline{r}|$, the dynamical matrix may be expressed in terms of its Fourier transform, $\phi(Q)$.

Assuming two-body interactions only, we note that $\Phi(\underline{R})$, the total potential energy, may be written as a sum of individual terms $\phi(|\underline{r}(\ell\ell')|) \equiv \phi(\ell\ell')$:-

$$\Phi(\underline{R}) = \frac{1}{2} \sum_{\ell\ell'} \phi(\ell\ell')$$

Thus

$$\phi_\alpha(\ell) = \left.\frac{\partial\Phi(\underline{R})}{\partial u_\alpha(\ell)}\right|_0 = \sum_{\ell'} \left.\frac{\partial\phi(\ell\ell')}{\partial u_\alpha(\ell)}\right|_0$$

and

$$\phi_{\alpha\beta}(\ell\ell') = \left.\frac{\partial^2\Phi(\underline{\underline{R}})}{\partial u_\alpha(\ell)\partial u_\beta(\ell')}\right|_o = \left.\frac{\partial^2\phi(\ell\ell')}{\partial u_\alpha(\ell)\partial u_\beta(\ell')}\right|_o .$$

Defining

$$\phi(r) = \frac{\Omega}{(2\pi)^3 N}\int \phi(Q)e^{i\underline{Q}\cdot\underline{r}}\, d^3Q \ , \qquad \text{(I-C14)}$$

where N/Ω is the number of cells per unit volume, we obtain

$$\frac{\partial^2\phi(\ell\ell')}{\partial u_\alpha(\ell)\partial u_\beta(\ell')} = \frac{\Omega}{(2\pi)^3 N}\int Q_\alpha Q_\beta \phi(Q)e^{i\underline{Q}\cdot\underline{r}(\ell\ell')}d^3Q$$

Therefore, using Eq. (I-C10),

$$D_{\alpha\beta}(\underline{q}) = \sum_{\ell'}{}' \phi_{\alpha\beta}(\ell\ell')[\exp\{-i\underline{q}\cdot\underline{r}(\ell\ell')\}-1]$$

$$= \frac{\Omega}{(2\pi)^3 N}\int Q_\alpha Q_\beta \phi(Q) \sum_{\ell'}{}' [\exp\{i(\underline{Q}-\underline{q})\cdot\underline{r}(\ell\ell')\}- \exp\{i\underline{Q}\cdot\underline{r}(\ell\ell')\}]d^3Q$$

Now

$$\sum_j{}' e^{i\underline{q}\cdot\underline{r}_j} = \frac{(2\pi)^3 N}{\Omega}\ \Delta(\underline{q}) \qquad \text{(I-C15)}$$

$$\text{where } \Delta(\underline{q}) = \begin{cases} 1 \text{ if } \underline{q} \text{ is a reciprocal lattice vector } \underline{G}. \\ 0 \text{ otherwise.}\end{cases} \qquad \text{(I-C16)}$$

Therefore

$$D_{\alpha\beta}(\underline{q}) = \sum_{\underline{G}}[(\underline{G}+\underline{q})_\alpha(\underline{G}+\underline{q})_\beta\phi(|\underline{G}+\underline{q}|) - G_\alpha G_\beta\phi(G)] \qquad \text{(I-C17)}$$

The displacements $u_\alpha(\ell)$ may be written in terms of phonon creation and destruction operators, $a^*(-\underline{q}j)$ and $a(\underline{q}j)$, in the following way. A general expression for $u_\alpha(\ell)$ is

$$u_\alpha(\ell) = \sum_{\underline{q}j} C(\underline{q}j)e_\alpha(\underline{q}j)\exp\{i[\underline{q}\cdot\underline{r}(\ell) - \omega(\underline{q}j)t]\}. \qquad \text{(I-C18)}$$

The total vibrational energy of the system is simply

$$E = 2T = m \sum_{\ell\alpha} <\dot{u}_\alpha(\ell)^2>$$

$$= m \sum_{\ell\alpha} \sum_{\underline{q}j} <|C(\underline{q}j)|^2>e_\alpha{}^2(\underline{q}j)\omega^2(\underline{q}j)$$

$$= Nm \sum_{\underline{q}j} <|C(\underline{q}j)|^2>\omega^2(\underline{q}j). \qquad \text{(I-C19)}$$

We may also write (Eq. III-A10):

$$E = \sum_{\underline{q}j} [n(\underline{q}j) + \tfrac{1}{2}]\hbar\omega(\underline{q}j),$$

where

$$n(\underline{q}j) = \{\exp(\hbar\omega(\underline{q}j)/k_BT)-1\}^{-1} \qquad \text{(I-C20)}$$

and therefore

$$[n(\underline{q}j) + \tfrac{1}{2}]\hbar\omega(\underline{q}j) = Nm<|C(\underline{q}j)|^2>\omega^2(\underline{q}j)$$

Defining phonon operators

$$A(\underline{q}j) = a(\underline{q}j) + a^*(-\underline{q}j) \qquad \text{(I-C21)}$$

we obtain

$$<|A(\underline{q}j)|^2> = 2n(\underline{q}j) + 1 \qquad \text{(I-C22)}$$

and

$$<|C(\underline{q}j)|^2> = \frac{\hbar}{2Nm\omega(\underline{q}j)} <|A(\underline{q}j)|^2> \qquad \text{(I-C23)}$$

and finally

$$u_\alpha(\ell) = (\frac{\hbar}{2Nm})^{\frac{1}{2}} \sum_{\underline{q}j} (\frac{1}{\omega(\underline{q}j)})^{\frac{1}{2}} A(\underline{q}j) e_\alpha(\underline{q}j) \exp\{i[\underline{q}\cdot\underline{r}(\ell) - \omega(\underline{q}j)t]\}. \qquad \text{(I-C24)}$$

(iii) Metals

In this section we apply the above results to the situation in metals. We consider three contributions to the interionic potential V(r) : (a) the repulsive Coulomb interaction between bare ions, $V^{(c)}(\underline{r}) = Z^2e^2/r$, where Z is the ionic charge, (b) the repulsive overlap potential, which is normally taken to be of the Born-Mayer type, $V^{(R)}(\underline{r}) = Ae^{-\alpha r}$, and (c) the indirect (attractive) interaction, $V^{(E)}(\underline{r})$, via the conduction electrons, including the electron-electron interaction. Ziman (1964) has shown that V(r) may be regarded as the effective potential between neutral "pseudoatoms" in a metal. We may take this as further justification for using the adiabatic approximation in the case of metals.

A number of calculations of the phonon dispersion relation in metals have been based on the "pseudopotential" method. On the other hand measured dispersion curves are commonly analysed to obtain empirical atomic force constants. We shall now consider these topics.

(a) The Pseudopotential Method

Only a brief outline of this important subject will be given. A useful account has been given by Harrison (1966).

The one-electron Schrödinger equation is written

$$(-\hbar^2/2m)\nabla^2\psi + V(\underline{r})\psi = E\psi \qquad \text{(I-C25)}$$

where $V(\underline{r})$ is the potential seen by an electron. The wavefunction ψ is written as a sum of orthogonalized plane waves:

$$\psi = \sum_{\underline{q}} a_{\underline{q}}(1-P)|\underline{k}+\underline{q}> = (1-P)\phi,$$

where P is a projection operator. Equation (I-C25) then becomes

$$[(-\hbar^2/2m)\nabla^2 + W]\phi = E\phi$$

where ϕ is the "pseudowavefunction" and W is the pseudopotential.

The effect of this rearrangement is to produce an equation which contains a relatively small potential W. Using second order perturbation theory, we obtain the energy of the state $\phi_{\underline{k}}$ as:

$$E(\underline{k}) = \frac{\hbar^2 k^2}{2m} + <\underline{k}|W|\underline{k}> + \sum_{\underline{q}}{}' \frac{|<\underline{k}+\underline{q}|W|\underline{k}>|^2}{(\hbar^2/2m)(k^2-|\underline{k}+\underline{q}|^2)} \qquad \text{(I-C26)}$$

We assume a local pseudopotential, and write

$$W(r) = \sum_j w(|\underline{r}-\underline{r}_j|) \qquad \text{(I-C27)}$$

so that

$$\langle \underline{k}+\underline{q}|W|\underline{k}\rangle = S(\underline{q})w(\underline{q}) \qquad \text{(I-C28)}$$

where the structure factor

$$S(\underline{q}) = \frac{1}{N}\sum_{j} \exp\{-i\underline{q}\cdot\underline{r}_j\} \qquad \text{(I-C29)}$$

and the form factor

$$w(q) = \frac{N}{\Omega}\int \exp\{-i\underline{q}\cdot\underline{r}\}w(r)d^3r \qquad \text{(I-C30)}$$

where Ω is the volume of the solid and N is the number of ions. The total electron energy per ion is then

$$E_{el} = \frac{1}{N}\sum_{k<k_F} E(k) = E_{fe} + E_{bs}$$

where the free electron contribution, E_{fe}, is

$$Z(\frac{3}{5}\frac{\hbar^2 k_F^2}{2m} + W_o)$$

and the band structure contribution, E_{bs}, is written

$$E_{bs} = \sum_{\underline{q}}{}' S^*(\underline{q})S(\underline{q})F(q) \qquad \text{(I-C31)}$$

Here the "energy-wave number characteristic", F(q), is

$$F(q) = \frac{2\Omega}{(2\pi)^3 N}|w(q)|^2 \frac{2m}{\hbar^2}\int_{k<k_F}\frac{d^3k}{(k^2-|\underline{k}+\underline{q}|)^2} \qquad \text{(I-C32)}$$

The summation over $k<k_F$ has been replaced by an integral. This yields the result

$$F(q) = \frac{-\Omega q^2}{8\pi e^2 N}|w(q)|^2[\varepsilon(q)-1] \qquad \text{(I-C33)}$$

where the Hartree dielectric function

$$\varepsilon(q) = 1 + \frac{me^2}{2\pi k_F \hbar^2 \eta^2} \left[1 + \frac{1-\eta^2}{2\nu} \ln \left|\frac{1+\eta}{1-\eta}\right|\right], \qquad \text{(I-C34)}$$

and $\eta = q/2k_F$.

The effect of screening is included in the following way. The pseudopotential is written as the sum of two terms:

$$w(r) = w^0(r) + w^1(r)$$

i.e.,

$$w(q) = w^0(q) + w^1(q) \qquad \text{(I-C35)}$$

Here w^0 is the potential due to Coulomb interaction with the ions, while w' is the potential due to Coulomb interaction with the electrons: w' is related through Poisson's equation to the fluctuation in electron charge density, which is in turn obtained from the first order wave functions. The same integral, which appears in Eq. (I-C32), enters this calculation, and we obtain

$$w(q) = w^0(q)/\varepsilon(q)$$

and finally

$$F(q) = \frac{-\,\Omega q^2}{8\pi e^2 N} \left| w^0(q) \right|^2 \left[1 - \frac{1}{\varepsilon(q)}\right]. \qquad \text{(I-C36)}$$

The dynamical matrix is written as the sum of three terms, corresponding to the three contributions to the interionic potential:

$$\underline{\underline{D}} = \underline{\underline{D}}^{(C)} + \underline{\underline{D}}^{(R)} + \underline{\underline{D}}^{(E)} \qquad \text{(I-C37)}$$

The Coulomb term may be treated by Ewald's method, as described by Kellermann (1940). The repulsive term is generally small and is often neglected. The electronic term is related to the electronic energy per ion, E_{el}, by

$$D_{\alpha\beta}^{(E)}(\underline{q}) = N \sum_{\ell'}{}' \left(\frac{\partial^2 E_{el}}{\partial u_\alpha(\ell)\partial u_\beta(\ell')}\right)[\exp\{i\underline{q}\cdot\underline{r}(\ell'\ell)\}-1] \qquad \text{(I-C38)}$$

The positions of the ions are only contained in E_{bs}, and we therefore have

$$\frac{\partial^2 E_{el}}{\partial u_\alpha(\ell)\partial u_\beta(\ell')} = \sum_{\underline{\kappa}}{}' F(\kappa) \left(\frac{\partial^2[S^*(\kappa)S(\kappa)]}{\partial u_\alpha(\ell)\partial u_\beta(\ell')}\right)$$

$$= \frac{1}{N^2} \sum_{\underline{\kappa}}{}' \kappa_\alpha\kappa_\beta F(\kappa)\{\exp[i\underline{\kappa}\cdot\underline{r}_{\ell'\ell}]+\exp[-i\underline{\kappa}\cdot r_{\ell'\ell}]\}$$

and therefore

$$D_{\alpha\beta}^{(E)}(\underline{q}) = \frac{1}{N} \sum_{\underline{\kappa}}{}' \kappa_\alpha\kappa_\beta F(\kappa) \sum_{\ell'}{}'\{\exp[i(\underline{q}+\underline{\kappa})\cdot\underline{r}_{\ell'\ell}] +$$

$$\exp[i(\underline{q}-\underline{\kappa})\cdot\underline{r}_{\ell'\ell}]-\exp[\underline{i\kappa}\cdot\underline{r}_{\ell'\ell}]-\exp[-i\underline{\kappa}\cdot\underline{r}_{\ell'\ell}]\},$$

or

$$D_{\alpha\beta}^{(E)}(\underline{q}) = 2 \sum_{\underline{G}}{}'\{(\underline{G}+\underline{q})_\alpha(\underline{G}+\underline{q})_\beta F(|\underline{G}+\underline{q}|)$$

$$- G_\alpha G_\beta F(G)\} \qquad \text{(I-C39)}$$

This expression is analogous to equation (I-C17). We shall discuss the application of this method to the alkali metals in Chapter II.

(b) Analysis of Dispersion Curves of Metals

The interatomic forces in a metal are expected to decrease with increasing interatomic separation. As an approximation, we may assume that these forces extend out to i'th nearest neighbours only. A linear least squares fit to the measured dispersion curves along the symmetry directions then yields a set of AFC's $\phi_{\alpha\beta}(\ell\ell')$, and the usefulness of the approximation is largely determined by the agreement between the measured frequencies and those calculated using the set of AFC's. In practice the dispersion curves of many metals, with the notable exception of lead (Brockhouse et al. 1962), are adequately described using AFC's out to fewer than 10 neighbours. Furthermore these AFC's may be used to calculate frequencies at a mesh of points in reciprocal space, and hence $g(\nu)$, the phonon frequency distribution or density of states. Knowing $g(\nu)$, thermodynamic properties of the material may be calculated. Corrections for departures from harmonicity may sometimes be estimated.

A detailed account of this method of analysis has been given by Svensson et al. (1967) with particular reference to copper. An analysis of the dispersion curves of rubidium is given in Chapter II.

(iv) Ionic Crystals

The simplest picture of the interionic forces in ionic crystals is the rigid ion model of Born (see Born and Huang

1954). The ions are regarded as rigid units, and the interionic potential contains a long range Coulomb term and a short range repulsive contribution of the Born-Mayer type. The equations of motion are then written:

$$\underline{\underline{m}}\omega^2\underline{U} = \underline{\underline{D}}\underline{U} = (\underline{\underline{R}} + \underline{\underline{Z}}\ \underline{\underline{C}}\ \underline{\underline{Z}})\underline{U} \qquad \text{(I-C40)}$$

where $\underline{U}$ contains the ionic displacements, $\underline{\underline{m}}$ and $\underline{\underline{Z}}$ are diagonal matrices containing the ionic masses and charges respectively, $\underline{\underline{D}}$ is the dynamical matrix, $\underline{\underline{R}}$ is the repulsive contribution, and $\underline{\underline{C}}$ is a matrix of "Coulomb coefficients",

$$C_{\alpha\beta}(\underline{q}kk') = - \sum_{\ell'k'}{}' \left[\frac{\partial^2((\underline{r})^{-1})}{\partial u_\alpha(\ell k)\,\partial u_\beta(\ell'k')} \left(e^{i\underline{q}\cdot\underline{r}} - 1\right)\right]$$

with $\underline{r} = \underline{r}(\ell'k',\ell k)$. These coefficients may be calculated by Ewald's method.

An extension of this model, which is generally necessary in order to obtain reasonable agreement with experiment, is the shell model which has been described by Cowley et al. (1963). We consider now displacements of an ion core relative to the outer shell of electrons in the ion. The equations of motion become:

$$\underline{\underline{m}}\omega^2\underline{U} = (\underline{\underline{R}}+\underline{\underline{Z}}\underline{\underline{C}}\underline{\underline{Z}})\underline{U} + (\underline{\underline{T}}+\underline{\underline{Z}}\underline{\underline{C}}\underline{\underline{Y}})\underline{W}$$

$$\underline{\underline{O}} = (\underline{\underline{\tilde{T}}}+\underline{\underline{Y}}\underline{\underline{C}}\underline{\underline{Z}})\underline{U} + (\underline{\underline{S}}+\underline{\underline{Y}}\underline{\underline{C}}\underline{\underline{Y}})\underline{W}$$

where $\underline{W}$ contains the shell displacements, $\underline{\underline{Y}}$ is a diagonal matrix containing the shell charges, and $\underline{\underline{T}}$ and $\underline{\underline{S}}$ represent the core-shell and shell-shell repulsive interactions. These equations may be solved for $\underline{W}$ yielding

$$\underline{\underline{m}}\omega^2\underline{U} = [(\underline{\underline{R}}+\underline{\underline{Z}}\,\underline{\underline{C}}\,\underline{\underline{Z}}) - (\underline{\underline{T}}+\underline{\underline{Z}}\,\underline{\underline{C}}\,\underline{\underline{Y}})(\underline{\underline{S}}+\underline{\underline{Y}}\,\underline{\underline{C}}\,\underline{\underline{Y}})^{-1}(\underline{\underline{\tilde{T}}}+\underline{\underline{Y}}\,\underline{\underline{C}}\,\underline{\underline{Z}})]\underline{U} \qquad \text{(I-C41)}$$

This expression simplifies when $\underline{q}$ lies along a symmetry direction.

Calculations based on the shell model invariably involve further approximations. The matrices $\underline{\underline{R}}$, $\underline{\underline{S}}$ and $\underline{\underline{T}}$ are commonly chosen to differ only by a scaling factor. For example Cowley et al. (1963) chose $\underline{\underline{R}} = \underline{\underline{T}} = \underline{\underline{S}}/\gamma_s$ where γ_s is a constant. Various other approximations and their validity are discussed in this paper. The short-range repulsive forces are often taken to be axially symmetric forces between first or first and second neighbours only, and sometimes further conditions are imposed. The matrices $\underline{\underline{Y}}$, $\underline{\underline{S}}$ and $\underline{\underline{T}}$ are normally expressed in terms of mechanical and electrical polarizabilities (Cowley et al. 1963).

The application of the shell model to the case of potassium chloride is described in a reprint at the end of this thesis (Copley et al. 1969).

This concludes our discussion of lattice dynamics in the harmonic approximation. In the remainder of this chapter, we shall consider the theory and practice of neutron scattering, with particular reference to the study of lattice vibrations.

D. NEUTRON SCATTERING THEORY

(i) The Born Approximation and Fermi Pseudopotential

We have already noted (Section IA) that there are many similarities between X-ray scattering and neutron scattering. The starting points for the two theories are however quite different, since there are fundamental differences in the form of interaction between the radiation and the scatterer.

X-rays are scattered by electrons. The scattered amplitude in the forward direction from a single atom or ion is proportional to the number of electrons, Z. The amplitude decreases away from the forward direction. This behaviour is described by the form factor $f_i(\sin\theta/\lambda)$, where i indicates that f depends on the atom or ion, θ is the Bragg angle, and λ is the wavelength. The form factor is not exactly known: it is generally calculated by a Hartree-Fock or related method.

Neutrons are predominantly scattered by nuclei. There is a further important interaction, in solids containing atoms with unpaired spins, between the magnetic moments of the atom and of the neutron (see e.g. Bacon 1962), but that interaction will not concern us here. An exhaustive list of the known interactions of slow neutrons with matter has been given by Shull (1967).

Slow neutron scattering is treated within the framework of the first Born approximation. At first sight this might seem inadmissible since the nuclear interaction potential cannot be regarded as a small perturbation compared with the energy of the neutron. This objection is avoided through representation of the nuclear interaction by the Fermi pseudopotential (Fermi 1936):

$$V(\underline{r}) = \frac{2\pi\hbar^2 b\delta(\underline{r})}{m_n} \qquad \text{(I-D1)}$$

where m_n is the neutron mass. This delta function representation is justified since the range of the nuclear interaction ($\sim 2 \times 10^{-13}$ cm) is very small compared with the wavelength of a thermal neutron ($\sim 10^{-8}$ cm). The "scattering amplitude", b, is determined by experiment (see e.g., Bacon 1962). The scattering properties of the nucleus are completely determined by the scattering amplitude.

Scattering amplitudes vary somewhat erratically with Z, in contrast with the smooth variation for X-rays. Furthermore, because of the short range of the interaction, neutrons are scattered isotropically by a nucleus, so that the "form factor" for neutrons is independent of scattering angle.

(ii) Van Hove's Treatment

Van Hove (1954) has developed an elegant method for treating the scattering of radiation within the first Born approximation. For the case of neutrons scattered by a system of identical particles with scattering length b, the differential scattering cross section per unit solid angle Ω, per unit energy interval ε, is written:

$$\frac{d^2\sigma}{d\Omega d\varepsilon} = AS(\underline{Q},\omega) \tag{I-D2}$$

where

$$A = \frac{b^2}{\hbar}\,\frac{k'}{k_o} \tag{I-D3}$$

and

$$S(\underline{Q},\omega) = \sum_n g(n) \sum_m \left|\langle m| \sum_{\ell=1}^{N} \exp(i\underline{Q}\cdot\underline{r}_\ell)|n\rangle\right|^2$$

$$\times\ \delta(\omega + (E_n - E_m)/\hbar)\,. \tag{I-D4}$$

Here $\underline{Q} = \underline{k}_o - \underline{k}'$ and $\hbar\omega = E_o - E'$ are the wave vector and energy transfer to the system, and $\underline{k}_o$ (E_o) and $\underline{k}'$ (E') are the wave vector (energy) of the incident and scattered neutrons respectively. E_n and E_m are the energies of the initial and final states of the system $|n\rangle$, $|m\rangle$; $g(n)$ is the relative population of state $|n\rangle$ given by

$$g(n) = \exp(-E_n/k_BT)/\sum_i \exp(-E_i/k_BT)\,. \tag{I-D5}$$

The positions of the N particles are described by the vectors $\underline{r}_\ell$.

The scattering cross section, Eq. (I-D2), is the product of two terms. The first term, A, contains information about the neutron and about the type of scatterer. The function $S(\underline{Q},\omega)$ contains information about the structure of the scattering system. It is the Fourier transform of the generalized pair distribution function $G(\underline{r},t)$ which, in the absence of quantum effects, has the following significance: given a particle at position $\underline{r}'$ at time t', $G(\underline{r},t)$ measures the probability that there is a particle at $\underline{r}'+\underline{r}$ at time $t'+t$.

We now distinguish two types of cross-section. Since the neutron has spin 1/2, a nucleus with non-zero spin has two scattering lengths corresponding to parallel and anti-parallel configurations. Furthermore different isotopes generally have different scattering lengths. Coherent scattering results when waves scattered by identical nuclei (i.e. nuclei of the same isotope, having the same spin) interfere with one another. Incoherent scattering, on the other hand, results from scattering by the individual nuclei. The total scattering cross section is related to the sum of the squared scattering amplitudes of the nuclei, whereas the coherent cross section is related to the square of the sum of the scattering amplitudes. The scattering cross section is then written as a sum of coherent and incoherent cross sections:

$$\frac{d^2\sigma}{d\Omega d\varepsilon} = \frac{d^2\sigma(\mathrm{COH})}{d\Omega d\varepsilon} + \frac{d^2\sigma(\mathrm{INC})}{d\Omega d\varepsilon} \qquad \text{(I-D6)}$$

where

$$\frac{d^2\sigma(\mathrm{COH})}{d\Omega d\varepsilon} = \frac{\langle b\rangle^2 k'}{\hbar \; k_o} S_{\mathrm{COH}}(\underline{Q},\omega)$$

and

$$\frac{d^2\sigma(\mathrm{INC})}{d\Omega d\varepsilon} = \frac{(<b^2>-<b>^2)}{\hbar}\frac{k'}{k_o}\ S_{\mathrm{INC}}(\underline{Q},\omega)$$

The expressions for $S_{\mathrm{COH}}(\underline{Q},\omega)$ and $S_{\mathrm{INC}}(\underline{Q},\omega)$ are given by Van Hove (1954). In the majority of experiments, including those reported here, incoherent scattering contributes an undesirable background beneath the observed resonance. Fortunately the incoherent scattering cross section is generally smaller than the coherent cross section. In certain cases important information about the phonon density of states has been obtained from measurements of incoherent scattering cross sections (Stewart and Brockhouse 1958, Page 1967).

The Van Hove formalism is particularly useful for treating scattering from liquids and magnetic systems. In these situations the interest lies in the correlation between atoms, or spins, at different sites. Truly elastic scattering ($\hbar\omega = 0$), inelastic scattering ($\hbar\omega \neq 0$), and scattering without regard to energy transfer ($\Delta(\hbar\omega) = \infty$), yield information about time-averaged correlations ($\Delta t = \infty$), correlations between two different times ($\Delta t \neq 0$), and correlations at a particular time ($\Delta t = 0$) respectively. These relationships result from the connection between $S(\underline{Q},\omega)$ and $G(\underline{r},t)$.

(iii) Scattering by a Crystal

The scattering of neutrons by a crystal may be treated using expression (I-D4) for the scattering function. Since the anharmonic situation will be considered in Chapter III, a brief outline of the harmonic theory (Sjölander 1958) will be given here. A simplified account (in which it is assumed that all modes of a given $\underline{q}$ are degenerate and that the polarization of one of the modes is parallel to $\underline{Q}$) is given by Kittel (1963).

Writing the atomic position $\underline{r}_\ell$ in Eq. (I-D4) as an equilibrium position $\underline{R}_\ell$ plus a displacement $\underline{u}_\ell$, the Heisenberg representation is utilized to obtain

$$S(\underline{Q},\omega) = \frac{1}{2\pi} \sum_{\ell\ell'} \exp[-i\underline{Q}\cdot\underline{R}_{\ell\ell'}] \int_{-\infty}^{\infty} e^{i\omega t}$$

$$\times <<\exp[-i\underline{Q}\cdot\underline{u}_\ell(t)]\exp[i\underline{Q}\cdot\underline{u}_{\ell'}(o)]>>dt \qquad \text{(I-D7)}$$

where the brackets <<...>> denote the thermal average, and the delta function in Eq. (I-D4) has been replaced by its Fourier transform.

The thermal average is simplified using the relation (Messiah 1962, p. 442):

$$e^A e^B = e^{A+B} \exp \frac{1}{2}[A,B].$$

The displacements $\underline{u}_\ell(t)$ are written in terms of the operators

$A(\underline{q}j)$, as in Eq. (I-C24). The thermal average in Eq. (I-D7) is then separated into a time-independent part, known as the Debye-Waller factor:

$$\exp[-2W(\underline{Q})] = \exp\{-\frac{\hbar Q^2}{2Nm}\sum_{\underline{q}j}\frac{2n(\underline{q}j)+1}{\omega(\underline{q}j)}\}$$

$$= \exp\{-<[\underline{Q}\cdot\underline{u}]^2>\} \qquad \text{(I-D8)}$$

and a time-dependent part:

$$\exp\{\frac{\hbar}{2Nm}\sum_{\underline{q}j}(\frac{[\underline{Q}\cdot\underline{e}(\underline{q}j)]^2}{\omega(\underline{q}j)}\exp(i\underline{q}\cdot\underline{R}_{\ell\ell'})$$

$$\times\ [(n(\underline{q}j)+1)\exp(-i\omega(\underline{q}j)t)+n(\underline{q}j)\exp(i\omega(\underline{q}j)t)])\} \qquad \text{(I-D9)}$$

Expression (I-D9) is expanded in a power series which, together with Eq. (I-D8), is substituted into Eq. (I-D7): sums such as $\sum_{\ell}\exp(i\underline{q}\cdot\underline{r}_{\ell})$ are replaced by multivalued delta functions $\Delta(\underline{q})$ using Eq. (I-C16), and the time-dependent exponential terms such as $\exp(i[\omega+\omega(\underline{q}j)]t)$ are integrated over time to give delta functions in energy. The first term in the final expression is the zero-phonon (elastic scattering) function:

$$S_o(\underline{Q},\omega) = (2\pi)^3N^2V^{-1}\exp[-2W(\underline{Q})]\delta(\omega)\Delta(\underline{Q}) \qquad \text{(I-D10)}$$

The delta functions simply express the conditions for Bragg reflection: V is the volume of the crystal.

The next term gives the one-phonon cross-section:

$$S_1(\underline{Q},\omega) = (2\pi)^3 \frac{N}{V} \exp[-2W(\underline{Q})]\frac{\hbar}{2m} \sum_{\underline{q}j} \frac{[\underline{Q}\cdot\underline{e}(\underline{q}j)]^2}{\omega(\underline{q}j)}$$

$$\times[(n(\underline{q}j)+1)\delta(\omega-\omega(\underline{q}j))+n(\underline{q}j)\delta(\omega+\omega(\underline{q}j))]\Delta(\underline{Q}-\underline{q}) \qquad \text{(I-D11)}$$

The delta functions in this expression express conservation of wave vector and energy. The cross section contains terms corresponding to phonon creation (neutron energy loss) and to phonon annihilation (neutron energy gain). Since these cross sections are proportional to n($\underline{q}$j)+1 and n($\underline{q}$j) respectively, measurements of high frequency excitations and/or measurements at low temperatures must be performed with neutron energy loss. Further consequences of equation (I-D11) will be discussed with particular reference to rubidium in Section IID.

We proceed now to a general discussion of the practical side of neutron scattering - the spectrometers and their operation.

E. NEUTRON SCATTERING METHODS

(i) Types of Instrument

A variety of instruments is used for measurements of slow neutron scattering cross sections. (see e.g. papers in General Reference 4, Vol. II, and General Reference 7).

As indicated in Section ID, the natural variables of a scattering experiment are the energy and wave vector transfers, $\hbar\omega$ and $\underline{Q}$. Instruments are therefore designed to define the direction and energy (and hence the wave vector) of the incident and scattered beams of neutrons. The energy is generally defined in one of two ways: by its time of flight over a measured distance, or by Bragg reflection from a single crystal.

In many time-of-flight machines a particular neutron velocity is selected by a system of beam choppers. The first chopper defines an origin in time, and the second chopper is phased to transmit neutrons of the desired velocity. Subsequent choppers reduce the fast neutron contribution to the beam. In an alternative arrangement a rotating crystal fulfils the twin functions of pulser and monochromator. The energy of a scattered neutron is deduced from its time of arrival at the detector. Such spectrometers are more suited to experiments on liquids than to measurements of excitations in single crystals.

The inelastic scattering measurements described in this thesis were made using the McMaster triple-axis spectrometer at the E2 hole of the NRU reactor, Chalk River (Brockhouse et al. 1968a). A schematic diagram of the spectrometer is shown in Fig. I-1. A particular wavelength λ_o is selected from the "white" reactor beam by Bragg reflection at the first monochromator crystal. A second crystal, mounted parallel to the first, reflects the beam parallel to its original direction. The monochromatic beam is incident on the specimen, and neutrons scattered through the angle ϕ are incident on the analyser crystal. Those of wavelength λ' are Bragg reflected into the signal detector (B). In order to compensate for fluctuations in reactor power, counting occurs for a preset number of counts accumulated in the fission monitor counter which is placed in the incident beam. Collimators serve to define the direction of the beam at each stage.

In many respects this spectrometer is typical. The twin monochromator system is however an unusual feature of the instrument. It has the advantage that the specimen table is fixed, and since the monochromator is in-pile the external shielding requirements are considerably reduced. The extra detector (labelled A in Fig. I-1) is useful for identifying various types of unwanted scattering process (see Appendix II).

In most measurements of elastic scattering intensities a double-axis spectrometer is employed. The analyser crystal is omitted and scattered neutrons of all energies are counted.

This procedure is justified because the ratio of inelastic to elastic events within the crystal is generally very small. On the other hand certain elastic scattering measurements are best performed using a triple axis spectrometer set to accept neutrons with wavelength $\lambda' = \lambda_o$ in the detector. For example the lattice constants of several alloys were measured in this way (Hallman 1969).

An undesirable feature of the present double monochromator system in the E2 triple-axis spectrometer is the existence of contaminant wavelengths in the incident beam. Since these contributions to the incident beam have shown up in some of the measurements (Section IID), it is worthwhile to describe how they are produced. The monochromator crystals are made of copper, with $(2\bar{2}0)$ axes vertical and (220) planes parallel to their major faces. With this arrangement other sets of planes are parallel in the two crystals (see the inset in Fig. I-1). For every setting of the monochromator Bragg angle Θ_M, there are therefore additional contaminant contributions to the beam incident on the specimen. The principal contaminant is reflected from (331) planes in the crystal: a weaker contaminant, which is present at large values of Θ_M, arises from $(33\bar{1})$ planes.

The wavelengths of the various components in the beam are easily evaluated. Defining $\beta = \cos^{-1}(\sqrt{19})$ as the angle between neighbouring (220) and (331) planes, we have

$$\begin{aligned} \lambda_o &= 2d_{220}\ \sin\Theta_M \\ \lambda_c &= 2d_{331}\ \sin(\Theta_M+\beta) \\ \lambda_c' &= 2d_{331}\ \sin(\Theta_M-\beta) \end{aligned} \qquad \text{(I-E1)}$$

where λ, λ_c, and λ_c' are the wavelengths of the (220), (331) and $(33\bar{1})$ components, and d_{220} and d_{331} are the spacings between (220) and (331) planes respectively.

The contaminants can be removed by rotating one of the monochromator crystals about the normal to the major (220) faces. This operation must await an extended reactor shutdown since it involves removal of the in-pile plug.

(ii) Operation of the Triple-Axis Spectrometer

The triple-axis spectrometer is particularly useful for studies of phonon (and other) dispersion relations in single crystals. Five conditions must be satisfied in order to observe a peak in the scattered intensity due to a (harmonic) excitation in the crystal.

$$\pm\hbar\omega = E_o - E' \qquad \text{(conservation of energy)} \qquad \text{(I-E2)}$$

$$\underline{q} + \underline{G} = \underline{Q} = \underline{k}_o - \underline{k}' \qquad \text{(conservation of wave vector)} \qquad \text{(I-E3)}$$

$$\omega = \omega(\underline{q}j) \qquad \text{(the dispersion relation).} \qquad \text{(I-E4)}$$

On the other hand there are only four angular variables: Θ_M and Θ_A (the monochromator and analyser Bragg angles respectively), ϕ, and ψ (the orientation of the specimen with respect to the incident beam, Fig. I-1). As a result peaks are only observed for certain settings of the spectrometer.

With the advent of the Constant $\underline{Q}$ and Constant E techniques, (Brockhouse 1961) the full capabilities of the triple-axis spectrometer were realized. In the Constant $\underline{Q}$ method, the angles are varied in such a way that $\underline{Q}$ remains fixed and the energy transfer $\hbar\omega$ is varied. Counts are accumulated at each point on the scan for a given monitor count. Typical peaks obtained in rubidium using this method are shown in Fig. II-2. The corresponding vector diagrams, indicating the initial and final positions on the scan, are also shown. Generally either Θ_M or Θ_A is kept constant throughout the run. Though corrections should be applied for the factor (k'/k_o) in the cross section formula, Eqs., (I-D2, I-D3),and for the variation of analyser efficiency with Θ_A, the "fixed Θ_M" mode is often chosen because the design of the spectrometer is simplified. At present the E2 spectrometer is operated only in this mode. The Constant E method is analogous to Constant $\underline{Q}$: both Θ_M and Θ_A are fixed, and ϕ and ψ are varied so that $\underline{Q}$ follows a straight line path in reciprocal space.

The bulk of the work described in this thesis was performed on the E2 spectrometer at Chalk River. Subsidiary measurements were made using the double- and triple-axis spectrometers installed at the McMaster reactor (Brockhouse et al. 1968a). Both triple-axis instruments are controlled by punched cards, as described by Rowe (1966). The cards are obtained as output from a computer programme which, in its present modification (due to the author in collaboration with Mr. A. Larose), can calculate scans along any straight line path in $(\underline{Q},\omega)$ space. In normal operation the spectrometer is run continuously and the angles are checked several times daily.

CHAPTER II

HARMONIC ASPECTS OF THE CRYSTAL DYNAMICS OF RUBIDIUM

A. INTRODUCTION

The elements lithium, sodium, potassium, rubidium, and caesium together with francium, whose most stable isotope has a 21 minute half-life, occupy Group 1A of the periodic table and are known as the alkali metals.* Atoms of these metals have the closed shell electronic structure of the inert gases He, Ne, Ar, Kr, Xe and Rn respectively, plus a single s-electron in the outer shell. In the condensed state, an alkali metal may be regarded as a collection of positive ion cores immersed in a negative sea of conduction electrons. The alkalis are considered the simplest of all metals and consequently a large body of experimental and theoretical work has been devoted to these materials.

Most of the experimental work has been performed on Na and K, since they are less reactive and more readily available than Rb and Cs (see e.g., Brotherton et al. 1962). A disadvantage of using Li or Na for many low temperature experiments is the occurrence of a partial martensitic transition from the body centred cubic (b.c.c.) phase to a low

---

*Apparently (Holmyard and Palmer 1939) Abu Mansur Muwaffak, a celebrated Persian physician in the 10th century A.D., was the first to distinguish between the carbonates of sodium and potassium. These substances were extracted from plant ashes by the Arabs, who described them as al-qali, "the ash", from which we obtain the moderm term, alkali.

temperature close-packed structure with stacking faults. No such transition has been observed in K, Rb or Cs (Barrett 1955, 1956).

Some properties of the stable alkali metals are listed in Table II-1. In order to demonstrate trends in certain properties, including the lattice constant and the thermal expansion, values for the five metals have been taken from the same reference. Martin (1965) has noted that "the temperature variations of the densities of the alkali metals are not established with any great certainty". For Rb and Cs the errors "may be as high as ±1%". An experimental determination of the lattice parameter of rubidium, by neutron diffraction, is reported in Appendix I.

The low temperature limiting values of the Debye temperature for the specific heat, θ_o^c, are also taken from Martin (1965). The slow neutron cross sections for absorption (σ_{abs}) and for coherent and incoherent scattering (σ_{coh}, σ_{inc}) are from the "barn book" of Hughes and Schwartz (1958). The value of σ_{coh} for Rb is given as 3.8 barns in this reference but a supplement (Goldberg et al. 1966) and a recent compilation in Acta Crystallographica (the Neutron Diffraction Commission, 1969) give the value 9.1 barns, which was reported by Mueller et al. (1963). More recent measurements of Copley (1970), Wang and Cox (1970), and Meriel (1970) favour a value between 5.7 and 6.7 barns (see Appendix VI).

TABLE II-1. Properties of the stable alkali metals

		Li	Na	K	Rb	Cs
Atomic Number		3	11	19	37	55
Atomic Weight		6.939	22.990	39.102	85.47	132.91
Isotopes		92.6% Li^7 7.4% Li^6	100% Na^{23}	93.1% K^{39} 6.9% K^{41} 0.02% K^{40} ($\tau_{\frac{1}{2}}=1.3\times10^9$y)	72.2% Rb^{85} 27.8% Rb^{87} ($\tau_{\frac{1}{2}}=4.7\times10^{10}$y)	100% Cs^{133}
Lattice Constant[a] (Å) (at 78°K)		3.49	4.238	5.247	5.605	6.07
Martensitic Transition Temperature		∿78°K	∿36°K			
Thermal Expansion[b] (10^{-6}°K^{-1})		∿47	∿68	∿83	∿90	∿97
Compressibility[c] (at 4°K) (10^{-5}atm.$^{-1}$)		0.78	1.39	2.88	3.48	4.41
Elastic Constants (at 78°K) (10^{10} dynes/cm^2)	C_{11} C_{12} C_{44}	14.44[d] 12.11 10.94	8.21[e] 6.83 5.78	4.10[f] 3.41 2.61	3.25[g] 2.73 1.98	2.46[h] 2.05 1.48
Debye temperature[j] θ_o^c (°K)		344	152.5	90.6	55.6	38.4

(continued next page)

TABLE II-1 (continued)

		Li	Na	K	Rb	Cs
Melting Temperature[k] T_M (°K)		453	371	337	312	303
Neutron Cross Sections[ℓ] (barns)	σ_{abs}	71	0.5	2.1	0.7	29
	σ_{coh}	0.4	1.55	1.5	5.9[m]	3.0
	σ_{inc}	0.8	1.9	0.7	1.7	4
Mohs Hardness[n]		0.6	0.4	0.5	0.3	0.2

[a] Barrett (1956). See also Appendix I.

[b] Values preferred by Martin (1965).

[c] Swenson (1955).

[d] Slotwinski and Trivisonno (1969).

[e] Diederich and Trivisonno (1966).

[f] Marquardt and Trivisonno (1965).

[g] Gutman and Trivisonno (1967)

[h] Kollarits and Trivisonno (1968).

[j] Martin (1965).

[k] Smithells (1962), p. 695.

[ℓ] Hughes and Schwartz (1958).

[m] Copley (1970). See also Appendix VI.

[n] Weast (1968).

Several properties of Rb are conveniently tabulated by Filyand and Semenova (1968). A book by Perel'man (1965) also contains much useful information on Rb and Cs.

The determination of the phonon dispersion relation in rubidium, which is reported in this chapter, was undertaken for several reasons.

(1) Though many authors have calculated dispersion curves for the alkali metals, generally by the pseudopotential method, the amount of experimental information is fairly limited. At the time this work was started, only the dispersion curves of sodium and potassium had been measured. It was felt that measurements on another of the alkali metals would be worthwhile.

(2) The volume thermal expansion coefficients, α_v, for the alkali metals, are considerably larger than those of any other metal at the same reduced temperature T/T_m, (T_m is the melting temperature). Borelius (1963) has compiled thermal expansion data for 16 metals: in order of increasing melting point, they are Hg, K, Na, Sn, Pb, Al, Ag, Au, Cu, Ni, Pd, Pt, Rh, Ir, Mo, and W. The volume expansivities (in units of $10^{-5}{}^{\circ}K^{-1}$), at the melting point, are 25 and 27 for Na and K respectively: in the same units $\alpha_v = 17$ for Hg. For the remaining metals the volume expansivity at T_m generally decreases

with increasing T_m. Aluminium (T_m = 933°K) has the largest value, $\alpha_v = 13$, whereas tungsten (T_m = 3650°K) has $\alpha_v \approx 4$ (obtained by extrapolation of data which exists up to 2700°K).

The large values of α_v for the alkali metals indicate that the effective interatomic potential is more anharmonic than in other metals, at the same reduced temperature, T/T_m. Anharmonic effects will therefore be more pronounced. In addition T_m is small for the alkalis so that these effects appear at relatively low (and therefore more accessible) temperatures. The effects of temperature on the phonon spectrum are consequently of some interest.

(3) Of the five alkali metals, rubidium has the best neutron cross sections (Table II-1), whereas the remaining two choices for a neutron scattering experiment (Li and Cs) have the worst cross sections.

(4) There is no martensitic transformation in rubidium (Barrett 1955, 1956).

(5) Both caesium and rubidium have melting points close to room temperature. This makes them preferable to lithium for anharmonic studies. The melting point of caesium is uncomfortably low, whereas precautions need only be taken to keep a rubidium crystal away from heat. (The unfortunate démise of the crystal, described in a later section, is not believed to result from its melting).

B. EXPERIMENTAL AND THEORETICAL WORK ON THE ALKALI METALS

The crystal dynamics of the alkali metals has been the subject of much theoretical work over past years. A useful review is given by Joshi and Rajagopal (1968). Cochran (1966) gives references to some of the earlier work.

The first fundamental calculation of the lattice vibration frequencies in a metal (Na) was that of Toya (1958). Following Fuchs (1935, 1936) he wrote the interionic potential as the sum of three terms, namely the Coulomb repulsion, the overlap repulsion, and the attractive interaction via the conduction electrons (Section I C(iii)). The dispersion curves of sodium were subsequently determined by Woods et al. (1962), and the agreement between these measurements and Toya's calculation is noteworthy.

More recent theoretical work on the phonon spectra of metals is due to many authors, including Vosko et al. (1965), Animalu et al. (1966), Schneider and Stoll (1966a, 1966b), Wallace (1968, 1969), Prakash and Joshi (1969) and Ashcroft (1968). Further references are contained in papers by Price et al. (1970) and by Blanchard and Varshni (1970). Most of these workers adopt the pseudopotential, or model potential, approach, which was outlined in Section I C. On the other hand, Vosko et al. (1965) used many-body perturbation theory to treat the electron-ion interaction term.

Cochran (1963) adopted a different approach, extracting an effective potential from the experimental measurements of Woods et al. (1962) on Na.

The dispersion curves of potassium were measured by Cowley et al. (1966), and found to be very similar in shape to those of sodium. These authors analyzed their results to obtain atomic force constants (as did Woods et al. for sodium), and they also obtained an effective potential using an extension of Cochran's method. More recently preliminary reports of experimental measurements on lithium (Smith et al. 1968) and rubidium (Copley et al. 1968) have appeared.

The present chapter reports further work on rubidium, including measurements at different temperatures. Attempts have been made to correct the measurements for experimental effects such as resolution and unwanted scattering processes, so that a reliable set of results is available for comparison with theory. Such corrections are particularly large in the case of rubidium, principally because the lattice spacing is large and the unit cell in reciprocal space is therefore unusually small. Furthermore the phonon frequencies in this metal are uncomfortably low with the result that unwanted elastic scattering processes are more commonly picked up. The details of these corrections are described in Appendices II and III .

Section IIE contains an analysis of the measurements, and calculations of the phonon frequency distribution for rubidium. The final section of the chapter is devoted to a detailed discussion of unexpected observations in the course of the measurements, together with a consistent explanation.

C. MEASUREMENT OF NORMAL MODE FREQUENCIES

The frequencies of the normal modes of vibration of body-centred cubic (b.c.c.)rubidium, for wave vectors along five symmetry directions in the reciprocal lattice, have been measured at several temperatures using the Chalk River (E2) triple-axis spectrometer (Section IB).

The specimen was a single crystal of cylindrical cross section, purchased from Research Crystals Inc., Richmond, Virginia. It measured 3-1/8" long by 1-1/2" diameter. A truncated cone at one end of the crystal occupied one third of the total length, narrowing to 3/8" diameter at the end (Fig. II-1). The crystal was examined, and subsequently sealed in an aluminium can, using a commercial dry box filled with argon. Protective grease, which surrounded the specimen, was first removed using facial tissues. A black film (of oxide/hydroxide?) was removed by wiping the surface with tissues soaked in xylene. The crystal was then transferred to an aluminium can having 0.040" walls, fitted with a re-entrant cap and an indium O-ring. The can was finally screwed up and sealed with epoxy cement.

After the first experimental run at low temperature, the specimen was removed from the cryostat and a small amount of material which had oozed through the indium seal caught fire. Since then there have been no further problems of this nature. It is clear that the metal must be treated with respect.

An event of more significance did however occur toward the end of the experimental work. A long series of measurements was made between October and December of 1969, using a helium cryostat. The specimen was left in the cryostat, under vacuum, until March 1970. At that time an attempt to check the alignment of the crystal was thwarted because of very poor intensity. On further examination the specimen was found to be largely polycrystalline, and the conical end contained three crystals at about 60° to each other. No explanation for this behaviour has yet been found. Attempts to purchase another crystal have been unsuccessful, and the experimental work was therefore concluded somewhat prematurely.

The crystal was initially aligned using the twin·axis spectrometer at the McMaster reactor (Brockhouse et al. 1968a) A $[1\bar{1}0]$ axis was found within 2° of the cylindrical axis, and the (200) rocking curves were 0.4° wide, indicating that the mosaic spread in the crystal was of this order. A careful search for extra crystals in the specimen in March 1969 (Appendix I) demonstrated that it was indeed single. Most of the measurements reported in this thesis were made with a (110) scattering plane. Certain branches were measured, at 120°K only, with a (100) scattering plane instead.

Inelastic scattering measurements of phonons were made using the McMaster triple axis spectrometer at Chalk River (Brockhouse et al. 1968a) almost exclusively in the constant $\underline{Q}$ mode of operation (Section ID). The monochromator used (220) planes of copper, and the analyser used (200) and (occasionally) (220) planes of copper. Soller collimators were employed to reduce the horizontal divergence of the beam. For most of the measurements, 8" collimators with 0.1" plate separation were used. For some of the measurements, two inches of single crystal quartz were inserted in the incident beam to reduce second-order contamination. The choice of collimation was determined by the conflicting requirements of good experimental resolution and good intensity. With the system described above, the collimation was fairly well matched to the mosaic spreads of the monochromator, specimen, and analyzer (Brockhouse 1966).

The fixed incident frequency ν_o was generally 4.79 THz (1 THz = 10^{12} cps). Some of the earlier measurements were made at other frequencies, between 3.8 and 5.5 THz. Several considerations affect the choice of ν_o. In particular, the energy resolution improves with larger θ_M, smaller ν_o. With ν_o = 4.79 THz, and the above collimation, the energy resolution was approximately 0.2 THz (full width at half maximum): this value was obtained from the width of a plot of scattered intensity against analyzer angle, using a vanadium specimen (which scatters almost completely incoherently (Brockhouse 1955)).

On the other hand, the proportion of second-order contaminant in the incident beam increases and (toward the low frequency end of the available range) the intensity of the main beam decreases, with decreasing ν_o. Furthermore in order to avoid detecting a peak resulting from elastic scattering by the specimen of the "(331) contaminant" (Section ID), followed by second-order Bragg reflection off the analyzer crystal, ν_o must be chosen greater than $[\nu_{max} + \nu_c/4]$, where ν_{max} is the maximum frequency in any scan, and ν_c is the frequency of the contaminant.

Most of the measurements were made using cryostats filled with liquid nitrogen. The more recent measurements were made with extra radiation shielding around the specimen. Furthermore two separate cryostats have been used. For these reasons, a number of temperatures ranging between 95 and 140°K were obtained for these measurements. Results have also been obtained at 205°K using dry ice, and a series of runs was made at 12°K using a liquid helium cryostat (made by Andonian Associates Inc.). With the inner well of this cryostat filled with liquid nitrogen, further measurements were made at 80°K. The tail section of the cryostat was modified to accommodate the large specimen (Fig. II-1). Temperatures

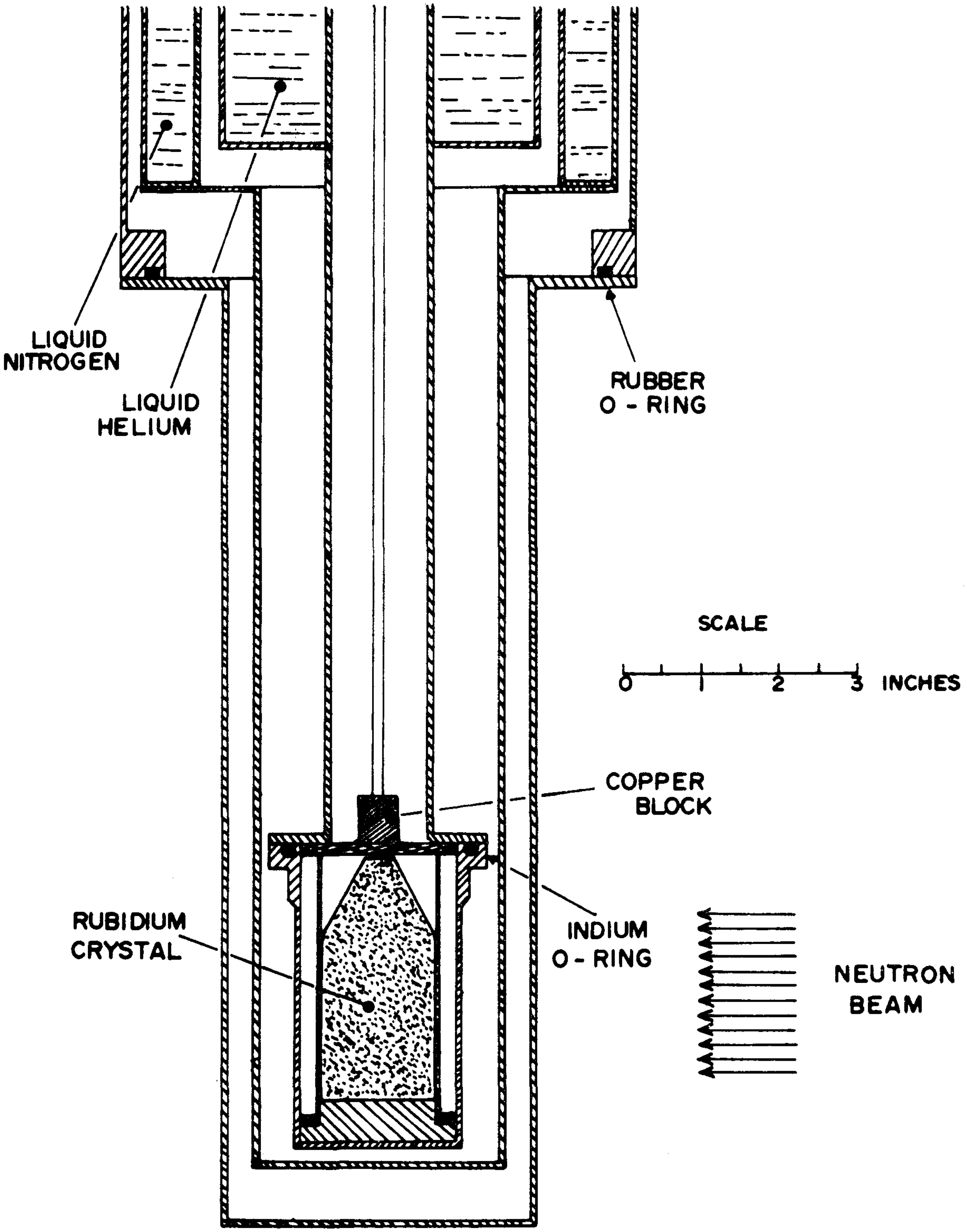

Fig. II-1. A scale drawing of the tail section of the helium cryostat which was used for the experiments at 12°K.

were generally measured using copper-constantan thermocouples; platinum and germanium resistance thermometers have also been employed.

D. TREATMENT OF RESULTS

Phonons with wave vector $\underline{q}$ lying along the $[00\zeta]$, $[\zeta\zeta\zeta]$, $[\zeta\zeta 0]$, $[\frac{1}{2}\frac{1}{2}\zeta]$ and $[\zeta\zeta 1]$ directions (i.e., directions Δ, Λ (and F), Σ, D and G in the notation of Koster (1957)), have been measured, using the constant $\underline{Q}$ technique (Section IE). (The first Brillouin zone of the face centred cubic (f.c.c.) reciprocal lattice is shown in Fig. AIV-1(a).

To optimize the intensity of a phonon, several factors had to be considered. The quantity $[\underline{Q}\cdot\underline{e}(\underline{q}j)]^2$ in Eq. (I-D11) was maximized by choosing $\underline{Q}$ as nearly parallel as possible to $\underline{e}(\underline{q}j)$. In many experiments $|\underline{Q}|$ itself is also maximized, but in the present situation the Debye-Waller factor is also an important consideration. For example the optimum value of $|\underline{Q}|$ at 110 and 220°K is about 3.6 $(2\pi/a)$ and 2.5 $(2\pi/a)$ respectively.

The results of several constant $\underline{Q}$ scans are shown in Figs. II-2 and II-3. In Fig. II-2 the (100) and $(1\bar{1}0)$ planes of the reciprocal lattice are shown, and vector diagrams for the first and last points on the scan are included appropriate to the measurements shown. These and subsequent vector diagrams correspond to a view from below the spectrometer.

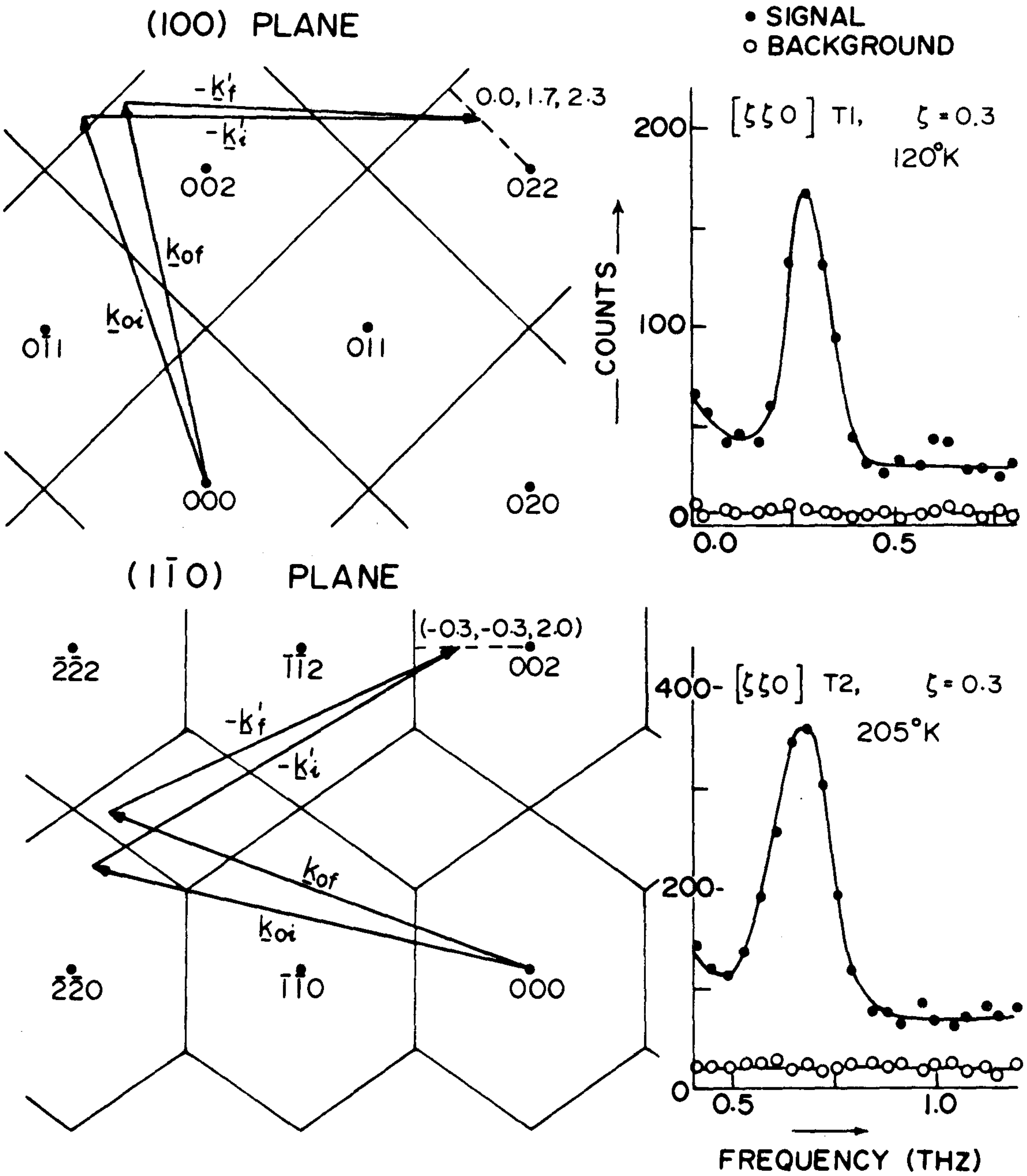

Fig. II-2. The (100) and (1$\bar{1}$0) planes of the reciprocal lattice for the body centred cubic structure. Two Constant $\underline{Q}$ neutron groups are shown on the right and corresponding vector diagrams are shown to the left.

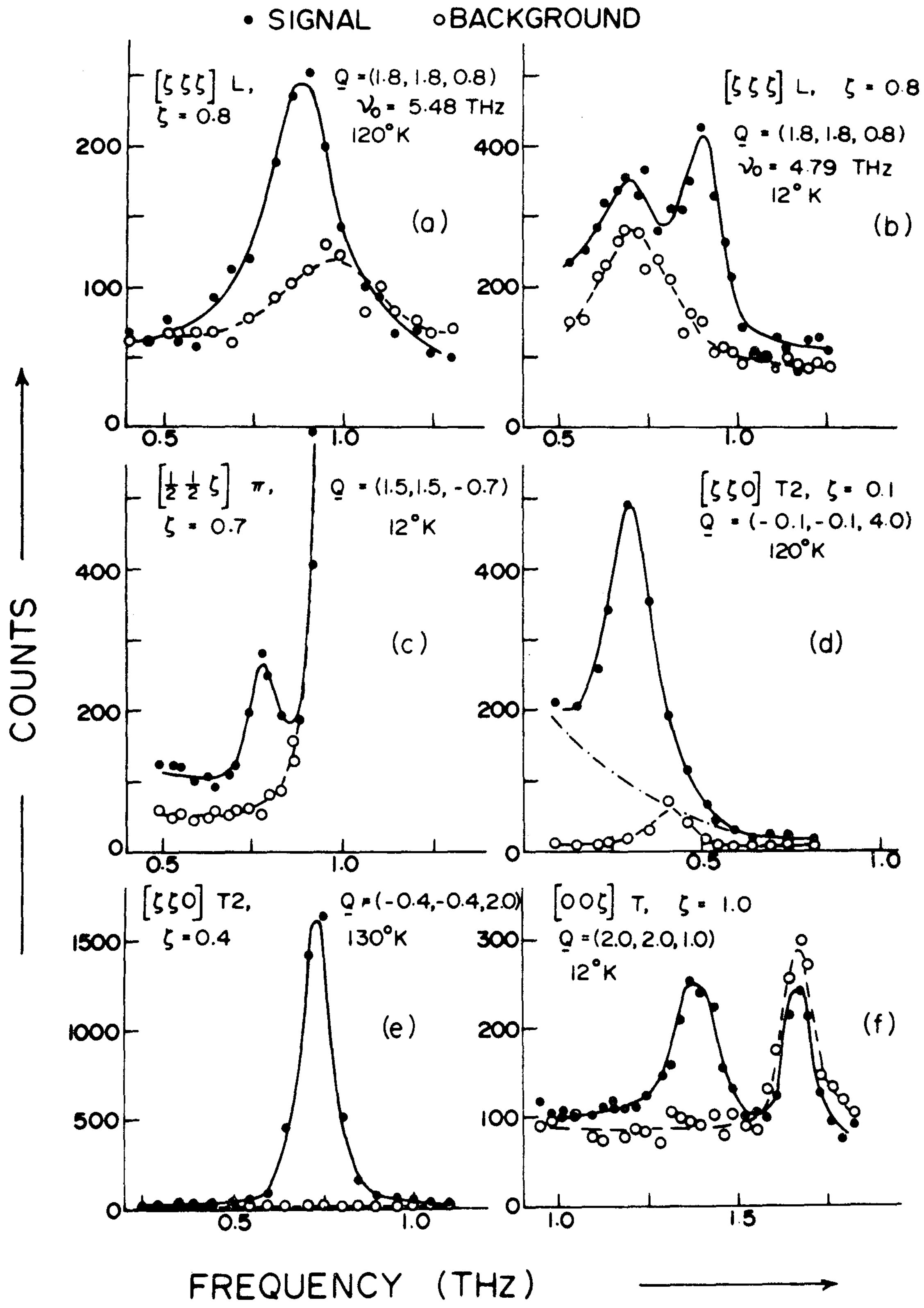

Fig. II-3. Six examples of spurious neutron groups

Many of the measured groups are similar in appearance to those of Fig. II-2. In such cases the frequency of the phonon, and its polarization (through the term $[\underline{Q}\cdot\underline{e}]^2$ in Eq. (I-D11)), are unambiguously determined.

In a number of cases the situation is more complicated. Some examples are shown in Fig. II-3. Additional peaks in the intensity distribution can arise in several ways. For example it can happen that the specimen is aligned to Bragg reflect neutrons in the incident beam into the analyzer. Elastic incoherent scattering from the analyzer will then give extra counts in both the signal and the background counters. Scans (a) to (d), and (f), show peaks in both counters. In (a) and (b) the peaks are believed to arise from elastic scattering off the aluminium container surrounding the specimen. The sharp rise at the high frequency end of scan (c), and the peak in (d), result from Bragg reflections in the specimen. The high frequency peak in (f) remains unexplained. The peak in scan (e) is caused by elastic incoherent scattering of the $(33\bar{1})$ component of the incident beam, and second order reflection in the analyzer.

Some of the additional peaks observed in Constant $\underline{Q}$ scans were easily identified by inspection. Most of the others have been identified using a computer programme which is described in Appendix II . Several peaks however have not been explained. Extra care has been taken in estimating the centre of the one-phonon peak when additional peaks have been observed.

Extra peaks at lower frequency have been rather consistently observed in a large number of scans of the $[00\zeta]L$ branch, under a wide variety of conditions. The effect, and its (somewhat unexpected) explanation, are discussed in Section IIF.

In many cases the intensity distribution "seen" by the signal counter contains a one-phonon peak superimposed on a residual curve which decreases with increasing frequency. For example the peak in Fig. II-3, scan (d), is superimposed on a residual curve indicated by the dot-dash line. The slope of this curve partly results from the variation of analyzer sensitivity with neutron energy, and from the factor k'/k_o in the cross section formula (Eqs. I-D2, I-D3). These variations with energy transfer are avoided if $\underline{k}_o$, rather than $\underline{k}'$, is varied during a scan (Section IE). There are also contributions from incoherent elastic and multiple phonon scattering off the specimen. The residual curve has been taken into account in assigning values to the peak positions.

The intensity in the background counter does not decrease with increasing frequency. Neutrons entering this counter have been incoherently scattered off the analyzer crystal. Therefore the frequency scale is not relevant to this counter, and no sloping curve is expected.

Considerable attention has been paid to the effects of instrumental resolution on the peak positions. These effects were calculated using a force constant model derived from the 1968 measurements. An account of this work is given in Appendix III. The results presented in the present section have been corrected for resolution.

The normal mode frequencies in rubidium are given in Table II-2. The columns labelled 85°K and 120°K include phonons measured between 80 and 95°K and between 120 and 140°K respectively. The 120°K measurements are shown in Fig. II-4.

The errors in the phonon frequencies were assigned with due regard to the width and shape of the group, and the counting statistics. In a number of cases more than one measurement of the same mode was made, and an error was assigned accordingly. For a well defined group the error is taken to be $\pm c\Gamma$ where Γ is the full width at half maximum of the group, and c is generally between 0.05 and 0.1. These errors are believed to be fairly realistic (see e.g. Svensson et al. (1967) for a discussion of errors). The analysis of Section IIE indicates that they may be overestimated by about 50%.

E. ANALYSIS OF RESULTS

(i) Force constant models

The dispersion curves of rubidium are similar in shape

TABLE II-2 Normal mode frequencies (in THz) for the symmetry branches in rubidium at 12, 85, 120 and 205°K.

Branch	ζ	12°K	85°K	120°K	205°K
[00ζ]T	0.1			0.215±0.01	
	0.15		0.305±0.015		
	0.2	0.41 ±0.01	0.405±0.01	0.40 ±0.01	0.355±0.01
	0.25		0.49 ±0.02	0.47 ±0.02	
	0.3	0.59 ±0.01	0.575±0.01	0.57 ±0.01	
	0.35		0.66 ±0.02		
	0.4	0.795±0.015	0.76 ±0.01	0.755±0.02	0.705±0.02
	0.5	0.96 ±0.01	0.93 ±0.01	0.895±0.025	
	0.6	1.12 ±0.02	1.08 ±0.01	1.065±0.015	1.01 ±0.02
	0.8	1.325±0.015	1.28 ±0.015	1.27 ±0.015	1.24 ±0.02
	0.9			1.30 ±0.015	
	1.0*	1.385±0.015	1.35 ±0.015	1.32 ±0.02	1.24 ±0.03
[00ζ]L	0.2	0.535±0.02	0.495±0.02	0.50 ±0.025	0.47 ±0.025
	0.25	0.64 ±0.02	0.61 ±0.03	0.62 ±0.02	0.565±0.025
	0.3	0.74 ±0.02	0.71 ±0.02	0.72 ±0.02	0.69 ±0.025
	0.35	0.82 ±0.015	0.82 ±0.02	0.82 ±0.02	
	0.4	0.93 ±0.015	0.91 ±0.025	0.88 ±0.025	0.87 ±0.02
	0.45	1.01 ±0.025		0.98 ±0.02	
	0.5	1.075±0.02		1.075±0.03	1.05 ±0.02
	0.6	1.23 ±0.03		1.225±0.05	
	0.65			1.23 ±0.04	
	0.7			1.23 ±0.04	1.20 ±0.04
	0.75			1.27 ±0.04	

(continued next page)

TABLE II-2 Normal mode frequencies (in THz) for the symmetry branches in rubidium at 12, 85, 120 and 205°K (cont'd)

Branch	ζ	12°K	85°K	120°K	205°K
[00ζ]L	0.8	1.34 ±0.05		1.275±0.03	
	0.9			1.305±0.02	
	1.0*	1.385±0.015	1.35 ±0.015	1.32 ±0.02	1.24 ±0.03
[ζζζ]T	0.1			0.235±0.03	
	0.15			0.35 ±0.03	
	0.2	0.45 ±0.02	0.435±0.025	0.48 ±0.02	0.42 ±0.04
	0.3	0.68 ±0.03	0.69 ±0.03	0.71 ±0.03	
	0.4	1.00 ±0.04	0.93 ±0.05	0.92 ±0.03	
	0.45			1.02 ±0.03	
	0.5*	1.13 ±0.015	1.08 ±0.02	1.10 ±0.02	1.03 ±0.03
	0.55			1.20 ±0.04	
	0.6			1.26 ±0.04	1.12 ±0.04
	0.7	1.32 ±0.04	1.33 ±0.03	1.325±0.02	
	0.8			1.32 ±0.03	1.21 ±0.04
	0.9			1.33 ±0.05	
	1.0*	1.385±0.015	1.35 ±0.015	1.32 ±0.02	1.24 ±0.03
[ζζζ]L	0.1	0.595±0.02	0.58 ±0.025	0.525±0.03	
	0.2	1.065±0.015	1.03 ±0.02	1.01 ±0.03	
	0.3	1.33 ±0.015	1.325±0.015	1.28 ±0.03	
	0.35			1.31 ±0.025	
	0.4	1.345±0.02	1.335±0.02	1.305±0.025	1.25 ±0.03
	0.45			1.24 ±0.04	

(continued next page)

TABLE II-2 Normal mode frequencies (in THz) for the symmetry branches in rubidium at 12, 85, 120 and 205°K (cont'd)

Branch	ζ	12°K	85°K	120°K	205°K
[ζζζ]L	0.5*	1.13 ±0.015	1.08 ±0.02	1.10 ±0.02	1.03 ±0.03
	0.55			0.935 ±0.03	
	0.6	0.775 ±0.02	0.74 ±0.02	0.72 ±0.03	0.68 ±0.025
	0.65			0.64 ±0.03	
	0.7	0.605 ±0.03		0.60 ±0.03	0.55 ±0.02
	0.75			0.685 ±0.025	
	0.8	0.90 ±0.02		0.87 ±0.03	0.805 ±0.015
	0.9			1.20 ±0.04	1.10 ±0.04
	0.95			1.285 ±0.03	
	1.0*	1.385 ±0.015	1.35 ±0.015	1.32 ±0.02	1.24 ±0.03
[ζζ0]T2	0.1			0.285 ±0.02	
	0.15			0.395 ±0.02	
	0.2			0.525 ±0.015	0.46 ±0.01
	0.25			0.66 ±0.03	
	0.3	0.75 ±0.015	0.735 ±0.015	0.735 ±0.02	0.66 ±0.01
	0.35			0.79 ±0.015	
	0.4			0.85 ±0.015	0.785 ±0.015
	0.45			0.89 ±0.015	
	0.5*	0.96 ±0.03	0.95 ±0.02	0.885 ±0.02	0.84 ±0.025
[ζζ0]T1	0.1			0.11 ±0.025	
	0.2			0.20 ±0.02	
	0.3			0.265 ±0.02	
	0.4			0.315 ±0.02	
	0.5*	0.34 ±0.02	0.34 ±0.03	0.32 ±0.025	-

(continued next page)

TABLE II-2 Normal mode frequencies (in THz) for the symmetry branches in rubidium at 12, 85, 120 and 205°K (cont'd)

Branch	ζ	12°K	85°K	120°K	205°K
$[\zeta\zeta 0]L$	0.1			0.41 ±0.02	0.395 ±0.02
	0.2	0.88 ±0.02	0.84 ±0.015	0.82 ±0.03	0.785 ±0.02
	0.3	1.235 ±0.02	1.17 ±0.02	1.185 ±0.025	1.125 ±0.02
	0.4			1.415 ±0.02	1.34 ±0.02
	0.5*	1.50 ±0.02	1.48 ±0.025	1.465 ±0.02	1.41 ±0.05
$[\frac{1}{2}\frac{1}{2}\zeta]\Lambda$	0.0*	0.96 ±0.03	0.95 ±0.02	0.885 ±0.02	0.84 ±0.025
	0.1			0.895 ±0.025	
	0.15			0.92 ±0.035	
	0.2			0.945 ±0.04	
	0.25			0.975 ±0.03	
	0.3	1.07 ±0.015			
	0.35			1.035 ±0.03	
	0.4			1.08 ±0.06	
	0.5*	1.13 ±0.015	1.08 ±0.02	1.10 ±0.02	1.03 ±0.03
$[\frac{1}{2}\frac{1}{2}\zeta]\pi$	0.0*	1.50 ±0.02	1.48 ±0.025	1.465 ±0.02	1.41 ±0.05
	0.2			1.42 ±0.02	
	0.3	1.39 ±0.02		1.34 ±0.02	
	0.4			1.25 ±0.025	
	0.5*	1.13 ±0.015	1.08 ±0.02	1.10 ±0.02	1.03 ±0.03
	0.6			0.965 ±0.015	
	0.7	0.785 ±0.015		0.77 ±0.015	
	0.8			0.59 ±0.015	
	0.9			0.405 ±0.015	
	1.0*	0.34 ±0.02	0.34 ±0.03	0.32 ±0.025	-

(continued next page)

TABLE II-2 Normal mode frequencies (in THz) for the symmetry branches in rubidium at 12, 85, 120 and 205°K (cont'd)

Branch	ζ	12°K	85°K	120°K	205°K
	0.0*	1.385±0.015	1.35 ±0.015	1.32 ±0.02	1.24 ±0.03
	0.1			1.27 ±0.02	
	0.2			1.04 ±0.03	
[ζζ1]Λ	0.3			0.78 ±0.03	
	0.4			0.49 ±0.025	
	0.45			0.37 ±0.03	
	0.5*	0.34 ±0.02	0.34 ±0.03	0.32 ±0.025	-
	0.0*	1.385±0.015	1.35 ±0.015	1.32 ±0.02	1.24 ±0.03
	0.1			1.29 ±0.025	
	0.2			1.205±0.02	
[ζζ1]π2	0.3			1.07 ±0.02	
	0.4			0.94 ±0.03	
	0.5*	0.96 ±0.03	0.95 ±0.02	0.885±0.02	0.84 ±0.025
	0.0*	1.385±0.015	1.35 ±0.015	1.32 ±0.02	1.24 ±0.03
	0.1			1.335±0.02	
[ζζ1]π1	0.2			1.36 ±0.05	
	0.3			1.42 ±0.03	
	0.4			1.47 ±0.03	
	0.5*	1.50 ±0.02	1.48 ±0.025	1.465±0.02	1.41 ±0.05

Note: an asterisk indicates that the same measurement is reported elsewhere in the table. For example the phonon frequency at symmetry point H is given for [00ζ]T and L,ζ = 1.0; [ζζζ]T and L,ζ = 1.0; and [½½ζ]Λ, π2, and π1 for ζ= 0.0.

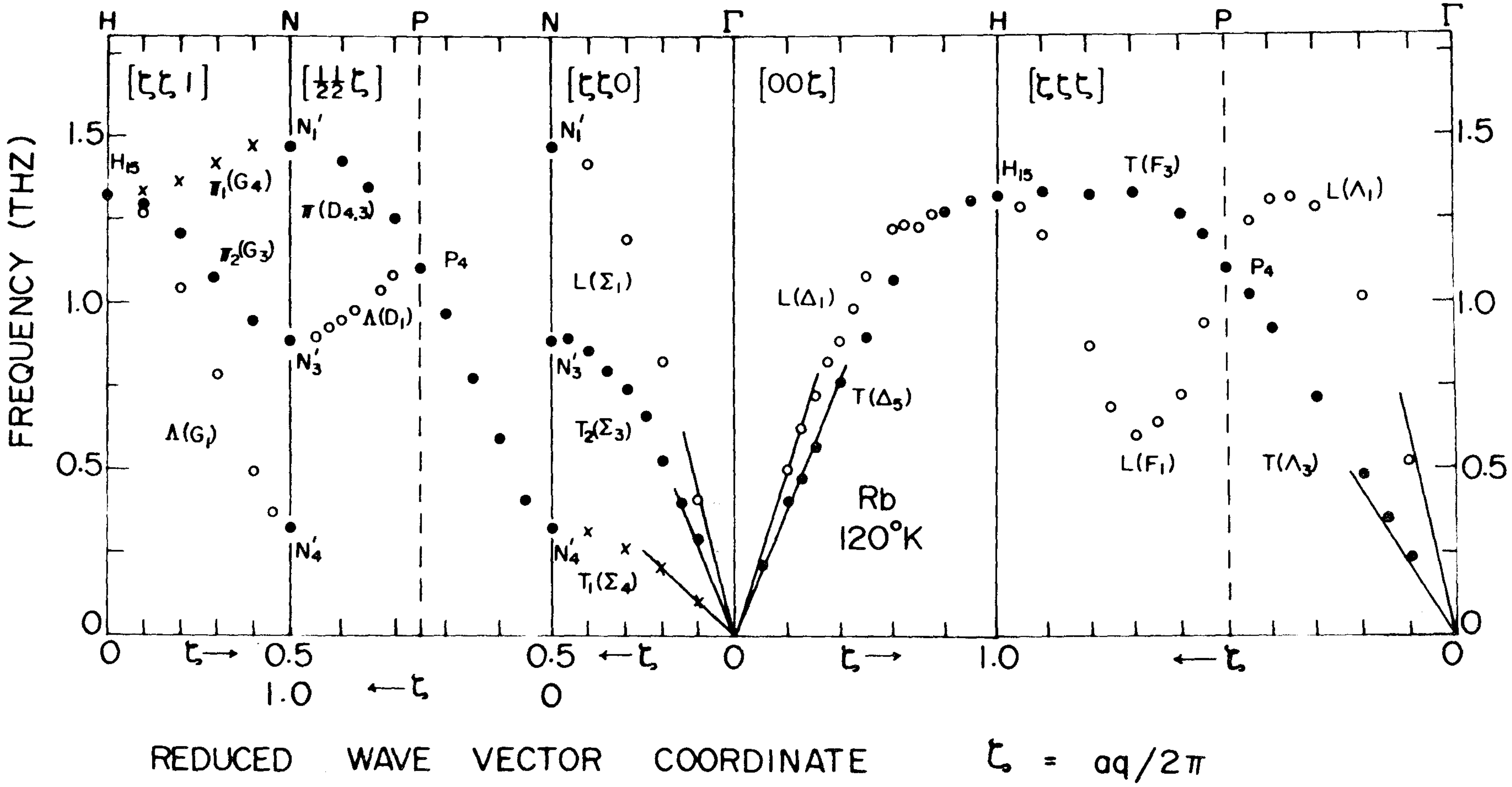

Fig. II-4. The dispersion curves of rubidium at 120°K. The group theoretical notation is due to Koster (1957). The solid lines represent appropriate sound velocities.

to those of sodium (Woods et al 1962) and potassium (Cowley et al 1966). The measurements have been analysed to obtain AFC's for different force models following the procedures of Svensson et al. (1967). Least squares fits are made to force models which include interactions out to n'th nearest neighbours, for n = 1, 2, ... 8. For each fit various statistical quantities are obtained including

$$\Delta_2 = [N^{-1} \sum_i^N (\nu_{ic}-\nu_i)^2]^{\frac{1}{2}} \qquad \text{(II-E1)}$$

$$\Delta_4 = [\sum_i^N W_i (m\nu_{ic}^2 - m\nu_i^2)^2 / \sum_i^N W_i]^{\frac{1}{2}} \qquad \text{(II-E2)}$$

$$\chi^2 = (N-K)^{-1} \sum_i^N [(\nu_{ic}-\nu_i)/\sigma_i]^2 \qquad \text{(II-E3)}$$

where ν_{ic} and ν_i are the calculated and measured frequencies, and σ_i is the assigned error, for the i'th measurement: N is the number of measurements, and K is the number of adjustable parameters (i.e., AFC's). The weights W_i are assigned according to the least-squares prescription

$$W_i = W_i'(\nu_i\sigma_i)^{-2}$$

where W_i' is a weight which is fed in. In the present case these weights (W_i') were set to unity with no loss of generality, since a change in W_i' is equally well expressed by altering σ_i.

Results of a run using the complete data at 120°K are shown in Fig. II-5(a). The plots of Δ_2, Δ_4 and χ^2 essentially tell the same story: first and second neighbour forces are

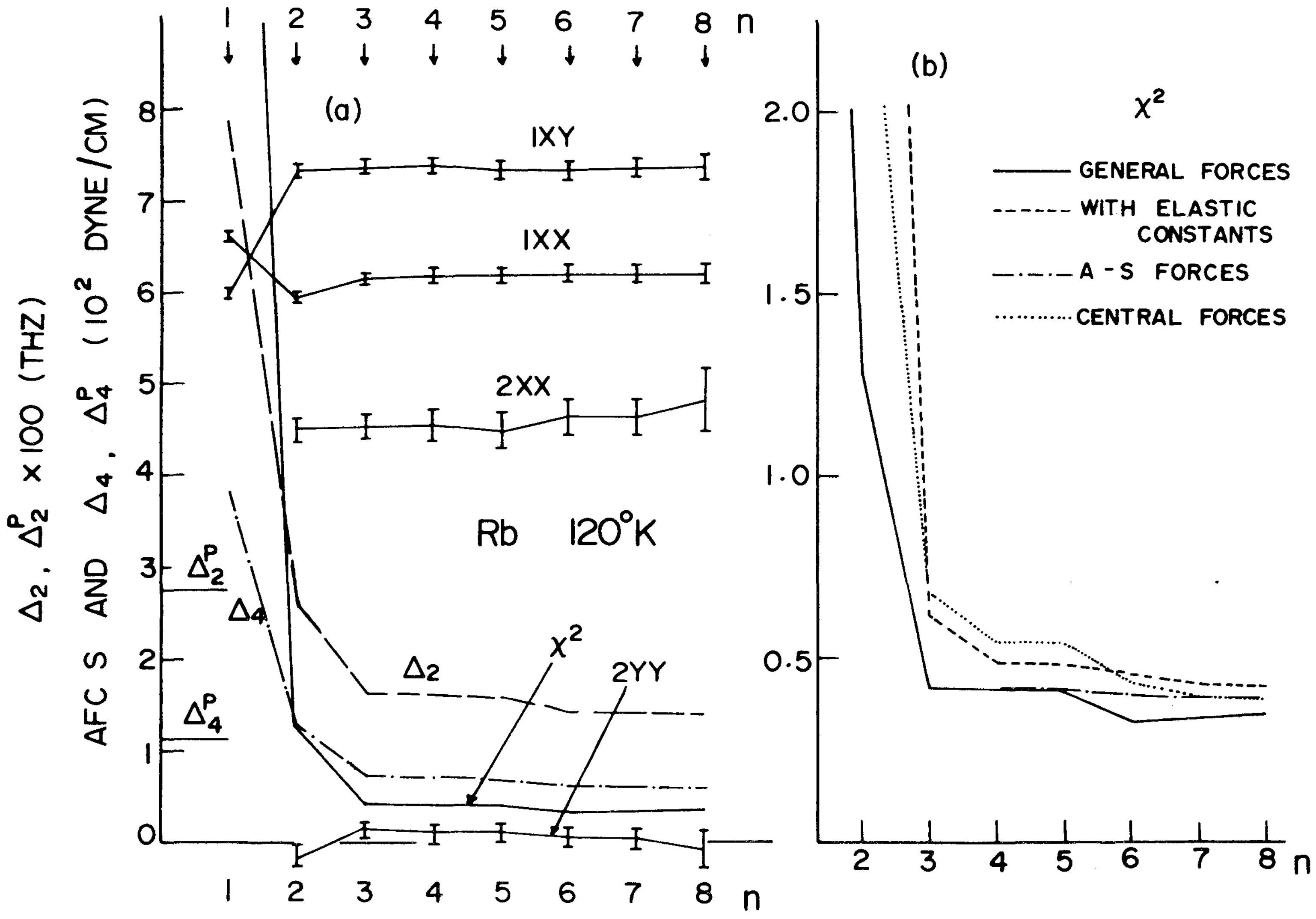

Fig. II-5. Atomic force constant fits to the data at 120°K. The "goodness of fit", χ^2, is dimensionless. Units for the remaining quantities are indicated.

sufficient to improve the fit considerably, whereas more distant neighbour forces are very weak. Svensson et al. (1967) note that the errors in the force constants are only physically meaningful "if an entirely adequate fit to the data was in fact obtained". With this in mind it is clear that forces out to third neighbours must be considered important. A third neighbour fit to the 120°K measurements is shown at the top of Fig. II-14.

It is noteworthy that χ^2 settles at about 0.35, and Δ_2 and Δ_4 settle to values of about $0.55 \times \Delta_2^P$ and $0.6 \times \Delta_4^P$ respectively, where the superscript P means the predicted value of the quantity, i.e., the value obtained by replacing $(\nu_{ic}-\nu_i)$ with σ_i in equations (II-E1, II-E2). This indicates that the assigned errors σ_i are overestimated by about 50%. Thus the assigned errors, which averaged about 0.075Γ for good groups (Section IID), should probably be made about 0.05Γ. Svensson et al. (1967) reached a similar conclusion for copper. Furthermore an analysis of the other alkali metal measurements (see Fig. II-6) leads to the same conclusion.

The slight improvement in fit, between n = 5 and n = 6 (Fig. II-5), largely results from an improvement in the fit to the $[\frac{1}{2}\frac{1}{2}\zeta]\Lambda$ branch. This is illustrated in Fig. II-7(a). The $[\frac{1}{2}\frac{1}{2}\zeta]\Lambda$ branch has been separately analysed to obtain inter-

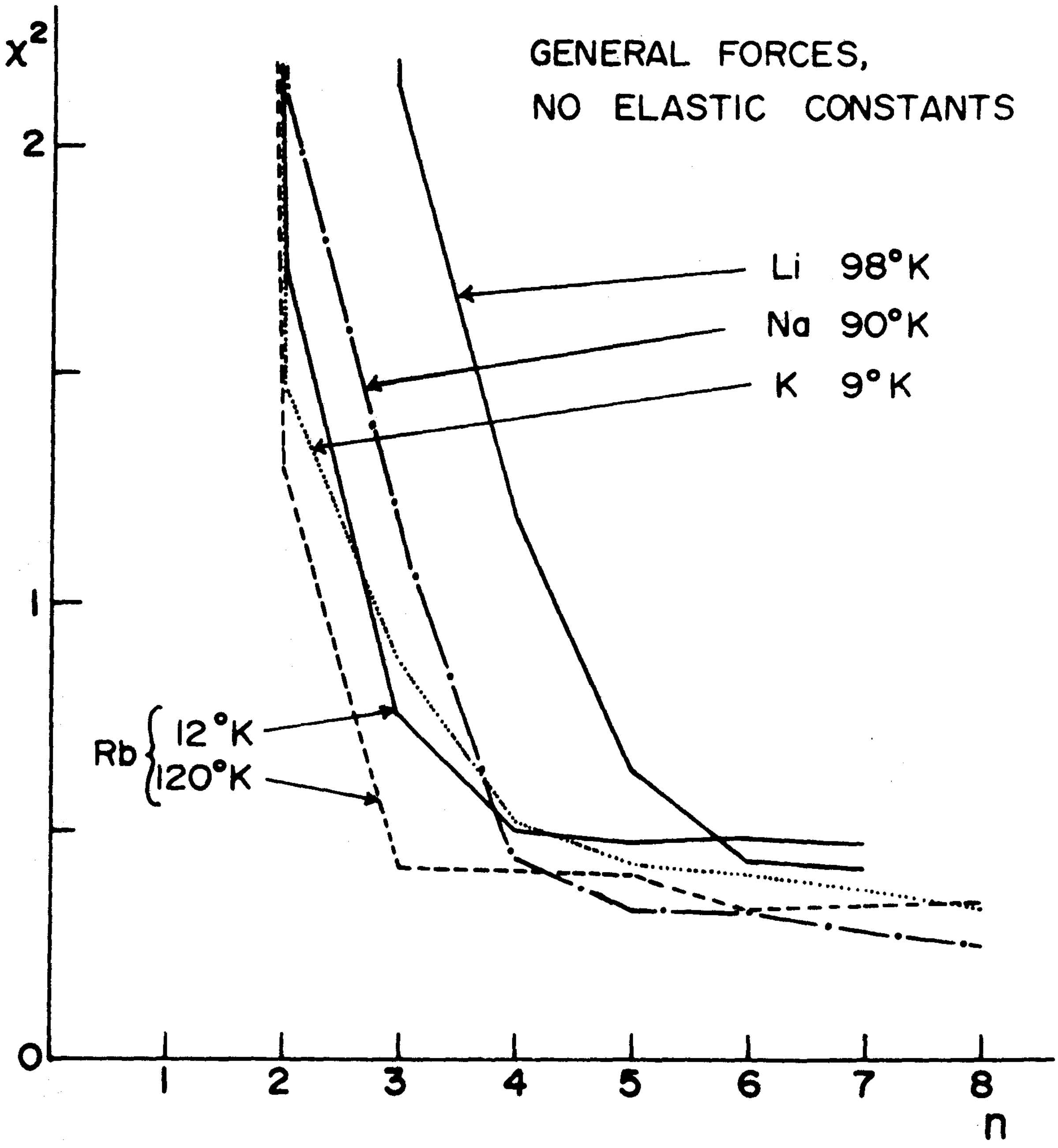

Fig. II-6. The "goodness of fit" for fits to Rb at 12 and 120°K, and to Li, Na, and K. In the cases of Li and of Rb at 12°K, there was insufficient data for a fit to 8 neighbours. In the case of Rb at 12°K, the elastic constant $(C_{11}-C_{12})/2$ was included in the fit to ensure stability of the lattice.

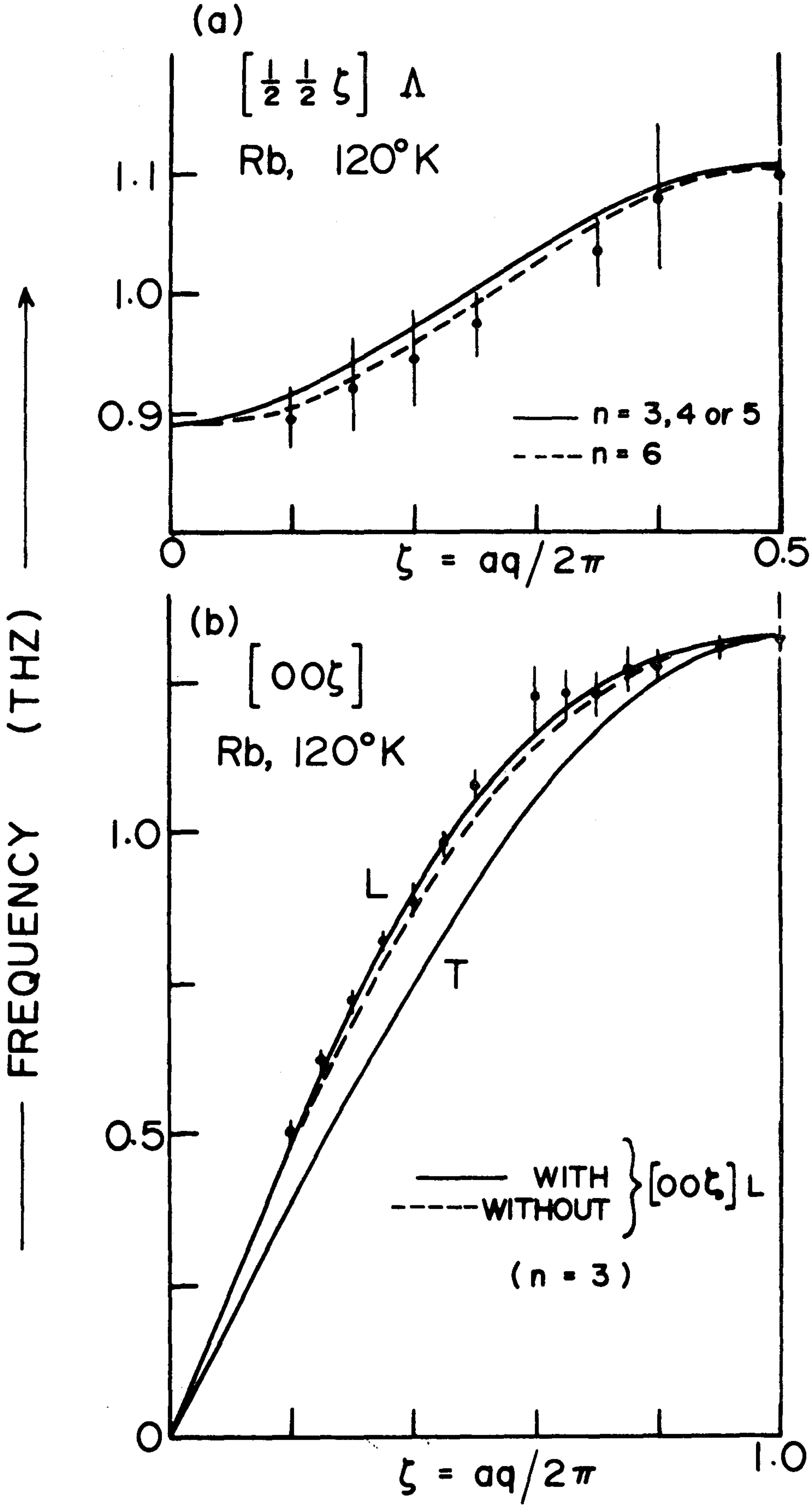

Fig. II-7. In (a), interplanar fits to the $[\frac{1}{2}\frac{1}{2}\zeta]\Lambda$ branch are shown. Third neighbour atomic force constant fits are shown in (b) for the $[00\zeta]$ direction.

planar force constants (Brockhouse et al. 1968b). These are given by

$$m\omega^2 = \phi_o + \sum_n \phi_n[1-\cos(n\pi\zeta)] \qquad \text{(II-E4)}$$

The analysis indicates that a good fit is obtained if three interplanar force constants are included. These quantities are related to the AFC's as follows:

$\phi_o = 8(1XX) + 8(2YY) + 16(3XX) + 8(4XX) + 16(4YY) \ldots$

$\phi_2 = 2(2XX) - 8(3XX) + 8(5XX) + 8(8YY)$

$\phi_4 = 2(6XX) - 8(8XX)$

$\phi_1 = \phi_3 = 0$.

The notation for the AFC's is explained in Table II-3. It is clear that the improvement in the AFC fit between n = 5 and n = 6 occurs because it corresponds to inclusion of a third interplanar force constant for the $[\frac{1}{2}\frac{1}{2}\zeta]\Lambda$ branch. An AFC fit to all the measurements except this branch is essentially identical to the fit which includes this branch.

Forces to third neighbours are nearly sufficient to fit the measurements of the $[00\zeta]$L branch (Fig. II-7(b)). Since the effects of instrumental resolution are particularly marked for this branch, and since the branch is thought to be more anharmonic than others, this fit is probably satisfactory. A fit was also made to all the measurements except the $[00\zeta]$L branch. Though the first neighbour force constants are unchanged, the remaining AFC's are somewhat different and their errors are considerably larger, whereas χ^2 is unaffected. It appears that there is insufficient orthogonal information to determine these parameters when the [00ζ]L branch is excluded. Fig. II-7(b) shows the [00ζ] branches calculated using AFC's from the fit to all but the [00ζ]L branch.

If the elastic constants of rubidium at 120°K (see Section IIE) are included in a fit to all branches, the quantities Δ_2, Δ_4 and χ^2 are somewhat larger (Fig. II-5(b)), but the first few AFC's are not changed. Since the ultrasonic measurements correspond to far smaller values of $\zeta(\lesssim 10^{-3})$, the elastic constant slopes need not coincide with neutron measurements for $\zeta \sim 0.1$. Indeed a difference in the sound velocity in these two ranges of wave vector is theoretically predicted (Cowley et al. 1968). For this reason no further fits have been made with the elastic constants included.

Fits to an axially symmetric force model are identical out to four neighbours (Fig. II-5(b)). Beyond n = 4 the general force model gives a slightly better fit, largely because it involves more parameters. The central force condition is very restrictive for small n, and χ^2 is considerably enhanced (Fig. II-5(b)). For $n \gtrsim 6$ the central force condition has little effect on χ^2. AFC's from various fits to the 120°K data are given in Table II-3.

General force model fits to measurements at different temperatures indicate that the interatomic forces in rubidium

TABLE II-3 Atomic force constants for various fits to the measurements on rubidium at 120°K
(units are dynes/cm)

Reference atom	AFC	GF(n=3)	GF(n=4)	AS(n=4)	CF(n=4)
(111)	1XX	615.2± 5.8	617.8± 8.1	613.0± 7.6	613.8± 7.6
	1XY	737.4± 7.6	739.5± 8.3	740.0± 8.2	735.6± 8.1
(200)	2XX	453.7±14.9	455.6±18.7	447.8±17.9	456.0±17.8
	2YY	16.9± 9.2	11.6±11.1	17.7± 9.7	17.5± 9.7
(220)	3XX	-37.6± 4.7	-34.0± 6.1	-40.2± 4.9	-43.6± 4.8
	3ZZ	- 2.2± 7.5	- 2.7±10.4	5.8± 7.7	7.6± 7.6
	3XY	-51.6± 7.9	-61.0±11.4	-47.2± 8.0	-50.3± 8.0
(311)	4XX	-	- 3.2± 7.1	3.6± 5.7	- 6.4± 4.9
	4YY	-	0.2± 3.6	- 0.8± 3.1	3.9± 2.8
	4YZ	-	4.1± 5.8	0.6± 1.5	-2.7± 1.1
	4XZ	-	3.2± 3.2	1.7± 2.5	-4.0± 2.0

GF:	General Forces
AS:	Axially Symmetric Forces
CF:	Central Forces

The force constant matrix, for n'th nearest neighbours, is

$$\begin{pmatrix} nXX & nXY & nXZ \\ nXY & nYY & nYZ \\ nXZ & nYZ & nZZ \end{pmatrix}$$

See also Brockhouse et al. (1968b).

are of longer range at low temperatures. This is illustrated in Fig. II-6. Clearly fourth neighbour interactions are appreciable at 12°K, but not at 120°K. There is insufficient data to obtain reliable information of this kind from the 85 and 205°K data. Table II-4 lists AFC's obtained from fourth neighbour fits to the measurements at different temperatures. We note that 1XX and 1XY decrease, but 2XX increases, with increasing temperature. This feature is discussed later in this section.

It is instructive to compare force systems in the different alkali metals, as determined from analyses of the dispersion curves. The "goodness of fit", χ^2, is shown in Fig. II-6, for general force model fits (with no elastic constants) to the experimental data. It is clear that the force system is of longer range in the lighter metals. Furthermore Table II-5 shows that the ratio of 2XX to 1XX (or 1XY) increases as the atomic mass increases. Thus we see that two types of trend occur (i) on going from the lighter to the heavier alkali metals, and (ii) on increasing the temperature (in Rb): the trends are (a) a decrease in the range of the interatomic forces, and (b) an increase in the ratio of second to first neighbour AFC's.

The first trend indicates that the electron-phonon interaction is weaker in the heavier metals. This conclusion is consistent with the fact that the ratio (ω/ω_p), where ω_p is the ion plasma frequency, increases with increasing atomic

TABLE II-4 Atomic force constants for four-neighbour general force model fits to rubidium at different temperatures. (Units are dynes/cm).

Reference atom	AFC	12°K*	85°K	120°K	205°K
(111)	1XX	669.4±11.3	657.4±18.1	617.8±8.1	590.7±15.6
	1XY	787.5±11.3	746.3±26.2	739.5±8.3	679.6±20.9
(200)	2XX	396.7±27.9	400.2±37.3	455.6±18.7	437.9±38.8
	2YY	21.7±16.8	7.1±26.7	11.6±11.1	-35.0±19.9
(220)	3XX	-36.8±8.8	-13.2±13.8	-34.0±6.1	-13.6±10.6
	3ZZ	-9.0±13.5	-24.9±13.6	-2.7±10.4	9.8±22.2
	3XY	42.6±13.9	-11.0±39.4	-61.0±11.4	-75.1±19.7
(311)	4XX	17.6±7.9	-12.5±16.3	-3.2±7.1	-16.4±11.3
	4YY	-3.8±5.1	-2.5±4.4	0.2±3.6	-11.3±6.5
	4YZ	-9.5±6.8	-26.7±9.3	4.1±5.8	-0.2±17.6
	4XZ	-8.8±3.8	-1.8±13.7	3.2±3.2	7.4±10.3

*The elastic constant $\frac{1}{2}(C_{11}-C_{12})$ was included in this fit to ensure stability of the lattice.

TABLE II-5 A comparison of first and second neighbour atomic force constants obtained from fits to the alkali metals. (Units are dynes/cm.)

	Li(98°K)(1)	Na(90°K)(2)	K(9°K)(3)	Rb(12°K)
1XX	2355	1178	786	669
1XY	2489	1320	895	788
2XX	631	472	432	397
2YY	50	104	29	22

(1) Smith et al. (1968)

(2) Woods et al. (1962)

(3) Cowley et al. (1966)

mass, being about 0.52 for Li and 0.61 for Rb, for the zone boundary [$\zeta\zeta$0]L mode.

The second trend, towards a larger ratio of second to first neighbour AFC's in the heavier metals, may be seen directly in the dispersion curves for the [00ζ] direction. The splitting of the L and T branches is largely determined by the AFC 2XX: a nearest neighbour only force model predicts degenerate L and T branches. This splitting is somewhat larger in the heavier metals, and the value of ζ at the crossover of the two branches (or for which they begin to overlap) becomes larger as Z increases. The increased splitting of the L and T branches in the heavier alkali metals is to be expected from an examination of the ratio $(C_{11}/C_{44})^{\frac{1}{2}}$, which is equal to the ratio of the slopes of the two branches at very small ζ. From Table II-1, the above ratio is 1.14, 1.19, 1.25 and 1.29 for Li, Na, K and Rb respectively. The first and second neighbour AFC's have been used to fit the parameters of a simple Morse potential (see Section IIIB). The results are shown in Figure II-8. It will be seen that, as a consequence of trend (b) above, the minimum in the potential moves nearer to the second neighbour position in the heavier metals. The second neighbour atoms, at (a,0,0) etc., will execute relatively large oscillations, and the [00ζ]L branch is expected to be rather anharmonic. In addition the Morse potential is shallower and less parabolic in the heavier metals.

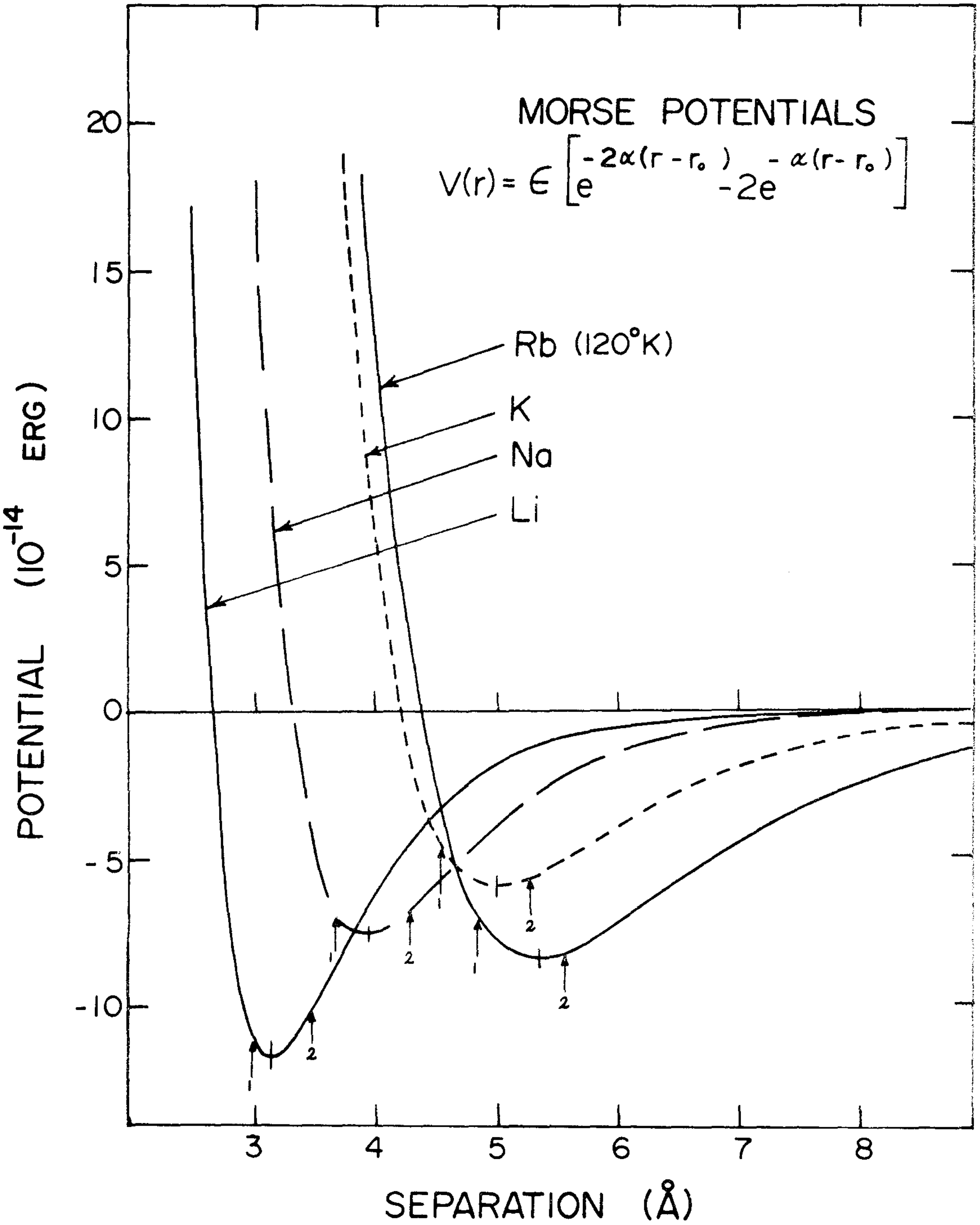

Fig. II-8. Morse potentials for the alkali metals, obtained by fitting to the first and second neighbour AFC's. The arrows show the first and second neighbour positions, and the short lines indicate the minimum in each potential.

(ii) Reciprocal Space Analysis

In the previous subsection, a real space analysis of the measurements was described. We now consider an analysis in terms of a potential in reciprocal space. The dynamical matrix may be written as a sum over reciprocal lattice vectors $\underline{G}$ (Eq. I-C17):

$$D_{\alpha\beta}(\underline{q}) = \sum_{\underline{G}} [(\underline{G}+\underline{q})_\alpha (\underline{G}+\underline{q})_\beta \phi(|\underline{G}+\underline{q}|) - G_\alpha G_\beta \phi(G)] ,$$

where $\phi(Q)$ is the Fourier transform of the real space potential $\phi(\mathbf{r})$, whose first and second derivatives are related to the AFC's of the previous subsection. Cochran (1963) showed how to extract a function $\phi(Q)$ from measurements of the normal mode frequencies in sodium. His method was extended by Cowley et al. (1966), who analysed the dispersion curves of K and Na in this way. Blanchard (1969) (see also Blanchard and Varshni 1970) analysed Na, K, and Rb using both methods. Following Cochran, he first subtracted the Coulomb contributions to the dynamical matrix, and then obtained an electronic potential function $\phi^E(Q)$.

The present measurements on Rb have been analysed to obtain the function H(Q) which is defined by

$$\phi(Q) = \frac{e^2}{Q^2} \frac{N}{\Omega} H(Q)$$

The procedure was exactly that of Cowley et al. (1966). Through the good offices of Dr. W.J.L. Buyers, extensive use was made of programmes belonging to the neutron scattering group at Chalk River, to calculate H(Q) and the real space potential $\phi(r)$.

Fits were made to the 12°K and the 120°K measurements, with and without elastic constants included, and for several values of the cutoff Q_c. In Fig. II-9 fits (which include the elastic constants) are compared for K and Rb, and for Rb at 12 and 120°K. It will be observed that the fits for Rb and K are similar: the larger fluctuations in peak height in the case of Rb are a consequence of the smaller body of experimental data. The fits to Rb at two different temperatures are very similar, as is expected. A typical fit to the 120°K measurements, using a cutoff of $2\times(2\pi/a)$, is shown in Fig. II-14.

The form of the function H(Q) is considerably influenced by the choice of Q-values for which the function is specified. This is especially true for large Q_c, as is shown on the left side of Fig. II-10. The symbols indicate the positions at which the function is specified. It will also be observed that the computed errors increase rapidly as Q_c is increased, since there is then insufficient data to determine H(Q). On the other hand it is difficult to obtain a good fit if Q_c is too small. On the right side of Fig. II-10 fits with and without elastic constants are compared, for different values of Q_c. Clearly fits with $Q_c = 1.6$ are relatively poor ($\chi^2 \simeq 1.6$). For large values of Q_c very large changes in peak height may occur unless the elastic constants are included in the fit.

Most of the above remarks have been made by Cowley et al.

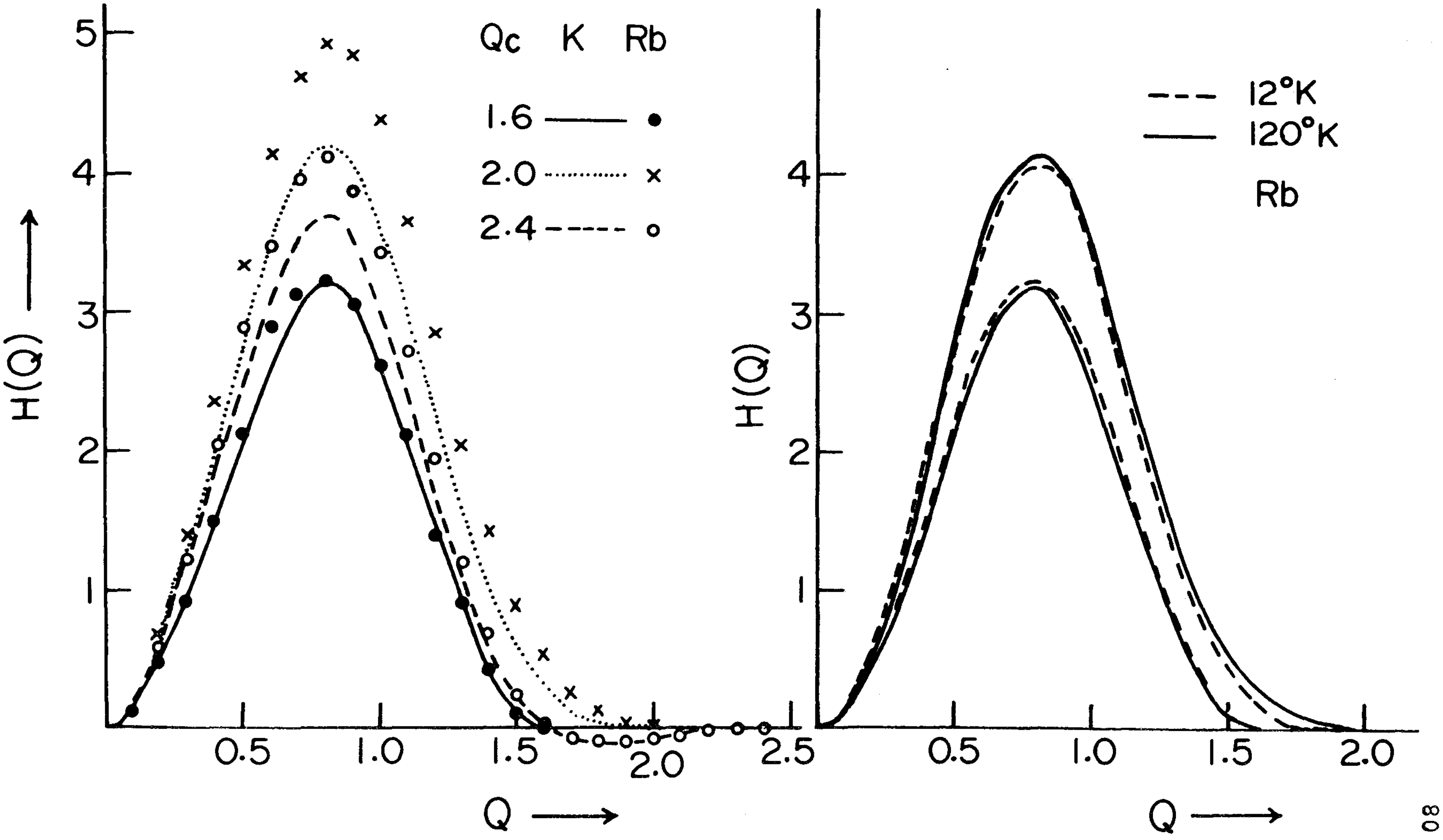

Fig. II-9. "Total potentials" for Rb and K, and for Rb at two temperatures, for different cutoffs Q_c.

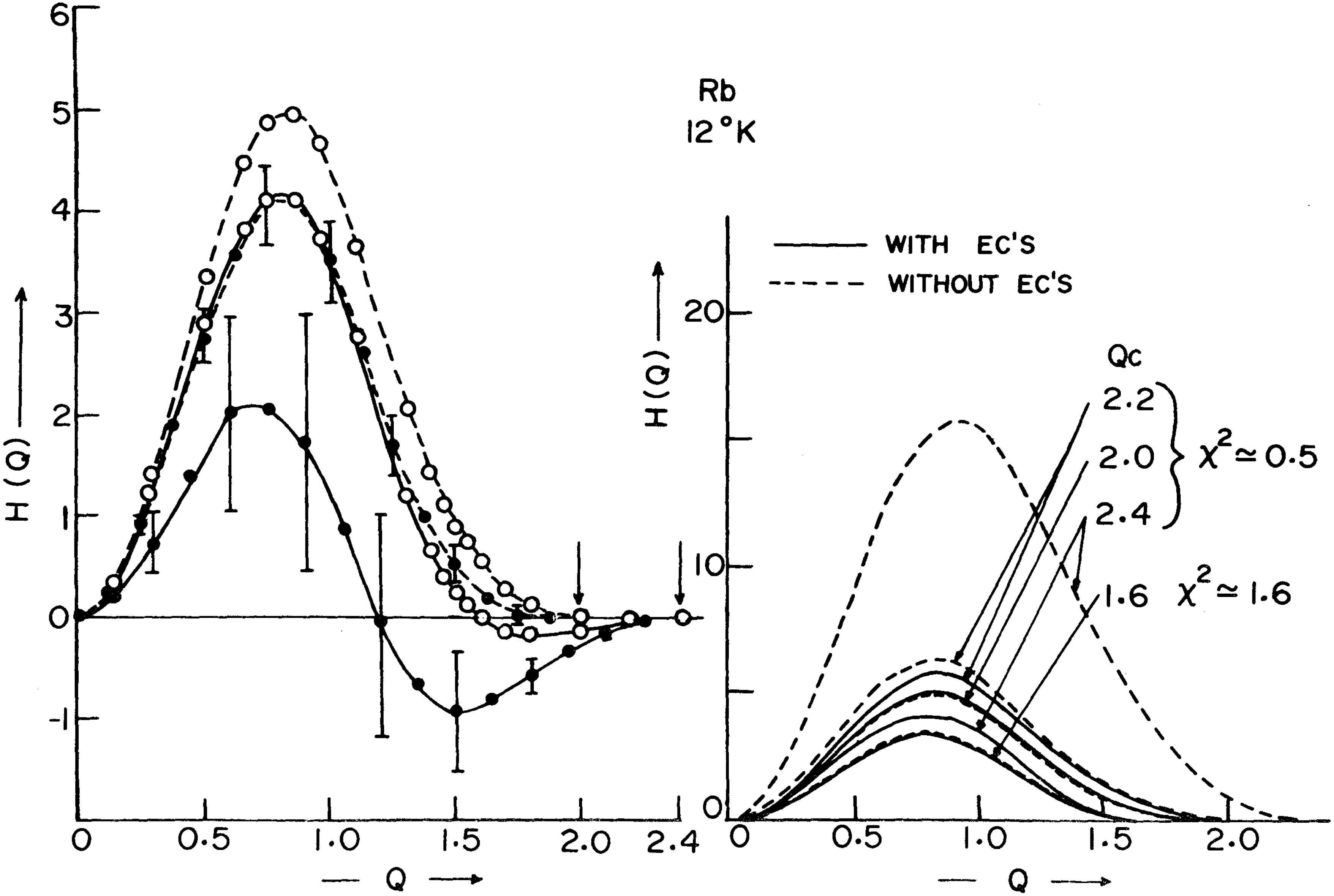

Fig. II-10. "Total potentials" for Rb, showing the effect of changing the cutoff and the values of Q for which H(Q) is specified. Functions obtained with and without elastic constants included, are also shown.

(1966) or by Buyers and Cowley (1969), regarding potassium.

In Chapter III we examine the Fourier transforms of some of these functions, and harmonic and anharmonic force constants derived therefrom are compared with force constants obtained by other methods.

(iii) Fundamental Calculations: Comparison with Experiment

Many authors have calculated dispersion curves for the alkali metals (see Section IIB). Toya (1958) presented calculations for Na, and later for K, Rb and Cs (Toya 1959). The agreement between experiment and these calculations is considerably poorer for Rb than for Na and K: Toya predicts a general trend toward smaller values of (ω/ω_p) (where ω_p is the plasma frequency), as the mass is increased, whereas the opposite trend is observed experimentally. Animalu et al. (1966) obtained curves which are in relatively good agreement with experiment for Na, K and Rb, but their calculations for Li were as much as 50% too high. Both Schneider and Stoll (1966b), and Ho (1968), presented calculations of phonon frequencies in Rb which are in good agreement with the measurements*. Direct comparisons with the published measurements for Rb (Copley et al. 1968) have been made by

---

*The author is grateful to Dr. T. Schneider and Dr. P. S. Ho, who kindly sent tables of calculated phonon frequencies.

Prakash and Joshi (1969), Price et al. (1970), and Blanchard and Varshni (1970).[†] The published frequencies were not corrected for resolution, and slightly better fits to experiment can probably be obtained using the corrected frequencies. For example Price et al. (1970) note that the $[\zeta\zeta 0]T1$ and the $[\frac{1}{2}\frac{1}{2}\zeta]\Lambda$ branches are less well predicted by theory than the others. Corrections to the measurements for resolution bring them into significantly better agreement with the theoretical curves.

Price et al. (1970) used an Ashcroft pseudopotential (Ashcroft 1966), which is defined by:

$$\begin{aligned} V(r) &= 0 && \text{for } r < r_A \\ V(r) &= -\, Ze^2/r && \text{for } r > r_A . \end{aligned}$$

They then fitted the measured dispersion curves using various choices for the dielectric function. The simplest type of screening is given by the Hartree function (Eq. I-C34). This function may be written as

$$\varepsilon_H(q) = 1 + V(q)L(q)$$

where $V(q) = 4\pi e^2/q^2$ and $L(q)$ is the Lindhard function. It is customary to include the effects of exchange and correlation by writing a generalized dielectric function in the form

---

[†] The author is grateful to Dr. David Price, and to Dr. Varshni, for sending preprints of these papers.

$$\varepsilon(q) = 1 + \frac{V(q)L(q)}{1-V(q)L(q)f(q)}$$

where f(q) is a generalized "Hubbard function". The problem is to obtain an expression for f(q) which is correct in its behaviour for all values of q. Various atomic properties may be fitted to experiment to obtain f(q): each property is sensitive to f(q) in a different way, so it is not surprising that functions f(q), obtained from different properties, are not identical. Conversely a Hubbard function which fits one property well is unlikely (at the present time at least) to predict other properties well.

In order to estimate the third and fourth derivatives of the effective potential in real space, quantities which are needed to perform the anharmonic calculations in Chapter III, the present measurements have been compared with calculations using an Ashcroft potential and the following form for f(q):

$$f(q) = \frac{1}{2}\left[\frac{\eta^2}{\eta^2+\beta^2}\right] \quad , \quad \text{with } \eta = q/2k_F$$

Following the suggestion of Dr. D. W. Taylor*, the quantity β^2 was made an adjustable parameter. The only other parameter is r_A, the cutoff of the Ashcroft potential.

---

*The author is very grateful to Dr. Taylor for many useful discussions, and for the computer programme used in these calculations.

Several values of r_A, and several values of β^2, have been tried: good agreement with experiment ($\chi^2 = 0.99$) was obtained for two sets of parameters:

$$\#1\ ;\ r_A/a_o = 2.38\ ,\ \beta^2 = 1.1$$
$$\#2\ ;\ r_A/a_o = 2.40\ ,\ \beta^2 = 0.7\ .$$

A calculation, using the second set of parameters, is shown in Fig. II-14.

The value of β^2 may also be determined by requiring that the long wavelength limiting value of $\varepsilon(q)$ be consistent with the compressibility of the electron gas. The formula of Geldart and Vosko (1966) (their equation 5.1) gives an unrealistic negative compressibility in the case of rubidium, so that this approach is not acceptable in the present situation. The idea of varying β^2 is therefore very reasonable.

Frequency shifts, corresponding to a 1% increase in volume, have also been calculated using the above model. The details of this calculation are given in Section IIIC.

(iv) Constant Frequency Contour Plots

Unsmoothed computer plots of constant frequency contours in the (100) and $(1\bar{1}0)$ planes are shown in Figs. II-11 and II-12. The dynamical matrix (obtained from 12°K AFC's) was diagonalized for a mesh of points in each plane, and the intersection of a particular contour with the line joining two adjacent mesh points was obtained by linear interpolation.

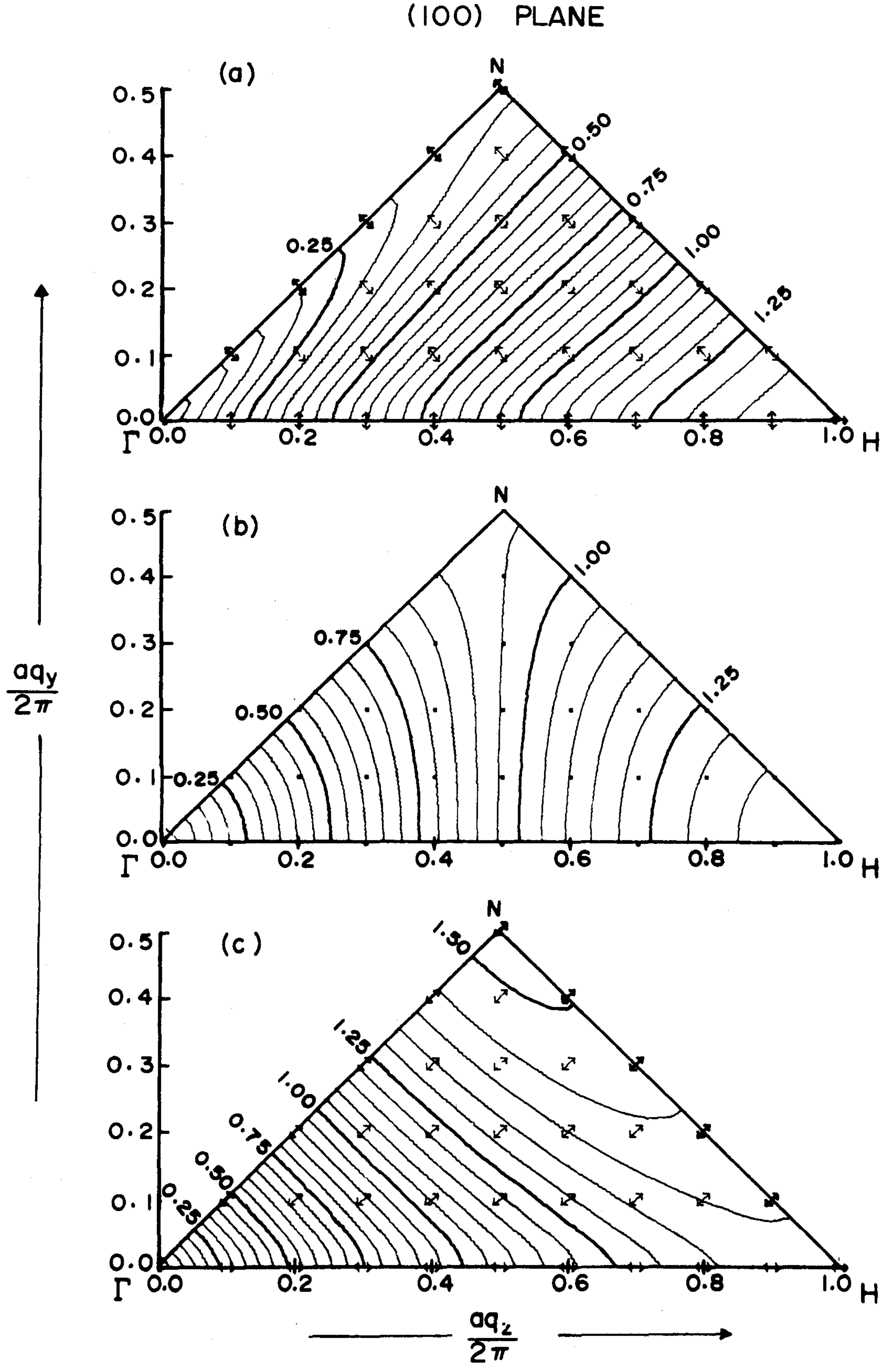

Figure II-11. Constant frequency contours in the (100) plane. The symmetry points are indicated. Every fifth contour is labelled with the frequency in THz.

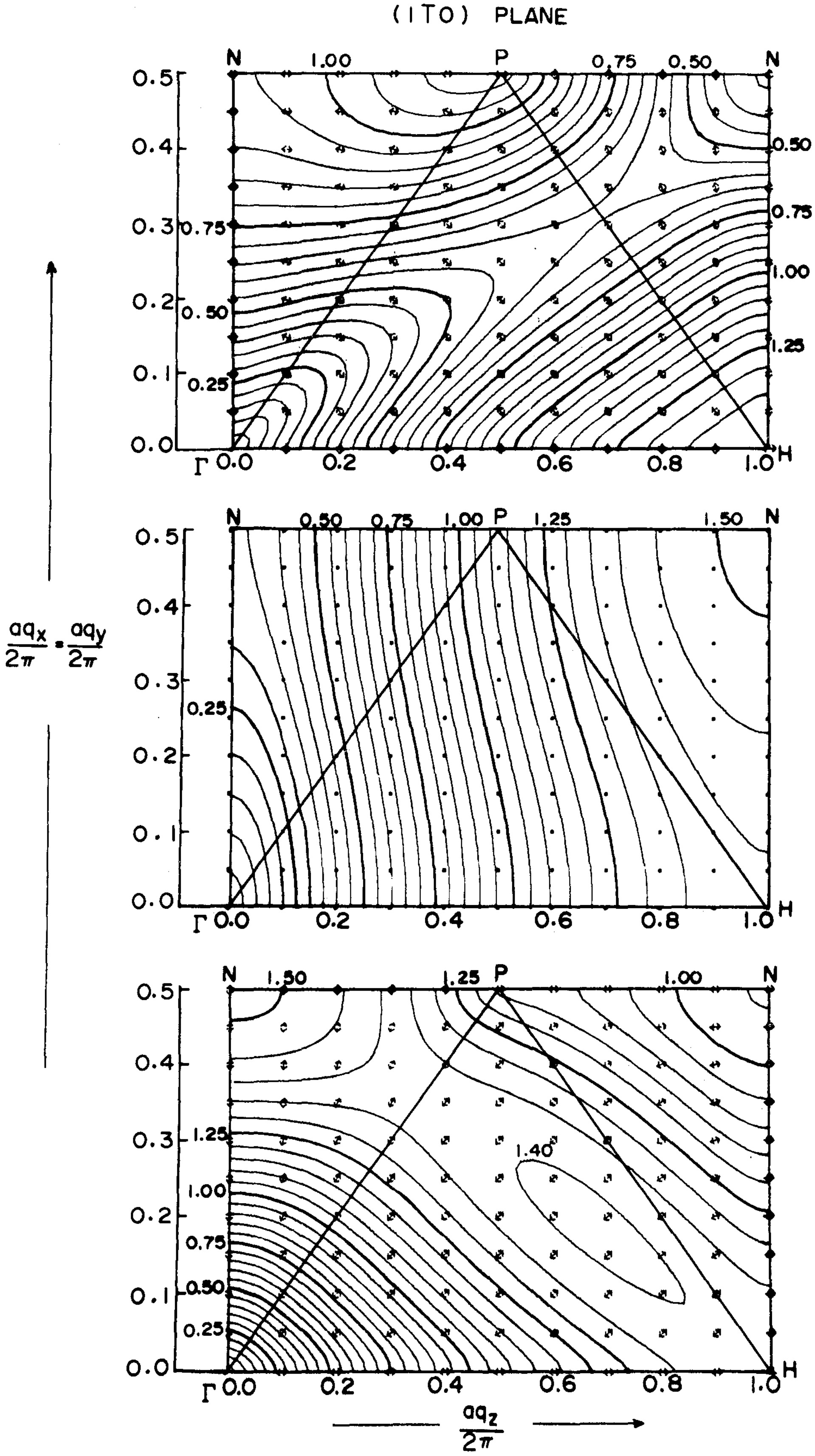

Figure II-12. Constant frequency contours in the (1$\bar{1}$0) plane. The symmetry points are indicated. Every fifth contour is labelled with the frequency in THz.

This section of the programme, together with the associated plotting routine, was obtained from the University Computing Centre. The polarization vectors in the plane are also plotted.

The plots for the (100) plane (Fig. II-11) were simply obtained by sorting the three frequencies at each mesh point into order of increasing size. This procedure yields continuous frequency contours and polarization vectors, as shown. Note in particular the sharp curvature of the contours near to the $[00\zeta]$ direction (plots (a) and (c)) and the rapid change in direction of the polarization vectors near to this direction. This feature is discussed in Section IIF.

The plots for the $(1\bar{1}0)$ plane (Fig. II-12) are more complicated, because two surfaces cross one another along the Λ and F directions (Γ to P, and P to H). This feature is mentioned in Appendix III. By including a few extra test statements in the frequency contour programme, continuous plots were obtained as shown. Note again the same type of behaviour near the $[00\zeta]$ direction as in the plots for the (100) plane. Another interesting feature is the maximum at $\sim(0.20,\ 0.20,\ 0.66)$ in plot (c). This feature is believed to produce the highest peak in the frequency distribution of rubidium (see below). Several other features of these curves will be mentioned in the discussion of resolution effects in Appendix III.

(v) Frequency Distributions

Phonon frequency distributions $g(\nu)$, at 12 and 120°K, have been calculated by the method of Gilat and Raubenheimer (1966), using AFC's from the general force model fits out to 4 and 3 neighbours respectively. The distributions are shown in Fig. II-13, normalized to the same area: a bin width of 0.0025 THz was employed, and the mesh number (n, in the notation of Gilat and Raubenheimer (1966)) was 40. The distributions are also given in Table II-6.

Several abrupt changes in slope occur in the function $g(\nu)$; these "critical points" may be correlated with certain features of the dispersion relation $\nu = \nu(\underset{\sim}{q})$. In the discussion which follows, it should be noted that the accuracy to which frequencies are quoted reflects the accuracy of the calculation of $g(\nu)$: it does not imply that the model is capable of predicting experimental frequencies to such accuracy. It may be useful to consult the constant frequency plots in Figs. II-11 and II-12, in order to visualize various features of the dispersion relation. If we consider the 12°K spectrum, we may readily identify critical points, following Dixon et al. (1963), at $\nu = 0.343$ and 0.947 THz (labelled N_1 and N_2) which result from saddle points in the two transverse branches at the point $(\frac{1}{2},\frac{1}{2},0)$. The cutoff at 1.513 THz (N3) corresponds to the maximum in the longitudinal branch at $(\frac{1}{2},\frac{1}{2},0)$. The sharp spike at 0.597 THz, labelled Λ_1', corresponds to a

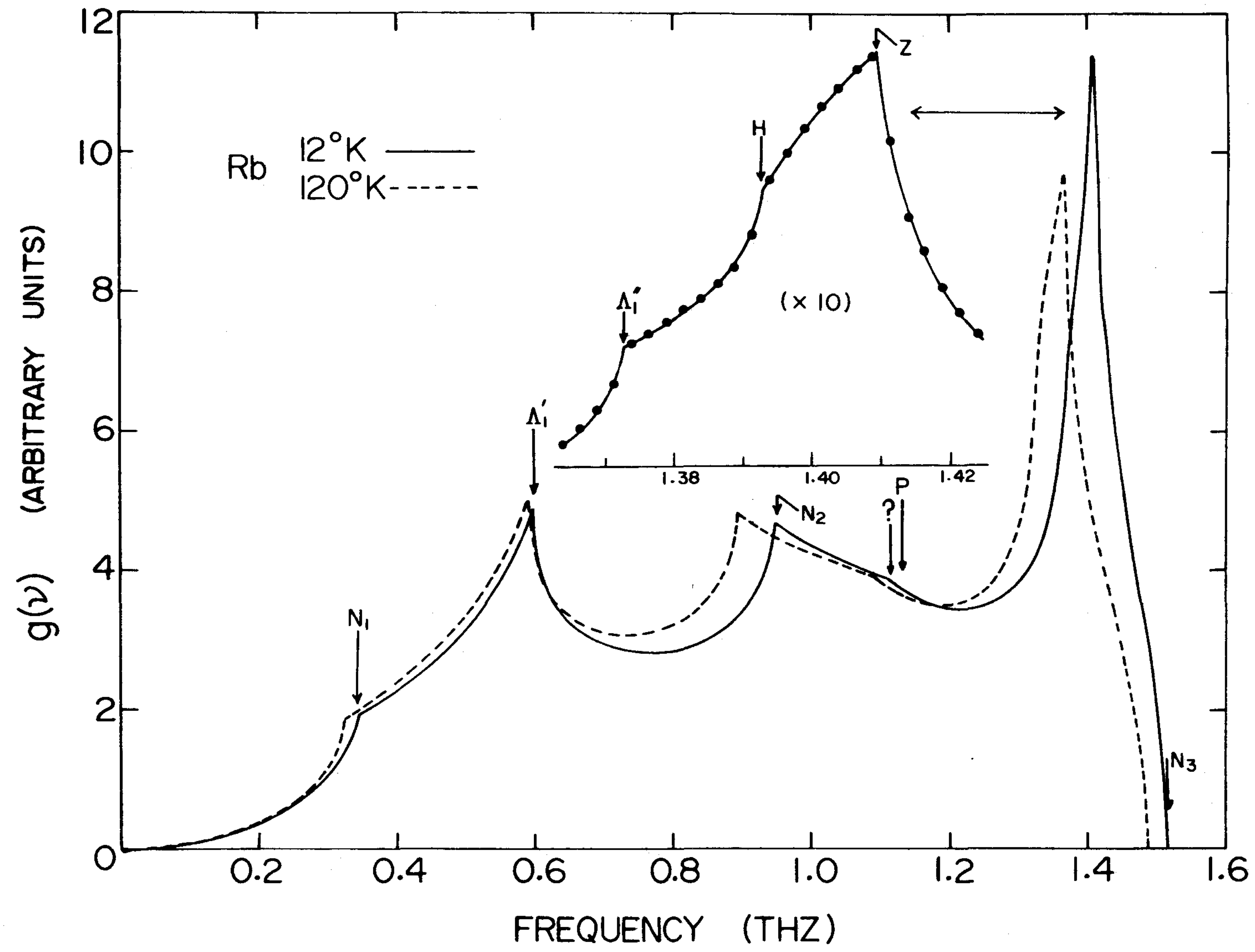

Fig. II-13 Phonon frequency distributions at two temperatures. The region between 1.365 and 1.42 THz is also shown on a ×10 scale.

TABLE II-6 Phonon frequency distributions for rubidium at (a) 12°K

FREQUENCY	.00125	.00375	.00625	.00875	.01125	.01375	.01625	.01875	.02125	.02375
0.000	1	7	20	41	65	95	134	177	227	295
.025	364	433	518	582	670	781	874	987	1163	1338
.050	1506	1618	1732	1917	2117	2342	2529	2679	2729	2704
.075	2735	2859	3102	3481	3877	4238	4523	4774	4983	5136
.100	5329	5603	5789	6141	6550	6901	7182	7384	7543	7703
.125	7954	8323	8765	9278	9830	10369	10767	11029	11356	11746
.150	12183	12599	12950	13273	13582	14020	14520	15088	15743	16372
.175	16756	16875	17198	17732	18477	19284	19911	20618	21284	21712
.200	22000	22583	23538	24532	25177	25631	26165	26420	26638	27358
.225	28583	29770	30684	31316	32185	32648	32872	33674	34816	35960
.250	37093	38132	39019	39590	40320	41728	43045	43893	44784	45557
.275	46352	47672	49412	50515	51242	52323	53451	54878	56924	58018
.300	60002	60645	61767	63763	65815	67786	69630	71263	73643	75970
.325	77683	79893	82987	85641	88678	92585	99197	105000	106515	106751
.350	107069	108192	109612	110656	111210	111706	112476	113496	114647	115722
.375	117138	118188	119003	119850	120362	121024	121895	123109	124253	124975
.400	125852	126935	127964	129286	130438	131106	131987	133081	134054	134975
.425	135883	137042	138373	139444	140623	142128	143515	144890	145704	146218
.450	147147	148404	149957	150820	151334	152791	154412	156082	157128	159036
.475	160426	161224	162133	163346	164468	166746	168575	169245	170671	172150
.500	174151	175624	177001	178143	180378	182725	183526	184383	186693	189193
.525	191080	192367	193590	194733	197212	199497	201755	204173	207305	209246
.550	210943	212989	215049	218030	220183	223673	226258	229704	231951	233228
.575	238483	241884	244366	247654	251987	256179	259992	265385	266885	251070
.600	234547	226919	219203	214064	210326	206771	203004	199535	196998	194839
.625	192574	190088	187786	185869	184088	182387	180735	179243	177778	176437
.650	175233	174219	173045	171909	170764	169627	168813	168182	167253	166195
.675	165560	165194	164462	163670	163298	162808	162089	161151	160565	160150
.700	159884	159452	158831	157944	157608	157589	157363	157291	156945	156293
.725	155830	155918	156059	155585	155161	155196	155127	155335	155145	155118
.750	155112	155123	155138	154200	153863	154170	154406	154923	155283	154931
.775	155015	154627	154593	155043	155404	155458	155563	155735	156373	157027
.800	157337	157165	157355	157603	157546	158335	158868	159306	159610	160170
.825	160366	160331	160571	161201	162140	162989	163463	163629	164332	165193
.850	166176	166557	167047	167845	169102	169761	170514	171468	172255	173213
.875	174145	175043	176346	177410	177432	178653	180395	181715	183345	184633
.900	185991	187289	189239	190958	192189	194101	196653	198685	201262	203215
.925	206062	208738	211853	215492	218818	223194	228006	235873	250148	255336
.950	254753	253155	252177	250974	250433	249376	248237	247758	246485	245852
.975	245183	244036	242982	241820	240884	240688	239347	237960	237377	236811
1.000	236590	235834	235491	234649	233791	233189	232799	232145	231386	231090
1.025	230471	229757	228992	228143	227642	226864	225991	224882	224972	224709
1.050	224266	223861	223305	222579	222175	221720	221227	220697	220074	219902
1.075	219417	218491	217698	216749	216137	215469	215059	214816	214728	213995
1.100	213177	212331	211868	211674	211416	210980	210148	209037	208027	206685
1.125	205288	204112	203092	202349	201559	200488	199598	198979	198212	197317
1.150	196531	195826	195250	194668	194054	193232	192659	192231	191861	191584
1.175	191338	191046	190715	190405	190039	189711	189362	189101	188883	188645
1.200	188369	188102	188123	188225	188220	188214	188410	188409	188231	188149
1.225	188236	188353	188412	188547	188779	189256	189439	189759	190204	190616
1.250	191108	191464	191752	192288	192841	193430	194166	194852	195569	196369
1.275	197292	198475	199554	200315	201299	202527	203875	205112	206317	207738
1.300	209358	211141	213064	215179	217156	219300	221327	223358	226010	228788
1.325	231483	234942	238204	241381	245308	249708	254263	259031	263483	268723
1.350	274753	281340	288789	297124	306373	316480	329581	343825	363559	395480
1.375	402875	412773	422737	431552	443144	454653	480720	523852	545859	565324
1.400	582307	596894	611616	621583	555572	494827	469018	440226	420458	404626
1.425	389769	372682	362165	349812	337276	326998	318004	308693	298967	289494
1.450	280814	272949	263595	256390	248332	240728	231388	224069	217090	208431
1.475	200485	192783	184872	175387	167997	159356	149822	141063	129773	121129
1.500	109078	96529	82781	66222	43417	6534	0	0	0	0

(continued next page)

TABLE II-6 Phonon frequency distributions for rubidium at (b) 120°K. (continued)

FREQUENCY	.00125	.00375	.00625	.00875	.01125	.01375	.01625	.01875	.02125	.02375
0.000	1	7	18	36	59	86	120	161	204	256
.025	315	399	453	533	612	702	771	848	974	1142
.050	1228	1465	1669	1711	1801	1996	2172	2364	2556	2566
.075	2701	2800	2945	3129	3392	3670	3941	4214	4464	4752
.100	5133	5262	5356	5566	5953	6276	6503	6729	6956	7196
.125	7463	7759	8073	8427	8934	9548	10077	10453	10646	10737
.150	10891	11412	12044	12522	13000	13591	14067	14256	14325	14690
.175	15352	16029	16528	17293	18010	18545	18762	18972	19612	20479
.200	21374	22102	22734	23576	24151	24408	25016	25591	26377	27173
.225	28017	28998	29642	30119	31271	32534	33412	33985	34738	35304
.250	36062	37704	39313	40535	41615	42396	43127	44325	46168	47425
.275	48722	49534	50816	52689	54615	56132	57141	58910	61343	63518
.300	65400	67756	70288	72632	75018	78341	82472	87674	94602	101729
.325	104457	104176	104559	105260	106916	108452	109266	109327	109701	110730
.350	112127	113409	114473	115444	116416	117263	118070	118807	119831	120789
.375	121705	123015	124370	125558	126627	127464	128016	128990	130112	131396
.400	132244	133133	134207	135458	136682	137544	138723	139796	141133	142522
.425	143191	144262	145645	147081	148630	150128	151332	152134	152318	153759
.450	155450	157274	158315	159072	160352	161900	163930	165395	166928	167972
.475	169225	170602	171862	173201	174020	175610	177924	180210	182529	184113
.500	184631	186098	188143	190490	191613	193123	195047	196434	198637	200795
.525	202903	205188	206868	208461	210068	213590	216264	217044	220500	221856
.550	224444	227631	231066	232649	234644	239919	238913	244685	248269	251129
.575	251043	256978	261570	262080	267994	271508	271745	251495	239089	231760
.600	225635	220518	215885	212429	209424	206547	203953	201408	199195	197398
.625	195565	193733	191379	189737	188412	186974	185870	184995	183208	182179
.650	181401	180356	179115	178449	177578	176251	175657	175096	174881	174623
.675	174253	173580	172043	171425	171172	171147	171195	170610	170121	169825
.700	168988	168087	168206	168189	168152	167935	167866	167973	167956	167768
.725	167204	167137	167378	167784	167793	167554	167805	167984	168161	168350
.750	168280	168308	167993	168018	168556	168887	169179	169642	170325	170723
.775	171055	171121	171270	171871	172255	172948	173811	174326	174877	175398
.800	175893	176779	177814	178469	178619	178968	179796	180796	181871	183255
.825	184166	185050	185945	187052	188460	189046	190619	192306	193848	195521
.850	196998	198332	200385	202314	204005	206036	208089	209815	211934	215533
.875	218385	222684	226135	230669	236399	243451	256891	263066	263026	261028
.900	260118	259028	258642	257618	256576	255352	253849	253485	252649	251295
.925	250380	249162	249068	248850	247771	246648	245503	244576	244074	243332
.950	243797	242884	242184	241450	240389	239773	239672	238901	237487	236234
.975	235759	235624	235688	235053	234337	233491	232691	232160	232405	232106
1.000	231514	230692	230052	229735	229210	228577	227846	226776	225796	225751
1.025	225770	225299	224942	224196	223531	223014	222851	222716	222352	221880
1.050	221308	220702	220206	219134	218314	217472	216702	216997	216683	215937
1.075	215058	214595	214228	214012	213867	213377	212556	211647	210143	208081
1.100	207710	206521	205423	204657	203780	203140	202431	201571	200731	199933
1.125	199213	198549	197912	197177	196464	195984	195468	194939	194753	194350
1.150	193945	193534	193134	192908	192593	192332	192109	191934	191636	191155
1.175	191038	191112	190926	190781	190772	190863	191012	191178	191205	191167
1.200	191098	191265	191655	191857	192000	192383	192886	193409	193913	194380
1.225	194398	194979	195893	196763	197363	198115	198949	199943	201017	201853
1.250	202858	204268	205512	206787	208378	209952	211744	213499	215540	217737
1.275	219919	222206	224463	226990	230168	233388	236532	240424	244292	249393
1.300	253858	259302	264810	270286	277522	285756	295012	306800	322222	350063
1.325	376786	396299	405420	422853	428922	442745	454838	457983	467350	482832
1.350	488314	494990	505695	512311	521856	529973	508343	455130	423011	403267
1.375	383277	367824	357302	343413	331547	323505	313698	304608	296282	288559
1.400	280619	272059	265308	259782	252757	245036	238552	233227	226935	219797
1.425	213867	208014	202734	196222	190101	183681	178465	172709	165671	160313
1.450	154121	148030	140529	134176	128865	121188	112825	106670	98291	89554
1.475	80689	70223	58506	44709	19150	83	0	0	0	0
1.500	0	0	0	0	0	0	0	0	0	0

saddle point (two maxima, one minimum) on the [ζζζ]L, or Λ_1, branch, at $\zeta \simeq 0.68$: this critical point occurs at very nearly the same value of ζ in the four alkali metals which have been studied.

The principal peak in the 12°K phonon spectrum is shown in detail in the inset to Fig. II-13. There are three distinct discontinuities in slope. The point labelled Λ_1'', at 1.373 THz, results from a saddle point on the [ζζζ]L branch at $\zeta \simeq 0.36$. The discontinuity at 1.393 THz (H) corresponds to the triply degenerate point (1,0,0). It is interesting to note that this high symmetry point does not correspond to the highest peak in g(ν) for Rb at 12°K, nor for Rb at 120°K, nor for K, whereas the principal peak in the distribution function for Na is indeed at the frequency of the point H(1,0,0). The peak marked Z, in the distribution for Rb at 12°K, occurs at 1.410 THz. It almost certainly results from a local maximum in the $(1\bar{1}0)$ plane at ∿(0.20, 0.20, 0.66), which is visible in Fig. II-12. A similar off-symmetry maximum occurs in K and in Rb at 120°K.

There remains a weak discontinuity at 1.11_5 THz, identified in Fig. II-13 by a question mark. It occurs at a frequency 1-1/2 to 2% lower than that of the point $(\frac{1}{2},\frac{1}{2},\frac{1}{2})$ labelled P (1.133 THz). A similar discrepancy obtains in both Na and K. The discontinuity occurs at 2.87 and 1.77_5 THz, whereas the point P has frequency 2.905 and 1.799 THz, respectively. No satisfactory explanation for this behaviour has been found.

The frequency distribution for Rb at 120°K shows a general shift to lower frequencies, as expected from the phonon measurements. The first moment of $g(\nu)$ is 0.971 and 0.939 THz at 12 and 120°K respectively. The positive moments of the 12°K distribution are in good agreement with the values given by Martin (1965) in his analysis of the specific heat data of Filby and Martin (1965), on the assumption that the specific heat below about half the Debye temperature is harmonic. The negative moments of the distribution are a few per cent smaller than those given by Martin (1965); these moments are sensitive to the low frequency end of the phonon spectrum, and therefore to the low frequency phonon measurements, which are the most difficult to correct for the effects of resolution. The discrepancy is not at all unreasonable in view of these considerations.

Various thermodynamic properties, such as the entropy and the heat capacity of the lattice, may be calculated from the frequency distribution function. Such calculations are presented in Section IIID, together with numerical estimates of the principal quasiharmonic and anharmonic corrections to these quantities.

(vi) Comparison with Elastic Constants

The limiting slopes of the phonon dispersion curves at very small $\underset{\sim}{q}$, i.e., very long wavelength, determine the velocities of sound propagation in this régime. Neutron measurements give information in the frequency range 10^{11} - 10^{13} cps, whereas ultrasonic velocity measurements are commonly made in the range 10^7 - 10^9 cps. It is none the less instructive to compare measured ultrasonic velocities with the neutron scattering measurements.

The elastic constants of rubidium have been measured using the ultrasonic pulse echo method by Roberts and Meister (1966) and by Gutman and Trivisonno (1967). The former measurements are on average about 15% lower than those of Gutman and Trivisonno, at 78°K. More recently Pauer (1968) has measured the pressure derivatives of the elastic constants of rubidium. His zero pressure measurements at 195°K agree to within 3% with the results of Gutman and Trivisonno (extrapolated to the same temperature). The latter measurements have therefore been used for comparison with the neutron scattering work.

Gutman and Trivisonno (1967) obtained the elastic constant C_{11}: (1) from measurements of the three wave velocities in the [110] direction, and (2) directly from the longitudinal wave velocity in the [001] direction. The latter values are about 3% higher at all temperatures, whereas the internal consistency of each set of measurements is better than 1%. Their measurements in the [110] direction alone have been used for the present comparison.

The straight lines from the points Γ in Fig. II-4 represent velocities of sound obtained from the elastic constants by interpolation to 120°K. The agreement with the neutron measurements is good for the [00ζ] and [ζζ0] directions. In the [ζζζ] direction the elastic constant lines have larger errors since the slopes are obtained by combining at least two measured elastic constants. In view of this the agreement is again satisfactory. The discrepancies noted by Copley et al. (1968) result from using the measurements of Roberts and Meister (1966).

At other temperatures the agreement, between the ultrasonic work of Gutman and Trivisonno (1967) and the neutron measurements, is again satisfactory. There is no experimental evidence for zero sound (Cowley et al. 1968) in rubidium.

(vii) Discussion

In previous sections we have described the measurement of phonon frequencies in rubidium, and several different methods of analysis have been explored. We have concentrated on the harmonic aspects of the lattice dynamics. The measurements at different temperatures have been independently analysed within the framework of the harmonic approximation, and the results of these analyses have then been compared.

No attempt has been made to examine the shifts in frequency of different modes as a function of temperature: this topic is discussed in the following chapter.

Looking at Fig. II-14 it is clear that there is no particular problem involved in fitting theoretical models to the dispersion curves of rubidium. The figure shows three different types of fit to the 120°K measurements on Rb. The pseudopotential calculation is not quite as good as the others, but it must be remembered that the model used only two adjustable parameters. It should be noted that no evidence of Kohn anomalies (Kohn 1959) exists for rubidium, nor is this unexpected: the electron-phonon interaction is weak in the alkali metals (weakening slightly more as the atomic mass increases), so that the strength of Kohn anomalies is very considerably reduced in comparison with a metal such as lead (Brockhouse et al. 1962).

Since phonon measurements now exist for four alkali metals, it is instructive to examine the degree of homology that exists between the vibrations in the different metals. Mean frequency ratios (R) for different pairs of alkali metals are given in Table II-7. The standard deviation of an individual ratio from the mean (σ), the average error of a ratio (estimated from the experimental errors, and denoted by δ), and the number of ratios (N), are also given. In every case, except for Li/Na, σ is smaller than δ, so that

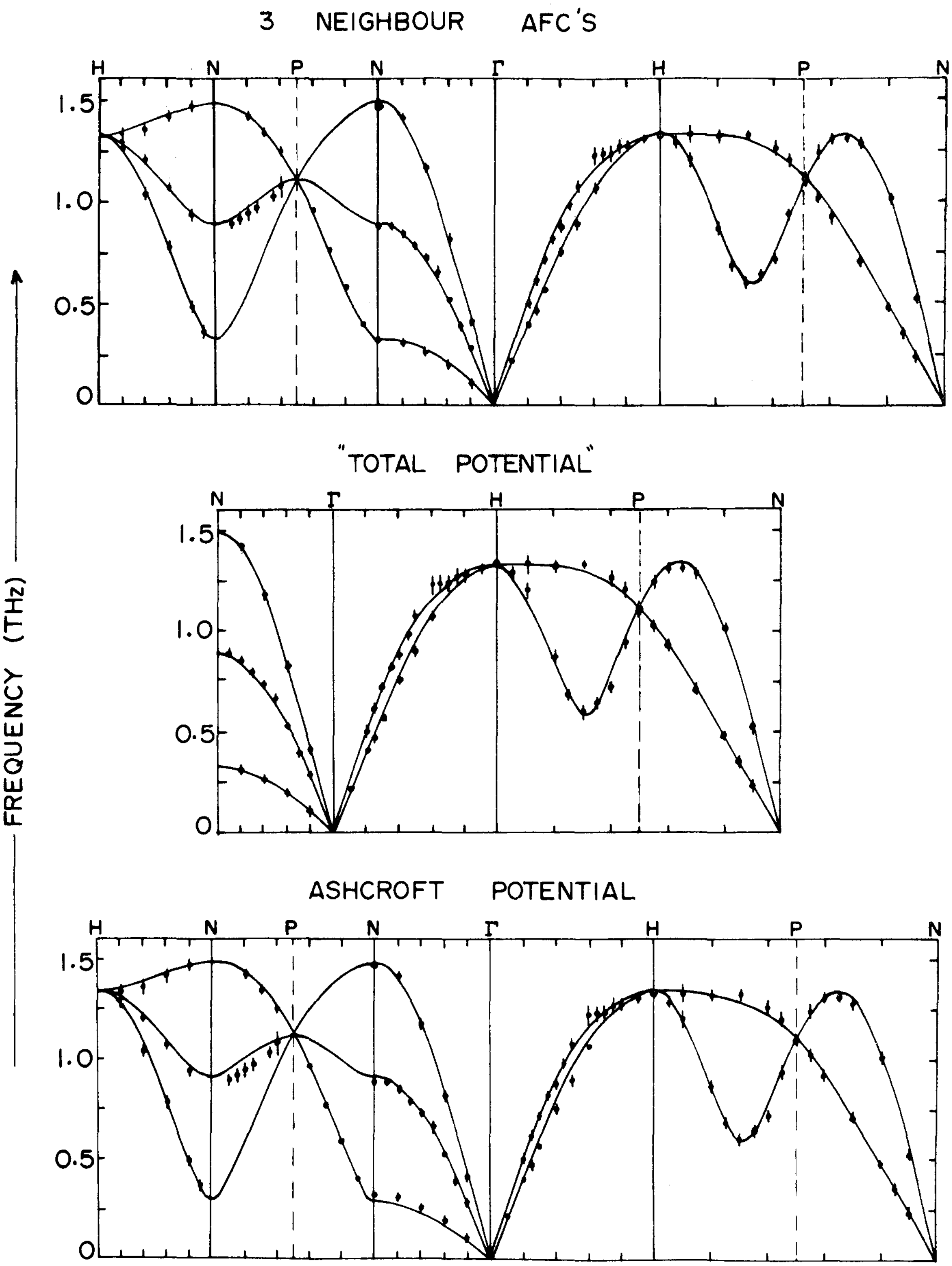
3 NEIGHBOUR AFC'S

"TOTAL POTENTIAL"

ASHCROFT POTENTIAL

Fig. II-14. Three different fits to the experimental normal mode frequencies in rubidium at 120°K.

(within experimental errors) the lattice vibrations are homologous. The values of δ given in Table II-7 differ from those listed by Copley et al. (1968) because an incorrect expression was used to compute the values given in that paper.

The fifth row of Table II-7 contains frequency ratios R_o appropriate to 0°K; these were obtained by correcting the ratios R using the measured temperature dependence of the elastic constants as a guide.

If the interatomic potentials in the alkali metals are identical in shape, differing only by a scaling factor proportional to the lattice constant, then the frequency ratio may be expressed as (Brockhouse 1959):

$$<\nu_1/\nu_2> = (M_2 a_2^2/M_1 a_1^2)^{\frac{1}{2}} .$$

On the other hand the Lindemann relation (Mott and Jones 1936) may be expressed as

$$<\nu_1/\nu_2> = (\theta_{D1}/\theta_{D2}) = (T_{M1} M_2 a_2^2/T_{M2} M_1 a_1^2)^{\frac{1}{2}} ,$$

where θ_{Di} is the Debye characteristic temperature of metal i, and T_{Mi} is its melting temperature.

The above ratios are also given in Table II-7. In every case the ratios R_o and $(\theta_{D1}/\theta_{D2})$ are close, and lie between the ratios predicted by the above relations. There is little to choose between them.

In conclusion, we have seen that the harmonic aspects of the crystal dynamics of the alkali metals are well understood, to the extent that theory and experiment are in accord. In addition several systematic trends are observable, as the mass is increased. In the following chapter we shall see that the situation is not as simple as regards the anharmonic properties of these metals.

F. THE [00ζ]L BRANCH

We have already noted that corrections for resolution,

TABLE II-7. Mean frequency ratios, and their errors, for different pairs of alkali metals. Other ratios of interest are also given. Values for M,a, T_M, and θ_D taken from Table II-1.

	Li/Na	Li/K	Li/Rb	Na/K	Na/Rb	K/Rb
$R=\langle\nu_1/\nu_2\rangle$	2.326 ±0.028	3.831 ±0.036	6.319 ±0.056	1.635 ±0.004	2.742 ±0.016	1.671 ±0.006
σ	0.155	0.189	0.304	0.040	0.119	0.052
δ	0.123	0.205	0.583	0.076	0.151	0.95
N	30	27	29	82	56	78
$R_o=\langle\nu_1/\nu_2\rangle_o$	2.31	3.89	6.14	1.67	2.68	1.60
$\sqrt{\frac{M_2a_2^2}{M_1a_1^2}}$	2.21	3.57	5.64	1.61	2.55	1.58
$\sqrt{\frac{M_2a_2^2T_{M1}}{M_1a_1^2T_{M2}}}$	2.44	4.14	6.79	1.69	2.78	1.64
θ_{D1}/θ_{D2}	2.26	3.80	6.19	1.68	2.74	1.63

as well as the occurrence of unwanted spurious peaks, are important considerations in the analysis of neutron scattering measurements on rubidium. These topics are discussed further in Appendices II and III. In this section we shall give detailed consideration to the $[00\zeta]L$ branch. Extra peaks were observed in Constant $\underline{Q}$ scans of this branch, and for a long time they defied explanation. We first describe the observations and some initial ideas regarding the origin of the extra peaks. A consistent explanation is then offered, and finally we discuss the possibility that such effects may be observed in other systems.

(i) Observation of Extra Peaks

Several examples of extra peaks observed in constant $\underline{Q}$ scans of the $[00\zeta]L$ branch are shown in Figs. II-15 and II-16. Fig. II-15 shows six scans for $\zeta = 0.3$ taken under various sets of conditions. From symmetry considerations, and because $\underline{Q}$ is (except for scan (d)) parallel to $\underline{e}_L$, the eigenvector for the longitudinal mode, we expect to see only one peak in each scan. From independent measurements of the $[00\zeta]T$ branch, which showed no unusual behaviour, we know that the frequency of the transverse mode is about 0.57 THz for $\zeta = 0.3$. This frequency lies between the two observed peaks in each scan of Fig. II-15, and we therefore associate the higher frequency peak with the L mode. Fig. II-16 shows the dependence of the effect on ζ at 205°K. The sharp rise in the counts at low frequency, for small ζ, results from elastic

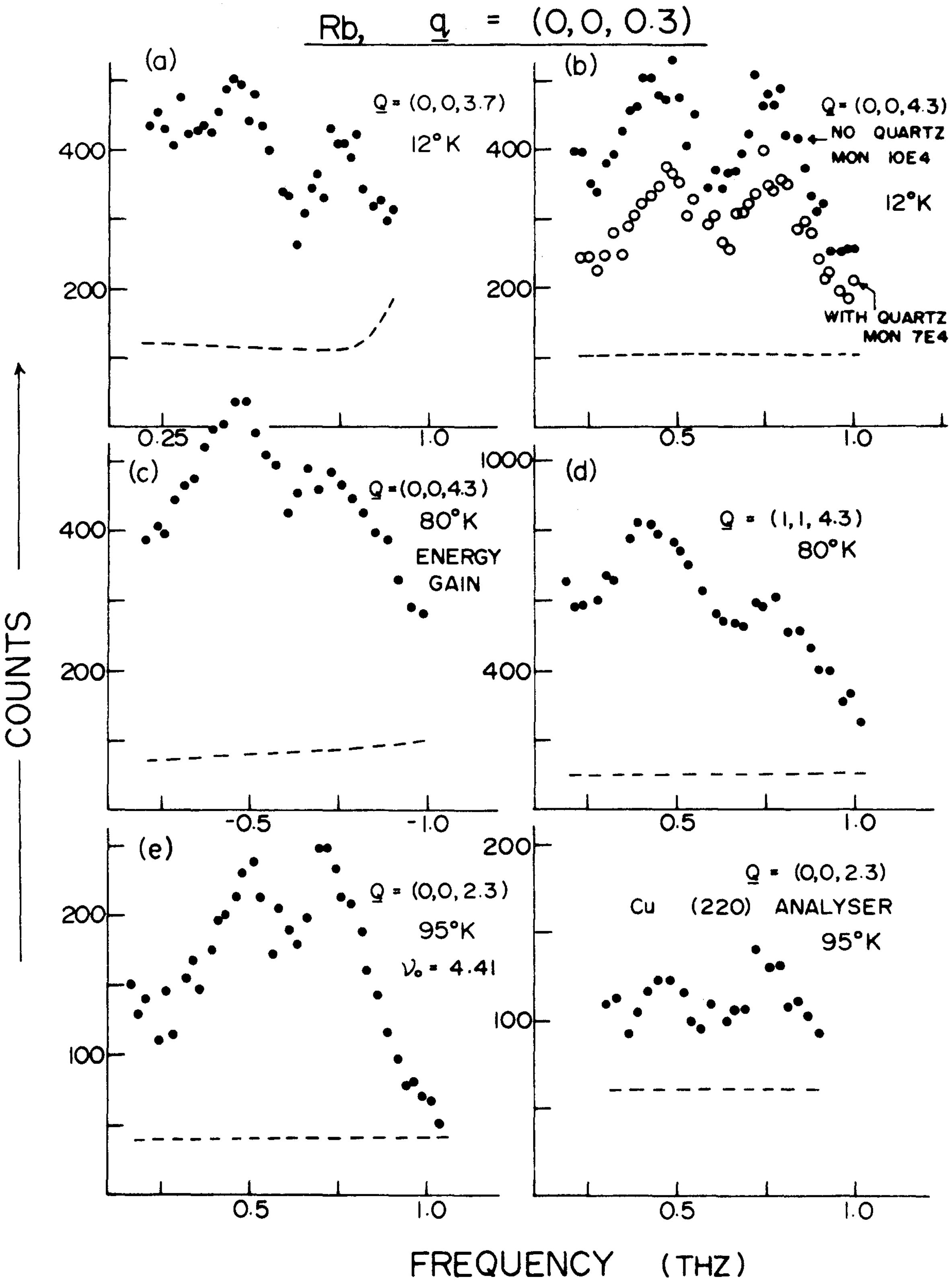

Fig. II-15. Examples of extra peaks observed in constant Q scans, for q = (0,0,0.3).

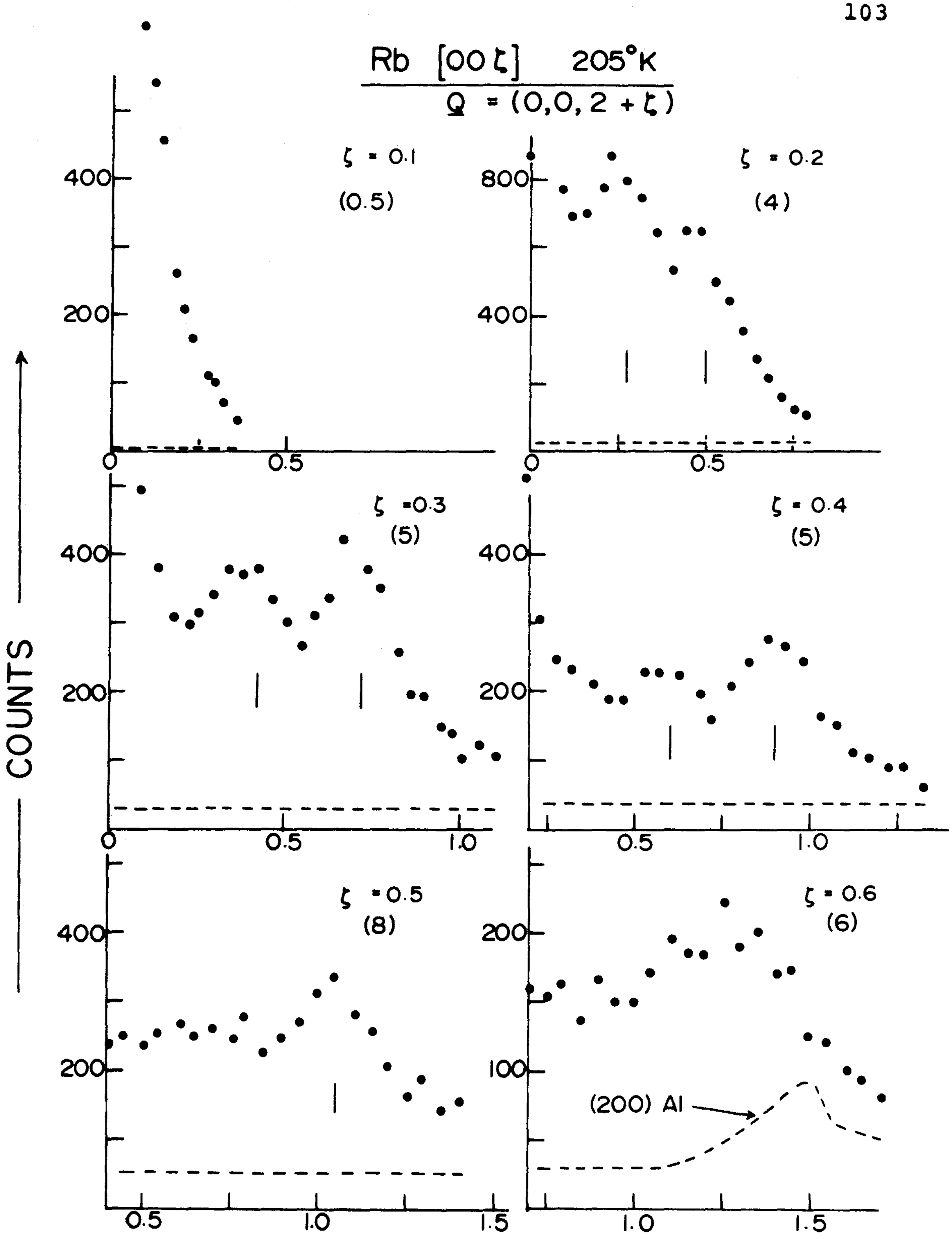

Fig. II-16. The dependence on ζ of the neutron groups observed with Q = (0,0,2+ζ) at 205°K.

incoherent scattering. We note from Fig. II-16 that two peaks are only observed clearly for ζ between 0.2 and 0.4, and in each case the transverse mode frequency lies between the two observed peaks.

The combined results at 85 and 120°K are shown in part (a) of Fig. II-17. The two "branches" observed in scans with $\underset{\sim}{Q}$ parallel to $\underset{\sim}{q}$ (i.e., longitudinal scans) are labelled L and L'. The L' "branch" lies about 15% below the transverse branch. Similar plots at other temperatures indicate that there is a general trend toward lower frequencies as the temperature is increased.

It should be remarked that Woods et al. (1962) observed peaks at lower energy transfer in scans of the [00ζ]L branch, and "their energy did not correspond exactly with that of the transverse branch." Furthermore Smith et al. (1968) mention that they observed "a number of extraneous peaks in the phonon spectrum". In a note added in proof (and in a private communication from Dr. H. G. Smith) it is stated that some low energy peaks in the [00ζ]L branch remain unexplained. To the author's knowledge no explanation for this type of behaviour has yet been advanced.

(ii) Ideas Regarding the Origin of the Extra Peaks

Since the extra peaks described above persist under a wide variety of experimental conditions, most of the possible

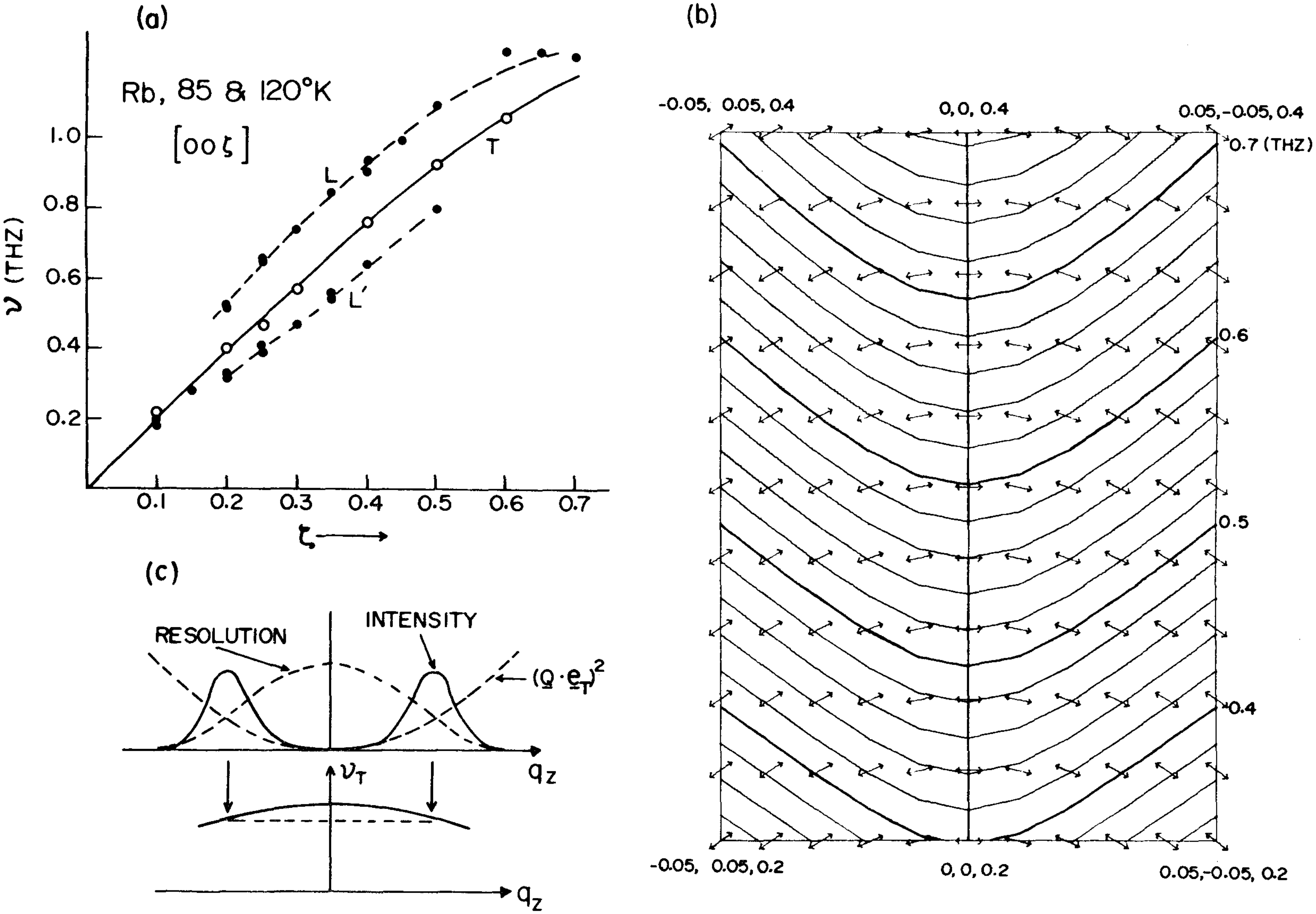

Fig. II-17. (a) The extra "branch" in Rb: (b) frequency contours close to (0,0,0.3)
(c) the explanation of the extra peaks.

spurious processes described in Appendix II can be discarded straightaway. The fact that the peaks are observed for different values of $\underline{Q}$, for example, indicates that it is not the result of a particular combination of wave vectors $\underline{k}_o, \underline{k}'$, leading to a Bragg peak. It is also noteworthy that the background counts do not show structure. The only possibility, of those listed in Appendix II , is multiple scattering. However it is difficult to understand why the extra peak does not occur at (or very near) the frequency of the transverse mode.

Extra peaks will result if a specimen containing more than one single crystal is used. A careful examination of the specimen was therefore undertaken (Appendix I), and it was established that only one crystal of sufficient size to produce observable one-phonon peaks existed in the specimen. It is in any case difficult to understand why an extra crystal would produce extra peaks in only one out of twelve branches. Furthermore it is noteworthy that the natural lithium crystal used by Smith et al. (1968) still gave extra peaks in this branch whereas the isotopic crystal (which was not single) gave extra peaks in several branches. (The double peaks in the $[\zeta\zeta\zeta]T$ branch in Li have been explained separately. (See Appendix III).

A tempting explanation for the extra peaks in Rb was that they resulted from marked anharmonicity in the branch.

Calculations by Cowley and Cowley (1965) indicate that certain modes in the alklai halides can have multiply peaked line shapes. However there was no indication of such line shapes in calculations by Buyers and Cowley (1969) on potassium.

A radically different idea was put forward by Overhauser (1970). On the assumption that the ground state of rubidium is a charge density wave state (see e.g., Overhauser 1968), he calculated the phonon spectrum of rubidium and was able to predict extra "longitudinal" modes. This occurs because the symmetry of the lattice may be lowered to tetragonal by a charge density wave. There are several objections to this idea, and it is not believed to be the correct explanation. In the following paragraphs, we consider experimental details which are fully able to explain the observations. It has been remarked that experimental considerations are more likely to be the reason for unexpected observations than are major changes in theory. This seems to be true in the present case.

(iii) The Explanation

It was remarked above that multiple scattering was a possible explanation, but that a 15% shift in frequency was difficult to understand. A small shift is possible however, as a result of finite instrumental resolution. To check this possibility, an existing computer programme (originally written by Dr. E. R. Cowley) would have had to be modified to allow for multiple scattering, and it was not clear how to formulate this modification. Fortunately no such changes were necessary. The programme, which is briefly described in Appendix III , was initially run without modification, and it immediately predicted double peaks for the $[00\zeta]$L branch!

The source of the extra peak was quickly established. Fig. II-17, part (b), shows constant frequency contours in a portion of the (110) plane, which is normal to the $(1\bar{1}0)$ scattering plane: the central line, which is the [001] direction, lies in the $(1\bar{1}0)$ plane. The diagram shows the behaviour of the transverse mode (eigenvector $\underline{e}_T$) lying in the (110) plane, for small displacements of $\underline{q}$ above and below the scattering plane. Referring now to part (c) of Fig. II-17, we observe that the resolution function drops off either side of the scattering plane (q_z is the component of $\underline{q}$ normal to the scattering plane). Furthermore the quantity $(\underline{Q}\cdot\underline{e}_T)^2$ increases, roughly as shown. Thus the intensity of scattering by this mode has the indicated type of behaviour. Referring now to the lower portion of (c), we see that the dispersion relation for this mode has considerable downward curvature with the result that a peak is observed at a frequency significantly lower than the value for $q_z = 0$.

To see why this effect is not observed in other branches, or in other types of system, we refer first to Figs. II-11, II-12. It is immediately apparent that, for modes with polarization in the plane, (a) the polarization vector changes direction rapidly for small displacements of $\underline{q}$ from the [001] direction, but only slowly for small displacements from other symmetry directions, and (b) the curvature of the frequency surfaces is very much more marked close to the [001] direction. The rapid change in direction of the polarization vectors results in a more intense extra mode, and the large curvature leads to a large shift of the mode.

These two effects are related. For small $\underline{q}$ we may use the long wavelength approximation to obtain, using standard perturbation theory:

$$\frac{\Delta\omega_{T'}}{\omega_{T'}} = \left[\frac{C_{11}+C_{12}+2C_{44}}{2C_{44}} - \frac{(C_{12}+C_{44})^2}{C_{44}(C_{11}-C_{44})}\right]\frac{\varepsilon^2}{\zeta^2} + O\left(\frac{\varepsilon^4}{\zeta^4}\right) \qquad \text{(II-F1)}$$

$$\frac{\Delta\omega_{T''}}{\omega_{T''}} = \left(\frac{C_{11}-C_{12}}{2C_{44}}\right)\frac{\varepsilon^2}{\zeta^2} \qquad \text{(II-F2)}$$

$$\frac{\Delta\omega_L}{\omega_L} = \left[\frac{C_{44}}{C_{11}} + \frac{(C_{12}+C_{44})^2}{C_{11}(C_{11}-C_{44})}\right]\frac{\varepsilon^2}{\zeta^2} + O\left(\frac{\varepsilon^4}{\zeta^4}\right) \qquad \text{(II-F3)}$$

$$\tan^2\alpha = \frac{2(C_{12}+C_{44})^2}{(C_{11}-C_{44})^2}\,\frac{\varepsilon^2}{\zeta^2} + O\left(\frac{\varepsilon^4}{\zeta^4}\right) \qquad \text{(II-F4)}$$

where the subscripts T' and T" refer to modes polarized in and normal to the plane; $\Delta\omega_L$, $\Delta\omega_{T'}$ and $\Delta\omega_{T''}$ are the changes in frequency of the three modes, and α is the change in direction of the polarization vectors in the plane, when $\underline{q}$ is changed from

$(0,0,\zeta)$ to $(\varepsilon,\varepsilon,\zeta)$ with $\varepsilon << \zeta$.

We now see that the extra peaks were observed as a result of relaxed vertical* resolution and the fact that $(C_{11}-C_{44})$, the energy denominator in Eqs. (II-F1, F3 and F4), is relatively small. The vertical resolution of the instrument is comparable with that of other instruments (for example Buyers and Cowley (1969) had 1° and 4° collimation in $\underset{\sim}{k}_o$ and $\underline{k}'$, which is very similar to the collimation of the McMaster spectrometer, 1.3° and 4°). Thus it is the small difference between C_{11} and C_{44}, together with the small size of the reciprocal lattice (Section IIB), which leads to pronounced extra peaks.

In Fig. II-18 experimental line shapes are compared with calculation. The experimental curves were obtained from the actual measurements (Fig. II-16) by subtracting off the background and the elastic incoherent contribution to the intensity. The solid curves were calculated using AFC's appropriate to 205°K, and parameters for the resolution function as in Appendix III. Somewhat better agreement (shown by dashed lines) was obtained using slightly poorer vertical resolution [$M_{33} = 100\ (a/2\pi)^2$: see Appendix III]. The agreement between theory and experiment is quite good considering that only one parameter can be varied: the calculated

---

[*] In the present discussion "vertical" means normal to the scattering plane.

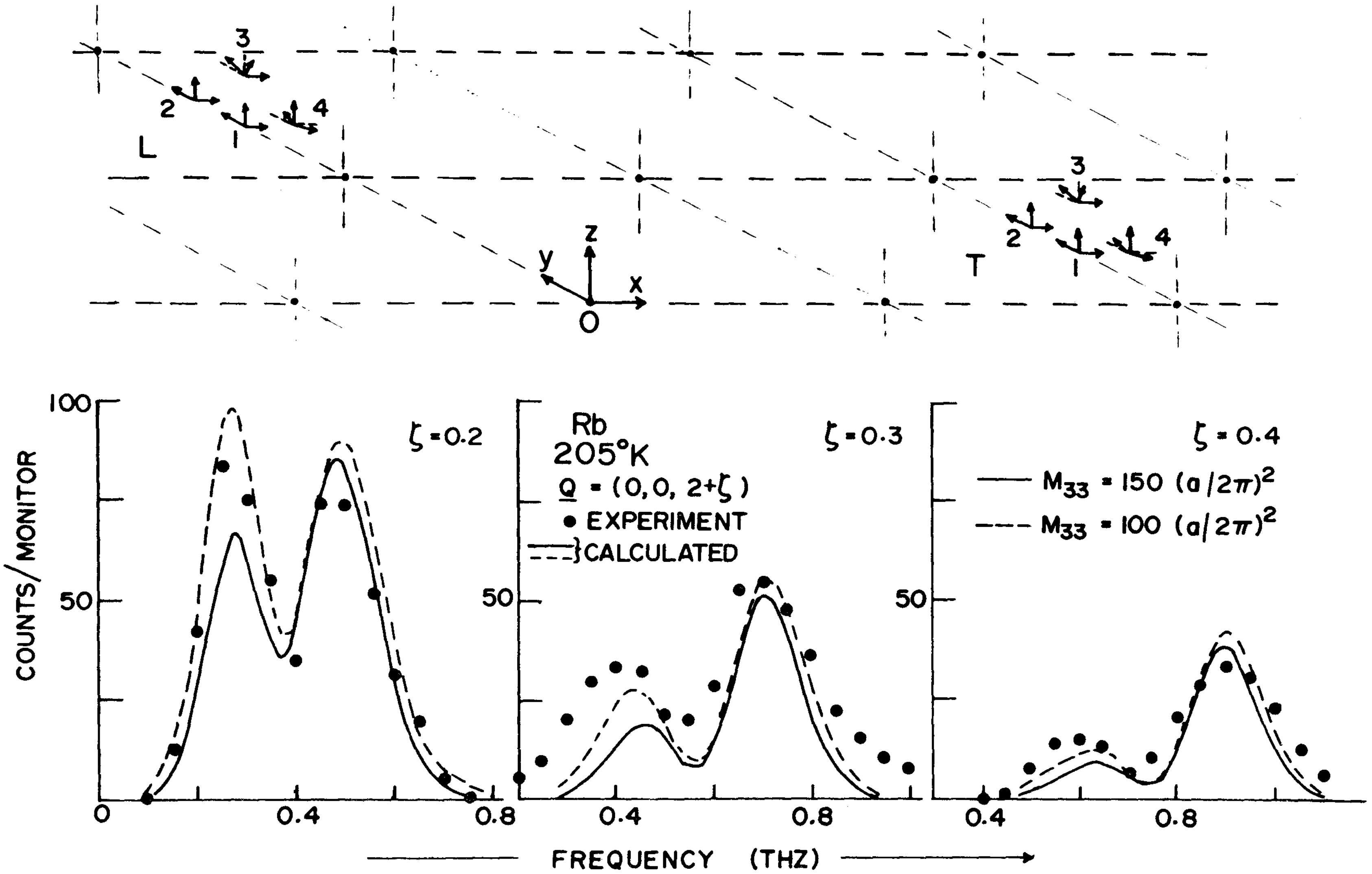

Fig. II-18. Above, behaviour of polarization vectors close to a symmetry direction. Below, observed and calculated neutron groups for [00ζ] direction.

intensities relative to one another are completely determined, but the ratio of the experimental intensity scale to the theoretical intensity scale is arbitrary. The discrepancies between calculation and experiment, particular for $\zeta = 0.3$, may result because no set procedure exists for subtracting off the large background from the experimental measurements.

(iv) Discussion

Clearly the above explanation can be tested by examining the behaviour of a scan as a function of vertical resolution. Such an experiment was planned in March 1970 but it was abandoned because the Rb crystal was no longer useable (see Section IIC). Instead an experiment on potassium was attempted using a crystal kindly lent by Dr. R. A. Cowley. The best run, with and without vertical collimation, is shown in Fig. II-19 (the inset shows the type of lineshape observed by Woods et al. (1962) in Na). Though the results are by no means conclusive, there is definite evidence of a low frequency peak in K which is reduced in intensity when vertical collimation (0.1" in 8" in the scattered beam) is put in.

No extra peaks were observed in K by Cowley et al. (1966) because detailed scans were restricted to a frequency range which did not extend low enough in frequency for the extra peak to be observed (Dolling 1970).

Let us now consider whether extra peaks are likely to

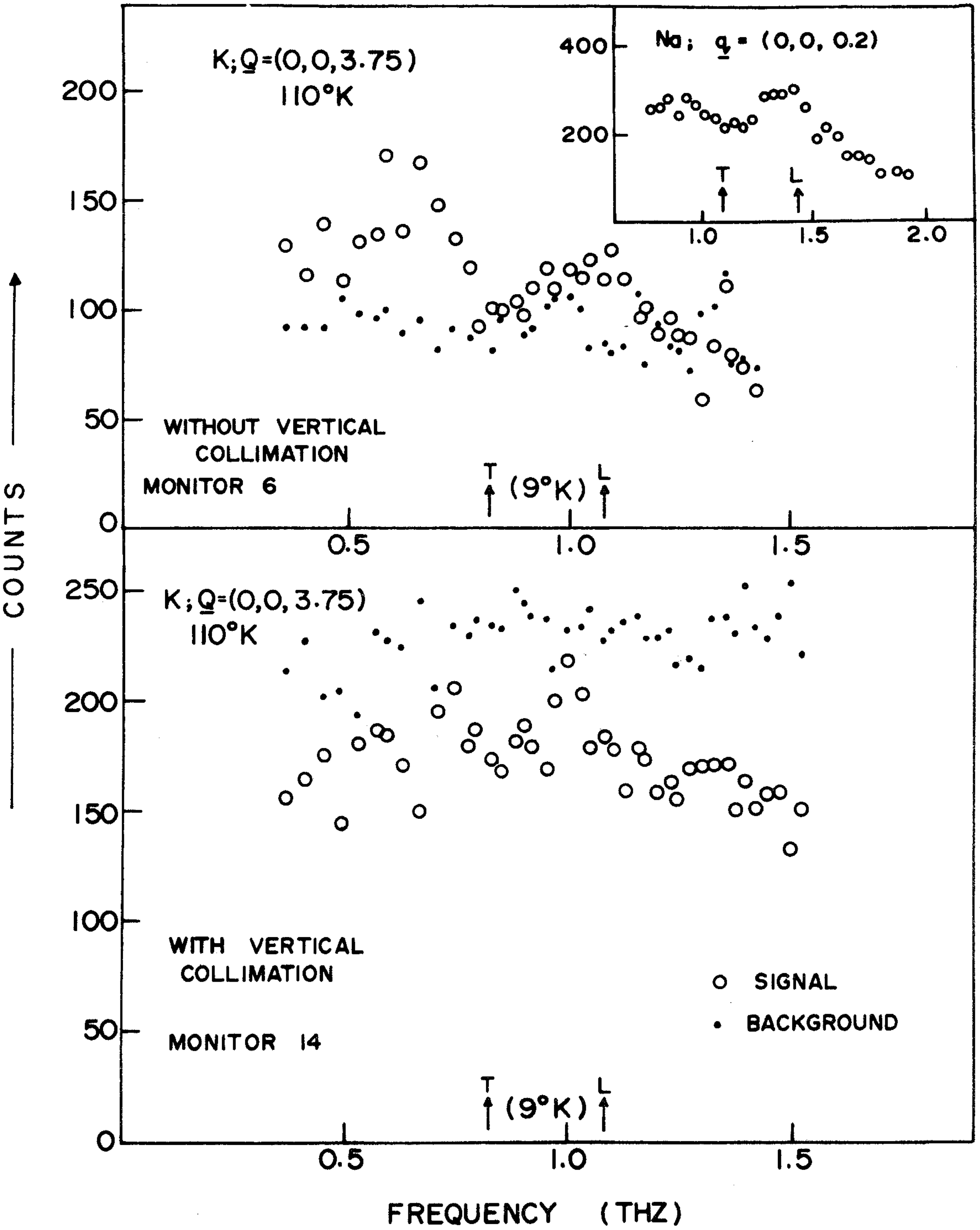

Fig. II-19. Neutron groups in K with and without vertical collimation. A group observed in Na by Woods et al (1962) is also shown. In each case the arrows indicate the positions of the T and L modes according to Woods et al (1962) and Cowley et al (1966).

show up in experiments on other types of systems, as a result of a rapid change in direction of the eigenvectors. Two questions arise: first, under what circumstances do such rapid changes occur, and second, what type of resolution function is necessary in order to see an extra peak?

Rapid changes in polarization direction are likely to occur when two modes have nearly the same frequency. However such changes can only occur if they are allowed by symmetry. Referring to either the lower left- or the lower right-hand side of Fig. II-18 we note that modes polarized parallel to the x- and y-directions (hereafter designated modes X and Y) can only interact if $\underline{q}$ is displaced in the x-direction, from position 1 to position 4: modes Y and Z can only interact if $\underline{q}$ is displaced vertically to position 3. In the left-hand diagram, which represents the measurement of a longitudinal phonon (mode Y), we see that poor resolution parallel to $\underline{Q}$ does not lead to interaction with modes X or Z: however poor vertical resolution can mix in mode Z. This is exactly the situation in the [00ζ]L branch in the alkali metals. In the case of a transverse phonon measurement, poor resolution parallel to $\underline{Q}$ results in the interaction of the transverse mode X with mode Y.

The crossing of the L and T2 branches in the [ζζ0] direction in an f.c.c. material (see e.g., Svensson et al. 1967) is a situation where the eigenvectors of the two branches change direction rapidly, if $\underline{q}$ is displaced slightly from the symmetry direction. The T2 mode is polarized parallel to [001]. It follows from the above arguments that:

(a) for measurements of the L mode conducted in the (001) scattering plane, poor vertical resolution will result in strong interaction with the T2 mode;

(b) for measurements of the L mode in the $(1\bar{1}0)$ plane, poor resolution in the plane, normal to $\underline{Q}$, has the same effect;

(c) for measurements of the T2 mode in the $(1\bar{1}0)$ plane, poor resolution parallel to $\underline{Q}$ results in strong interaction with the L mode.

Furthermore we should note that, though two peaks may not be observed, considerable shifts may still occur as a result of interactions with other modes. If the energy resolution is poor the two peaks may not be resolved with the result that the modes appear to be attracted to one another. Clearly extra precautions should be taken if measurements are contemplated where this type of complication is likely to occur.

(v) Phonon Frequencies for the $[00\zeta]$L Branch

The shift in frequency of the $[00\zeta]$L modes in Rb, as a result of relaxed vertical collimation, is easily calculated for small ζ. The "true" frequencies lie 0.02 to 0.03 THz below the measured frequencies in Rb, for $\zeta \lesssim 0.5$. For $\zeta \gtrsim 5$

the type of correction is not clear. Assuming the extra peak is still resolved, but too weak to be separated from the background, the shift Δ_R is still positive: on the other hand Δ_R is negative if we assume that the extra peak is not resolved.

An additional complication is that the neutron groups for the upper part of the branch were very weak. This is reflected in the large errors assigned to these measurements. For this reason the shifts are not significant since they are at most ±0.02 THz whereas the errors are of order ± 0.04 THz.

The $[00\zeta]$L branch in the alkali metals is believed to be more anharmonic than the other branches. Glyde and Cowley (1970) predict a crossover in this direction for b.c.c. He^3 when cubic anharmonicity is taken into account. A crossover was observed in lithium by Smith et al. (1968), and Brockhouse (1968) suggested that it resulted from anharmonicity. Furthermore Millington (1969) found evidence of anharmonicity in the $[00\zeta]$L branch in an analysis of his own room temperature time-of-flight measurements on sodium. It may well be that the weak, poorly defined, groups observed in Rb result from considerable anharmonic damping of these modes.

Wallace (1968) has noticed a "kink" in the measured $[00\zeta]$L branch in Na and K, for ζ between 0.6 and 0.7. There is also slight evidence of such behaviour in Rb, but the present results are by no means conclusive.

CHAPTER III

ANHARMONIC PROPERTIES

A. THEORY OF ANHARMONICITY

(i) Introduction

The harmonic approximation, which has been described in previous sections, is evidently a good approximation, capable of explaining many of the observed dynamical properties of real crystals. On the other hand, the approximation predicts a number of results which are not satisfied in real crystals. Among these predictions, (a) there is no thermal expansion, (b) the adiabatic and isothermal elastic constants are equal, and independent of temperature and pressure, and (c) the heat capacity tends to a constant value at high temperatures. It is clear that the theory must be extended to allow for departures from harmonicity.

In this section we shall first discuss the quasi-harmonic theory, in which the phonon frequencies are assumed to be volume-dependent, but independent of temperature at constant volume. We shall then consider the principal effects of intrinsic anharmonicity, which we may think of as anharmonicity at constant volume, with particular reference to the lattice vibrations. Finally, we take a brief look at the idea of effective frequency distributions, and the anharmonic contributions to thermodynamic functions.

The discussion that follows is generally restricted to monatomic cubic lattices, and in particular the b.c.c. lattice.

(ii) The Quasiharmonic Approximation

In this subsection we shall determine the volume dependence of the normal mode frequencies in terms of the anharmonic atomic force constants (AAFC's) $\phi_{\alpha\beta\gamma}(\ell\ell'\ell'')$. This will enable us to calculate the thermal expansion.

We first demonstrate that the AAFC's are non-zero. Owing to the rotational invariance condition (Leibfried 1965, Born and Huang 1954), these quantities are related to both the second and third derivatives, V" and V'" of the potential $V(\underline{r})$. Clearly V" is non-zero, and therefore at least some of the anharmonic coefficients are non-zero. Furthermore Leibfried (1965) states that, in the case of an f.c.c.nearest neighbour central force model, setting V'" = V"" = 0 leads to the unexpected result that the thermal expansion is negative.

We now derive the shift in frequency, due to thermal strain, of the mode $\lambda \equiv (\underline{q}j)$. This problem has been treated by Maradudin (1962). The frequency of the mode λ, in the harmonic approximation, is given by (Eqs. I-C10, I-C11):

$$m\omega^2(\lambda) = \sum_{\alpha\beta} e_\alpha(\lambda)e_\beta(\lambda) \sum_{\ell'}{}' \phi_{\alpha\beta}(\ell\ell')[\exp\{i\underline{q}\cdot\underline{r}(\ell'\ell)\}-1]. \quad \text{(III-A1)}$$

We consider an isotropic strain $\eta = \Delta a/a$, which we shall regard below as a thermal strain (rather than as a mechanical strain). The atomic positions are changed by amounts $\eta \underline{r}(\ell)$, and the AFC $\phi_{\alpha\beta}(\ell\ell')$ becomes

$$\phi_{\alpha\beta}(\ell\ell') + \eta \sum_{\ell''\gamma} \phi_{\alpha\beta\gamma}(\ell\ell'\ell'')r_{\gamma}(\ell'').$$

The change in frequency of the mode λ is therefore obtained from Eq. (III-A1) as:

$$2m\omega(\lambda)\Delta\omega(\lambda) = \eta \sum_{\alpha\beta} e_{\alpha}(\lambda)e_{\beta}(\lambda) \sum_{\substack{\ell'\neq\ell \\ \ell''\ \gamma}} \phi_{\alpha\beta\gamma}(\ell\ell'\ell'')r_{\gamma}(\ell'')[\exp\{i\underline{q}\cdot\underline{r}(\ell'\ell)\}-1] \tag{III-A2}$$

The Grüneisen parameter for the mode, given by

$$\gamma(\lambda) = \frac{d\ \ell n\ \omega(\lambda)}{d\ \ell n\ \ V} = -\frac{a}{3\omega(\lambda)}\frac{d\omega(\lambda)}{da} \tag{III-A3}$$

is simply obtained from Equation (III-A2).

In the absence of external stresses, the condition which determines η is that the Helmholtz free energy F be a minimum*. We write (Born and Huang 1954)

$$F = -k_B\ T\ \ell n\ Z \tag{III-A4}$$

where the partition function, Z, is a sum over all possible configurations ℓ of the system:

$$Z = \sum_{\ell} \exp(-E_{\ell}/k_B T)$$

In the harmonic approximation, the energy of configuration E_{ℓ} is the sum of two terms,

---

*Throughout this thesis the term "free energy" signifies the Helmholtz free energy, and is denoted by F.

$$E_\ell = \Phi_o + \sum_\lambda [n(\lambda)+\tfrac{1}{2}]\hbar\omega(\lambda), \qquad \text{(III-A5)}$$

where $\Phi_o \equiv \Phi(\underline{R})|_o$. A particular configuration ℓ may be expressed as a set of occupation numbers $n(\lambda)$, and therefore we obtain

$$Z = \exp(-\Phi_o/k_BT)\prod_\lambda \sum_{n=0}^{\infty} \exp\{-[n(\lambda)+\tfrac{1}{2}]\hbar\omega(\lambda)/k_BT\}$$

which gives after some manipulations

$$F = \Phi_o + k_BT \sum_\lambda \ell n[2 \sinh x(\lambda)], \qquad \text{(III-A6)}$$

where

$$x(\lambda) = \hbar\omega(\lambda)/2k_BT \qquad \text{(III-A7)}$$

Furthermore the entropy is

$$S = -\frac{\partial F}{\partial T} = k_B \sum_\lambda \{x(\lambda)\coth x(\lambda) - \ell n[2 \sinh x(\lambda)]\}, \qquad \text{(III-A8)}$$

the heat capacity is

$$C_v = T \left.\frac{\partial S}{\partial T}\right|_v = k_B \sum_\lambda \{x^2(\lambda)\text{cosech}^2\, x(\lambda)\}, \qquad \text{(III-A9)}$$

and the internal energy is

$$E=F+TS = \Phi_o + k_BT \sum_\lambda x(\lambda)\coth x(\lambda) = \Phi_o + \sum_\lambda \hbar\omega(\lambda)[\bar{n}(\lambda)+\tfrac{1}{2}], \qquad \text{(III-A10)}$$

where $\bar{n}(\lambda)$ is the Bose-Einstein population factor*,

$$\bar{n}(\lambda) = \{\exp[\hbar\omega(\lambda)/k_BT] - 1\}^{-1}.$$

---

*Note that elsewhere in this thesis the Bose-Einstein population factor is simply denoted by $n(\lambda)$ or $n(\underline{q}j)$.

The derivative of F with respect to thermal strain η is, to lowest order (Ludwig 1967):

$$\frac{\partial F}{\partial \eta} = \frac{\partial \Phi_o}{\partial \eta} + \sum_\lambda \left(\frac{\partial F}{\partial \omega(\lambda)}\right)\left(\frac{\partial \omega(\lambda)}{\partial \eta}\right) . \qquad \text{(III-A11)}$$

The second term may be written in terms of Grüneisen parameters $\gamma(\lambda)$. The change in Φ_o with thermal strain is related to its change with mechanical strain, and for cubic crystals the appropriate equation is

$$\frac{\partial \Phi_o}{\partial \eta} = 3BV\eta ,$$

where B is the bulk modulus. We now put $\partial F/\partial \eta$ equal to zero, to obtain

$$3BV\eta - \frac{1}{2}\sum_\lambda \hbar\omega(\lambda)\coth x(\lambda)\gamma(\lambda) = 0 \qquad \text{(III-A12)}$$

Comparing Eqs. (III-A10) and (III-A12) we see that

$$\eta = \frac{1}{3VB}\sum_\lambda E(\lambda)\gamma(\lambda) \qquad \text{(III-A13)}$$

and the thermal expansion coefficient, $\alpha = d\eta/dT$, is given by

$$\alpha = \frac{1}{3VB}\sum_\lambda C(\lambda)\gamma(\lambda) . \qquad \text{(III-A14)}$$

In these expressions $E(\lambda)$ and $C(\lambda)$ are respectively the energy and heat capacity of the mode λ.

Various measured thermodynamic quantities (e.g., heat capacity, Debye-Waller factor) are sometimes expressed in terms of equivalent Debye temperatures θ (see Barron et al. (1966),

§4.1, for a helpful discussion). The corresponding frequency $\omega = k_B\theta/\hbar$ defines the cutoff of the Debye frequency distribution which correctly predicts the thermodynamic quantity. If the actual frequency distribution were a Debye distribution, θ would be independent of temperature T, and the same for every property. In practice θ varies with T and depends on the property.

In the limits of low and high temperature, various Debye temperatures may be written as expansions involving Debye frequencies $\omega_D(n)$: these are defined as the cutoff of the Debye distribution which has the same n'th moment as the true distribution. For example the leading term in the high temperature expansion for $\theta^c(T)$, the Debye temperature characteristic of the heat capacity, is

$$\lim_{T\to\infty} \theta^c(T) = \hbar\omega_D(2)/k_B$$

It is sometimes desirable to correct Debye θ's for the effect of thermal expansion, in order to facilitate comparison with theory. The corrections involve bulk Grüneisen parameters $\gamma(n)$, which are defined by

$$\gamma(n) = \frac{\sum_\lambda \gamma(\lambda)\omega^n(\lambda)}{\sum_\lambda \omega^n(\lambda)} \qquad \text{(III-A15)}$$

For example high temperature values of $\theta^c(V,T)$ may be corrected to the fixed volume V_o by writing (Barron et al. 1964)

$$\frac{\theta^c(V_o,T)}{\theta^c(V, T)} = (\frac{V}{V_o})^{\gamma(2)}$$

We now have two types of Grüneisen parameter, $\gamma(\lambda)$ and $\gamma(n)$, in addition to the well known thermodynamic function $\gamma(V,T)$ which is given by

$$\gamma(V,T) = \frac{3\alpha VB_T}{C_v} = \frac{3\alpha VB_S}{C_p} \qquad \text{(III-A16)}$$

where B_T and B_S are the isothermal and adiabatic bulk moduli, and C_v and C_p are heat capacities at constant volume and constant pressure respectively.

Clearly a calculation of the mode γ's can give important information about the quasiharmonic corrections to physical quantities. Such a calculation is presented in Section IIIC.

(iii) Intrinsic Anharmonicity

There are several indications that the correction for thermal expansion, outlined above, is not always sufficient to account for differences between experimental measurements and the appropriate harmonic theory.

For example, an analysis by Newsham (1966) of heat capacity data for silicon and germanium shows that , at high temperatures, there is an extra contribution to the heat capacity, of the form AT, with $A \sim 3 \times 10^{-4}$ cals/°K^2/gm atom; this is attributed to anharmonicity. Furthermore, measurements of the elastic constants of several materials

(Cu, Al, CuZn, KCl and NaCl), as a function of both temperature and pressure, enabled Lazarus (1949) to calculate the intrinsic temperature dependence (i.e. the temperature dependence at constant volume) of the elastic constants. It was found comparable to the temperature dependence at constant pressure: in the quasiharmonic approximation there is no intrinsic dependence on temperature.

We shall see below that anharmonicity introduces interactions between the previously independent normal modes of a crystal. These interactions largely account for thermal resistivity; furthermore, finite phonon lifetimes, which result from phonon-phonon interactions, show up as an increase in the natural width of a phonon with temperature, first observed in aluminium by Larsson et al. (1961) and in lead by Brockhouse et al. (1961).

A useful qualitative discussion of anharmonicity has been given by Barron (1965a). Let us consider the potential energy of a system, and write it as

$$\phi = \phi_o + \phi_1 + \phi_2 + \phi_3 + \phi_4 + \dots \qquad \text{(III-A17)}$$

The terms in this equation bear a one-to-one correspondence to the terms in Eq. (I-C1). The term ϕ_1 vanishes (Section IC), and in the harmonic approximation terms beyond ϕ_2 are neglected: the normal mode frequencies are determined by the coefficients $\phi_{\alpha\beta}(\ell\ell')$, which enter ϕ_2. To allow for thermal expansion we go to the quasiharmonic approximation, which gives shifts in the normal mode frequencies in terms of ϕ_3.

To the next order in (u/r) (the ratio of a vibrational amplitude to the interatomic spacing), there are terms in $|\phi_3|^2$ and in ϕ_4. These are the terms which concern us here. When they are included, the normal modes are no longer independent. Instead they have finite lifetimes, and in general a shift in frequency will occur. Because ϕ_2, ϕ_3 and ϕ_4 are functions of the (temperature dependent) amplitudes, the widths and shifts will also be dependent on temperature.

Maradudin and Fein (1962) have shown that the delta functions in Eq. (I-D11) become "pseudo-Lorentzian" functions, when anharmonic interactions are introduced:

$$\pi\delta[\Omega\pm\omega(\lambda)] \rightarrow \frac{\Gamma(\lambda,\Omega)}{[\Omega\pm\{\omega(\lambda)+\Delta(\lambda,\Omega)\}]^2+\Gamma^2(\lambda,\Omega)} \qquad \text{(III-A18)}$$

Here, and in later equations, Ω denotes the energy transfer. The shift Δ and width Γ are seen to be functions of Ω, so that the line shape can have structure. However, if Δ and Γ are small compared with ω, as is often the case, the line shape is approximately Lorentzian. The half width at half height is then Γ, and the shift of the peak is Δ.

A variety of techniques has been employed to study anharmonic effects in solids. Cowley (1963,1968) gives references to much of the earlier work. The mathematics is long and involved, and will not be reproduced here. Instead we shall very briefly examine the differences between the harmonic and the anharmonic derivations of the scattering cross section.

In both cases the starting point is Van Hove's equation (I-D4). The displacements are written in terms of phonon operators, using Eq. (I-C24), and a time independent Debye-Waller factor is then separated out. The anharmonic Debye-Waller factor (Maradudin and Flinn 1963) retains terms to all powers of u^2. A one phonon scattering cross section, which may be defined as the contribution to $S(\underline{Q},\omega)$ proportional to Q^2, is then written as

$$S_1(\underline{Q},\omega) = \frac{2\pi^2 N\hbar}{Vm} \exp[-2W] \sum_{\lambda} \frac{[\underline{Q}\cdot\underline{e}(\lambda)]^2}{\omega(\lambda)} \Delta(\underline{Q}-\underline{q}) J(\Omega) \qquad \text{(III-A19)}$$

where the spectral function $J(\Omega)$ is

$$J(\Omega) = \int_{-\infty}^{\infty} \exp(i\Omega t) \langle\langle A(\lambda,t)A(-\lambda,0)\rangle\rangle dt \qquad \text{(III-A20)}$$

In the harmonic approximation the spectral function is simply obtained because the only time dependence in $A(\lambda,t)$ is of the form $\exp(i\omega t)$. It is given below in Eq. (III-A29).

The anharmonic case is quite different. The modes are no longer independent of each other, and the displacement of an atom, due to a particular mode, is no longer a simple periodic function of time. On the other hand the probability of creation or annihilation of a phonon is essentially independent of time: that is, the phonon operators are not functions of time. In the present treatment, however, we regard the modes as non interacting, so that the operators assume a complicated time dependent form. This is the Heisenberg picture. The advantage of this approach is that normal mode frequencies and eigenvectors, determined using a harmonic model, may be inserted into the final anharmonic expressions.

The evaluation of the spectral function, $J(\Omega)$, for an anharmonic crystal, is a formidable task. Cowley (1963) shows that it may be written as

$$J(\Omega)=[1-\exp(-\hbar\Omega/k_BT)]^{-1}\frac{8\omega^2(\lambda)\Gamma(\lambda,\Omega)}{[\omega^2(\lambda)-\Omega^2+2\omega(\lambda)\Delta(\lambda,\Omega)]^2+4\omega^2(\lambda)\Gamma^2(\lambda,\Omega)} \qquad \text{(III-A21)}$$

and that, to lowest non-vanishing order, the function $\Delta(\lambda,\Omega)$ is given by

$$\Delta(\lambda,\Omega) = \Delta_T(\lambda) + \Delta_3(\lambda,\Omega) + \Delta_4(\lambda) \ , \qquad \text{(III-A22)}$$

where the thermal shift $\Delta_T(\lambda)$ has already been given,

$$\Delta_3(\lambda,\Omega) = -\frac{18}{\hbar^2}\sum_{\lambda_1,\lambda_2} |V(\lambda,\lambda_1,\lambda_2)|^2 R(\Omega) \ , \qquad \text{(III-A23)}$$

$$\Delta_4(\lambda) = \frac{12}{\hbar}\sum_{\lambda_1} V(\lambda,-\lambda,\lambda_1,-\lambda_1)(2n_1+1), \qquad \text{(III-A24)}$$

and $\Gamma(\lambda,\Omega)$ is given by

$$\Gamma(\lambda,\Omega) = \frac{18\pi}{\hbar^2}\sum_{\lambda_1\lambda_2} V(\lambda,\lambda_1,\lambda_2)|^2 S(\Omega) \qquad \text{(III-A25)}$$

with

$$R(\Omega) = (n_1+n_2+1)[(\omega_1+\omega_2+\Omega)_p^{-1} + (\omega_1+\omega_2-\Omega)_p^{-1}]$$

$$+ (n_2-n_1)[(\omega_1-\omega_2-\Omega)_p^{-1} + (\omega_1-\omega_2+\Omega)_p^{-1}] \qquad \text{(III-A26)}$$

and

$$S(\Omega) = (n_1+n_2+1)[\delta(\omega_1+\omega_2-\Omega)-\delta(\omega_1+\omega_2+\Omega)]$$
$$- (n_2-n_1)[\delta(\omega_1-\omega_2-\Omega)-\delta(\omega_1-\omega_2+\Omega)]. \qquad \text{(III-A27)}$$

In the above expressions n_i and ω_i refer to the mode λ_i, and the subscript p indicates the principal value. The coefficients $V(\lambda,\lambda_1,\lambda_2)$ and $V(\lambda,-\lambda,\lambda_1,-\lambda_1)$ are explained in Section IIIB.

Note that there is only one contribution to Γ, and that the cubic terms (Δ_3 and Γ) are functions of Ω, whereas the quartic shift (Δ_4) is not. More generally Δ_3, Γ and Δ_4 are functions of $\lambda = (\underset{\sim}{q}j)$ and $\lambda' = (\underset{\sim}{q}, j')$: wave vector is conserved, but the polarization of the mode may be altered by the anharmonic interaction. However the off diagonal contributions, such as $\Delta_3(\lambda\lambda',\Omega)$, with $\lambda'\neq\lambda$, are identically zero for the symmetry directions which we shall consider (see e.g. Buyers and Cowley 1969).

In the harmonic approximation Δ and Γ vanish. Using the representation

$$\delta(x) = \frac{1}{\pi} \lim_{\varepsilon\to 0} \left[\frac{\varepsilon}{x^2+\varepsilon^2}\right], \qquad \text{(III-A28)}$$

we find that

$$J_{HAR}(\Omega) = [1-\exp(-\hbar\Omega/k_BT)]^{-1} 4\omega(\lambda)\pi\delta[\omega^2(\lambda)-\Omega^2]$$
$$= 2\pi\{[n(\lambda)+1]\delta[\omega(\lambda)-\Omega]+n(\lambda)\delta[\omega(\lambda)+\Omega]\}. \qquad \text{(III-A29)}$$

Substituting Eq. (III-A29) into Eq. (III-A19), we get back the harmonic expression, Eq. (I-D11).

Calculations of cubic shifts and widths, and quartic shifts, are reported in Section IIIC. We now pass to a consideration of the thermodynamic properties of an anharmonic crystal.

(iv) Effective Frequency Distributions

In the harmonic approximation, various thermodynamic properties of a system (such as the free energy and the entropy) may be expressed as a sum of individual contributions from each normal mode (see e.g. Eqs. III-A6, III-A8). In each of these expressions the summand only depends on ($\underline{q}j$) through the frequency of the mode. The thermodynamic properties may therefore be written:

$$F = \Phi_o + k_B T \int \ell n[2 \sinh \frac{\hbar\omega}{2k_B T}] g(\omega) d\omega \qquad \text{(III-A30)}$$

$$S = k_B \int [\frac{\hbar\omega}{2k_B T} \coth \frac{\hbar\omega}{2k_B T} - \ell n(2 \sinh \frac{\hbar\omega}{2k_B T})] g(\omega) d\omega \qquad \text{(III-A31)}$$

where the frequency distribution is normalized to 3N, and N is the number of atoms in the solid.

The above expressions are valid in the quasiharmonic approximation, in which case the frequency distribution, $g(\omega)$, is volume dependent.

Anharmonic contributions to thermodynamic properties may be calculated using perturbation theory. The principal contributions to the free energy are (Leibfried and Ludwig 1961)

$$\Delta F_3 = -\frac{6}{\hbar} \sum_{\lambda_1\lambda_2\lambda_3} |V(\lambda_1\lambda_2\lambda_3)|^2 N_3(\omega_1\omega_2\omega_3) \qquad \text{(III-A32)}$$

$$\Delta F_4 = 3 \sum_{\lambda_1\lambda_2} V(\lambda_1,-\lambda_1,\lambda_2,-\lambda_2) N_4(\omega_1\omega_2) \qquad \text{(III-A33)}$$

where

$$N_3(\omega_1\omega_2\omega_3) = \frac{(n_1+1)(n_2+n_3+1)+n_2n_3}{\omega_1+\omega_2+\omega_3} + 3\,\frac{n_1(n_2+n_3+1)-n_2n_3}{-\omega_1+\omega_2+\omega_3} \qquad \text{(III-A34)}$$

and

$$N_4(\omega_1\omega_2) = (2n_1+1)(2n_2+1). \qquad \text{(III-A35)}$$

Anharmonic contributions to the entropy and to the heat capacity are obtained by differentiating the above expressions with respect to temperature.

Comparing Eqs. (III-A24) and (III-A33), we have

$$\Delta F_4 = \frac{\hbar}{4} \sum_{\lambda} (2n+1)\Delta_4(\lambda). \qquad \text{(III-A36)}$$

Cowley (1963) states that, "after some manipulation" an exactly similar expression may be obtained for ΔF_3 in terms of $\Delta_3(\lambda) \equiv \Delta_3(\lambda,\omega)$. Overton (1968) has shown how to obtain this result.

By differentiating Eq. (III-A30) we may obtain an expression for the change in free energy ΔF resulting from changes $\Delta(\lambda)$ in the normal mode frequencies:

$$\Delta F = \frac{1}{2} \sum_{\lambda} \coth x(\lambda)\, \hbar\Delta(\lambda) = \frac{\hbar}{2} \sum_{\lambda} (2n+1)\Delta(\lambda) \qquad \text{(III-A37)}$$

This equation correctly gives the change in the free energy resulting from thermal expansion, with $\Delta(\lambda)$ denoting the corresponding change in frequency of the mode λ. However the change in free energy resulting from anharmonicity is only predicted correctly by Eq. (III-A37) when $\Delta(\lambda)$ is replaced by $\frac{1}{2}[\Delta_3(\lambda)+\Delta_4(\lambda)]$, rather than by $[\Delta_3(\lambda)+\Delta_4(\lambda)]$.

The quasiharmonic phonon density of states

$$g^{qh}(\omega) = \sum_\lambda \delta[\omega^{qh}(\lambda)-\omega] \qquad \text{(III-A38)}$$

is simply corrected for anharmonicity by writing

$$g(\omega) = \sum_\lambda \delta[\omega^{qh}(\lambda)+\Delta_3(\lambda)+\Delta_4(\lambda)-\omega]. \qquad \text{(III-A39)}$$

If this expression is substituted into Eq. (III-A30), the anharmonic contribution to F is too large by a factor of two. In order to obtain the correct anharmonic free energy, we must use the following "effective frequency distribution for the free energy":

$$g^F(\omega) = \sum_\lambda \delta[\omega^{qh}(\lambda)+\frac{1}{2}(\Delta_3(\lambda)+\Delta_4(\lambda))-\omega] \qquad \text{(III-A40)}$$

The quartic anharmonic entropy is obtained as

$$\Delta S_4 = - \left.\frac{\partial \Delta F_4}{\partial T}\right|_V$$

$$= - 6 \sum_{\lambda_1\lambda_2} V(\lambda_1,-\lambda_1,\lambda_2,-\lambda_2)(2n_1+1) \frac{2dn_2}{dT}$$

$$= - \hbar \sum_\lambda \frac{dn}{dT} \Delta_4(\lambda) \ . \qquad \text{(III-A41)}$$

We see that the quantity $(S^{qh}+\Delta S_4)$ is correctly predicted by substituting $(\omega^{qh}+\Delta_4)$ for ω in Eq. (III-A31) for the entropy; this is also true of the cubic anharmonic term ΔS_3 (Barron 1965b). Thus the "effective frequency distribution for the entropy" is simply

$$g^S(\omega) = g(\omega).$$

The situation regarding the heat capacity is somewhat more complicated. We shall return to this subject in our discussion of thermodynamic properties in Section IIID.

B. THE ANHARMONIC POTENTIAL

(i) Definition

In the previous section, the quantities $V(\lambda,\lambda_1,\lambda_2)$ and $V(\lambda,-\lambda,\lambda_1,-\lambda_1)$ were introduced. They are related to the third and fourth derivatives of the real space potential in the following manner.

The first two anharmonic terms in the expansion of the total potential energy, Eq. (I-C1), are

$$\Phi_3 = \frac{1}{6} \sum_{\substack{\ell\ \alpha \\ \ell'\beta \\ \ell''\gamma}} \phi_{\alpha\beta\gamma}(\ell\ell'\ell'')u_\alpha(\ell)u_\beta(\ell')u_\gamma(\ell'')$$

$$\Phi_4 = \frac{1}{24} \sum_{\substack{\ell\ \ \alpha \\ \ell'\ \ \beta \\ \ell''\ \ \gamma \\ \ell'''\sigma}} \phi_{\alpha\beta\gamma\sigma}(\ell\ell'\ell''\ell''')u_\alpha(\ell)u_\beta(\ell')u_\gamma(\ell'')u_\sigma(\ell''')$$

Writing $u_\alpha(\ell)$ in terms of phonon operators (Eq. I-C24), we obtain

$$\Phi_3 = \sum_{\lambda_1\lambda_2\lambda_3} V(\lambda_1\lambda_2\lambda_3)A(\lambda_1)A(\lambda_2)A(\lambda_3)$$

$$\Phi_4 = \sum_{\lambda_1\lambda_2\lambda_3\lambda_4} V(\lambda_1\lambda_2\lambda_3\lambda_4)A(\lambda_1)A(\lambda_2)A(\lambda_3)A(\lambda_4),$$

where

$$V(\lambda_1\lambda_2\lambda_3) = \frac{1}{6}\left\{\frac{\hbar^3}{8\omega_1\omega_2\omega_3N^3m^3}\right\}^{\frac{1}{2}} \sum_{\substack{\ell\ell'\ell'' \\ \alpha\beta\gamma}} \phi_{\alpha\beta\gamma}(\ell\ell'\ell'')$$

$$\times\ e_\alpha(\lambda_1)e_\beta(\lambda_2)e_\gamma(\lambda_3)\exp\{i[\underline{q}_1\cdot\underline{r}(\ell)+\underline{q}_2\cdot\underline{r}(\ell')$$

$$+\ \underline{q}_3\cdot\underline{r}(\ell'')]\}\Delta(\underline{q}_1+\underline{q}_2+\underline{q}_3) \qquad \text{(III-B1)}$$

and

$$V(\lambda_1\lambda_2\lambda_3\lambda_4) = \frac{1}{24}\left\{\frac{\hbar^4}{16\omega_1\omega_2\omega_3\omega_4 N^4 m^4}\right\}^{\frac{1}{2}} \sum_{\substack{\ell\ell'\ell''\ell'''\\ \alpha\beta\gamma\sigma}}$$

$$\times\ \phi_{\alpha\beta\gamma\sigma}(\ell\ell'\ell''\ell''')e_\alpha(\lambda_1)e_\beta(\lambda_2)e_\gamma(\lambda_3)e_\sigma(\lambda_4)$$

$$\times\ \exp\{i[\underline{q}_1\cdot\underline{r}(\ell)+\underline{q}_2\cdot\underline{r}(\ell')+\underline{q}_3\cdot\underline{r}(\ell'')+\underline{q}_4\cdot\underline{r}(\ell''')]\}$$

$$\times\ \Delta(\underline{q}_1+\underline{q}_2+\underline{q}_3+\underline{q}_4)\,. \qquad \text{(III-B2)}$$

In both the above expressions, the sum over ℓ may be simply replaced by an additional factor N multiplying the right hand side. Note too that we are only interested in $V(\lambda_1,-\lambda_1,\lambda_2,-\lambda_2)$ so that the Δ function in the second expression is automatically satisfied.

In the previous section expressions were given for the principal contributions to the shift and width of a mode resulting from anharmonicity. These expressions contain the anharmonic force constants $\phi_{\alpha\beta\gamma}(\ell\ell'\ell'')$ and $\phi_{\alpha\beta\gamma\sigma}(\ell\ell'\ell''\ell''')$. In the remainder of this section we describe several methods which have been used to estimate these quantities.

(ii) Estimates of the Anharmonic Atomic Force Constants

We assume a two body central potential V(r). The AAFC's are related to the derivatives of this potential (see Eq. AIV-1). In this work we perform calculations out to second nearest neighbours, so that we are interested in knowing the values of V_i''' and V_i'''' for i = 1 and 2, where i denotes the shell of neighbours. It seems reasonable to work with only first and second neighbours, since we have already seen that the harmonic frequencies are well fitted by considering forces out to third or fourth neighbours.

(a) Volume Dependence of the Elastic Constants

Probably the most direct experimental information concerning the third derivatives of the interatomic potential in rubidium comes from experimental measurements of the elastic constants as a function of pressure. Pauer (1968) measured the change in the transit time of an ultrasonic pulse with pressure for the three modes propagating in the [110] direction at 195°K. Using the relation

$$\gamma_i = -B_T d(\ell n t)/dP, \qquad \text{(III-B3)}$$

where γ_i is the long wavelength limit of the Grüneisen parameter of the mode i, and B_T is the isothermal bulk modulus, which Pauer gives as 26.3 kbar at 195°K, he obtained

$$\begin{aligned} \gamma(L) &= 1.37 \pm 0.04 \\ \gamma(T2) &= 1.06 \pm 0.01 \\ \gamma(T1) &= 1.20 \pm 0.04 \end{aligned} \qquad \text{(III-B4)}$$

For a central force model we may relate these quantities to the first three derivatives of the potential, in the following way. We first write

$$m\omega^2(\underset{\sim}{q}) = \sum_n \Phi_n[1-\cos(n\pi q/q_{max})]$$

where Φ_n are interplanar force constants. These may be expressed in terms of AFC's (Brockhouse et al. 1968b), and hence in terms of the derivatives V_i', V_i''. For very small q, we obtain, considering first and second neighbours only,

$$\omega_L^2 = \frac{\pi^2 q^2}{2mq_{max}^2} \{\frac{4V_1'}{3r_1} + \frac{8}{3} V_1'' + \frac{2}{r_2} V_2' + 2V_2''\} \qquad \text{(III-B5a)}$$

$$\omega_{T2}^2 = \frac{\pi^2 q^2}{2mq_{max}^2} \{\frac{8V_1'}{3r_1} + \frac{4}{3} V_1'' + \frac{4}{r_2} V_2'\} \qquad \text{(III-B5b)}$$

$$\omega_{T1}^2 = \frac{\pi^2 q^2}{2mq_{max}^2} \{\frac{4}{r_1} V_1' + \frac{2}{r_2} V_2' + 2V_2''\} \qquad \text{(III-B5c)}$$

where $r_1 (= \sqrt{3}a/2)$, and $r_2 (=a)$, are the first and second neighbour distances respectively.

$$\text{Now} \qquad \gamma = -\frac{d\ell n\omega}{d\ell nV} = -\frac{1}{6}\frac{d(\ell n\omega^2)}{da}$$

so that (after some manipulations) we have

$$\gamma_L = -\frac{[(4r_1/3)V_1''' + r_2V_2''' + 2\beta_1 + \alpha_2 - \beta_2]}{6[2\alpha_1 + 2\beta_1 + \alpha_2 + \beta_2]} \qquad \text{(III-B6a)}$$

$$\gamma_{T2} = -\frac{[(4r_1/3)V_1''' + 8\beta_1 + 4\alpha_2 - 4\beta_2]}{24[\alpha_1 + \beta_2]} \qquad \text{(III-B6b)}$$

$$\gamma_{T1} = -\frac{[r_2V_2''' + 6\beta_1 + \alpha_2 - \beta_2]}{6[2\alpha_1 - 2\beta_1 + \alpha_2 + \beta_2]} \qquad \text{(III-B6c)}$$

Using the 12°K and 120°K AFC's given in Table II-4, the following values are respectively obtained:

from Eq. (III-B6b)

$(4r_1/3)V_1''' = (-25380\pm170)$ and (-23730 ± 150) dynes/cm.

from Eq. (III-B6c)

$$r_2V_2^{'''} = (-6410\pm45) \text{ and } (-6490\pm55) \text{ dynes/cm.}$$

from Eq. (III-B6a)

$$(4r_1/3)V_1^{'''} + r_2V_2^{'''} = (-31800\pm210) \text{ and } (-30200\pm210) \text{ dynes/cm.}$$

Though these results are not completely compatible, they give one a good idea of the sign and magnitude of the third derivatives.

In particular, note from Eq. (III-B6c) that γ_{T1} is very sensitive to $r_2V_2^{'''}$. This means that this derivative is rather well determined by this method.

It is interesting to note that the normal mode frequencies in Rb are predicted to better than 10% using a three force constant model (1XX, 1XY and 2XX nonzero), with the force constants determined from the elastic constants. This indicates that the anharmonic force constants derived above are fairly realistic. The harmonic and anharmonic force constants derived from elastic constant data are listed in Table III-1.

(b) The Morse Potential

The AFC's, which are obtained from an analysis of the phonon dispersion curves (Section IIE) may be related to the first and second derivatives of an interatomic potential (see Eq. I-C5). In order to obtain higher derivatives, the first and second derivatives, for first and second neighbours, have been fitted to a Morse potential:

$$V(r) = \varepsilon[e^{-2\alpha(r-r_o)} - 2e^{-\alpha(r-r_o)}] , \qquad \text{(III-B7)}$$

whose n'th derivative is given by

$$V^n(r) = 2(-\alpha)^n\varepsilon[2^{n-1}e^{-2\alpha(r-r_o)} - e^{-\alpha(r-r_o)}].$$

The best values of the parameters are, at 12 and 120°K respectively:

$$\alpha = 0.779 \text{ and } 0.700 \text{ Å}^{-1}$$
$$r_o = 5.256 \text{ and } 5.341 \text{ Å}$$
$$\varepsilon = 746 \text{ and } 850 \text{ ergs.} \qquad \text{(III-B8)}$$

Using these parameters, the derivatives listed in Table III-1 were obtained.

These parameters differ markedly from those obtained by Girifalco and Weizer (1959), by fitting to the energy of sublimation, the compressibility, and the lattice constant. On the other hand Bruno (1970) obtained the following values:

$$\alpha = 0.692\text{Å}^{-1}$$
$$r_o = 5.345\text{Å}$$
$$\varepsilon = 875 \text{ ergs,}$$

by fitting to the energy of vacancy formation, the compressibility, and the lattice constant. The latter values are in good agreement with those obtained by fitting to the AFC's.

The derivatives of the Morse potentials at 12 and 120°K are listed in Table III-1.

(c) Fourier Transform of the "Total Potential" in Reciprocal Space

The Fourier transform of the "total" potential $\phi(\underline{Q})$, introduced in Section IIE, is the real space potential whose first and second derivatives give the AFC's. Values for the AFC's and for the third and fourth derivatives, for three different fits to the 12°K measurements are listed in Table III-1. These quantities were obtained using a programme which was kindly made available by Dr. W.J.L. Buyers at Chalk River. The sets of values labelled 1, 2 and 3 in Table III-1 correspond to the functions shown on the left side of Fig. II-9 , with cutoffs of 1.6, 2.0 and 2.4 respectively. Clearly #2 and #3 are very similar, but #1 predicts a very different value for V_1'''' .

Blanchard (1969) analysed the dispersion curves of Rb using the method of Cowley et al. He obtained an electronic potential function $\phi^E(Q)$ which he then transformed into real space and added to the real space Coulomb potential. The derivatives of this potential* have been evaluated by numerical differentiation. They are given in Table III-1. These values are comparatively inaccurate, since V(r) was only specified at intervals of 0.2 Å. It is satisfying to note that the first and second derivatives are in reasonable agreement with those derived from the AFC analysis (Section IIE).

---

*The author is very grateful to Dr. Blanchard for sending numerical values of the real space potential.

(d) Effective Potentials Obtained from Pseudopotentials

Ho (1968) calculated phonon dispersion curves for the alkali metals using a Heine-Abarenkov pseudopotential, and a modified Hubbard function to allow for exchange and correlation effects. The parameters of his calculation were fitted to measured elastic contents. Ho also presented effective real space potentials which were obtained by Fourier transforming the pseudopotential, and adding in the Coulomb potential, e^2/r. In every case the minimum in the effective potential lies close to the second neighbour position.

Blanchard (1969) fitted the parameters of a model, based on a Bardeen (1937) pseudopotential and an exchange and correlation term of his own, to the measured frequencies for Na, K, and Rb. He then obtained interatomic potentials which are similar in shape to those of Ho (1968).

In Section IIE, calculations of phonon frequencies using a simple Ashcroft potential were reported. The two pseudopotentials which gave the best agreement with experiment have been Fourier transformed to yield interatomic potentials.

The integral we require is

$$V_e(r) = \frac{\Omega}{2\pi^2} \int_0^\infty V_e(q) q^2 \frac{\sin(qr)}{qr} dq,$$

where

$$V_e(q) = - \frac{4\pi e^2}{\Omega q^2} \cos^2(qr_A) \frac{\varepsilon(q)-1}{\varepsilon(q)} .$$

Since $V_e(q)$ dies away rapidly at large q, the function was arbitrarily set equal to zero after the second zero ($q\ r_A \geq 1.5\pi$). At very small q, $V_e(q)$ goes as $-4\pi e^2/q^2$, so that it cancels the Coulomb potential $V_c(q)$. To avoid infinities at q=0, we write

$$
\begin{aligned}
V(r) &= V_c(r) + V_e(r). \\
&= \frac{2e^2}{\pi r}\int_0^\infty \frac{\sin(qr)}{(qr)}\, d(qr) + \frac{\Omega}{2\pi^2}\int_0^\infty V_e(q)q^2\, \frac{\sin(qr)}{(qr)}\, dq \\
&= \frac{e^2}{r} - \frac{2e^2}{\pi r}\int_0^{r\Delta} \frac{\sin x}{x}\, dx + \frac{\Omega}{2\pi^2 r}\int_\Delta^{q_c} V_e(q)q\, \sin(qr)dq
\end{aligned}
$$

The first integral is simply

$$
-\frac{2e^2}{\pi r}\left(r\Delta - \frac{(r\Delta)^3}{3!3} + \ldots.\right)
$$

so that for $r\Delta \ll 1$, we need retain only the first term. The second integral was evaluated using Filon's method (Fröberg 1965). The derivatives of V(r) were subsequently obtained by numerical differentiation. They are listed in Table III-1.

(iii) <u>Choice of Values</u>

The values of r_1V_1''', r_2V_2'''', and $r_2^2V_2''''$, listed in Table III-1, show a spread of roughly ± 20%, so that the "preferred values", given at the bottom of the table, can be used with some confidence. The third derivatives, in particular r_2V_2''', were chosen to reproduce the measured long wavelength Grüneisen parameters of Pauer (1968). This is discussed in Section IIIC.

The derivative $r_1^2V_1''''$ shows considerably more spread. Neglecting values obtained from the Morse potential, which is probably the poorest of the methods described above, and the value obtained from "total potential" #1, the spread is about ±20%.

We come now to the calculation of shifts and widths, and in Section IIID to the calculation of thermodynamic properties.

TABLE III-1 The first four derivatives of the interatomic potential in rubidium for 1st and 2nd neighbours, evaluated by several different methods (see text). The units are dynes/cm throughout.

		$r_1^{-1}V_1'$	$r_2^{-1}V_2'$	V_1''	V_2''	r_1V_1'''	r_2V_2'''	$r_1^2V_1''''$	$r_2^2V_2''''$
Elastic Constants	12°K	(108)	(0)	(1783)	(354)	-19,000	-6400		
	120°K					-17,800	-6500		
Morse Potential	12°K	-130	35	2243	389	-21,600	-6450	180,000	69,000
	120°K	-124	31	2089	447	-18,200	-6200	140,000	60,000
"Total Potential"	#1	-130	51	2142	447	-13,500	-8990	21,000	60,000
	#2	-146	29	2231	388	-17,900	-7590	81,000	76,000
	#3	-145	30	2243	385	-17,900	-7510	72,000	77,000
Ashcroft Potential	#1	-155	18	2100	375	-16,500	-7200	86,000	66,000
	#2	-120	42	2150	425	-17,000	-7400	87,000	67,000
Blanchard		-133	34	2040	408	-15,000	-8000	68,000	57,000
Harmonic AFC's	12°K	-118	22	2244	397	-	-	-	-
	120°K	-122	17	2090	454	-	-	-	-
Preferred Values		-118	22	2244	397	-17,000	-6250	80,000	70,000

C. CALCULATIONS OF PHONON FREQUENCY SHIFTS AND WIDTHS

In this Section we present calculations of the effects of thermal expansion and intrinsic anharmonicity on the frequency and width of phonons in rubidium.

Equations for the various quantities have been given in Section IIIA. These expressions are very considerably simplified in Appendix IV. In that appendix, the particular case of an axially symmetric potential is considered, and the symmetry of the b.c.c. lattice is fully exploited. The final expressions obtained in Appendix IV are derived for first and second nearest neighbours.

In Section IIIB we have considered various methods of calculating the anharmonic atomic force constants. The preferred values listed in Table III-1 were used in the present calculations.

We consider first the quasiharmonic shifts, resulting from thermal expansion.

(i) Thermal Expansion

Grüneisen parameters have been calculated, for $\underline{q}$ along the five major symmetry directions in Rb. Comparing Eqs. (III-A3) and (AIV-B1) it is clear that

$$\gamma(\underline{q}j) = \frac{-1}{3m\omega^2(\underline{q}j)} \sum_{\alpha\beta\gamma} e_\alpha(\underline{q}j)\, e_\beta(\underline{q}j)\, f_{\alpha\beta\gamma}(\underline{q})$$

$$= -\frac{Ia}{3m\omega^2(\underline{q}j)}$$

where I is given by Eq. (AIV-C3). Results for the [00ζ] and [ζζ0] directions are shown in Fig. III-1. The solid lines represent values calculated using the preferred values for the third derivatives. It will be observed that the agreement between calculation and experiment (Pauer 1968), for long wavelength modes in the [ζζ0] direction, is quite good. The dotted and dashed lines indicate the effects of increasing $|r_1V_1^{'''}|$ and $|r_2V_2^{'''}|$ respectively, by 10%. Note that certain modes are only sensitive to one of these quantities. For example the [00ζ]T and the [ζζ0]T2 modes are independent of $r_2V_2^{'''}$. On the other hand the [ζζ0]T1 mode is very sensitive to this quantity (but independent of $r_1V_1^{'''}$), as was mentioned in Section IIIB. This means $r_2V_2^{'''}$ can be rather reliably obtained from the elastic constant work.

Complete results, for all five symmetry directions, are shown in Fig. III-2 as solid lines. The dashed lines represent calculations based on an Ashcroft model (Section IIE (iii)). Phonon frequencies were calculated for two volumes differing by 1%, and values of $\gamma(\underset{\sim}{q}j)$ were then trivially obtained. This procedure is related to that of Wallace (1968), who obtained his results by differentiating the dynamical matrix. The behaviour of the T1 branch in Rb is probably a result of the finite difference method of calculation which was employed with the Ashcroft potential. The present calculations compare quite well with those of Wallace (1968)

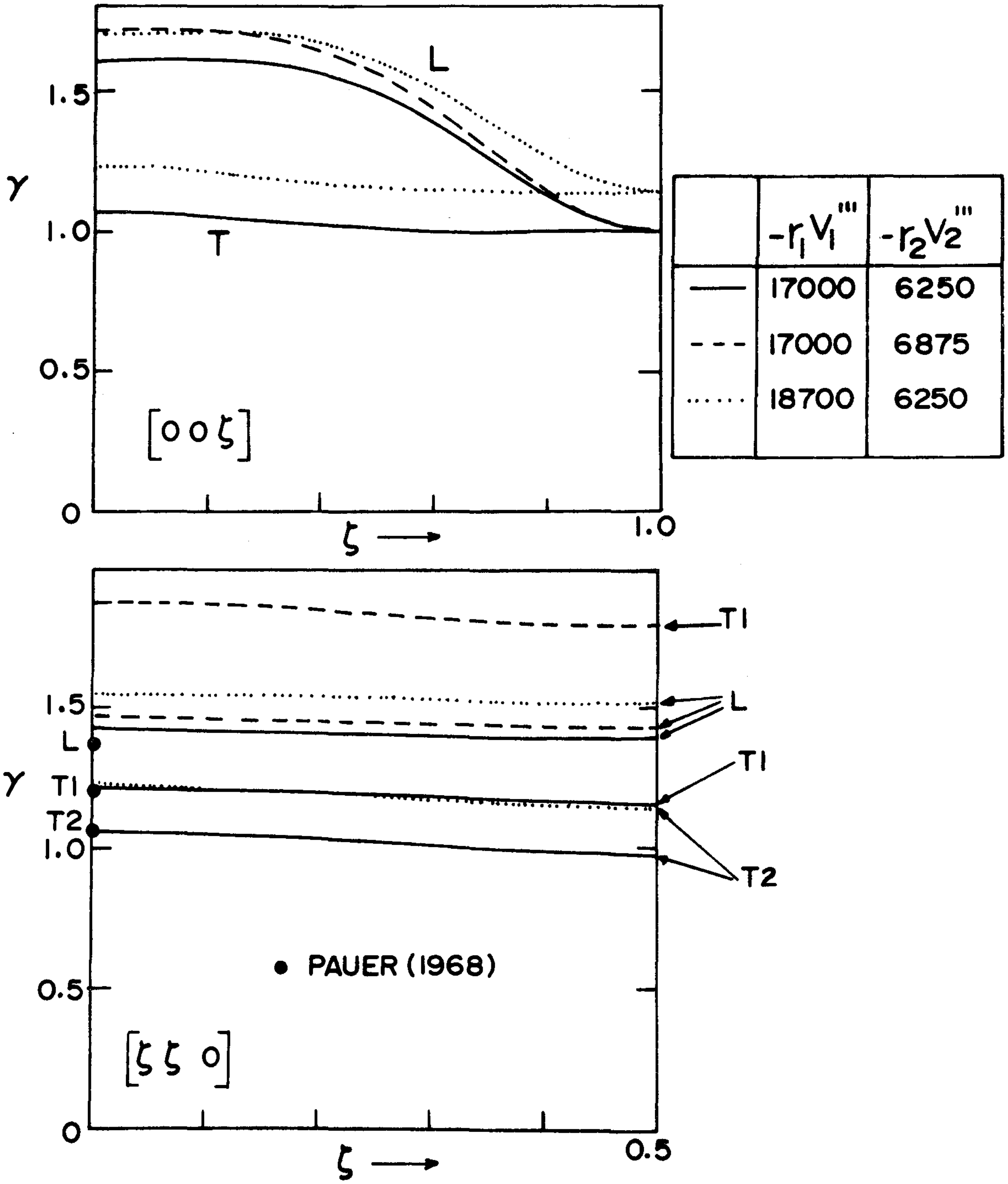

Fig. III-1. Grüneisen parameters calculated with different sets of values of V_1''' and V_2''', for two directions in rubidium.

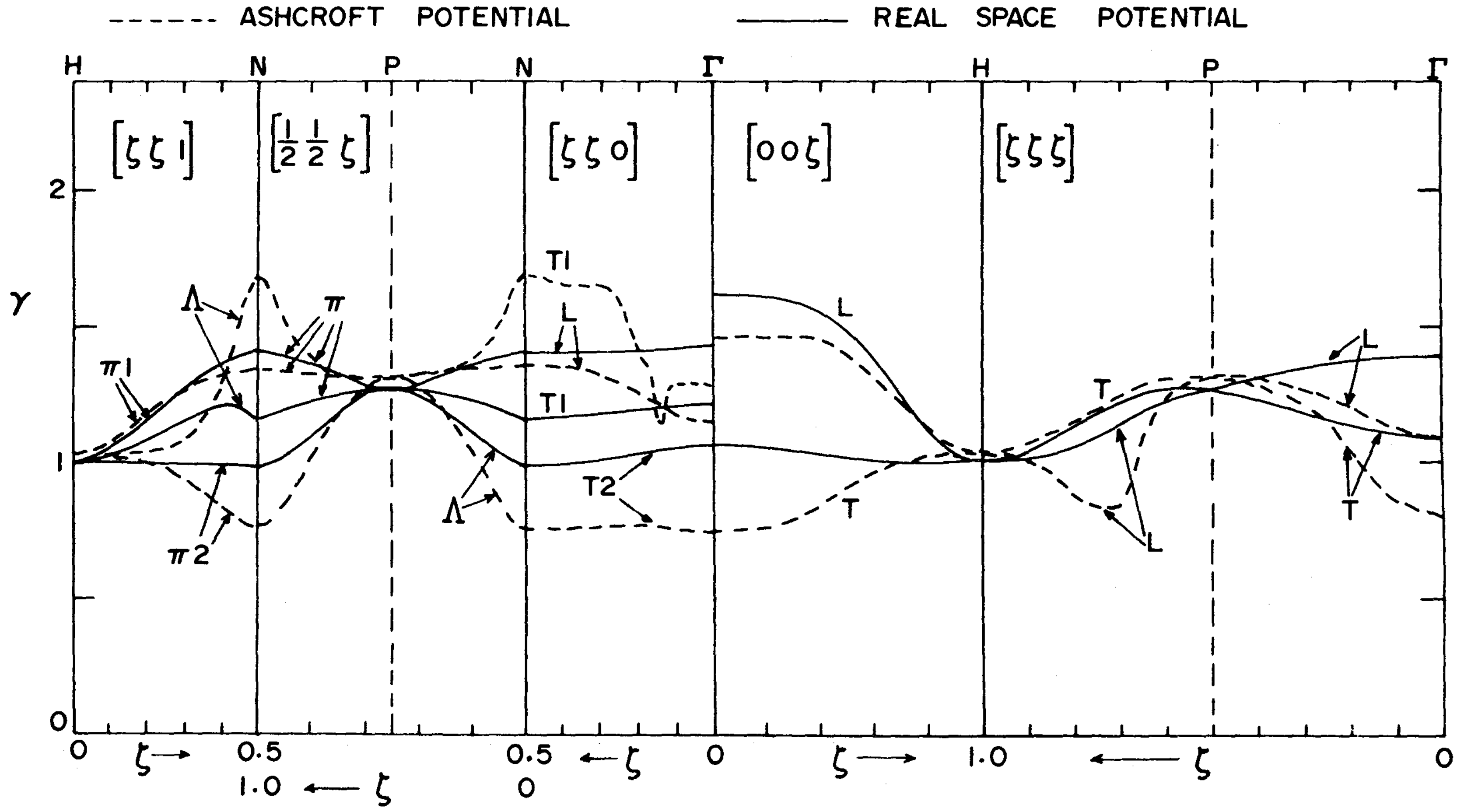

Fig. III-2. Grüneisen parameters in rubidium calculated in two different ways.

for Na and K. Coulthard (1970) has also examined the effects of volume changes in his calculations of phonons in Na, Al and Pb.

The thermal strain η, and the ratio (α/β), where β is the compressibility, are shown in Fig. III-3. These curves were obtained by summing over 14 points in the IBZ. Identical results,to within 0.2%, were obtained by summing over 70 points in the IBZ. The "experimental values", shown in Fig. III-3, were obtained by using values of α and β respectively due to Hackspill (1911) and Swenson (1955). The isothermal compressibility has been measured by Swenson (1955) (see Table II-1) and by Bridgman (1942, 1948), by static methods. Rice (1965) used the shock-wave method to obtain the adiabatic compressibility, and this quantity may also be obtained from measurements of elastic constants (Gutman and Trivisonno 1967). Ginell and Quigley (1965) analysed the work of Swenson and of Bridgman, and concluded that both sets of data are good, although some of the earlier measurements (Bridgman 1942) must be regarded with suspicion. Swenson's low temperature value was used to obtain the thermal strain curve shown in Fig. III-3.

The experimental thermal expansion coefficient is not well known. The situation has been summarized by Kelly and Pearson (1955). Early macroscopic measurements (Hackspill 1911),gave $\alpha \simeq 90 \times 10^{-6}$ °K^{-1}, but x-ray measurements favour a value nearer 66×10^{-6} °K^{-1}. In view of this large uncer-

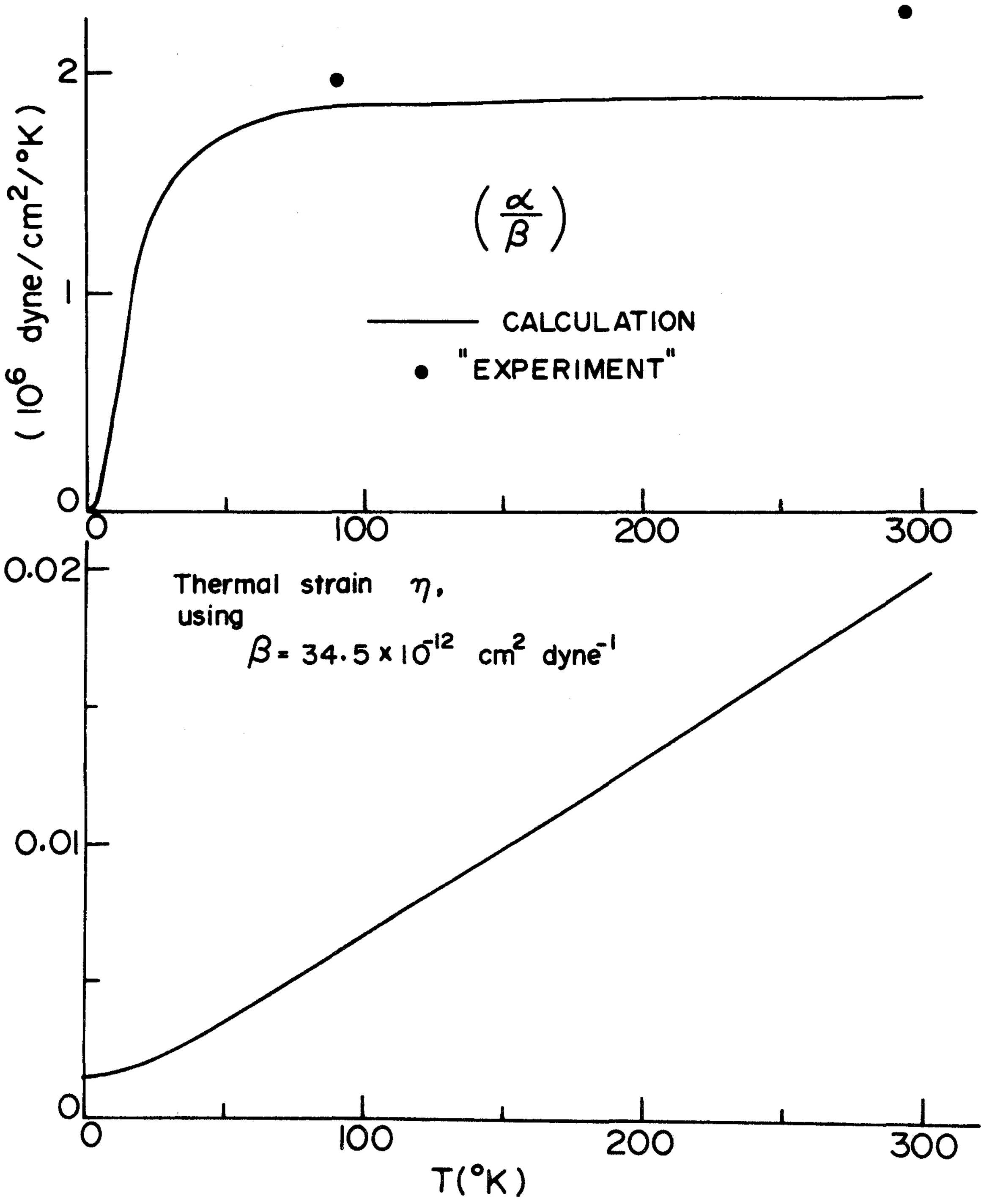

Figure III-3. The ratio of thermal expansion coefficient to compressibility, and the thermal strain.

tainty in the experimental numbers, no useful comments can be made regarding the adequacy of the present calculation of (α/β).

Thermal shifts for individual modes $(\underset{\sim}{q}j)$ are obtained from $\gamma(\underset{\sim}{q}j)$ and from the change in thermal strain with temperature. The results are discussed in a later subsection.

(ii) Quartic Shifts

The quartic shifts $\Delta_4(\lambda)$ were calculated using Eq. (AIV-C6). The sum over $\underset{\sim}{q}_2$ converged rapidly as the density of points in the IBZ was increased. Shifts calculated with 70 and 204 points in the IBZ (M_n = 10 and 15 respectively) differed by <0.5%. The results, for the three major symmetry directions, are shown in Fig. III-4. The effect of changing the fourth derivatives is also illustrated. Note that the quartic shifts for the $[\zeta\zeta 0]$T1 branch are independent of $r_1^2 V_1''''$, and for the $[00\zeta]$T and $[\zeta\zeta 0]$T2 branches the shifts are independent of $r_2^2 V_2''''$. An analogous situation was found in the case of the thermal shifts. Note in particular the strong dependence on $r_2^2 V_2''''$ of the quartic shift for the symmetry point H.

The temperature dependence of the quartic shift of the mode at H is shown in Fig. III-4. The behaviour of the other quartic shifts is similar.

Using values for the derivatives of the interatomic potential in potassium, kindly supplied by Dr. G. Dolling,

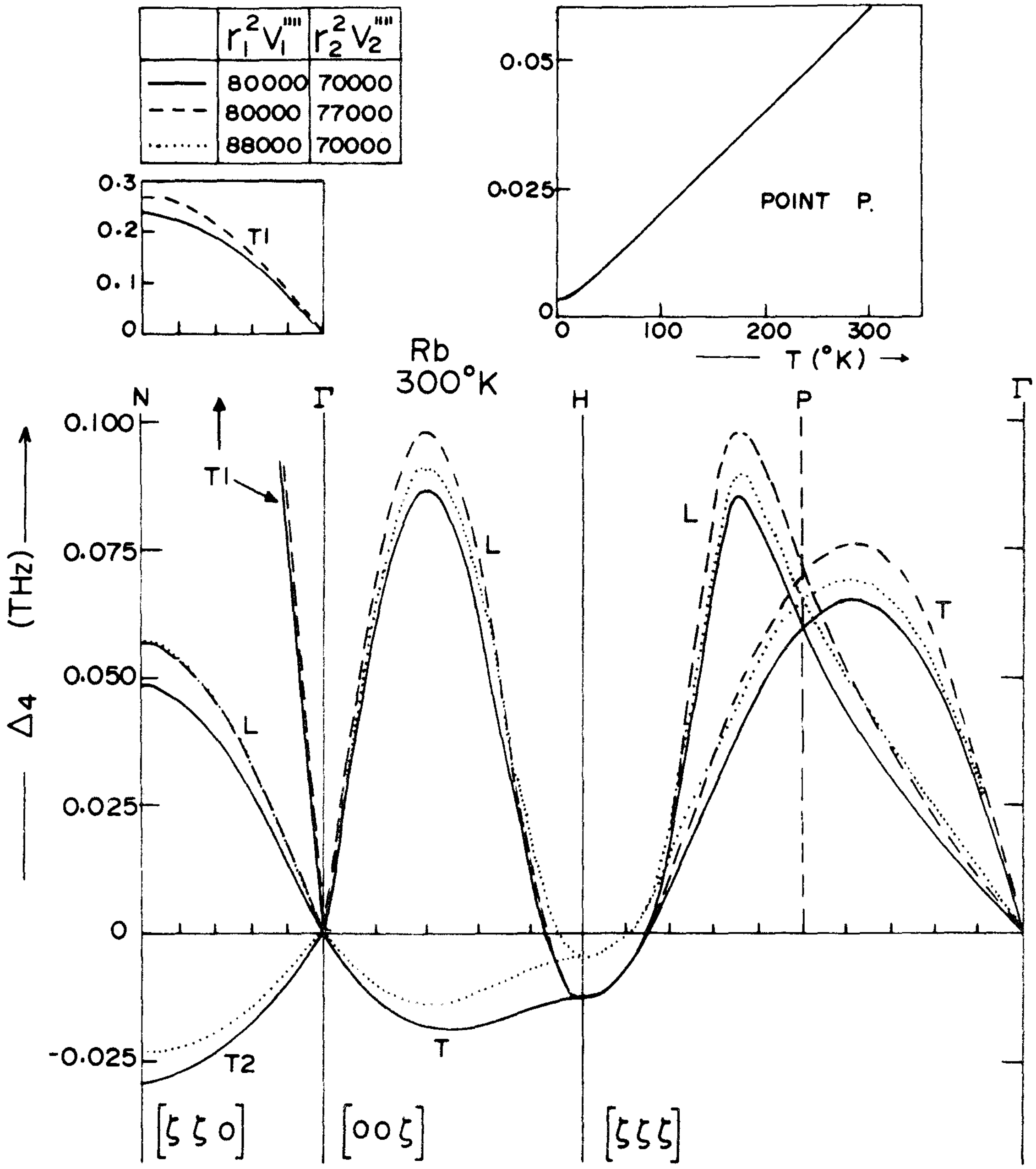

Figure III-4. Quartic shifts, calculated with different sets of values of V_1'''' and V_2''''.

quartic shifts at 299°K have been calculated and are shown in Fig. III-5. The shifts calculated by Buyers and Cowley (1969) are also shown. The present calculations used derivatives appropriate to a potential having a cutoff of 2.0, whereas Buyers and Cowley used a cutoff of 1.6. In view of this difference, the agreement between the two calculations is not bad: in particular the shape of the curves, and the signs of the shifts, are the same, with the exception of the $[\zeta\zeta 0]$L and $[\zeta\zeta\zeta]$L branches (the latter at small $\underset{\sim}{q}$). By adjusting the derivatives within reasonable limits, considerably improved agreement can be achieved. Note that very large values of $\Delta_4(\underset{\sim}{q})$ for the $[\zeta\zeta 0]$T1 branch (more than 50% of $\nu(\underset{\sim}{q})$ itself) are predicted by both the real space and the reciprocal space calculations.

(iii) Cubic Shifts and Widths

We have already noted that $\Delta_3(\lambda,\Omega)$ and $\Gamma(\lambda,\Omega)$ are considerably more complicated quantities to calculate than $\Delta_T(\lambda)$ and $\Delta_4(\lambda)$. There are several complications. In the first place, Δ_3 and Γ are functions of Ω, so that an extra "do loop" is involved in the computations. Secondly, the calculation for a general mode λ involves a sum over the whole zone, whereas Δ_4 only requires a sum over the irreducible 1/48th of the zone. In this work we restrict our attention to the high symmetry directions, in which case sums over smaller fractions of the whole zone are sufficient (Appendix IV, Section E).

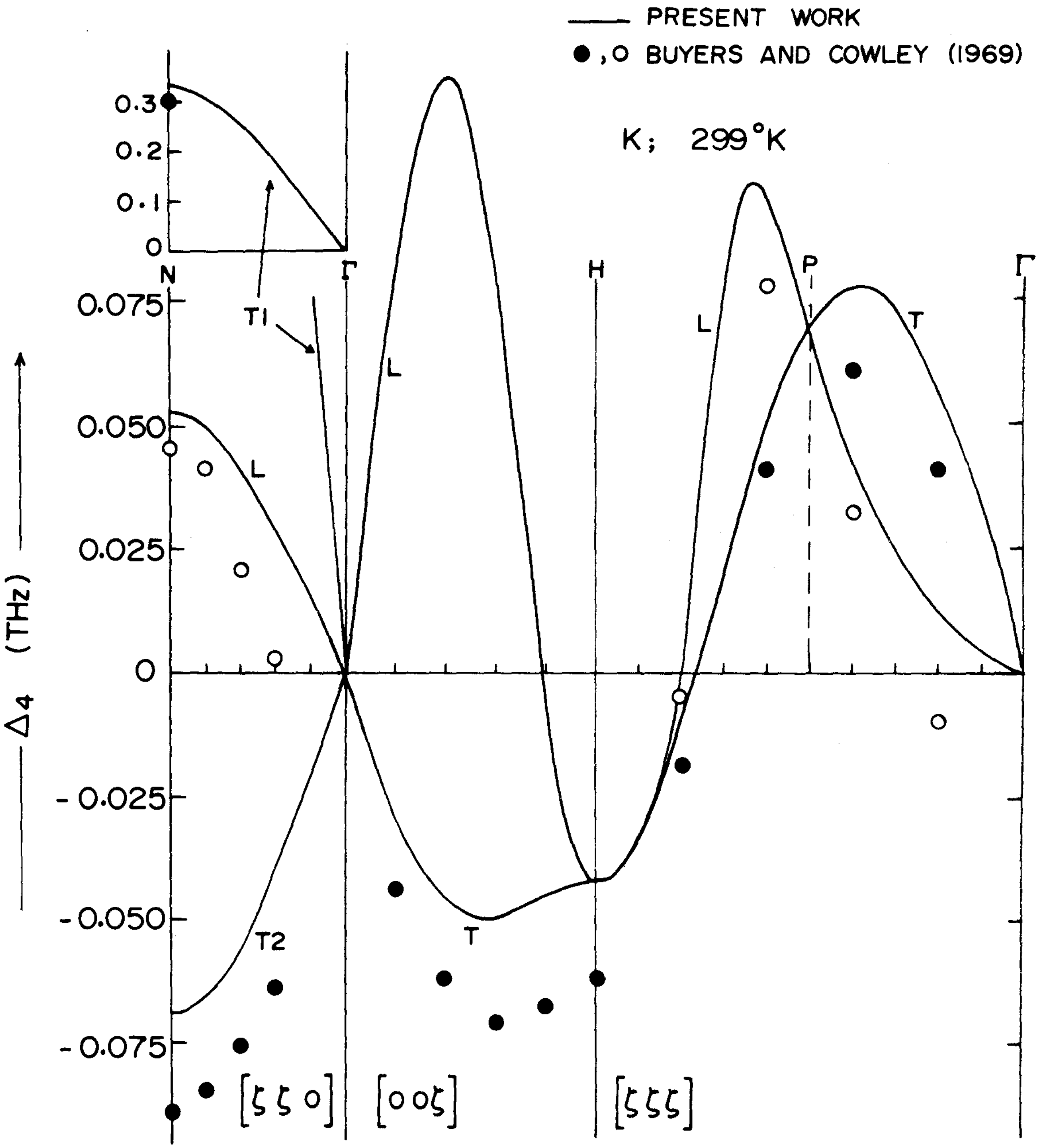

Figure III-5. Quartic shifts in potassium, compared with the calculation of Buyers and Cowley (1969).

The most troublesome computational problem is the representation of the Cauchy principal values and the delta functions which appear in the expressions for $\Delta_3(\lambda,\Omega)$ and $\Gamma(\lambda,\Omega)$. Maradudin et al. (1962) discuss this problem, and suggest that the principal value and the delta function be written as series in Legendre polynomials. In this work we have used the simpler representation (Maradudin and Fein 1962):

$$\left(\frac{1}{x}\right)_p - i\pi\delta(x) = \lim_{\varepsilon\to 0+}\left(\frac{1}{x+i\varepsilon}\right). \qquad \text{(III-C1)}$$

The choice of ε is dictated by conflicting requirements. To obtain a faithful representation, ε must be very small; on the other hand ε must be larger than the smallest increment in x which results from the use of a finite mesh of points in $\underset{\sim}{q}$ space (Maradudin et al. 1962). This point has also been discussed by Bohlin and Högberg (1968). The separation of values of Ω for which the function is calculated (designated $\Delta\Omega$) is also important.

To get an idea of suitable values for ε and M_n (the mesh number, defined in Appendix IV), let us consider the frequency distribution function (Eq. III-A38), with the above representation for $\delta(x)$. Fig. III-6 shows calculations of $g(\nu)$ using three different values of ε, and three values of M_n. For comparison, consult Fig. II-13 which shows an accurate calculation of this function. In Fig. III-6 we see that, for a particular value of ε, an increase in M_n tends to dampen the wiggles in the function. For smaller values

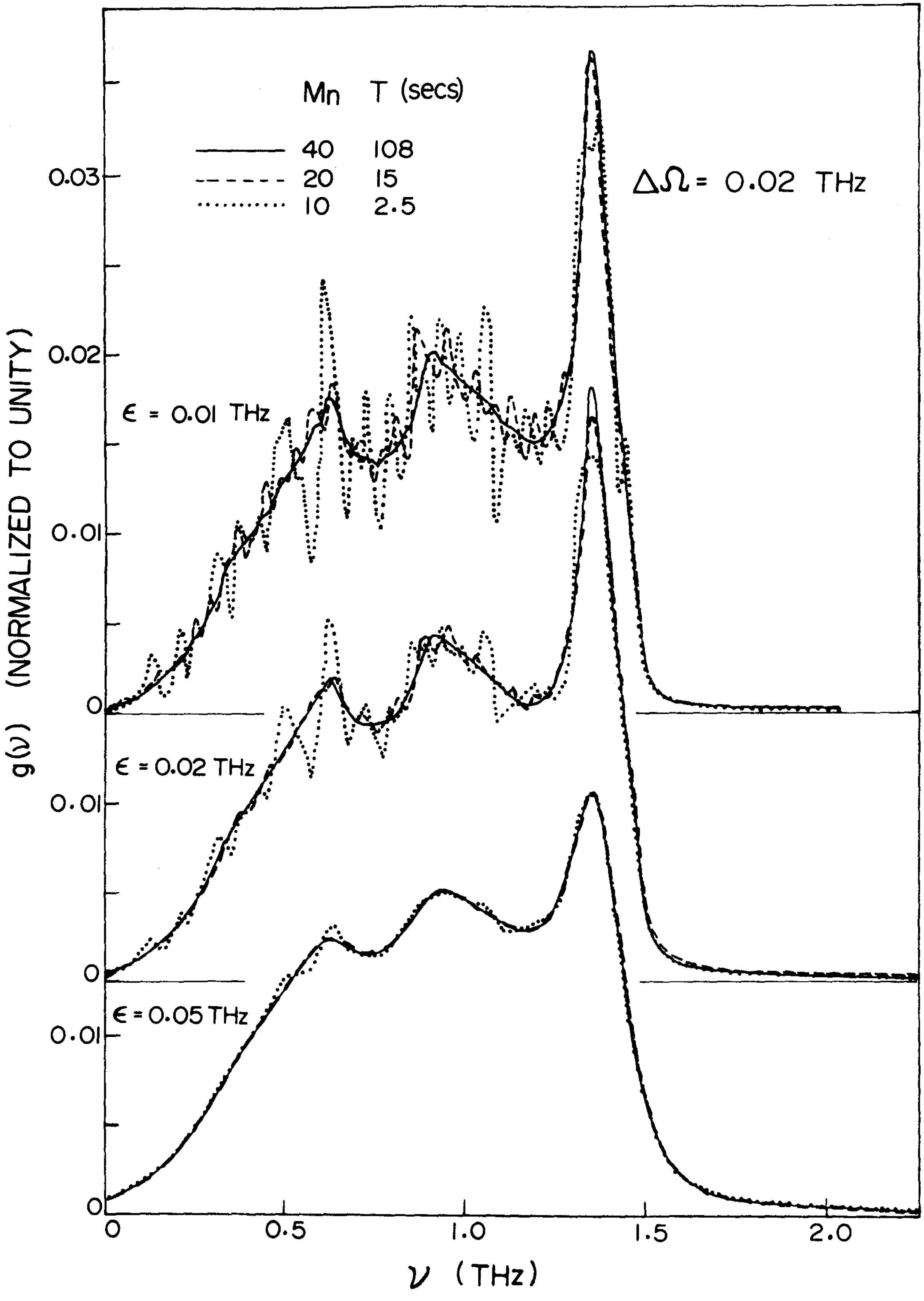

Figure III-6. The phonon frequency distribution in rubidium, calculated using a representation of the delta function.

of ε, it is necessary to go to larger values of M_n (and therefore longer computing times) in order to remove the wiggles, but the end result is considerably closer to the "true" function, which is shown in Fig. II-13. Further tests indicate that $\Delta\Omega$ should be roughly equal to ε for optimum results. Bohlin and Högberg (1968) have examined the effects, of changing ε and M_n, on the cubic shifts and widths themselves.

The frequency distribution shown in Fig. II-13 was calculated by the method of Gilat and Raubenheimer (1966). Recently Gilat and Kam (1969) extended this method to include functions of the form

$$I(\omega) = C \sum_j \int_{IBZ} F(\underset{\sim}{q}j)\delta[\omega-\omega(\underset{\sim}{q}j)]d^3\underset{\sim}{q},$$

and Gilat and Bohlin (1969) showed how to calculate the corresponding principal value function

$$G(\omega) = -\frac{C}{\pi}\sum_j \int_{IBZ} \frac{F(\underset{\sim}{q}j)}{[\omega-\omega(\underset{\sim}{q}j)]} d^3\underset{\sim}{q} .$$

This method assumes a knowledge of the derivatives $(\partial F(\underset{\sim}{q}j)/(\partial q_\alpha)$, and involves considerable programming to obtain areas of surfaces in reciprocal space. To the author's knowledge the method has not been used to calculate anharmonic properties.

Another method of calculation would be to obtain the widths by an accurate histogram method. The shifts could then be obtained utilizing the Kramers-Kronig relations (Pines and Nozières 1966). Gilat and Bohlin (1969) have stressed the problems involved with this method, and we have not attempted to use it.

(iv) Results of the Calculations

Lineshapes have been calculated for modes in the three major symmetry directions. The lineshape is given by

$$L(\lambda,\Omega) = \frac{2\omega(\lambda)\Gamma(\lambda,\Omega)}{[\omega^2(\lambda)-\Omega^2+2\omega(\lambda)\Delta(\lambda,\Omega)]^2+4\omega^2(\lambda)\Gamma^2(\lambda,\Omega)}$$

where $\Delta(\lambda,\Omega)$ contains three contributions (Eq. III-A22). Some examples of lineshapes at 205°K are shown in Fig. III-7. Clearly they depart from the Lorentzian shape in some cases. From these plots, widths and shifts have been obtained and are shown by solid lines in Fig. III-8. The measured shifts, obtained from Table II-2, are also shown with their error bars.

The agreement between the theoretical and experimental shifts is satisfactory in the case of the [00ζ]T and the [ζζ0]T2 branches. The shifts for the longitudinal directions are generally underestimated by the theory. In the case of the [00ζ]L branch the experimental shifts may be in error because of the additional complication of the "extra branch" (Section IIF). A large positive shift is predicted for the [ζζ0]T1 branch. Though no measurements of this branch were made at 205°K, the measurements of the zone boundary mode at lower temperatures indicate that the shift is small and,

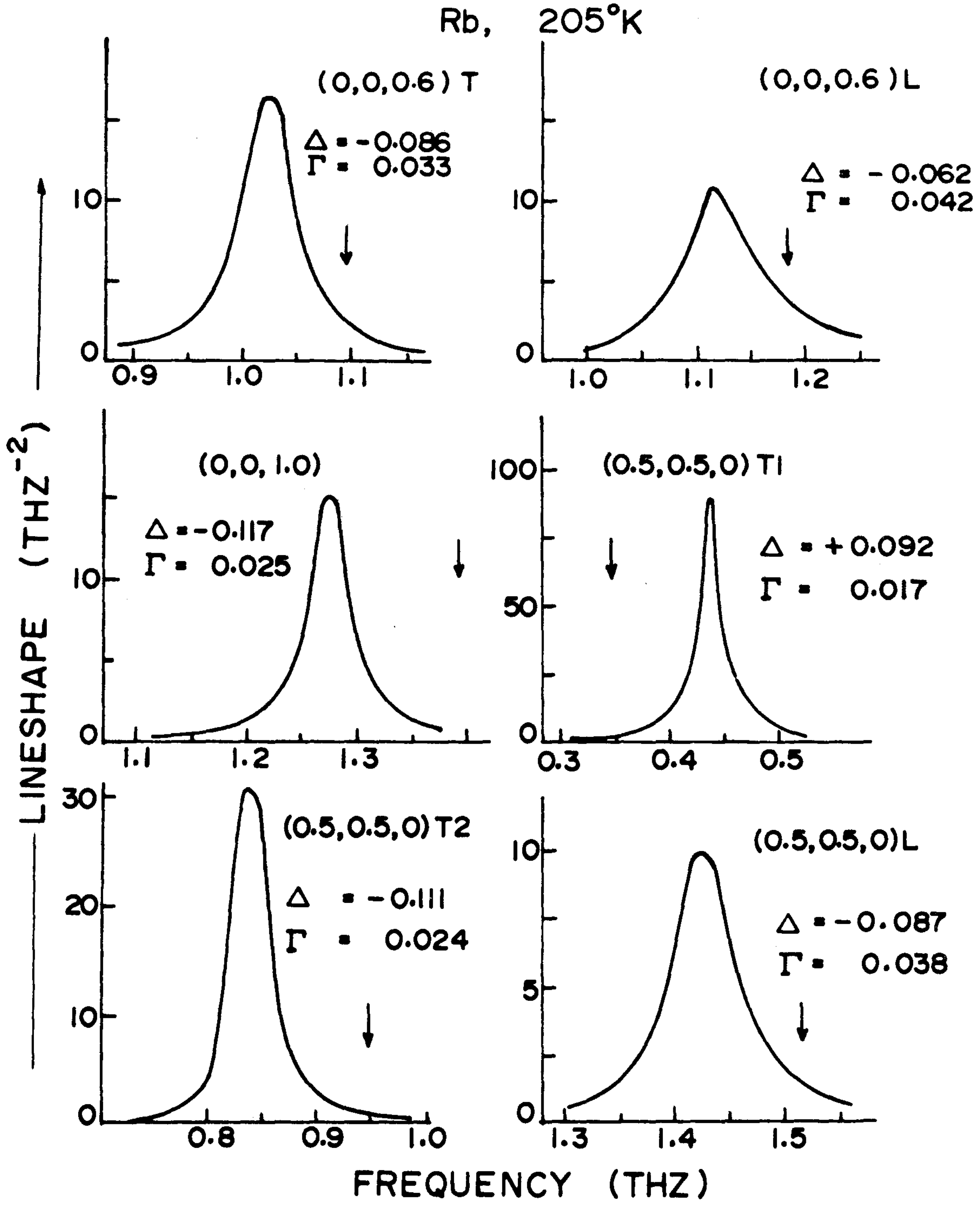

Fig. III-7 Calculated lineshapes in rubidium. The arrows indicate the harmonic frequency in each case.

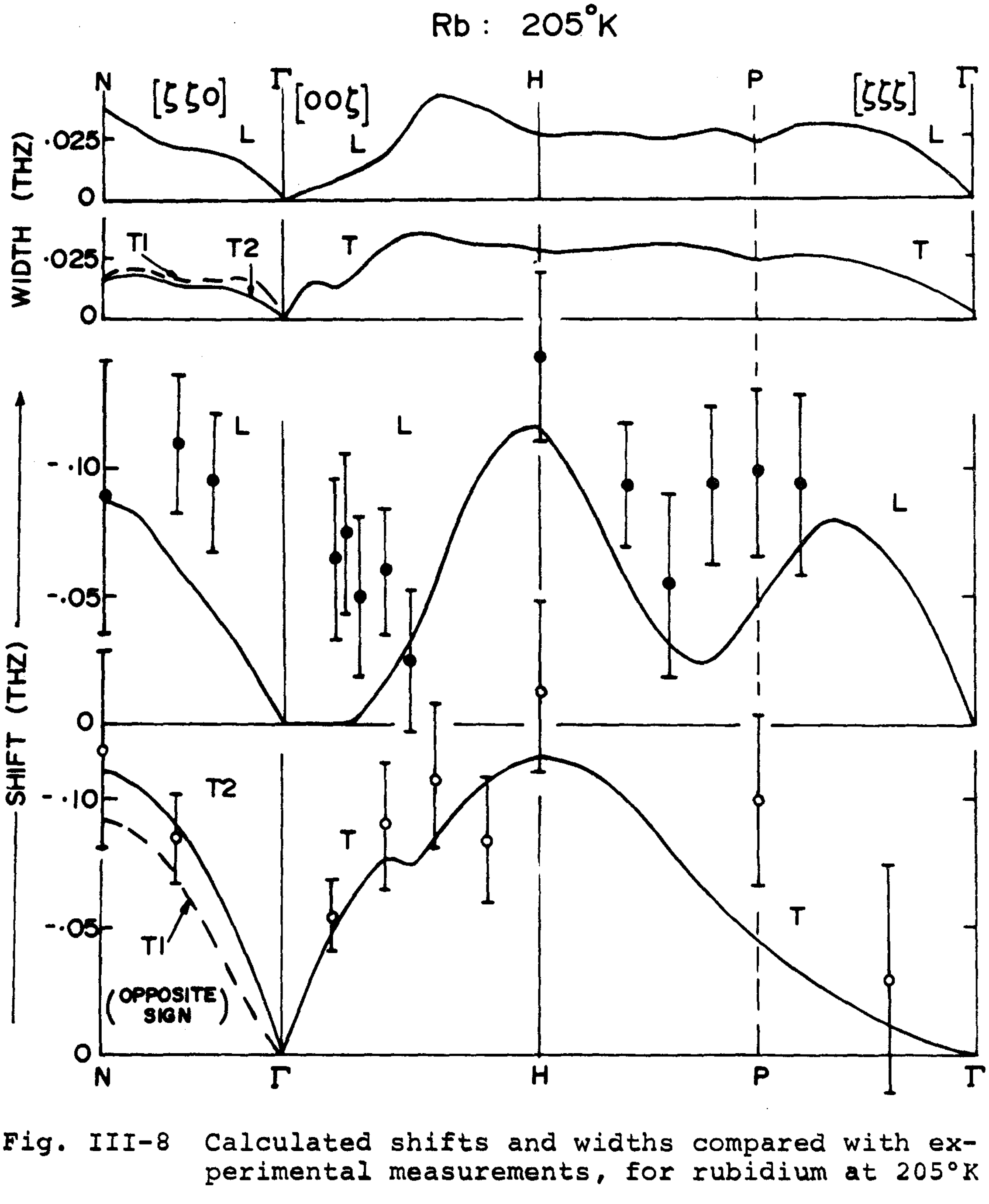

Fig. III-8 Calculated shifts and widths compared with experimental measurements, for rubidium at 205°K if anything, negative. An analogous situation exists in potassium (Buyers and Cowley 1969). We shall return to this aspect of the work in Section IIIE.

It is interesting to note that the theory predicts an increase in the separation of the L and T branches in the [00ζ] direction as the temperature is increased. This behaviour is manifest in the measurements, as can be seen from the fact that the ratio of second to first neighbour AFC's increases with increasing temperature (Section IIE(i)).

No comparison between theory and experiment has been made in the case of the widths, because reliable experimental widths are not available. The problem of extracting reliable anharmonic widths is considerable, and in the present case the errors would be at least as large as the widths themselves.

Further discussion of the shifts and widths in rubidium will be postponed until after calculations of the heat capacity have been described (Section IIID).

In order to examine the validity of these calculations, cubic shifts and widths, defined as $\Delta[\lambda,\omega(\lambda)]$ and $\Gamma[\lambda,\omega(\lambda)]$, have been computed for potassium at 299°K using the derivatives supplied by Dr. Dolling. The (somewhat fortuitous) good agreement between this calculation and that of Buyers and Cowley (1969) is illustrated in Fig. III-9. The sizeable disagreement for the [ζζ0]T2 branch is surprising and has not been explained.

Several groups have performed calculations of anharmonic

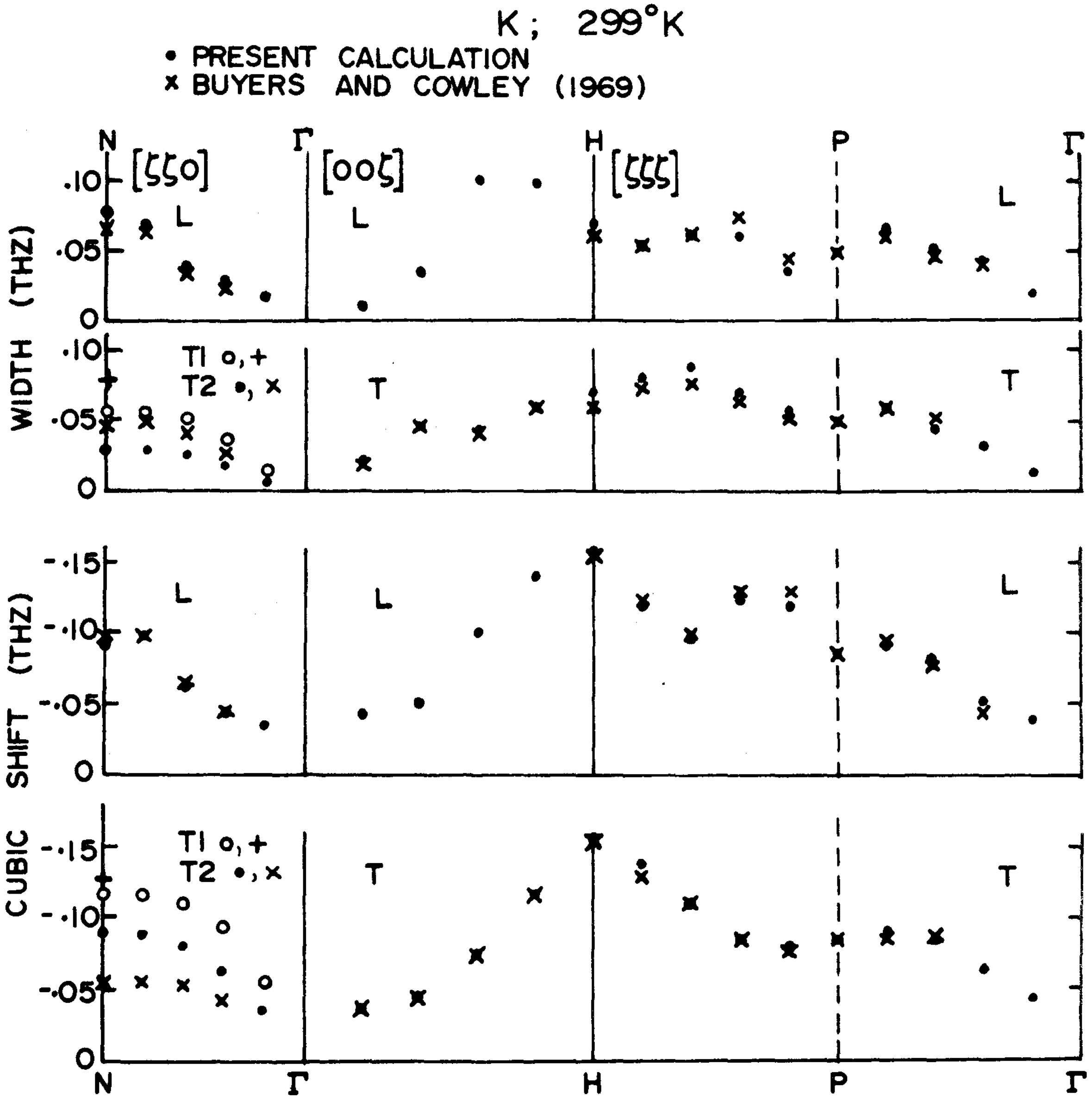

Fig. III-9 Cubic shifts and widths in potassium, compared with the calculation of Buyers and Cowley (1969) phonon frequency shifts and widths. Cowley and Cowley (1965) calculated these quantities for the [111] direction in the alkali halides, using a shell model obtained from experimentally measured phonon frequencies. More recently Buyers and Cowley (1969) performed calculations on potassium. Furthermore Bohlin and Högberg (1968) and Högberg and Sandström (1969) have looked at the inert gas solids and at aluminium: these calculations were based on a Lennard-Jones potential and on a pseudopotential approach respectively. Koehler et al. (1970) also computed shifts and widths in aluminium, but they performed sums in real space, obtaining derivatives from the Fourier transform of a pseudopotential fitted to phonon measurements. These latter calculations are therefore similar in many respects to the work reported here. A major difference is that the present calculations were made for a body centred cubic metal. Glyde and Cowley (1970) and Horner (1970) reported calculations of cubic anharmonic effects in b.c.c. ^{3}He, and find them to be relatively large.

D. THERMODYNAMIC PROPERTIES

Harmonic expressions for the free energy and the entropy, in terms of $g(\omega)$, have been given in Eqs. (III-A30) and (III-A31). The heat capacity is simply given by (cf. Eq. III-A9)

$$C_v = k_B \int \left(\frac{\hbar\omega}{2k_BT}\right)^2 \operatorname{cosech}^2\left(\frac{\hbar\omega}{2k_BT}\right) g(\omega)\, d\omega. \qquad \text{(III-D1)}$$

In order to calculate the true entropy and heat capacity, including both harmonic and anharmonic contributions, several approaches are possible.

(1) One may first calculate normal mode frequencies in the harmonic approximation, and from them the harmonic entropy S^h, and heat capacity C^h. The three shifts Δ_T, Δ_3 and Δ_4 for each mode may then be calculated, and from them the corresponding quantities ΔS_T, ΔS_3 and ΔS_4 etc. are obtained. (We shall discuss the difference between $(\Delta C_v)_T$ and $(\Delta C_p)_T$ below.)

(2) Given a model with volume dependent parameters, one may first calculate normal mode frequencies in the quasi-harmonic approximation as a function of volume. All that remains then is to calculate Δ_3 and Δ_4 as functions of volume, and hence the changes in S and C resulting from anharmonicity.

(3) Using a temperature dependent frequency distribution, ob-

tained from measurements of phonon frequencies at different temperatures, the total entropy may be calculated directly. The heat capacity is then obtained by differentiation. The procedure adopted by Miiller (1969) (see also Miiller and Brockhouse 1970) is closely related to this method.

Cowley and Cowley (1966) adopted method (1) above to calculate thermodynamic properties of KBr and NaI. The harmonic g(ω) was essentially obtained by taking the frequency distribution calculated from measurements of phonon frequencies at 90°K, and correcting it to 0°K for the effect of thermal expansion. On the other hand Cowley (1970) has used method (2) to make more detailed computations of various properties of the alkali halides. Owing to the very large degree of cancellation between the cubic and quartic contributions to these properties, and because the resultant anharmonic contribution is sensitive to volume changes, the two methods give dissimilar results. Method (2) is felt to be more realistic.

In the present calculations we have concentrated on method (1). The harmonic frequencies were obtained from AFC's fitted to the 12°K measurements on Rb. They therefore include the shift resulting from zero point motion, plus a very small shift appropriate to the temperature of the measurements. The latter shift has been neglected in the present work.

Let us now consider the various contributions to the thermodynamic properties. Expressions for the harmonic contributions have already been given (Eqs. III-A31, III-D1). They were calculated using the frequency distribution at 12°K, shown in Fig. II-13. In the next three subsections we consider the remaining contributions to the anharmonic properties. The results of the calculations are evaluated in the final subsection.

(i) Quasiharmonic Contribution

For the free energy we have (using Eq. III-A37),

$$\Delta F_T = \hbar \sum_{\lambda} (n + \tfrac{1}{2}) \Delta_T(\lambda) .$$

Now $\gamma(\lambda) = -\frac{1}{3\eta} \frac{\Delta_T(\lambda)}{\omega(\lambda)}$ so that we obtain

$$\Delta F_T = -3\eta \sum_{\lambda} E(\lambda)\gamma(\lambda)$$

$$= -9VB\eta^2 . \qquad \text{(III-D2)}$$

For the entropy we have

$$\Delta S_T = -\hbar \sum_{\lambda} n' \Delta_T(\lambda) ,$$

where the prime indicates differentiation with respect to T. It follows that

$$\Delta S_T = 9VB\eta\alpha . \qquad \text{(III-D3)}$$

The change in C_v is obtained as

$$(\Delta C_v)_T = -\hbar T \sum_{\lambda} n'' \Delta_T(\lambda)$$

$$= 3\eta \sum_{\lambda} T\, C'(\lambda)\gamma(\lambda) \qquad \text{(III-D4)}$$

To obtain $(\Delta C_p)_T$ we must include an extra term, since the shift $\Delta_T(\lambda)$ is a function of T if the volume is not held constant. We then have

$$(\Delta C_p)_T = (\Delta C_v)_T - \hbar T \sum_{\lambda} n' \, \Delta_T'(\lambda)$$

(cf. Cowley and Cowley 1966).

Now

$$\Delta_T'(\lambda) = - \frac{d}{dT} [3\omega(\lambda)\gamma(\lambda)\eta]$$

$$= - 3\omega(\lambda)\gamma(\lambda)\alpha \;\; + \text{higher order terms.}$$

Therefore

$$\begin{aligned}(\Delta C_p)_T - (\Delta C_v)_T &= 3\hbar T\alpha \sum_{\lambda} n'\omega(\lambda)\gamma(\lambda) \\ &= 9VB\alpha^2 T \qquad \text{(III-D5)}\end{aligned}$$

This is the well known thermodynamic relation for C_p-C_v (Zemansky 1957).

The above quantities are trivially obtained, once α and η have been calculated (Section IIIC). The exception is $(\Delta C_v)_T$, which is easily calculated by modifying the thermal expansion programme to do the appropriate sum.

As with the thermal strain calculation in Section IIIC, the 0°K compressibility value of Swenson (1955) was used for these calculations. The temperature dependence of $(\Delta C_v)_T$ and of $(\Delta C_p)_T$ - $(\Delta C_v)_T$ is shown in Fig. III-10. Note that the former quantity tends to zero at high temperatures. This is because in the quasiharmonic approximation, where no interactions between modes occur, the high temperature limit for C_v

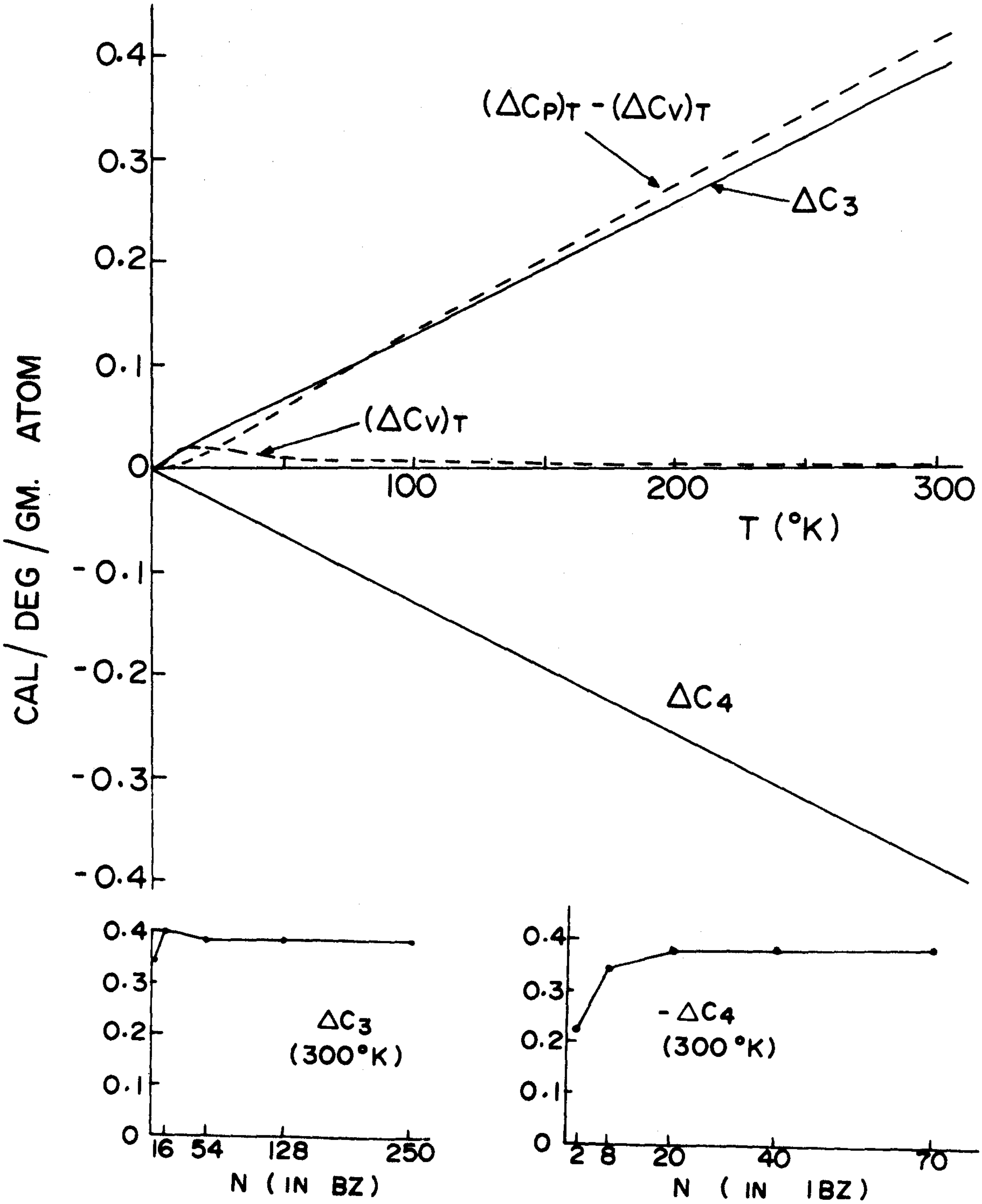

Figure III-10. The quasiharmonic and anharmonic contributions to the heat capacity. The convergence of the sums is also indicated.

is simply $3Nk_B$, regardless of the frequencies of the phonons.

(ii) Quartic Contribution

Expressions for ΔF_4 and ΔS_4, in terms of the quartic shifts $\Delta_4(\lambda)$, have been given in Eqs. (III-A36) and (III-A41). The quartic heat capacity is given by

$$\Delta C_4 = T \frac{d(\Delta S_4)}{dT}$$

$$= -24T \sum_{\lambda_1\lambda_2} V(\lambda_1,-\lambda_1,\lambda_2,-\lambda_2)[(n_1+\tfrac{1}{2})n_2'' + n_1'n_2']$$

$$=-T\hbar \sum_{\lambda_2} n_2''\Delta_4(\lambda_2)-24T \sum_{\lambda_1\lambda_2} n_1'n_2'V(\lambda_1,-\lambda_1,\lambda_2-\lambda_2)$$

These quantities have been calculated using an extended version of the programme which calculates quartic shifts (Section IIIC). The convergence of the sums is illustrated (for the case of ΔC_4) in Fig. III-10. As more wave vectors are included, $|\Delta C_4|$ increases monotonically, and quickly saturates. A sum over 40 wave vectors in the IBZ is sufficient to obtain numbers to an accuracy of 1%.

The temperature dependence of ΔC_4 is also illustrated in Fig. III-10. It is negative, and at high temperatures it is about 7% smaller in magnitude than the contribution resulting from thermal strain.

(iii) Cubic Contribution

The cubic contribution to the free energy is given by Eq. (III-A32). The expression may be written as a sum over cubic shifts analogous to Eq. (III-A36). The cubic shifts, in Section IIIC above, were obtained using a programme which was specialized to treat the three principal symmetry directions only, whereas shifts for all values of $\underset{\sim}{q}$ are required in the present case. In addition it is important to optimize the speed of this type of programme, so a separate programme, named FREE3, was written to calculate cubic contributions to the thermodynamic properties. The details of this programme are given in Appendix V.

The convergence of the sums is illustrated in Fig. III-10. The quantity ΔC_3 is shown as a function of the number of wavevectors $\underset{\sim}{q}_2$ in the full zone. Unlike the situation with ΔC_4, the sum to give ΔC_3 oscillates, but again the convergence is rapid. The temperature dependence of ΔC_3 is also shown in Fig. III-10. It is almost identical in size, but opposite in sign, to ΔC_4. The resultant anharmonic heat capacity is therefore very small. We shall discuss this further below.

(iv) The Experimental Heat Capacity

The most reliable measurements of the heat capacity of rubidium are those of Filby and Martin (1965). More recent measurements by Martin (1970), for temperatures below 3°K, are the most accurate for this temperature range. In order to obtain suitable numbers for comparison with calculation, we have taken the constant pressure (C_p) measurements of Filby and Martin (1965), and we have subtracted (a) an electronic contribution,

$$C_e = \gamma T = 6.25 \times 10^{-4}\ T\ \text{cal/°K/gm atom}$$

using the value of γ obtained by Martin (1970), and (b) a lattice vacancy formation contribution,

$$C_{vac} = (6.79\times10^{9}/T^{2})\exp(-3.63\times10^{3}/T)\text{cal/°K/gm atom}$$

as given by Martin (1965). At 300°K, $C_e = 0.19$ and $C_{vac} = 0.42$ cal/°K/gm atom: at 200°K however $C_e = 0.13$ and $C_{vac} = 0.002$ cal/°K/gm atom. The remaining heat capacity is the lattice heat capacity C_ℓ. Both C_p and C_ℓ are shown in Fig. III-11.

(v) Comparison of Theory and Experiment

In the upper half of Fig. III-11, the solid line shows the harmonic lattice heat capacity which was calculated using Eq. (III-D1) and the 12°K $g(\omega)$ presented in Fig. II-13. The dashed line shows the total lattice heat capacity, calculated by a method similar to that of Miiller and Brockhouse (1970). We shall return to this below.

The lower half of Fig. III-11 shows the difference between various experimental and calculated heat capacities and the calculated harmonic value. The dot-dash line shows the sum of the quasiharmonic and anharmonic heat capacities. It is essentially the same as the quasiharmonic contribution alone, since the anharmonic terms are found to cancel out.

Clearly there is a discrepancy between the calculated

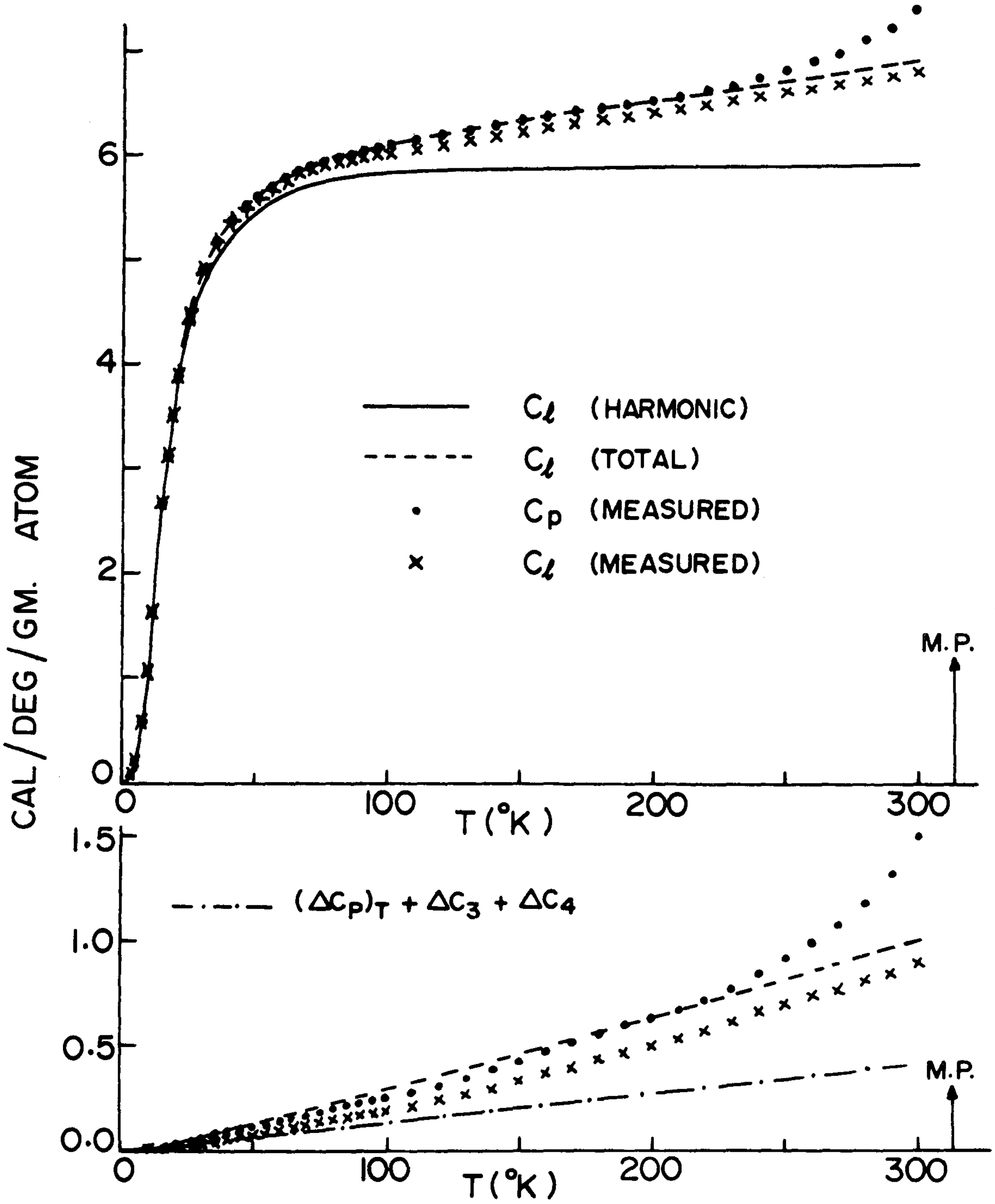

Fig. III-11 The heat capacity of rubidium, and the difference between the heat capacity and the harmonic value (see text).

and experimental lattice heat capacities. Assuming that the experimental values are correct, and that the computer programmes are working properly, it appears that the quasiharmonic and/or the anharmonic contributions to C_ℓ are too small. We shall consider the two possibilities in turn.

At high temperatures the quasiharmonic contribution to C_ℓ is essentially the (C_p-C_v) correction, Eq. (III-D5). This may well be underestimated, by several per cent at room temperature, because 0°K values for the compressibility and the atomic volume have been used throughout: note however that these two quantities change in the same way with temperature, so that the correction is small. Filby and Martin (1965) used Hackspill's (1911) macroscopic value of $\alpha = 90 \times 10^{-6}$ deg^{-1}, to obtain $(C_p-C_v) = 0.70$ cal/°K/gm atom at 290°K. The present calculations give $\alpha = 65 \times 10^{-6}$ deg^{-1}, and $(C_p-C_v) = 0.40$ cal/°K/gm atom at that temperature. This value for α is in reasonable agreement with microscopic (diffraction) measurements. In this work no comparison is made with the C_v values of Filby and Martin (1965).

It is harder to evaluate the accuracy of the calculations of ΔC_3 and ΔC_4. There are no new adjustable parameters in ΔC_3, but ΔC_4 involves the fourth derivatives of the potential. We have already noted that the quartic shifts for the $[\zeta\zeta 0]T1$ branch were unusually large. It appears that a theory which predicts smaller shifts for this branch will also predict a net positive anharmonic contribution to C_ℓ. We will return to this in Section IIIE.

To the author's knowledge, this work represents the first calculation of the anharmonic heat capacity of a metal using a realistic potential: the early work of Keller and Wallace (1962), based on a Lennard-Jones potential, predicts a large negative anharmonic contribution to C_ℓ, which is clearly in disagreement with experiment. Apart from the work of Cowley and Cowley (1966) on alkali halides, recent calculations of anharmonic thermodynamic quantities have been devoted to the inert gas solids (see e.g. Klein et al 1969).

The dashed lines in Fig. III-11 represent a calculation of the total lattice heat capacity $C_\ell(T)$ using a method similar to that of Miiller and Brockhouse (1970). Their equation [8] may be written

$$C_\ell(T) = k_B\{1 - \frac{TG'(T,T_o)}{G(T,T_o)}\} \int_o^{\nu_{max}} g(\nu,T_o) \frac{x^2 e^x}{(e^x-1)^2} d\nu$$

where $x = (h\nu/k_BT)G(T,T_o)$; $g(\nu,T_o)$ is the frequency distribution at $T = T_o$, and $G(T,T_o)$ is the mean ratio of the frequencies at temperatures T and T_o,

$$G(T,T_o) = \left\langle \frac{\nu(\underline{q},j,T)}{\nu(\underline{q},j,T_o)} \right\rangle_{\underline{q},j}$$

Experimental ratios, for T = 85, 120 and 205°K, and T_o = 12°K, are given in Table III-2: the quantities σ, δ and N are explained in Section IIE(vii). The ratios have been fitted to a function of the form

$$1 - \frac{C}{[\exp(\theta/T)-1]}$$

and the result is shown in Fig. III-12. This function has the correct behaviour at low temperatures, and it gives a reasonable fit to the data.

The results of this calculation are in fair agreement with experiment; this indicates that the measured frequency shifts in rubidium are consistent with the measured anharmonic heat capacity, but it says nothing about the origin of these effects.

TABLE III-2. Mean frequency ratios, and their errors, for rubidium at 85, 120 and 205°K relative to 12°K.

T(°K)	85	120	205
$\langle\nu(T)/\nu(12°K)\rangle$	0.972 ± 0.004	0.965 ± 0.006	0.907 ± 0.006
σ	0.021	0.034	0.027
δ	0.058	0.057	0.055
N	28	36	21

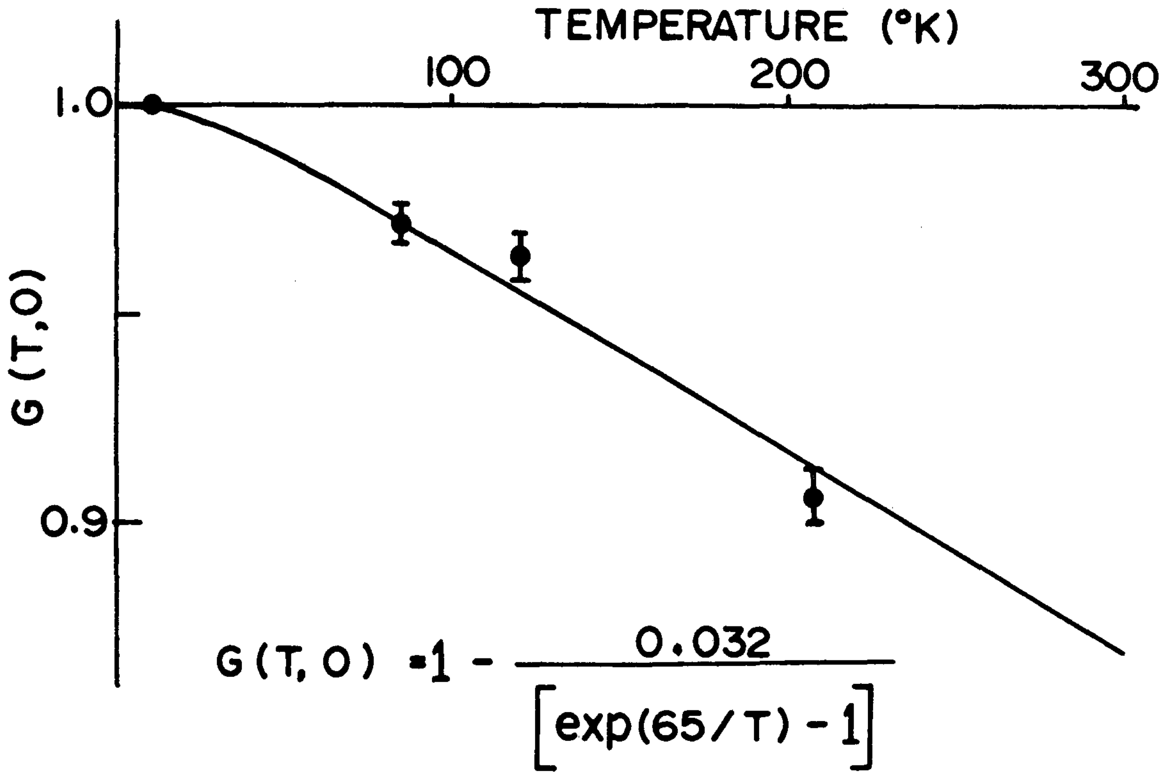

Fig. III-12. Mean frequency ratios for rubidium at 85, 120 and 205°K, relative to 0°K. The line shows a fit to the points. The difference between the frequencies at 0 and 12°K has been neglected.

E. CONCLUSIONS

In Sections IIIC and IIID we have looked at calculations of the quasiharmonic and anharmonic contributions, to lowest order, to the vibrational modes and the heat capacity in rubidium. To a large extent the calculations account for the observed frequency shifts, and there is no reason to suppose this will not be the case with the widths, when such measurements become available for comparison with theory. The discrepancies which exist may result from uncertainties in the third and, to a larger extent, the fourth derivatives of the potential, which are required for this calculation. Another possibility is that the calculations would be improved if the sums over neighbours were extended to more distant shells. The agreement between the present (real space) calculations and the reciprocal space calculations of Buyers and Cowley (1969) indicates that this is unlikely to be very important.

In view of the very large cancellation between the cubic and quartic contributions to the heat capacity, it is possible that a calculation based on method (2) of Section IIID would yield superior results. Koehler et al (1970) calculated shifts and widths in aluminium using this method.

The large positive shifts calculated for the [$\zeta\zeta0$]T1 branch (Section IIIC) are not observed experimentally, either in Rb or in K. If we assume a possible 20% uncertainty (which is probably pessimistic) in each contribution to the calculated shifts, then the calculations are not in disagreement with experiment. On the other hand, the fact that the present calculations compare well with those of Buyers and Cowley (1969), indicates that there may be a real difference. It is possible that higher order terms in the anharmonic expansion must be considered. Since this is a very time-consuming, complicated task, and since even higher derivatives of the interatomic potential are required, it is felt that such a calculation should only be attempted when more accurate experimental numbers are available for comparison with theory. It is also possible that a calculation to higher order will yield values for the anharmonic heat capacity in better agreement with experiment.

There is clearly plenty of room for improvement in the experimental determination and the theoretical calculation of anharmonic effects in the simple metals. No doubt the next few years will see increased activity in this important and exciting field.

APPENDIX I

THE LATTICE SPACING OF RUBIDIUM, AND A DETAILED EXAMINATION OF THE LARGE RUBIDIUM CRYSTAL

A. THE LATTICE SPACING OF RUBIDIUM

Several workers have measured the lattice spacing of rubidium by x-ray methods: Pearson (1958) summarizes the available data and remarks that "the lattice spacings appear to be somewhat uncertain". The x-ray measurements are shown in Figure AI-1. To the author's knowledge the only macroscopic measurements of the thermal expansion coefficient of Rb, apart from those of Kelly and Pearson (1955), who obtained very variable results, are due to Hackspill (1911) and Deuss (1911), both of whom obtained $\alpha = 90 \times 10^{-6}\ {}^\circ K^{-1}$, in the range 0 - 30°C.

In this appendix, neutron diffraction measurements of the lattice spacing of Rb at several temperatures are reported. The neutron method has the advantage that the beam "sees" the whole crystal whereas, because of high absorption, x-rays are scattered by a very thin region near the surface of the crystal ($\sim$ 0.1 mm thick for Rb). This is particularly relevant to the work of Kelly and Pearson (1955), who noted that the alkali metal tended to stick to its glass container. This can produce undesirable strains in the surface region. Furthermore any surface contamination (such

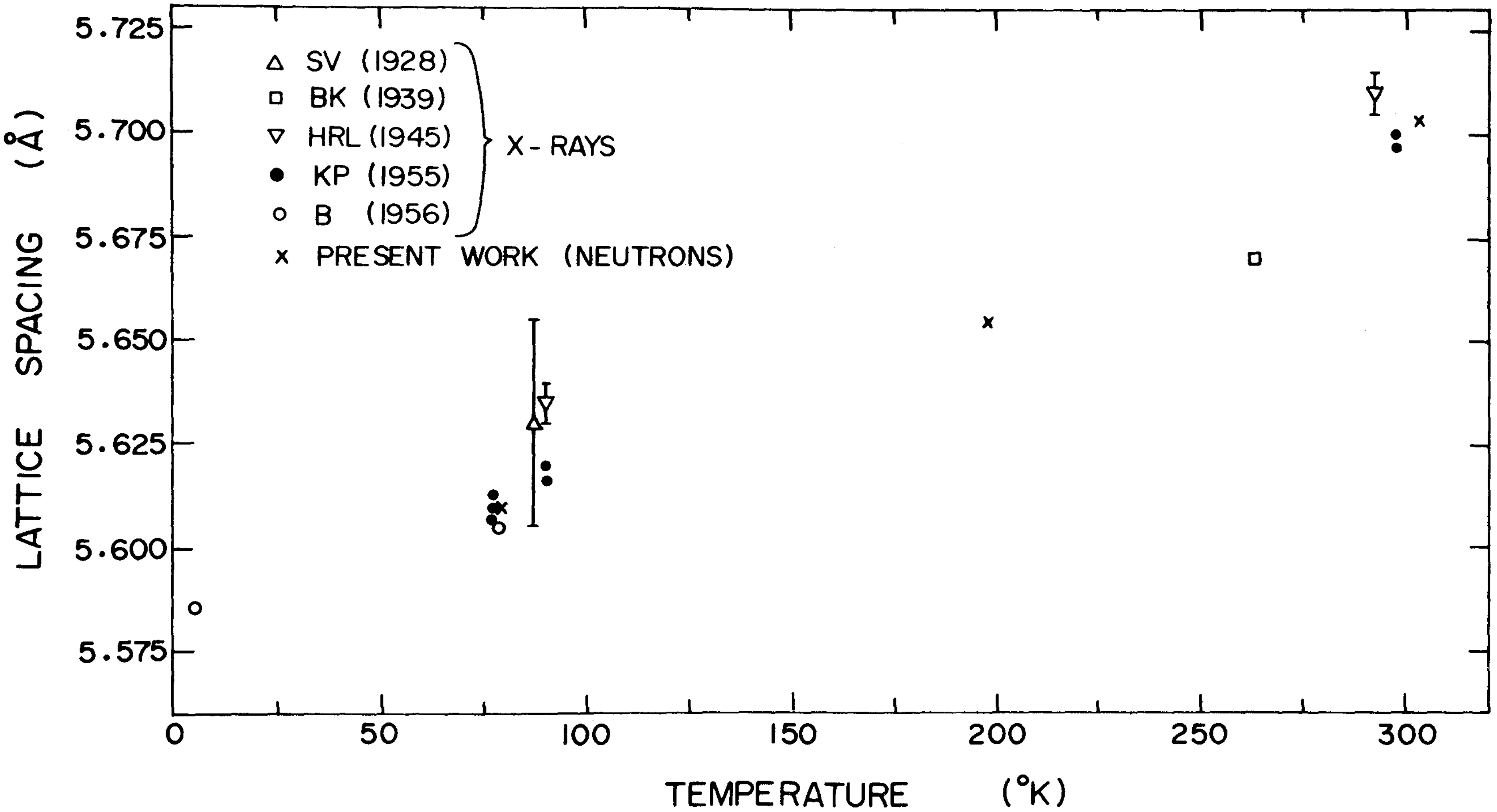

Fig. AI-1 The lattice spacing of rubidium metal as a function of temperature. The x-ray measurements are due to Simon and Vohsen (SV)(1928), Böhm and Klemm (BK)(1939), Hume-Rothery and Lonsdale (HRL)(1945), Kelly and Pearson (KP)(1955), and Barrett (B)(1956). No errors were quoted by Böhm and Klemm (1939). The errors in the measurements since 1950 are ± 0.001Å.

as oxide or hydroxide) is of more consequence in x-ray work.

Measurements were initially made using the McMaster (E2) spectrometer at Chalk River, operated as a diffractometer (Hallman and Brockhouse 1969). Subsequent analysis of these results suggested that the temperature of the specimen had not been properly determined, so further experiments were performed using the triple-axis spectrometer at the McMaster reactor with a much improved method of measuring the temperature. Since rubidium has a low Debye temperature (∿ 56°K), the elastic scattering intensity (for all but the lowest index reflections) drops rapidly with increasing temperature. The experiments at the low flux McMaster reactor were therefore restricted to the lower temperatures, and the room temperature result obtained using the much higher flux of the Chalk River reactor was retained.

The method was essentially that of Ng et al (1967). The instrumental parameters are given in Table AI-1. Vertical Soller collimators were employed, with the indicated length and slit separation. Poorer resolution had to be tolerated for the experiment at McMaster, because of the low beam intensity. For maximum resolution a large scattering angle (ϕ) is desirable. On the other hand the Debye-Waller factor restricts one to low index reflections, particularly at the higher temperatures. For example, the (440) reflection is roughly 35 times weaker than the (330) reflection, at room temperature. Kelly and Pearson (1955) were only able to obtain reflections out to $\phi \approx 60°$ at this temperature. Another complication is the necessity of avoiding peaks from the aluminium container: since the lattice spacings of Al and Rb are very nearly in the ratio $1:\sqrt{2}$, this is a severe limitation.

Measurements were made of the (330) and $(\bar{3}\bar{3}0)$ reflections ($\phi \approx 110°$ to $115°$) in a small (1" diam. by 2" high) crystal of rubidium. The specimen contained two crystals, which gave reflections with intensities in the approximate ratio 3:1, about 0.4° wide and separated by about 1.5°, but this did not complicate the measurements. The spectrometer was calibrated by measuring reflections in powders of copper and germanium, and in single crystals of copper, germanium and silicon. The temperature of the rubidium crystal was monitored using copper-constantan thermocouples at each end of the specimen. The thermocouple wires were fed through a small hole in the top of the cryostat, sealed with a high vacuum wax, to avoid introducing extra junctions at this point.

The results are presented in Table AI-2 and in Fig. AI-1. They are clearly in good agreement with the measurements of Kelly and Pearson (1955). The present measurements do not fall on a straight line, which is the behaviour predicted by the simple quasiharmonic theory except at low temperatures (cf. Fig. III-3). In view of this, it would be well worth while to perform further measurements over the full temperature range, in order to determine the detailed behaviour of the lattice spacing as a function of temperature.

TABLE AI-1. Instrumental parameters for the lattice spacing measurements. The mosaic spreads are denoted by η.

Experiment	1	2
Spectrometer	E2 (Chalk River) (triple-axis)	McMaster Reactor (triple-axis)
Wavelength	2.268 Å	2.207 Å
Monochromator	Cu(220);$\eta \simeq 20'$	Cu(200);$\eta \simeq 20'$
Analyser	Cu(220);$\eta \simeq 20'$	Cu(220);$\eta \simeq 20'$
Collimation ($\underline{k}_o$ and $\underline{k}'$)	0.05" in 8"	0.1" in 8"

TABLE AI-2. Results of the lattice spacing measurements.

Temperature (°K) (± 1°K)	78	197	303
Lattice spacing (Å) (± 0.001 Å)	5.609	5.655	5.703_5

B. A DETAILED EXAMINATION OF THE LARGE RUBIDIUM CRYSTAL

In order to check that the large (1-1/2×3") crystal of rubidium was indeed single, in connection with the observations described in Section IIF, a series of ψ rocking curves was run for different tilt angles χ. The χ drive shaft of a commercial two-circle x-ray goniometer was fitted with a motor, cam and microswitch assembly similar to those used to control the other angles on the McMaster spectrometers. The crystal was mounted on the goniometer head, and measurements were made at room temperature using the triple-axis spectrometer at McMaster, operated as a diffractometer with a wavelength of 1.41 Å. The scattering angle was fixed at 20.2°, the value appropriate to the (110) plane spacing. Because of the large Debye-Waller factor of Rb at room temperature, examination of higher index reflections would have taken a prohibitively long time.

With no Soller collimators in the beam path, the crystal was tilted about the [001] axis (Fig. AI-2), through 90° in steps of 2.5°. At each setting of the tilt χ, the crystal was rocked through 180° about the vertical axis between $(0,0,\sqrt{2})$ and $(0,0,-\sqrt{2})$. In this way one quarter of the spherical scattering surface was scanned, bounded by the planes (100) and (010).

The results are presented in Fig. AI-2. As expected, $1 + (4 \times 1/2) = 3$ [110] reflections are observed. The peak intensity of these reflections was typically 25,000 counts.

Fig. AI-2 Constant intensity contours for the large crystal of rubidium, as a function of ψ and χ (see diagram top right). Successive contours correspond to 200, 300, 400, 1000 and 10,000 counts in the main diagram, and to 200, 400, 600, 800, N/2, 1500 and 2000 counts in the inset at bottom right: N is the number of counts at the peak height. The resolution function is indicated in each case by a half intensity contour labelled Ge (germanium).

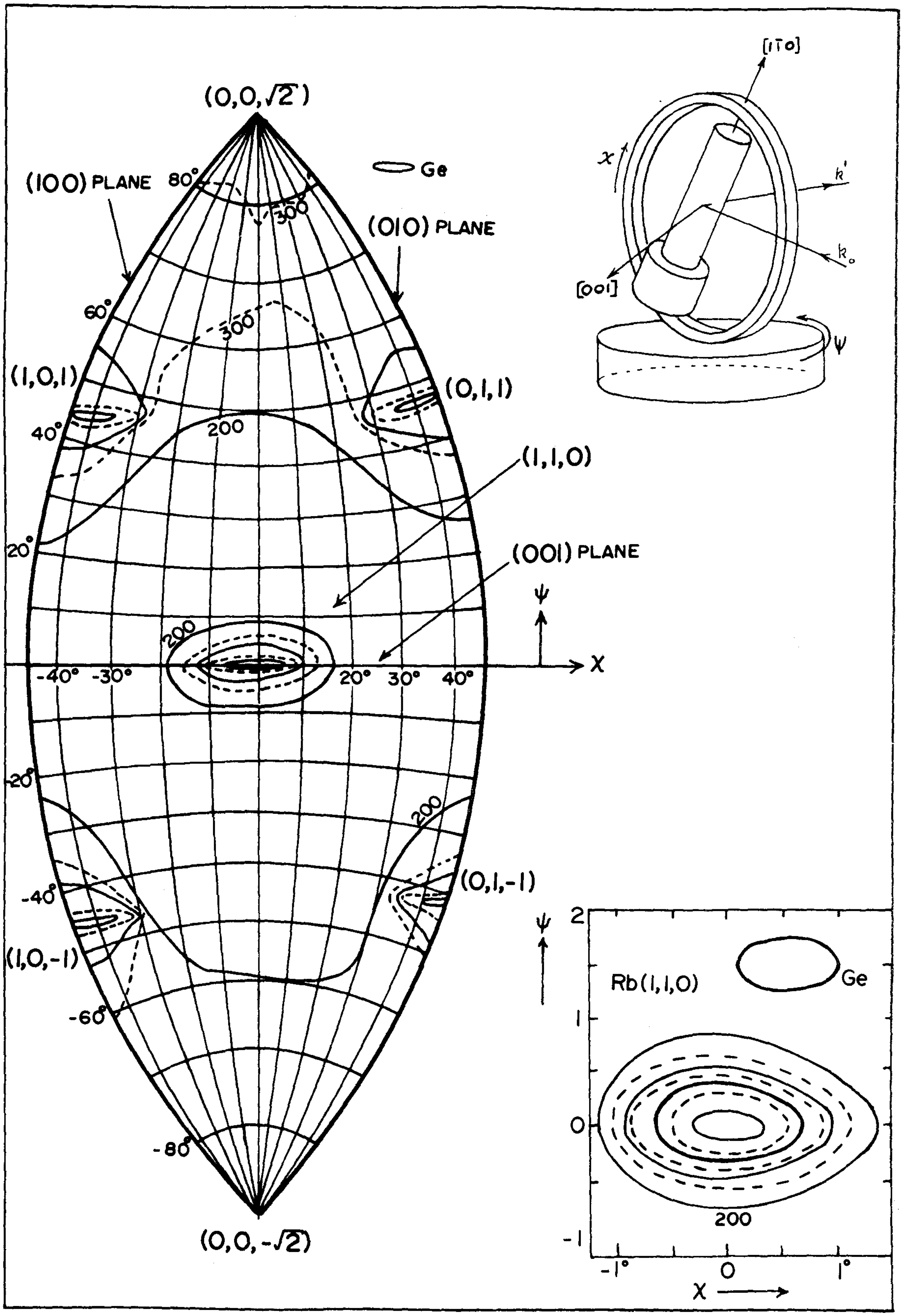
(0,0,√2)
Ge
(100) PLANE
80°
300
(010) PLANE
60°
300
(1,0,1)
(0,1,1)
40°
200
(1,1,0)
20°
(001) PLANE
200
ψ
χ
-40°
-30°
20°
30°
40°
-20°
200
(0,1,-1)
-40°
(1,0,-1)
-60°
-80°
(0,0,-√2)
[1$\bar{1}$0]
χ
k'
k₀
[001]
ψ
2
Rb(1,1,0)
Ge
1
0
200
-1
-1°
0
1°
χ

The half peak intensity contour for a (111) reflection from a (relatively) perfect germanium crystal is included in Fig. AI-2 to indicate the resolution of the experiment.

The (220) reflection in rubidium, and a (220) reflection from the germanium crystal (which occurs at very nearly the same scattering angle), were examined with 1/10" in 8" horizontal Soller slit collimators (to improve the resolution in χ), in the incident and scattered beams. The results are shown in the inset to Fig. AI-2.

It is clear from this work that (at the time of the experiment, March 1969) the crystal was indeed single. The comparatively small ratio of signal to background occurs because no Soller collimators were used. The increase in background for $|\psi| \gtrsim 45°$ occurred because the χ motor assembly, as well as the goniometer circle, were partially in the neutron beam.

APPENDIX II

SPURION - A COMPUTER PROGRAMME WHICH SEARCHES FOR SPURIOUS NEUTRON SCATTERING PROCESSES

It was mentioned in Section IID that a number of constant $\underline{Q}$ scans in rubidium exhibited structure in addition to the expected one-phonon peak. Initial attempts to explain these observations were only moderately successful. A computer programme, called SPURION, was therefore written by the author. With this programme, a systematic search for possible spurious processes is made. In the present context a spurious process includes any process other than the intended one-phonon scattering process. Depending on its cross section, a spurious process may or may not result in an observable spurious peak, or "spurion". The programme indicates which spurious processes can occur for a particular setting of the spectrometer: the user then decides whether these processes explain, both qualitatively and at least semi-quantitatively, the observations.

Fig. AII-1 shows a simplified flowchart of the programme. The master card contains information common to a series of constant $\underline{Q}$ scans, including the (principal) incident frequency ν_{o1} and the lattice constant of the specimen. Given this information, the other components of the incident beam, with frequency ν_{oI} and wave vector $\underline{k}_{oI}$ (I>1) are calculated. These

FLOWCHART OF PROGRAMME "SPURION"

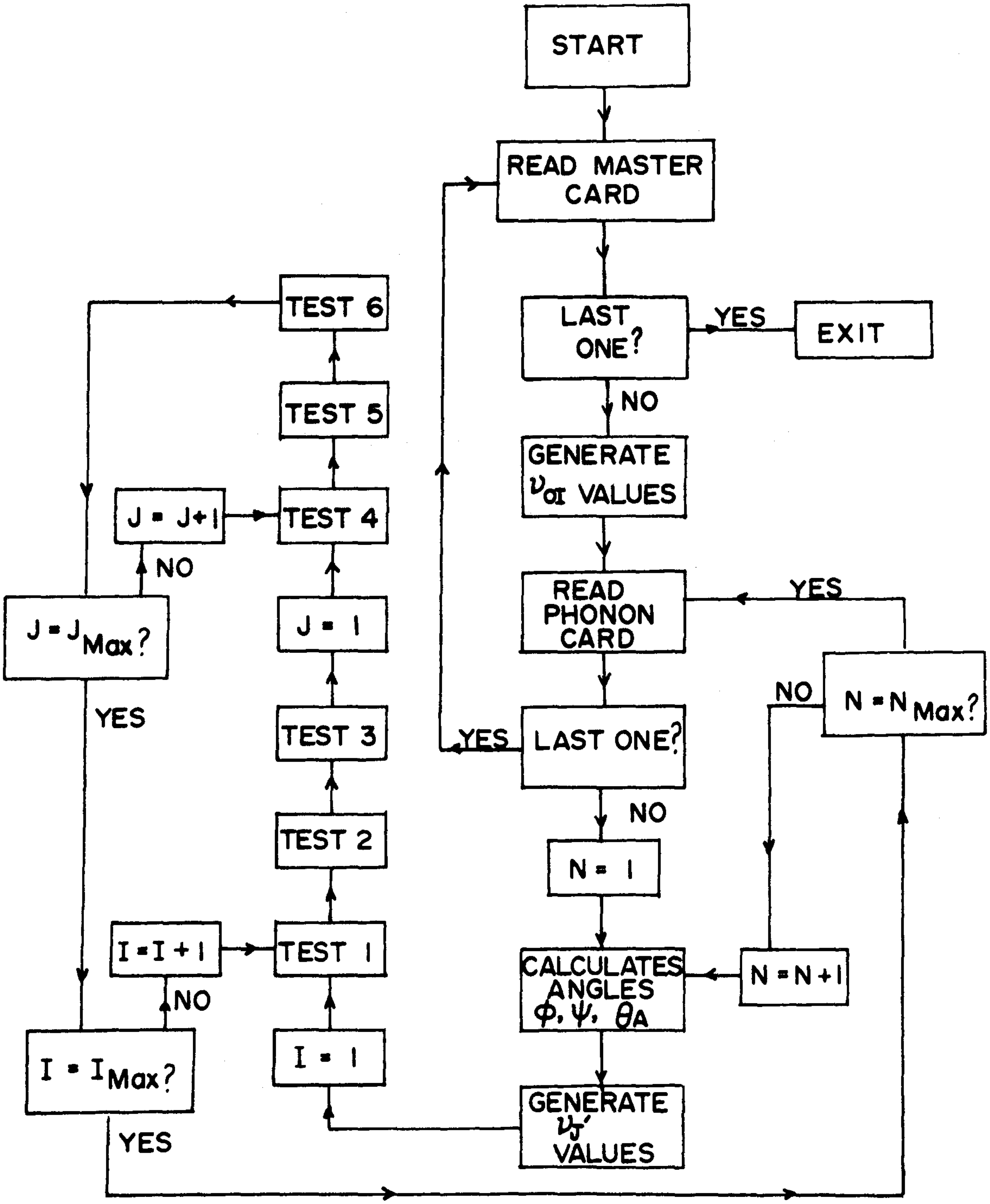

Fig. AII-1. A simplified flowchart of the programme SPURION.

include the (331) and (33$\bar{1}$) contaminants (see Section IE) and higher order components. A phonon card is then read. This card contains details of a particular scan, i.e., the components of $\underline{Q}$, the range of the scan, and the number of steps. For each point (N) on the scan, ν_1' and the angles ϕ, ψ , and θ_A are calculated, and the higher order components with frequency ν_J' and wave vector $\underline{k}_J'$ (J>1), which can be Bragg reflected by the analyser, are generated.

For each ν_{oI}(including ν_{o1}), tests 1 to 3 below are performed. In each case, a message is printed if a possible process is detected.

Test 1. Bragg reflection in specimen, into analyser

Consider the vector diagram at the top of Fig. AII-2. This represents a particular spectrometer setting characterized by a wave vector transfer $\underline{Q}$, and a positive energy transfer (since $|\underline{k}'| < |\underline{k}_o|$). If the line AB is produced to C, such that AC=OA, the vector diagram OAC represents an elastic scattering process. If C lies close to a reciprocal lattice point R, as in the diagram (the dashed circle represents schematically the instrumental resolution), then the incident beam may be Bragg reflected into the analyser. Part of this beam will be incoherently scattered by the analyser into both detectors. There will therefore be an

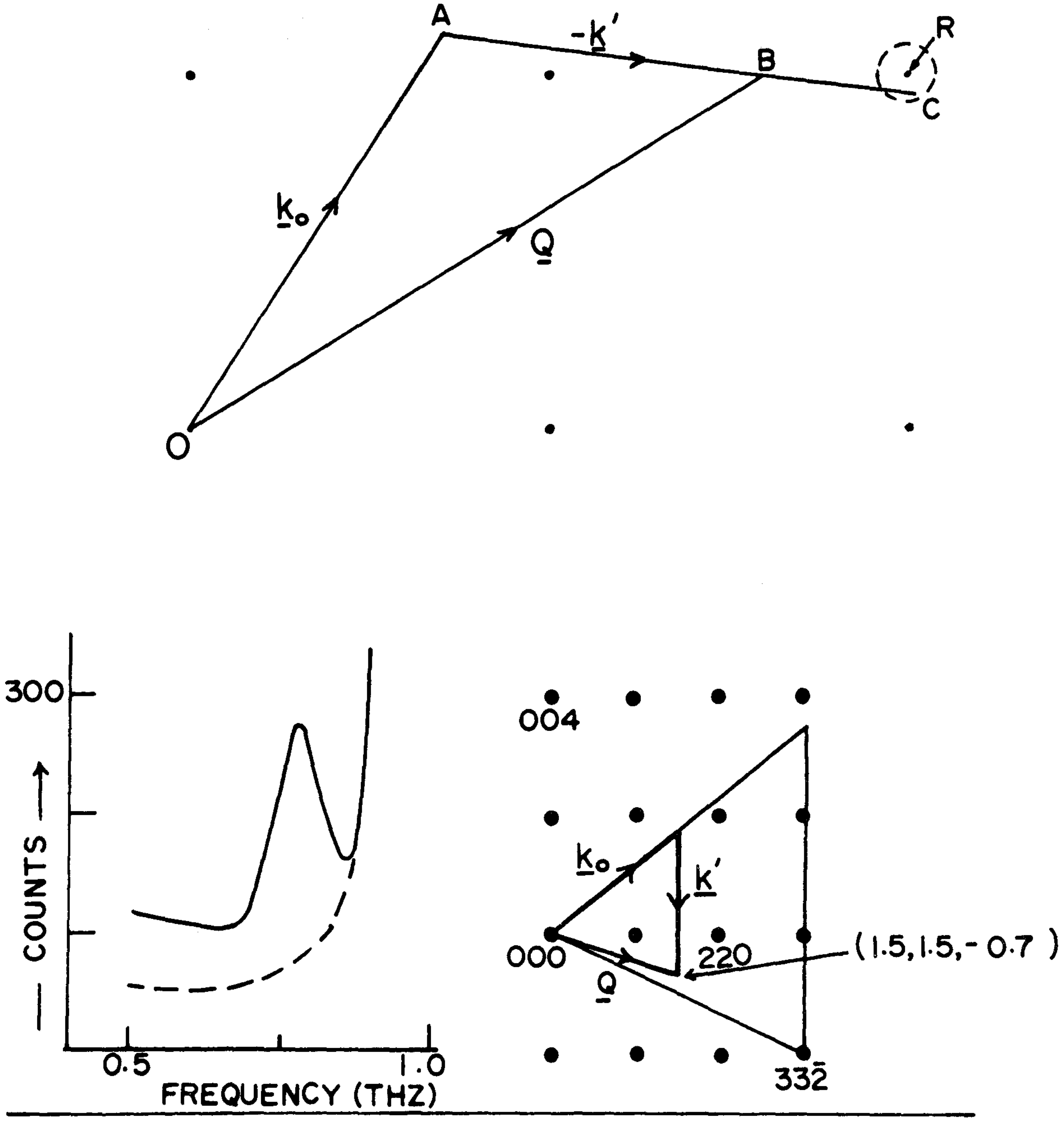

Figure AII-2. Illustrating the production of a peak in a constant $\underline{Q}$ scan, resulting from Bragg reflection in the specimen and incoherent scattering in the analyser.

increase in the count rate in both counters. In the programme, the vector

$$\underline{S} = \underline{k}_{oI} - |\underline{k}_{oI}|\underline{n}'$$

where $\underline{n}'$ is a unit vector in the direction of $\underline{k}'$, is formed. If $\underline{S}$ is approximately equal to a reciprocal lattice vector, a Bragg reflection can occur in the specimen and an appropriate message is printed out. Scans (c) and (d) in Fig. II-3 show this type of behaviour. The sharp upward rise in (c) is a $(33\bar{2})$ reflection in the specimen off the second order (i.e.,the 440) component of the incident beam. The situation is illustrated in the lower part of Fig. AII-2.

Test 2. "Powder" peak off aluminium container

If $\phi/2$ is approximately equal to the Bragg angle for reflection from a set of planes in the aluminium can which encloses the specimen, a "powder" peak may be observed. The peaks in both counters in scans (a) and (b), Fig. II-3, are believed to result from (200) reflections in the can. The effect is more pronounced in the 12°K result since there is an extra can in the beam when the helium cryostat is used (Fig. II-1).

Test 3. Reflections into the background counter

The angle between the two counters in the analyser is approximately 40°. If the background counter is at the smaller scattering angle (case 1 in Fig. AII-3), it may be in a position to pick up neutrons which pass straight through the analyser. This can occur over a range of about 10° in θ_A.

In both case 1 and case 2 (Fig. AII-3), there is the possibility that neutrons will be Bragg reflected by the analyser into the background counter. Since the collimation between the analyser and the counter is poor, the scattering plane can be at an angle anywhere between about 15° and 25° to the (200) plane. The programme searches for (420) and (311) Bragg reflections into the counter , since these are the most likely ones to occur.

Fig. AII-3 illustrates a peak in the background counter attributed to elastic incoherent scattering off the specimen and a (311) reflection in the analyser. Though such a reflection lies out of the plane, it is still allowed: the active section of the detector subtends an angle of at least 30° to the analyser crystal. Real and reciprocal space diagrams of the situation in the analyser are shown at the bottom of Fig. AII-3. Note that the reciprocal space diagram shows the projection on to the (100) plane, so that the reciprocal lattice point (311) becomes (310).

For each ν_{oI} (including ν_{o1}), and furthermore for each ν'_J (including ν'_1), three further tests are performed. As

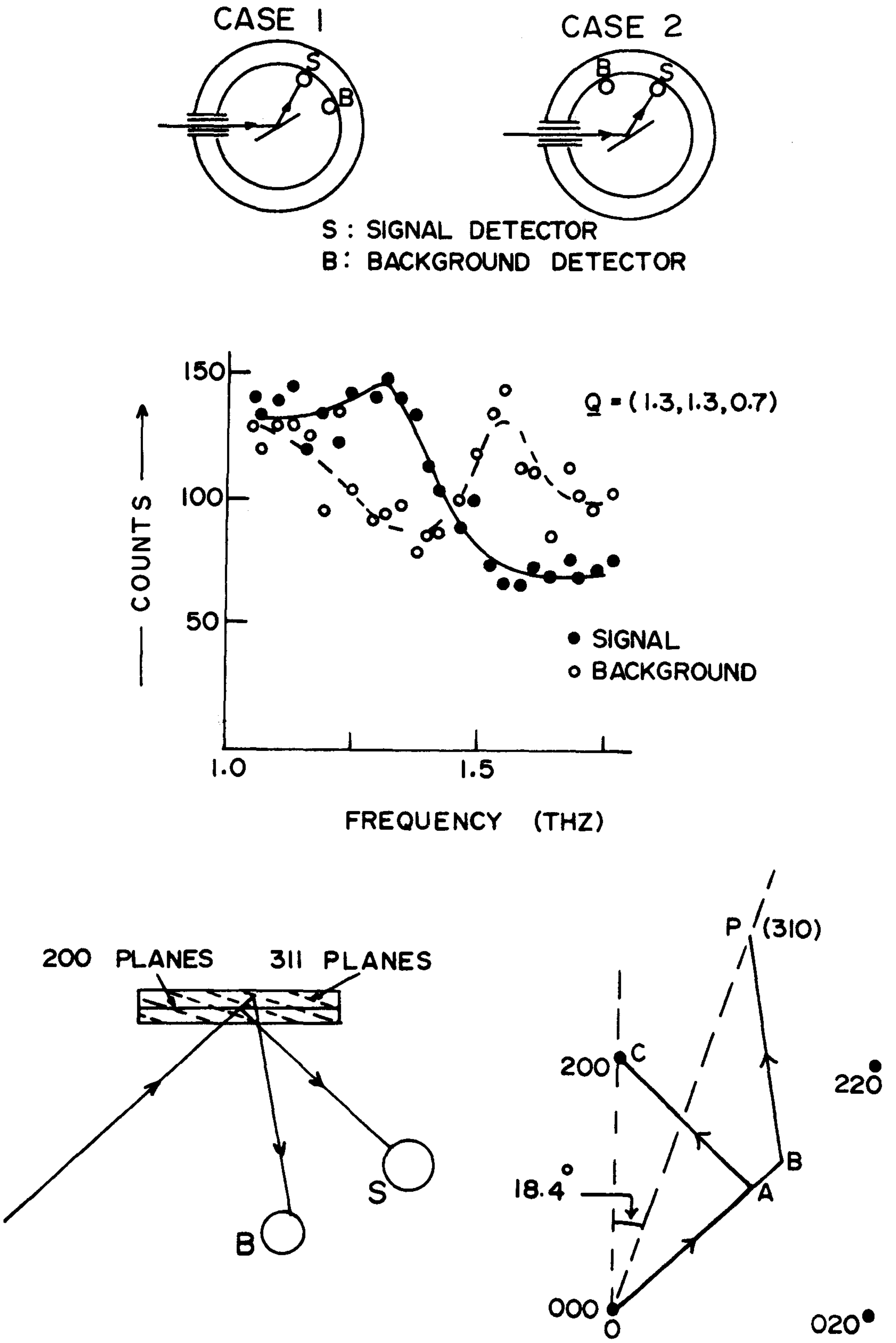

Figure AII-3. Illustrating the way an increase in counting rate can occur in the background detector alone.

before, appropriate messages are printed when a possible spurious process is found.

Test 4. Incoherent elastic process in the specimen

If $\nu_{oI} \simeq \nu'_J$, an incoherent elastic process in the specimen can occur, leading to a peak in the signal counter. Scan (e) (Fig. II-3) shows a very large peak due to incoherent elastic scattering of the $(33\bar{1})$ contaminant (frequency 12.49 THz) and then second order (i.e. 400) reflection in the analyser.

Test 5. Other phonons

We have seen that there are several contributions to the incident beam, and furthermore several frequencies (corresponding to different order reflections) can be detected by coherent scattering from the analyser. With each combination we associate an energy transfer

$$h\nu_{IJ} = h\,(\nu_{oI} - \nu'_J)$$

and a wave vector transfer

$$\underline{Q}_{IJ} = \underline{k}_{oI} - \underline{k}'_J \ .$$

It has already been remarked (Section IE) that one-phonon peaks are only observed for certain spectrometer settings. There are four angular variables, but five equations to be satisfied: conservation of energy and wave vector (i.e. the above equations with I=J=1), and in addition the phonon dispersion relation - all these must be satisfied.

It can happen that the energy and wave vector transfer $h\nu_{IJ}$ and $\underline{Q}_{IJ}$, for I and/or J greater than 1, satisfy the dispersion relation. In this case a peak could be observed in the signal counter .

In the programme, $h\nu_{IJ}$ and $\underline{Q}_{IJ}$ are first evaluated. Using a simple force constant model the 3 frequencies appropriate to $\underline{Q}_{IJ}$ are then found. If one or more of the frequencies is approximately equal to ν_{IJ}, a message is printed. The products $[\underline{e}(\underline{Q}_{IJ},j)]^2$ are also given, since they largely determine the intensity of such a spurion.

This message has appeared on many occasions but no peaks have been identified as resulting from this cause.

Test 6. Multiple scattering

A common cause of trouble in certain materials is multiple scattering (Brockhouse et al. 1961). This is illustrated in Fig. AII-4. In the situation called Type 1, the incident neutron is Bragg reflected within the crystal:

$$\underline{G} = \underline{k}_o - \underline{k}''$$
$$|\underline{k}_o| = |\underline{k}''|$$

It is then inelastically scattered into the analyser:

$$\underline{Q}_{MS} = \underline{k}'' - \underline{k}' \quad .$$

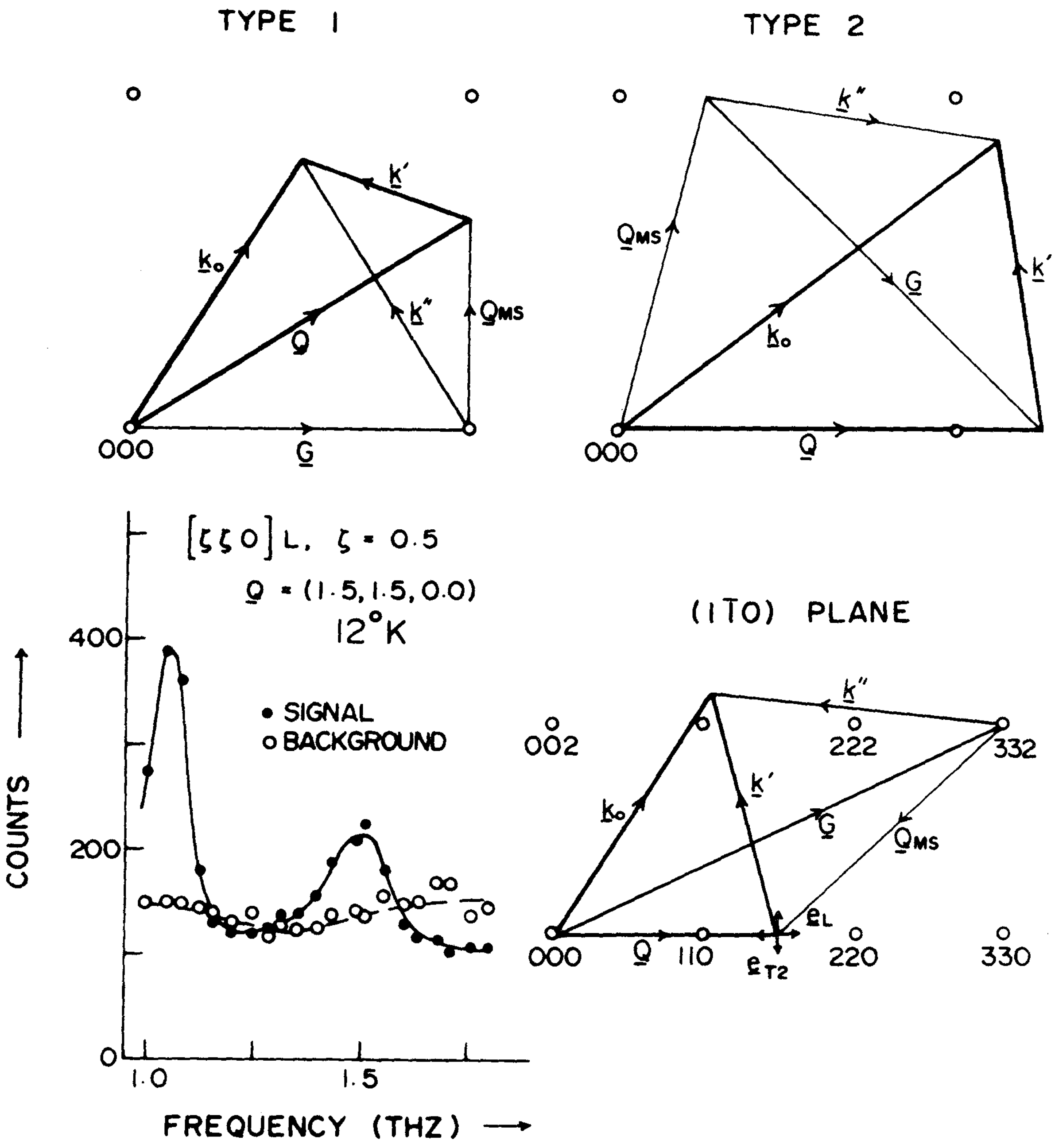

Figure AII-4. Multiple scattering diagrams, and a peak attributed to multiple scattering.

The energy transfer is still $(\nu_o - \nu')$, and the total wave vector transfer is still $\underline{Q}$, since

$$\underline{G} + \underline{Q}_{MS} = \underline{Q}.$$

The factor $(\underline{Q}\cdot\underline{e})^2$ in the one-phonon scattering cross section (Eq. I-D11) is replaced by $(\underline{Q}_{MS}\cdot\underline{e})^2$. Thus modes with the same $\underline{q}$, but with polarization other than the intended polarization, may be detected. The alternative situation (Type 2) is also depicted in Fig. AII-4. Here an inelastic process is followed by an elastic process.

To check for multiple scattering (Type 1), the distance from the terminus of $\underline{k}_{oI}$ to all reciprocal lattice points in the vicinity is determined. If this distance is nearly equal to $|\underline{k}_{oI}|$, this type of scattering can occur. A related procedure is involved in testing for type 2.

Tests for multiple scattering have been limited to the principal wave vectors $\underline{k}_{o1}$ and $\underline{k}_1'$. In this case it is a simple matter (given some knowledge of the dispersion relation) to check first to see which peaks could possibly result from multiple scattering. Such a peak must occur at a frequency appropriate to the reduced wave vector $\underline{q}$ of the scan. Unless this is so, Test 6 (Fig. AII-1) is generally avoided, since it is a relatively lengthy procedure.

The scan shown in Fig. AII-4 shows two well defined peaks. The upper peak is the zone boundary [ζζ0] longitudinal mode. The lower peak is very probably the T2 mode, observed by multiple scattering. The vector diagram (which is of type 1) shows that $\underline{Q}_{MS}$ has a sizeable component parallel to $\underline{e}_{T2}$. The frequency of the T2 phonon at 12°K is 0.96 THz (Table II-2) whereas the peak in the scan occurs at about 1.05 THz. This difference occurs because the Bragg condition for the incident wave vector is best satisfied at a frequency transfer significantly greater than the frequency of the T2 phonon.

APPENDIX III

EFFECTS OF FINITE RESOLUTION IN THE TRIPLE-AXIS SPECTROMETER

A. Previous Work

The resolution of the triple-axis spectrometer has been discussed by several authors. Møller and Nielsen (1970) give a useful review, with references to earlier work.

In a conventional experiment using a triple-axis spectrometer, counts are accumulated at a series of settings of the various angles of the spectrometer. With each setting we may associate a frequency transfer ω and wave vector transfer $\underline{Q}$, where

$$\omega = \omega_o - \omega'$$

$$\underline{Q} = \underline{k}_o - \underline{k}'.$$

Here $\omega_o(\underline{k}_o)$ and $\omega'(\underline{k}')$ are the frequency (wave vector) of the incident and scattered beams respectively.

Finite collimation of the beam, and finite mosaic spreads in the monochromator and analyser, lead to uncertainties in ω_o, $\underline{k}_o$, ω' and $\underline{k}'$ and therefore to uncertainties in ω and $\underline{Q}$. In energy-wave vector space the most probable values of $\underline{Q}$ and ω are represented by the point $(\tilde{\underline{Q}},\tilde{\omega})$. The probability that $\underline{Q}$ and ω have particular values is given by the "resolution function"

$$R_{\tilde{\underline{Q}},\tilde{\omega}}(\Delta\underline{Q},\Delta\omega)$$

where $\Delta\underline{Q} = \underline{Q} - \tilde{\underline{Q}}$, $\Delta\omega = \omega - \tilde{\omega}$, and the subscripts indicate that the function depends parametrically on $\tilde{\underline{Q}}$ and $\tilde{\omega}$.

Following Cooper and Nathans (1967) we assume Gaussian distributions of mosaic blocks in the monochromator and analyser, and Gaussian transmission functions for each collimator. The resolution function may then be written as

$$R_{\tilde{\underline{Q}},\tilde{\omega}}(\Delta\underline{Q},\Delta\omega) = R_o \exp\{- \frac{1}{2} \sum_{k=1}^{4} \sum_{\ell=1}^{4} X_k M_{k\ell}(\tilde{\underline{Q}},\tilde{\omega}) X_\ell\}$$

where $X_1 = \Delta Q_x$, $X_2 = \Delta Q_y$, $X_3 = \Delta Q_z$ and $X_4 = \Delta\omega$: for convenience the x direction is chosen parallel to $\underline{Q}$, and the z direction is chosen normal to the scattering plane. The 4×4 matrix $\underline{\underline{M}}$, known as the resolution matrix, is a complicated function of the spectrometer setting, the mosaic spreads, and the collimations. R_o is the value of $R_{\tilde{\underline{Q}},\tilde{\omega}}(\underline{O},0)$.

The equation

$$\sum_{k\ell} X_k M_{k\ell} X_\ell = 2(\ell n2)$$

defines an ellipsoid in $(\underline{Q},\omega)$ space such that $R = R_o/2$ for every point on its surface. One axis of this "resolution ellipsoid" is normal to the scattering plane. $\underline{\underline{M}}$ may therefore be factorized into a 3×3 matrix and the element M_{33}. In many experiments the resolution normal to the scattering plane is relatively poor, so that M_{33} is comparatively small.

In the common "parallel" setting of the spectrometer, illustrated in Fig. AIII-1(a), the neutron beam is scattered alternately to the left and to the right by the monochromator, sample and analyser. With this arrangement another axis of the resolution ellipsoid lies roughly parallel to $\underline{Q}$ and the remaining axes lie in the $(\Delta Q_y, \Delta\omega)$ plane. The slope of the major axis in this plane corresponds to a typical slow neutron velocity (e.g., a few km/sec). The focussing properties of the triple-axis spectrometer have been considered by Collins (1963), Peckham (1964), Bergsma and van Dijk (1965), and by Peckham et al. (1967). Graphical methods may be used to determine the optimum setting of the spectrometer for observation of a well focussed peak, i.e., an intense, narrow peak. The directions of scattering at monochromator, sample and analyser, and the position of $\underline{Q}$ relative to the nearest reciprocal lattice point, are chosen to optimize the focussing diagram.

This last point is illustrated in Fig. AIII-1. With the "parallel" setting of the spectrometer there is considerable correlation between ΔQ_y and $\Delta\omega$, as mentioned earlier. In Fig. AIII-1 one of the transverse dispersion curves either side of a reciprocal lattice point is shown. The ellipses represent the resolution in the (Q_y, ω) plane. The resolution function varies slowly within this region of $\underline{\tilde{Q}}$ and $\tilde{\omega}$ and is here assumed to be constant. In situation 1 the ellipse passes slowly through the dispersion curve during a constant $\underline{Q}$ scan and the

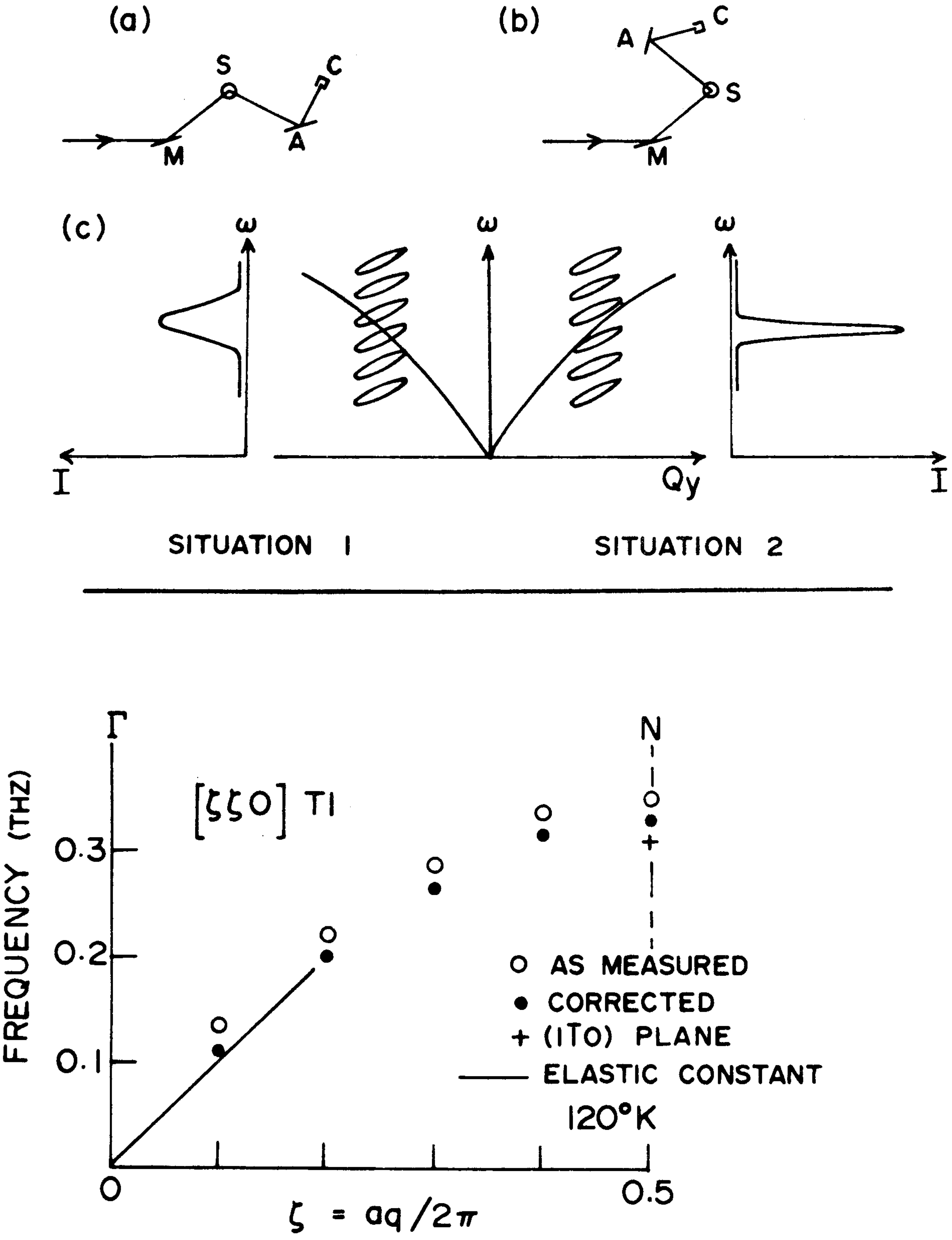

AIII-1. The upper diagram illustrates the idea of focussing. Below, the effect of a correction for resolution, on the [ζζ0]T1 branch.

observed peak is broad. Situation 2 is quite different: the ellipse passes rapidly through the dispersion curve, and the resonance is narrow.

The measurements reported in this thesis were made with the McMaster spectrometer at Chalk River in the "parallel" setting. Wherever possible measurements were made in a focussed position following certain "rules-of-thumb" for this spectrometer (see e.g. Brockhouse 1966).

The fact that the width of an observed resonance depends on instrumental resolution, was noted by Brockhouse et al. (1961), and widths of high temperature phonons were obtained by comparison with the widths of corresponding groups at 100°K. Though this procedure is still widely used (see e.g. Buyers and Cowley 1969), an alternative approach is sometimes adopted. This involves a calculation of the instrumental resolution in terms of the various mosaic spreads and collimating elements of the spectrometer. It is generally done in one of two ways. Cooper and Nathans (1967) give an expression for the width in terms of the resolution matrix elements. They consider a planar dispersion surface and assume the scattering cross section is constant, over the region of $(\underline{Q},\omega)$ space where the resolution function is appreciable. Stedman and Nilsson (1966) instead calculate individual contributions from each collimator and each monochromating crystal, and hence they obtain the instrumental width. The effect of specimen mosaic spread, which broadens transverse peaks, is readily included in such calculations.

Brockhouse et al. (1961) noted that finite instrumental resolution can also shift a peak position. In a later paper (Brockhouse et al. 1962) they considered the shift which results because of finite energy resolution. For a peak with centre at frequency ν_M, having a width W, they give the shift as

$$\Delta\nu \approx W^2/4\nu_M.$$

Shifts in peak positions, resulting from finite resolution, were observed in LiF by Dolling et al. (1968). These workers remarked that two effects will introduce shifts which can become apparent in the case of long wavelength acoustic modes. For wave vectors slightly removed from a symmetry direction, the frequency surface is normally of the form:

$$\nu(\delta_y,\delta_z) = \nu(0,0) + A\delta_y{}^2 + B\delta_z{}^2$$

where $\nu(\delta_y,\delta_z)$ is the frequency at a point δ_y from the symmetry direction in the scattering plane, and δ_z above the scattering plane: A and B may be positive or negative. This parabolic dependence can produce a shift in the peak position. Secondly the variation of the scattering cross section with frequency is most marked at low frequency. For this reason the spread in wave vectors along the symmetry direction introduces a small downward shift in the observed position of the peak. In this work (Dolling et al. 1968) shifts of 2-3% were reported. More recently Raunio (1969) has observed shifts of about 8% in similar measurements on KCl.

Collins et al. (1969) observed marked asymmetry in neutron groups from long wavelength magnons in iron. This asymmetry arises from the curvature of the magnon dispersion curve and the fact that the resolution out of the scattering plane was relatively poor.

Another effect of resolution which has received attention recently is the artificial splitting of a neutron group for [$\zeta\zeta\zeta$]T modes in cubic and similar crystals (Cowley and Pant 1970). Such splittings have been observed in calcite (Cowley and Pant 1970), and in KCl by Raunio and Almqvist (1969) and by the author. Double peaks observed by Smith et. al. (1968) for small $\underset{\sim}{q}$ modes in this branch in lithium probably result from the same cause.

B. Resolution Effects in Rubidium

In the present work on rubidium, we have already noted the appearance of extra peaks in the [00ζ]L branch. Seeking an explanation for this effect, it became clear that the behaviour of the dispersion relation near to the [00ζ] direction was influencing the observed neutron groups. In this section we consider the effect of resolution on measurements of the other branches. The [00ζ]L branch is discussed separately in Section IIF.

For a particular setting of the spectrometer, corresponding to wave vector transfer $\tilde{\underline{Q}}$ and frequency transfer $\tilde{\omega}$, the scattered intensity is simply

$$I(\tilde{\underline{Q}},\tilde{\omega}) = \iint \sigma(\underline{Q},\omega)R(\underline{Q}-\tilde{\underline{Q}},\omega-\tilde{\omega})d\underline{Q}d\omega$$

where $\sigma(\underline{Q},\tilde{\omega})$ is the differential scattering cross section, and the subscripts $\tilde{\underline{Q}},\tilde{\omega}$ have been omitted from R. The one-phonon scattered intensity $I_1(\tilde{\underline{Q}},\tilde{\omega})$ is obtained if the one-phonon differential scattering cross section is used. For energy loss this is (cf. Eq. I-D11):

$$\sigma_1(\underline{Q},\omega) = A \sum_{\underline{q}j} \frac{[\underline{Q}\cdot\underline{e}(\underline{q}j)]^2}{\omega(\underline{q}j)} [n(\underline{q}j)+1]\delta(\omega-\omega(\underline{q}j)) \times \Delta(\underline{Q}-\underline{q}) \qquad \text{(AIII-B1)}$$

where A is a constant, so that we obtain

$$I_1(\tilde{\underline{Q}},\tilde{\omega}) = A \int \sum_{j} \{\frac{[\underline{Q}\cdot\underline{e}(\underline{q}j)]^2}{\omega(\underline{q}j)} [n(\underline{q}j)+1]R(\underline{Q}-\tilde{\underline{Q}},\omega(\underline{q}j)-\tilde{\omega})\}d\underline{Q} \qquad \text{(AIII-B2)}$$

where $\underline{q}$ is the reduced wave vector associated with $\underline{Q}$.

Using Equation (AIII-B2), with an early set of atomic force constants (Copley et al. 1968), shifts Δ_R resulting from vertical resolution (i.e., resolution normal to the scattering plane) have been calculated using a programme originally written by Dr. E. R. Cowley. Since the resolution in the plane is much better than it is normal to the plane (e.g. M_{11} is typically at least an order of magnitude larger than M_{33}), this procedure is justified. Finite energy resolution is incorporated into the calculation, mainly because the intensity $I_1(\tilde{\underline{Q}},\tilde{\omega})$ is calculated for a discrete set of values of $\tilde{\omega}$ and the integration over $\underline{Q}$ is replaced by a sum over a set of values of $\underline{Q}$. If very good energy resolution is used, the delta functions in Eq. (AIII-B1) are very unlikely to peak at any of the values of $\tilde{\omega}$ for which $I_1(\tilde{Q},\tilde{\omega})$ is calculated. For these calculations M_{33} was chosen as 150 $(a/2\pi)^2$ where a is the lattice constant of rubidium. This corresponds to a full width at half height in q_z of $0.11(2\pi/a)$. This choice of M_{33} is consistent with values obtained using the expressions of Cooper and Nathans (1967) with vertical collimations of 1 in 45 and 1 in 15 in the incident and scattered beams respectively. These numbers were determined from the geometry of the spectrometer.

We now consider the effects on the different branches in turn. In the following, a positive shift means that the measured frequency is higher than the true frequency. Shifts are given below in THz.

(i) $\underline{[00\zeta]T}$. The shifts Δ_R are small, ∿ 0.005, whether measurements are made in the (001) or the $(1\bar{1}0)$ scattering planes.

(ii) $\underline{[00\zeta]L}$. See Section IIF .

(iii) $\underline{[\zeta\zeta\zeta]T}$. Δ_R is generally negative and small. For small $\underline{q}$ the groups can split if the vertical resolution is sufficiently relaxed (Cowley and Pant 1970). Close to the degenerate points P and H, the longitudinal mode can influence the lineshape. For example, with $\underline{Q}$ = (0.1, 0.1, 2.9), the contributions from both polarizations are unresolved, and the resulting peak is shifted ∿ 0.05 THz below the transverse frequency.

(iv) [ζζζ]L. Again the shifts are small. They may be of either sign, depending on Q. Near to P the shifts are slightly larger, i.e., ∿ ± 0.01(5).

(v) [ζζ0]T2. The situation at the zone boundary, point N, is discussed with the $[\frac{1}{2}\frac{1}{2}\zeta]\Lambda$ branch below. For ζ ∿ 0.15, Δ_R ∿ 0.015 whereas for ζ ∿ 0.4, Δ_R ∿ 0.01.

(vi) [ζζ0]T1. This branch is especially sensitive to the resolution of the instrument. For small displacements normal to the [ζζ0] direction the frequency increases rapidly. This is clearly visible in Fig. II-12. The measured frequencies lie well above the true frequencies: Δ_R ∿ 0.02. Fig. AIII-1 (lower half) shows the effect of resolution on this branch. The elastic constant line is the same as in Fig. II-4. The situation at the zone boundary is discussed with the [ζζ1]Λ branch below.

(vii) [ζζ0]L. Shifts for this branch (including the point N) are negligible, whether measurements are made in the (001) or the $(1\bar{1}0)$ plane.

(viii) $[\frac{1}{2}\frac{1}{2}\zeta]\Lambda$ This branch is of particular interest. Since it is symmetrical about the point P, it may be completely determined by measuring phonons between neighbouring points N and P, with Q nearly parallel to the line joining these points (Fig. AIII-2(a)). A general point N in the $(1\bar{1}0)$ plane is of the form $(1/2 + h, 1/2 + h, \ell)$ where h and ℓ are integers. We may distinguish even and odd points depending whether ℓ is even or odd. We now consider the vertical (110) plane through the line $N_e P N_o$ (subscripts e and o refer to even and odd points respectively). This plane is illustrated in Fig. AIII-2(b). Constant frequency contours in the (110) plane, which join to the $[\frac{1}{2}\frac{1}{2}\zeta]\Lambda$ branch, are shown in Fig. AIII-2(c) (cf. Fig. II-12). It is clear from this figure that the shift Δ_R is positive (negative) for measurements between N_e and P (N_o and P). This predicted behaviour is observed experimentally, as shown in Fig. AIII-2(d). The calculated shifts are sufficient to account for the observed differences between the measurements taken nearer even and odd points N.

The $[\frac{1}{2}\frac{1}{2}\zeta]\Lambda$ phonon at N itself, i.e., the zone boundary $[\zeta\zeta 0]$T2 phonon frequency, is affected in the same way.

(ix) $\underline{[\frac{1}{2}\frac{1}{2}\zeta]\pi}$. The shifts for this branch are very small.

(x) $\underline{[\zeta\zeta 1]\Lambda}$. This branch, including the mode with $\zeta = 0.5$, which is the zone boundary $[\zeta\zeta 0]$ T1 phonon, may be measured in either scattering plane. Modes measured in the $(1\bar{1}0)$ plane are not shifted, whereas negative shifts ~ 0.015 occur when modes with $\zeta \lesssim 0.25$ are measured in the (001) plane: nearer N the shifts are small, whereas at N $\Delta_R \sim +0.02$.

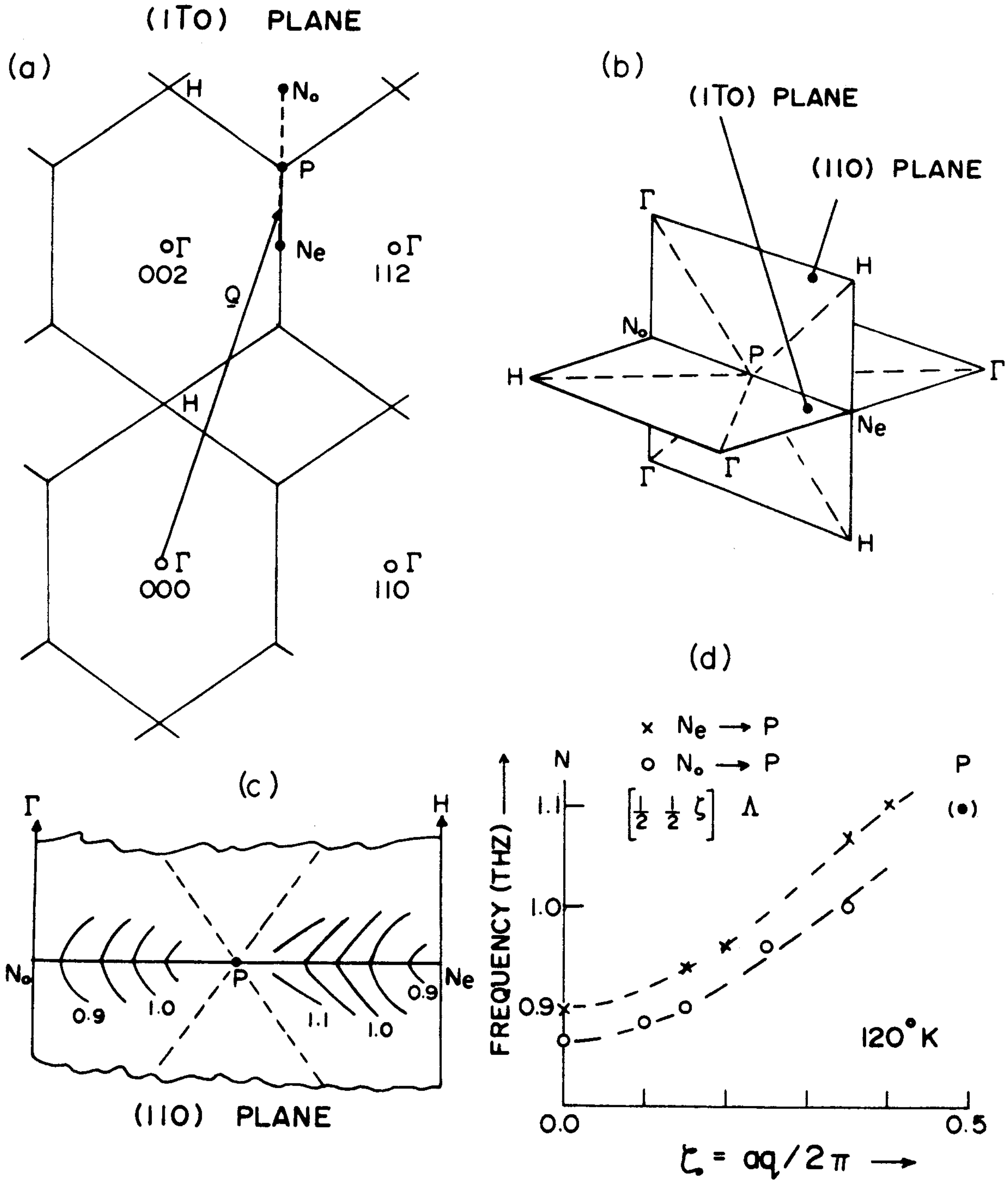

Fig. AIII-2. Illustrating the effects of vertical resolution on the $[\frac{1}{2}\frac{1}{2}\zeta]\Lambda$ branch.

(See Figs. II-11, II-12).

Experimental measurements of the [ζζ0]T1 zone boundary mode in both scattering planes confirm this prediction. The best values, from three measurements in the (001) plane and three in the $(1\bar{1}0)$ plane (at 120°K), are 0.35 ± 0.02 and 0.31 ± 0.02 THz respectively. The correction for resolution lowers the first value to 0.33 ± 0.02 THz, in improved agreement with measurements in the $(1\bar{1}0)$ plane. This is illustrated in the lower part of Fig. AIII-1.

(xi), (xii) [ζζ1]π2,π1. The shifts for these branches are small.

APPENDIX IV

SIMPLIFICATION OF ANHARMONIC MATRIX ELEMENTS

In Section IIIA, expressions were derived for the shift in frequency of a mode $\lambda \equiv (\underline{q}j)$, caused by thermal expansion (Δ_T), and for the principal contributions to the shift and width of a **mode** resulting from "true" anharmonicity, Δ_3, Δ_4 and Γ. In this appendix we shall simplify these expressions, making particular use of the symmetry properties of the cubic lattice.

First we shall examine the important symmetry properties of the anharmonic atomic force constants (the AAFC's), with particular reference to the two body axially symmetric force system which is assumed in this work. In Section B the summations over atomic positions (in the expressions for the shifts and widths) are performed. In each case one or two examples of the method are shown, and the complete results out to third neighbours are given in tables. Section C contains a discussion of the summations over $\underline{q}$-vectors related by symmetry and over cartesian coordinates. Since eigenvectors enter the summations it is generally insufficient to sum over the irreducible volume within the first Brillouin zone. An alternative procedure for simplifying the matrix elements entering the cubic and quartic expressions is briefly discussed in Section D. The final section contains a discussion of various weighting schemes and the generation of wave vectors within various "irreducible" volumes in reciprocal space.

In subsections treating the cubic shift Δ_3 it is to be understood that the cubic width Γ is treated in exactly the same fashion as Δ_3, with $R(\Omega)$ replaced by $-i\pi S(\Omega)$: see Eqs. (III-A23), (III-A25).

A. Properties of the Anharmonic Atomic Force Constants

In the following, we assume a two body axially symmetric force system. The cartesian second derivatives of this potential (i.e., the AFC's) are given by Eq. (I-C5). The third and fourth derivatives (i.e., the AAFC's) are then

$$\phi_{\alpha\beta\gamma}(\ell\ell\ell') = s_\alpha s_\beta s_\gamma C_3(R) + (s_\alpha \delta_{\beta\gamma} + s_\beta \delta_{\gamma\alpha} + s_\gamma \delta_{\alpha\beta}) C_2(R)/R,$$

and

$$-\phi_{\alpha\beta\gamma\sigma}(\ell\ell\ell\ell') = s_\alpha s_\beta s_\gamma s_\sigma C_4(R) + (s_\alpha s_\beta \delta_{\gamma\sigma} + s_\alpha s_\gamma \delta_{\beta\sigma}$$

$$+ s_\alpha s_\sigma \delta_{\beta\gamma} + s_\beta s_\gamma \delta_{\alpha\sigma} + s_\beta s_\sigma \delta_{\alpha\gamma} + s_\gamma s_\sigma \delta_{\alpha\beta}) C_3(R)/R$$

$$+ (\delta_{\alpha\beta}\delta_{\gamma\sigma} + \delta_{\alpha\gamma}\delta_{\beta\sigma} + \delta_{\alpha\sigma}\delta_{\beta\gamma}) C_2(R)/R^2, \qquad \text{(AIV-A1)}$$

where

$$C_2(R) = \phi^{II} - \phi^{I}/R$$

$$C_3(R) = \phi^{III} - 3\phi^{II}/R + 3\phi^{I}/R$$

$$C_4(R) = \phi^{IV} - 6\phi^{III}/R + 15\phi^{II}/R^2 - 15\phi^{I}/R^3 \qquad \text{(AIV-A2)}$$

In these expressions $R = |\underline{r}(\ell'\ell)|$ and $s_\alpha = R_\alpha/R$. Furthermore

$$\phi^{I} = \left.\frac{d\Phi}{dr}\right|_{r=R} , \quad \phi^{II} = \left.\frac{d^2\Phi}{dr^2}\right|_{r=R} \quad \text{etc.} \qquad (A^{I}V\text{-}A3)$$

The following properties of the AAFC's will be used in subsequent sections. The first four properties are quite general.

(1). Since the order of differentiation is immaterial, we may permute pairs of indices so that

$$\phi_{\alpha\beta\gamma}(\ell\ell'\ell'') = \phi_{\beta\alpha\gamma}(\ell'\ell\ell'') \text{ etc.,}$$

$$\phi_{\alpha\beta\gamma\sigma}(\ell\ell'\ell''\ell''') = \phi_{\beta\gamma\alpha\sigma}(\ell'\ell''\ell\ell''') \text{ etc.}$$

(2). The AAFC's depend only on separations so that, in an obvious notation:

$$\phi_{\alpha\beta\gamma}(\ell\ell'\ell'') = \phi_{\alpha\beta\gamma}(0,\ell'-\ell,\ell''-\ell) \text{ etc.,}$$

$$\phi_{\alpha\beta\gamma\sigma}(\ell\ell'\ell''\ell''') = \phi_{\alpha\beta\gamma\sigma}(\ell-\ell'',\ell'-\ell'', 0,\ell'''-\ell'') \text{ etc.}$$

(3). Translational invariance requires that (Born and Huang 1954, p. 221):

$$\sum_{\ell\ell'} \phi_{\alpha\beta\gamma}(\ell\ell'\ell'') = 0$$

$$\sum_{\ell\ell'\ell''} \phi_{\alpha\beta\gamma\sigma}(\ell\ell'\ell''\ell''') = 0 \text{ .}$$

(4). On inversion of the atomic coordinates we obtain

$$\phi_{\alpha\beta\gamma}(\ell\ell'\ell'') = -\phi_{\alpha\beta\gamma}(-\ell,-\ell',-\ell'')$$

$$\phi_{\alpha\beta\gamma\sigma}(\ell\ell'\ell''\ell''') = +\phi_{\alpha\beta\gamma\sigma}(-\ell,-\ell',-\ell'',-\ell''').$$

Hence (using property 2 above)

$$\phi_{\alpha\beta\gamma}(\ell\ell\ell) = \phi_{\alpha\beta\gamma}(000) = 0.$$

For the two-body axially symmetric interaction, there are additional properties. In this approximation only two of the indices $\ell,\ell'\ldots$ can be different.

(5). Examining Eqs. (AIV-A1) we note that the cartesian indices may be permuted independently of the labels ℓ,ℓ'. Therefore

$$\phi_{\alpha\beta\gamma}(\ell\ell\ell') = \phi_{\beta\alpha\gamma}(\ell\ell\ell') \text{ etc.,}$$

$$\phi_{\alpha\beta\gamma\sigma}(\ell\ell\ell\ell') = \phi_{\alpha\gamma\sigma\beta}(\ell\ell\ell\ell') \text{ etc.}$$

(6). Performing one of the differentiations with respect to the other end of the vector $\underline{r}(\ell'\ell)$, we obtain

$$\phi_{\alpha\beta\gamma}(\ell\ell\ell') = -\phi_{\alpha\beta\gamma}(\ell\ell'\ell')$$

$$\phi_{\alpha\beta\gamma\sigma}(\ell\ell\ell\ell') = -\phi_{\alpha\beta\gamma\sigma}(\ell\ell\ell'\ell')$$

See also Leibfried and Ludwig (1961), p. 295.

Using properties (1) - (6) above, it is convenient to obtain some further relations.

(7). From (1) and (5) it is clear that the labels ℓ and ℓ' may be permuted independently:

$$\phi_{\alpha\beta\gamma}(\ell\ell\ell') = \phi_{\alpha\beta\gamma}(\ell\ell'\ell) \text{ etc.,}$$

$$\phi_{\alpha\beta\gamma\sigma}(\ell\ell\ell\ell') = \phi_{\alpha\beta\gamma\sigma}(\ell\ell'\ell\ell) \text{ etc.}$$

(8). Using (2) and (4),

$$\phi_{\alpha\beta\gamma\sigma}(\ell\ell\ell\ell') = \phi_{\alpha\beta\gamma\sigma}(000h) \text{ where } h=\ell'-\ell$$

$$= \phi_{\alpha\beta\gamma\sigma}(000-h)$$

Finally, using (2) again,

$$\phi_{\alpha\beta\gamma\sigma}(\ell\ell\ell\ell') = \phi_{\alpha\beta\gamma\sigma}(\ell'\ell'\ell'\ell)$$

Similarly (using (7) also),

$$\phi_{\alpha\beta\gamma}(\ell\ell\ell') = -\phi_{\alpha\beta\gamma}(\ell\ell'\ell')$$

which is the same result as in (6) above.

(9). Using properties (2) and (3) we have

$$\sum_{\ell'\ell''\ell'''} \phi_{\alpha\beta\gamma\sigma}(0\ell'\ell''\ell''') = 0.$$

For two-body forces ($\ell',\ell'',\ell''' = 0$ or ℓ), we have

$$\phi_{\alpha\beta\gamma\sigma}(0000) + \sum_{\ell}{}'[\phi_{\alpha\beta\gamma\sigma}(000\ell) + \phi_{\alpha\beta\gamma\sigma}(00\ell0)$$

$$+ \phi_{\alpha\beta\gamma\sigma}(0\ell00) + \phi_{\alpha\beta\gamma\sigma}(0\ell\ell0) + \phi_{\alpha\beta\gamma\sigma}(0\ell0\ell)$$

Using property (6), we obtain

$$+ \phi_{\alpha\beta\gamma\sigma}(00\ell\ell) + \phi_{\alpha\beta\gamma\sigma}(0\ell\ell\ell)] = 0$$

Using property (6), we obtain

$$\phi_{\alpha\beta\gamma\sigma}(0000) = - \sum_{\ell}{}' \phi_{\alpha\beta\gamma\sigma}(000\ell).$$

This result is used to simplify the expression for the quartic shift.

B. The Summations Over Atomic Positions

As the first stage in simplifying the expressions obtained in Chapter III, we shall perform the sums over atomic positions. We consider first, second and third neighbours in the b.c.c. lattice, but it should be noted that first and second neighbours in the f.c.c. lattice have the same symmetry as third and second neighbours in the b.c.c. lattice, so that the results presented in this section are also applicable to the f.c.c. lattice, with only a few small modifications.

(i) The Thermal Expansion

The shift in frequency of the mode λ, due to a thermal strain η, is written (Eq. III-A2):

$$\Delta_T(\lambda) = [\eta/m\omega(\lambda)]\sum_{\alpha\beta} e_\alpha(\lambda)e_\beta(\lambda)\sum_{\gamma} f_{\alpha\beta\gamma}(\underline{q}) \qquad \text{(AIV-B1)}$$

with

$$f_{\alpha\beta\gamma}(\underline{q}) = \frac{1}{2}\sum_{\substack{\ell'\neq\ell \\ \ell''}} \phi_{\alpha\beta\gamma}(\ell\ell'\ell'')r_\gamma(\ell'')[\exp\{i\underline{q}\cdot\underline{r}(\ell'\ell)\}-1].$$

Since we are assuming two body forces, we consider only $\ell'' = \ell$ or $\ell'' = \ell'$. Therefore

$$f_{\alpha\beta\gamma}(\underset{\sim}{q}) = \frac{1}{2}\sum_{\ell'\neq\ell}[\phi_{\alpha\beta\gamma}(\ell\ell'\ell)r_\gamma(\ell) + \phi_{\alpha\beta\gamma}(\ell\ell'\ell')r_\gamma(\ell')]$$

$$\times\ [\exp\{i\underset{\sim}{q}\cdot\underline{r}(\ell'\ell)-1] .$$

Using properties (6) and (7) above, we obtain

$$f_{\alpha\beta\gamma}(\underset{\sim}{q}) = \frac{1}{2}\sum_{\ell'\neq\ell}\phi_{\alpha\beta\gamma}(\ell\ell\ell')r_\gamma(\ell'\ell)[1-\exp\{i\underset{\sim}{q}\cdot\underline{r}(\ell'\ell)\}]$$

$$= \sum_{\ell>0}\phi_{\alpha\beta\gamma}(00\ell)r_\gamma(\ell)[1-\cos(\underset{\sim}{q}\cdot\underline{r}(\ell))] \qquad \text{(AIV-B2)}$$

where we have taken the origin at $\underline{r}(0)$. Note that the first expression above is written in the form of differences $r_\gamma(\ell'\ell)$, indicating that the expression is independent of the choice of ℓ.

The notation $\ell > 0$ indicates that the summation is performed over half the neighbours such that only one member of each pair of neighbours related by the inversion operation is included. For example, of the six second nearest neighbours one member of each pair, $(200, \bar{2}00)$, $(020, 0\bar{2}0)$, $(002, 00\bar{2})$ is included.

We rewrite Eq. (AIV-B1) as

$$f_{\alpha\beta\gamma}(\underset{\sim}{q}) = \sum_i f^{(i)}_{\alpha\beta\gamma}(\underset{\sim}{q})$$

with

$$f^{(i)}_{\alpha\beta\gamma}(\underset{\sim}{q}) = \sum_{\ell_i>0}\phi_{\alpha\beta\gamma}(00\ell_i)r_\gamma(\ell_i)[1-\cos\underset{\sim}{q}\cdot\underline{r}(\ell_i)],$$

where i denotes the i'th nearest neighbour shell. The quantities $f^{(i)}_{\alpha\beta\gamma}(\underset{\sim}{q})$ are readily evaluated in terms of the derivatives

C_{2i}, C_{3i}, and C_{4i} (Table AIV-1). We need only consider four distinct cases, for each i:

(i) α, β, γ all different,

(ii) $\alpha = \beta = \gamma$,

(iii) $\alpha = \beta \neq \gamma$,

(iv) $\alpha \neq \beta = \gamma$.

As an example we shall evaluate $f^{(1)}_{xxx}(\underline{q})$.

$$\begin{aligned} f^{(1)}_{xxx}(\underline{q}) &= \phi_{xxx}(0,0,111)\cdot(a/2)\cdot[1-\cos(q_x+q_y+q_z)] \\ &+ \phi_{xxx}(0,0,\bar{1}11)\cdot(-a/2)\cdot[1-\cos(-q_x+q_y+q_z)] \\ &+ \phi_{xxx}(0,0,1\bar{1}1)\cdot(a/2)\cdot[1-\cos(q_x-q_y+q_z)] \\ &+ \phi_{xxx}(0,0,\bar{1}\bar{1}1)\cdot(-a/2)\cdot[1-\cos(-q_x-q_y+q_z)] \end{aligned}$$

In the above expression, and in similar expressions later in this appendix the components of $\underline{q}$ are given in units of (2/a).

Now

$$\begin{aligned} \phi_{xxx}(0,0,111) &= C_{31}/3\sqrt{3} + \sqrt{3}\, C'_{21} \equiv \frac{1}{2} A_{31} \\ \phi_{xxx}(0,0,\bar{1}11) &= -\frac{1}{2} A_{31} \\ \phi_{xxx}(0,0,1\bar{1}1) &= \frac{1}{2} A_{31} \\ \phi_{xxx}(0,0,\bar{1}\bar{1}1) &= -\frac{1}{2} A_{31} \end{aligned}$$

Hence

$$f^{(1)}_{xxx}(\underline{q}) = aA_{31}(1-\cos q_x \cos q_y \cos q_z).$$

Complete results for i = 1, 2 and 3 are given in Table AIV-2.

(ii) The Quartic Shift

From Eqs. (III-A24) and (III-B2) we have

$$\Delta_4(\lambda) = \frac{\hbar}{Nm^2\omega_1} \sum_{\underline{q}_2 j_2} \left(\frac{n_2+\frac{1}{2}}{\omega_2}\right) \sum_{\alpha\beta\gamma\sigma} e_\alpha(1)e_\beta(1)e_\gamma(2)e_\sigma(2)h_{\alpha\beta\gamma\sigma}(12)$$

where

$$h_{\alpha\beta\gamma\sigma}(12) = \frac{1}{4} \sum_{\ell'\ell''\ell'''} \phi_{\alpha\beta\gamma\sigma}(\ell\ell'\ell''\ell''')\exp\{i[\underline{q}_1\cdot\underline{r}_{\ell\ell'}+\underline{q}_2\cdot\underline{r}_{\ell''\ell'''}]\}$$

(AIV-B3)

In the above, $e_\alpha(1) \equiv e_\alpha(\lambda_1)$ etc.

Again considering two body forces, with one atom at the origin ($\ell = 0$), we obtain:

$$h_{\alpha\beta\gamma\sigma}(12) = \frac{1}{4}\phi_{\alpha\beta\gamma\sigma}(0000) + \frac{1}{4}\sum_{\ell}{}' [\phi_{\alpha\beta\gamma\sigma}(000\ell)e^{-i\underline{q}_2\cdot\underline{r}(\ell)}$$

$$+ \phi_{\alpha\beta\gamma\sigma}(00\ell0)e^{i\underline{q}_2\cdot\underline{r}(\ell)} + \phi_{\alpha\beta\gamma\sigma}(0\ell00)e^{-i\underline{q}_1\cdot\underline{r}(\ell)}$$

$$+ \phi_{\alpha\beta\gamma\sigma}(0\ell\ell0)e^{i(\underline{q}_2-\underline{q}_1)\cdot\underline{r}(\ell)} + \phi_{\alpha\beta\gamma\sigma}(0\ell0\ell)e^{-i(\underline{q}_1+\underline{q}_2)\cdot\underline{r}(\ell)}$$

$$+ \phi_{\alpha\beta\gamma\sigma}(00\ell\ell) + \phi_{\alpha\beta\gamma\sigma}(0\ell\ell\ell)e^{-i\underline{q}_1\cdot\underline{r}(\ell)}]$$

Using properties (6) - (9) above, this becomes

$$h_{\alpha\beta\gamma\sigma}(12) = \frac{1}{4}\sum_{\ell}{}'[\phi_{\alpha\beta\gamma\sigma}(000\ell)\{e^{-i\underline{q}_2\cdot\underline{r}(\ell)} + e^{i\underline{q}_2\cdot\underline{r}(\ell)}$$

$$+ e^{i\underline{q}_1\cdot\underline{r}(\ell)} - e^{i(\underline{q}_2-\underline{q}_1)\cdot\underline{r}(\ell)} - e^{-i(\underline{q}_1+\underline{q}_2)\cdot\underline{r}(\ell)}$$

$$+ e^{-i\underline{q}_1\cdot\underline{r}(\ell)} - 2\}]$$

Since

$$\sum_{\ell}{}' \phi_{\alpha\beta\gamma\sigma}(000\ell)e^{-i\underline{q}_1\cdot\underline{r}(\ell)} = \sum_{\ell}{}' \phi_{\alpha\beta\gamma\sigma}(000\ell)e^{i\underline{q}_1\cdot\underline{r}(\ell)},$$

Eq. (AIV-B2) reduces to the form

$$h_{\alpha\beta\gamma\sigma}(12) = -\sum_{\ell>0} \phi_{\alpha\beta\gamma\sigma}(000\ell)[1-\cos(\underline{q}_1\cdot\underline{r}(\ell))][1-\cos(\underline{q}_2\cdot\underline{r}(\ell))]$$

This is written as

$$h_{\alpha\beta\gamma\sigma}(12) = \sum_{i}\sum_{\kappa=1}^{5} h^{(i)}_{\alpha\beta\gamma\sigma,\kappa}(12)$$

where

$$h^{(i)}_{\alpha\beta\gamma\sigma,\kappa}(12) = -\sum_{\ell>0} \phi_{\alpha\beta\gamma\sigma}(000\ell)\mu_\kappa \cos \underline{q}_\kappa\cdot\underline{r}(\ell).$$

In this expression

$$\mu_1 = \mu_2 = -1 ; \mu_3 = \mu_4 = \frac{1}{2} ; \mu_5 = 1;$$

$$\underline{q}_3 = \underline{q}_1 + \underline{q}_2 ; \underline{q}_4 = \underline{q}_1 - \underline{q}_2 ; \underline{q}_5 = 0.$$

and $\underline{q}_1$, $\underline{q}_2$ are as before.

Then there are four distinct cases for each i:

(i) $\alpha = \beta = \gamma = \sigma$,

(ii) $\alpha = \beta = \gamma \neq \sigma$,

(iii) $\alpha = \beta \neq \gamma = \sigma$,

(iv) $\alpha = \beta \neq \gamma \neq \sigma$, with $\alpha \neq \sigma$.

We consider two examples.

First we evaluate $h^{(2)}_{xxyy,\kappa}(12)$.

$$h^{(2)}_{xxyy,\kappa}(12) = -\phi_{xxyy}(0,0,0,100)\mu_\kappa \cos(2q_{\kappa x})$$

$$-\phi_{xxyy}(0,0,0,010)\mu_\kappa \cos(2q_{\kappa y})$$

$$-\phi_{xxyy}(0,0,0,001)\mu_\kappa \cos(2q_{\kappa z})$$

Now $-\phi_{xxyy}(0,0,0,100) = C'_{32}+ C''_{22}$ (Table AIV-1)

$$-\phi_{xxyy}(0,0,0,010) = C'_{32}+C''_{22}$$

$$-\phi_{xxyy}(0,0,0,001) = C''_{22} \; .$$

Therefore

$$h^{(2)}_{xxyy,\kappa}(12) = \mu_\kappa\{(C'_{32}+C''_{22})[\cos(2q_{\kappa x})+\cos(2q_{\kappa y})]+C''_{22} \cos(2q_{\kappa z})\}$$

Secondly, consider

$$\begin{aligned} h^{(3)}_{zxyz,\kappa}(12) = &-\phi_{zxyz}(0,0,0,110)\mu_\kappa \cos(2q_{\kappa x}+2q_{\kappa y}) \\ &-\phi_{zxyz}(0,0,0,1\bar{1}0)\mu_\kappa \cos(2q_{\kappa x}-2q_{\kappa y}) \\ &-\phi_{zxyz}(0,0,0,101)\mu_\kappa \cos(2q_{\kappa x}+2q_{\kappa z}) \\ &-\phi_{zxyz}(0,0,0,10\bar{1})\mu_\kappa \cos(2q_{\kappa x}-2q_{\kappa z}) \\ &-\phi_{zxyz}(0,0,0,011)\mu_\kappa \cos(2q_{\kappa y}+2q_{\kappa z}) \\ &-\phi_{zxyz}(0,0,0,01\bar{1})\mu_\kappa \cos(2q_{\kappa y}-2q_{\kappa z}) \end{aligned}$$

Now

$$-\phi_{zxyz}(0,0,0,110) = C'_{33}/2$$

$$-\phi_{zxyz}(0,0,0,1\bar{1}0) = -C'_{33}/2$$

The remainder vanish, so that

$$h^{(3)}_{zxyz,\kappa}(12) = -\mu_\kappa C'_{33} \sin(2q_{\kappa x})\sin(2q_{\kappa y}) .$$

The results for i = 1, 2, and 3 are given in Table AIV-3. Since the indices α, β, γ, σ may be permuted in $h^{(i)}_{\alpha\beta\gamma\sigma,\kappa}(12)$, only one permutation of each set of indices is given.

(iii) The Cubic Shift

The cubic contribution to the shift is (Eq. III-A23):

$$\Delta_3(\lambda_1,\Omega) = -\frac{18}{\hbar^2}\sum_{\lambda_2,\lambda_3}\left|V(\lambda_1\lambda_2\lambda_3)\right|^2 R(\Omega) \qquad \text{(AIV-B4)}$$

Here (Eq. III-B1):

$$V(\lambda_1\lambda_2\lambda_3)=\frac{1}{6}\left\{\frac{\hbar^3}{8\omega_1\omega_2\omega_3 Nm^3}\right\}^{\frac{1}{2}}\sum_{\alpha\beta\gamma} e_\alpha(\lambda_1)e_\beta(\lambda_2)e_\gamma(\lambda_3)\ [2ig_{\alpha\beta\gamma}(\underline{q}_1\underline{q}_2\underline{q}_3)]$$

where

$$2ig_{\alpha\beta\gamma}(\underline{q}_1\underline{q}_2\underline{q}_3) = \sum_{\ell'\ell''}\phi_{\alpha\beta\gamma}(\ell\ell'\ell'')\exp\{i[q_1\cdot\underline{r}(\ell)$$
$$+\underline{q}_2\cdot\underline{r}(\ell')+\underline{q}_3\cdot\underline{r}(\ell'')]\}\Delta(\underline{q}_1+\underline{q}_2+\underline{q}_3).$$

For convenience we drop the Δ-function, keeping in mind that the wave vector is conserved. With the origin at $\ell = 0$, and for two body forces, we have

$$2ig_{\alpha\beta\gamma}(\underline{q}_1\underline{q}_2\underline{q}_3) = \phi_{\alpha\beta\gamma}(000) + \sum_{\ell}{}'\ \{\phi_{\alpha\beta\gamma}(00\ell)$$
$$\times\ \exp[i\underline{q}_3\cdot\underline{r}(\ell)]+\phi_{\alpha\beta\gamma}(0\ell 0)\exp[i\underline{q}_2\cdot\underline{r}(\ell)]+\ \phi_{\alpha\beta\gamma}(0\ell\ell)$$
$$\times\ \exp[i(\underline{q}_2+\underline{q}_3)\cdot\underline{r}(\ell)]\} \qquad \text{(AIV-B5)}$$

Using properties (4), (6) and (7) and remembering conservation of wave vector, Eq. (AIV-B5) becomes

$$g_{\alpha\beta\gamma}(\underline{q}_1\underline{q}_2\underline{q}_3) = \sum_{\ell>0} \phi_{\alpha\beta\gamma}(00\ell) \sum_{\kappa=1}^{3} \sin \underline{q}_\kappa \cdot \underline{r}(\ell).$$

We now write

$$g_{\alpha\beta\gamma}(\underline{q}_1\underline{q}_2\underline{q}_3) = \sum_{i} \sum_{\kappa=1}^{3} g^{(i)}_{\alpha\beta\gamma,\kappa}(\underline{q}_1\underline{q}_2\underline{q}_3)$$

where

$$g^{(i)}_{\alpha\beta\gamma,\kappa}(\underline{q}_1\underline{q}_2\underline{q}_3) = \sum_{\ell_i>0} \phi_{\alpha\beta\gamma}(00\ell_i)\sin[\underline{q}_\kappa \cdot \underline{r}(\ell_i)] \ .$$

There are three distinct cases for each i:

(i) α, β, γ all different,

(ii) $\alpha = \beta = \gamma$,

(iii) $\alpha = \beta \neq \gamma$.

As an example we evaluate $g^{(1)}_{xyz,\kappa}(\underline{q}_1\underline{q}_2\underline{q}_3)$

$$\begin{aligned} g^{(1)}_{xyz,\kappa}(\underline{q}_1\underline{q}_2\underline{q}_3) &= \phi_{xyz}(0,0,111)\sin(q_{\kappa x}+q_{\kappa y}+q_{\kappa z}) \\ &+ \phi_{xyz}(0,0,\bar{1}11)\sin(-q_{\kappa x}+q_{\kappa y}+q_{\kappa z}) \\ &+ \phi_{xyz}(0,0,1\bar{1}1)\sin(q_{\kappa x}-q_{\kappa y}+q_{\kappa z}) \\ &+ \phi_{xyz}(0,0,\bar{1}\bar{1}1)\sin(-q_{\kappa x}-q_{\kappa y}+q_{\kappa z}) \end{aligned}$$

Now

$$\phi_{xyz}(0,0,111) = C_{31}/3\sqrt{3} = \frac{1}{2} A_{11} \quad \text{(Table AIV-1)}$$

$$\phi_{xyz}(0,0,\bar{1}11) = -\frac{1}{2} A_{11}$$

$$\phi_{xyz}(0,0,1\bar{1}1) = -\frac{1}{2} A_{11}$$

$$\phi_{xyz}(0,0,\bar{1}\bar{1}1) = \frac{1}{2} A_{11}$$

Therefore

$$g^{(1)}_{xyz,\kappa}(\underline{q}_1\underline{q}_2\underline{q}_3) = -2A_{11} \sin q_{\kappa x} \sin q_{\kappa y} \sin q_{\kappa z}.$$

The results for i = 1, 2 and 3 are given in Table AIV-4. Since the indices α, β, γ may be permuted in $g^{(i)}_{\alpha\beta\gamma,\kappa}(\underset{\sim}{q}_1\underset{\sim}{q}_2\underset{\sim}{q}_3)$, only one permutation of each set of indices is given.

C. The Summations over Equivalent Wave Vectors and Over Cartesian Coordinates

The expressions for the thermal expansion α, and the quantities Δ_3, Δ_4 and Γ, contain summations over wave vectors uniformly distributed throughout the first Brillouin zone (BZ). Since the summands contain eigenvectors, it is not necessarily true that a summation over the irreducible (1/48)th of the BZ (the IBZ) is equivalent. In this section we shall show that (i) in the case of α a summation over the IBZ is equivalent, (ii) the summand in the expression for Δ_4 may be cast in such a form that a summation over the IBZ is sufficient and equivalent, and (iii) the situation is considerably more complicated in the case of Δ_3 (see below).

The summations over α, β, γ (and σ in Δ_4) are also performed. We consider the thermal expansion first, and then the quartic shift. The cubic terms are considered last, in view of their additional complications.

(i) The Thermal Expansion

From Eqs. (III-A14), (III-A3), and (AIV-B1) we have

$$\alpha(T) = \frac{-1}{9VB} \sum_{\underset{\sim}{q}j}^{BZ} \frac{C(\underset{\sim}{q}j)}{M\omega^2(\underset{\sim}{q}j)} \sum_{\alpha\beta} e_\alpha(\underset{\sim}{q}j)e_\beta(\underset{\sim}{q}j) \sum_{\gamma} f_{\alpha\beta\gamma}(\underset{\sim}{q})$$

where the first summation is over $\underset{\sim}{q}$ in the first Brillouin zone. We may rewrite the above expression as

$$\alpha(T) = \frac{-1}{9VB} \sum_{\underset{\sim}{q}j}^{IBZ} \frac{C(\underset{\sim}{q}j)}{m\omega^2(\underset{\sim}{q}j)} S_T \qquad \text{(AIV-C1)}$$

where

$$S_T = \sum_{48} \sum_{\alpha\beta\gamma} e_\alpha(\underset{\sim}{q}'j) e_\beta(\underset{\sim}{q}'j) f_{\alpha\beta\gamma}(\underset{\sim}{q}') \quad .$$

The notation $\sum_{48}$ indicates a summation over the 48 wave vectors $\underset{\sim}{q}'$ which are equivalent to $\underset{\sim}{q}$ in the IBZ. Writing $\underset{\sim}{q} = (r,s,t)$, $\underset{\sim}{e}(\underset{\sim}{q}j) = (u,v,w)$, and using Table AIV-2, we obtain

$$I = a^{-1} \sum_{\alpha\beta\gamma} e_\alpha(\underset{\sim}{q}j)\ e_\beta(\underset{\sim}{q}j) f_{\alpha\beta\gamma}(\underset{\sim}{q}) \qquad \text{(AIV-C2)}$$

$$= -(A_{31}+2A_{21})D_2+2(A_{11}+2A_{21})P_2+A_{22}P_4+A_{12}P_6 \qquad \text{(AIV-C3)}$$

where D_2, P_2, P_4 and P_6 are defined in Table AIV-5. The above expression includes contributions from first and second neighbours. The contribution from third neighbours is similarly evaluated. We note that I is invariant with respect to all the operations of the cubic group ($\underset{\sim}{e}$ transforms in the same way as $\underset{\sim}{q}$). We may therefore write

$$S_T = 48I\ a \qquad \text{(AIV-C4)}$$

and a summation over the IBZ is sufficient.

(ii) The Quartic Shift

The quartic shift may be written as

$$\Delta_4(\lambda_1) = \frac{\hbar}{Nm^2\omega_1} \sum_{\underset{\sim}{q}_2 j_2}^{IBZ} \left(\frac{n_2+\frac{1}{2}}{\omega_2}\right) \sum_i S_i \qquad \text{(AIV-C5)}$$

where the first summation is over the irreducible volume of the first Brillouin zone and the second is over shells of neighbours. The quantity S_i is a sum over the 48 wave vectors equivalent to $\underset{\sim}{q}_2$:

$$S_i = \sum_{\alpha\beta\gamma\sigma} e_\alpha(1)e_\beta(1) \sum_{48} e_\gamma(2)e_\sigma(2) \sum_\kappa h^{(i)}_{\alpha\beta\gamma\sigma,\kappa}(12).$$

We first simplify the sums over κ. For $i = 1$ there are two types of sum:

(a) $$I_1 = \sum_\kappa \cos(q_{\kappa x})\cos(q_{\kappa y})\cos(q_{\kappa z})$$

$$= 1 - c_{1x}c_{1y}c_{1z} - c_{2x}c_{2y}c_{2z}$$
$$+ \frac{1}{2}(c_{3x}c_{3y}c_{3z} + c_{4x}c_{4y}c_{4z})$$

where c_{1x} denotes $\cos(q_{1x})$, etc. This simplifies to

$$I_1 = (1-c_{1x}c_{1y}c_{1z})(1-c_{2x}c_{2y}c_{2z}) + c_{1x}s_{1y}s_{1z}c_{2x}s_{2y}s_{2z}$$
$$+ s_{1x}c_{1y}s_{1z}s_{2x}c_{2y}s_{2z} + s_{1x}s_{1y}c_{1z}s_{2x}s_{2y}c_{2z},$$

where of course s_{1x} denotes sin (q_{1x}) etc.

(b) $$I_{2(3)} = \sum_\kappa \sin(q_{\kappa x})\sin(q_{\kappa y})\cos(q_{\kappa z})\mu_\kappa.$$

In a similar way this becomes

$$I_{2(3)} = s_{1x}s_{1y}c_{1z}(c_{2x}c_{2y}c_{2z}-1)+s_{2x}s_{2y}c_{2z}(c_{1x}c_{1y}c_{1z}-1)$$

$$-s_{1x}c_{1y}s_{1z}c_{2x}s_{2y}s_{2z} - c_{1x}s_{1y}s_{1z}s_{2x}c_{2y}s_{2z}.$$

For i = 2 there is only one type of sum:

$$I_{3(1)} = \sum_{\kappa} \cos(2q_{\kappa x})\mu_{\kappa}$$

$$= [1-\cos(2q_{1x})][1-\cos(2q_{2x})].$$

The sum over equivalent wave vectors may now be performed. For $\alpha = \beta$ there are four types of sum and for $\alpha \neq \beta$ there are another four:

(i) $\alpha = \beta = \gamma = \sigma$
(ii) $\alpha = \beta \neq \gamma = \sigma$
(iii) $\alpha = \beta = \gamma \neq \sigma$
(iv) $\alpha = \beta \neq \gamma \neq \sigma \neq \alpha$
(v) $\alpha = \gamma = \sigma \neq \beta$
(vi) $\alpha = \gamma \neq \beta = \sigma$
(vii) $\alpha = \gamma \neq \beta \neq \sigma \neq \alpha$
(viii) $\alpha \neq \beta \neq \gamma = \sigma \neq \alpha$

For case (i), with $\alpha = x$, the contribution to S_1 is

$$e_x^2(1) \sum_{48} e_x^2(2) \sum_{\kappa} h^{(1)}_{xxxx,\kappa}(12)$$

$$= A_{41}e_x^2(1) \sum_{48} e_x^2(2) I_1$$

$$= 16A_{41}e_x^2(1)[1-c_{1x}c_{1y}c_{1z}][1-c_{2x}c_{2y}c_{2z}].$$

The contribution to S_2 is

$$e_x^2(1) \sum_{48} e_x^2(2) \sum_{\kappa} h^{(2)}_{xxxx,\kappa}(12)$$

$$= A_{32}e_x^2(1) \sum_{48} e_x^2(2)I_{3(1)} + A_{42}e_x^2(1) \sum_{48} e_x^2(2)[I_{3(2)} + I_{3(3)}]$$

$$= 16A_{32}e_x^2(1)[1-\cos(2q_{1x})][1-u^2\cos(2r)-v^2\cos(2s)-w^2\cos(2t)]$$

$$+ 8A_{42}e_x^2(1)[2-\cos(2q_{1y})-\cos(2q_{1z})][2-u^2(\cos(2s)$$

$$+\cos(2t))-v^2(\cos(2t)+\cos(2r))-w^2(\cos(2r)+\cos(2s))].$$

Here (r,s,t) and (u,v,w) are components of the unrotated wave vector $\underline{q}_2$ and eigenvector $\underline{e}(2)$ respectively.

As a further example, we consider case (iii), with $\alpha = x$, $\sigma = y$. For i = 1, the contribution is

$$A_{51}e_x^2(1) \sum_{48} e_x(2)e_y(2)I_{2(3)}$$

$$= A_{51}\, e_x^2(1)[c_{1x}c_{1y}c_{1z}-1] \sum_{48} e_x(2)e_y(2)s_{2x}s_{2y}c_{2z}$$

$$=16A_{51}e_x^2(1)[c_{1x}c_{1y}c_{1z}-1][uv\sin(r)\sin(s)\cos(t)+$$

$$vw\sin(s)\sin(t)\cos(r)+wu\sin(t)\sin(r)\cos(s)].$$

For i = 2 there is no contribution.

A complete list of contributions, for i = 1 and 2, is given in Table AIV-6. Note that the contribution for case (vi), i = 2 vanishes. We may see this in the following way. The contribution is simply (for $\alpha = \gamma = x$, $\beta = \sigma = y$):

$$e_x(1)e_y(1) \sum_{48} e_x(2)e_y(2) \sum_{\kappa} h^{(2)}_{xyxy,\kappa}(12)$$

$$= A_{62}e_x(1)e_y(1) \sum_{48} e_x(2)e_y(2)I_{3(3)}+A_{52}e_x(1)e_y(1)$$

$$\times \sum_{48} e_x(2)e_y(2)[I_{3(1)}+I_{3(2)}] \ .$$

Since the functions $I_{3(\ )}$ are even, we see that the summands are odd with respect to x or y or both. The term therefore vanishes.

The final step in simplifying S_i is to perform the sums over α, β, γ, and σ. The results are given in Table AIV-7, for the eight cases. The quartic shift, to second neighbours may now be written as:

$$\Delta_4(\lambda_1) = \frac{\hbar}{Nm^2\omega_1} \sum_{\underset{\sim}{q}_2 j_2}^{IBZ} \left(\frac{n_2+\frac{1}{2}}{\omega_2}\right)(S_1+S_2), \qquad \text{(AIV-C6)}$$

where

$$S_1 + S_2 = K_1D_2 + K_2P_2 + K_3P_4 + K_4P_6 \qquad \text{(AIV-C7)}$$

Here K_1, K_2, K_3 and K_4 are independent of $(\underset{\sim}{q}_2 j_2)$, and given by

$$K_1 = 16(A_{41} + 2A_{61})D_1 + 32(2A_{51} + A_{71})P_1$$

$$K_2 = 32(A_{71} + 2A_{51})D_1 + 64(A_{61} - 2A_{71})P_1$$

$$K_3 = 16A_{32}P_3 + 16A_{52}P_5$$

$$K_4 = 16A_{52}P_3 + 8(A_{42} + A_{62})P_5 \qquad \text{(AIV-C8)}$$

and D_2, P_2, P_4 and P_6 are simple invariant functions of $\underset{\sim}{q}_2$ and $\underset{\sim}{e}(2)$, given in Table AIV-5. The quantities appearing in equations (AIV-C8) are defined in Tables AIV-1 and AIV-5.

(iii) The Cubic Shift

The expression for the cubic shift, Eq. (AIV-B4), involves three wave vectors. The summation over $\underline{q}_3$ in Eq.(AIV-B4) is trivial because of the Δ-function in $V(\lambda_1\lambda_2\lambda_3)$. The summation over j_3 must however be retained.

The 48 wave vectors $\underline{q}_3'$, given by $\underline{q}_3' = -\underline{q}_1 - \underline{q}_2'$ (where $\underline{q}_2'$ are the 48 wave vectors equivalent to $\underline{q}_2$), are in general inequivalent. In certain cases, depending on $\underline{q}_1$, there is a smaller group of equivalent wave vectors $\underline{q}_2$ such that the corresponding vectors $\underline{q}_3$ are equivalent. In this work we consider three cases:

(a) If $\underline{q}_1 = (0,0,\zeta)$, the 8 vectors $\underline{q}_2 = (\pm r, \pm s, t)$ and

$\underline{q}_2 = (\pm s, \pm r, t)$ define 8 equivalent vectors

$\underline{q}_3 = (\mp r, \mp s, -t-\zeta)$ and $(\mp s, \mp r, -t-\zeta)$.

(b) If $\underline{q}_1 = (\zeta,\zeta,\zeta)$, there are 6 vectors $\underline{q}_2 = (r,s,t)$, (s,r,t), (r,t,s), etc., such that vectors $\underline{q}_3$ are equivalent.

(c) If $\underline{q}_1 = (\zeta,\zeta,0)$ there are 4 vectors $\underline{q}_2 = (r,s,\pm t)$ and $(s,r,\pm t)$, such that the vectors $\underline{q}_3$ are equivalent.

We may therefore write

$$\Delta_3(\lambda,\Omega) = \left(\frac{\hbar}{4Nm^3\omega_1}\right) \sum_{\underline{q}_2 j_2 j_3}^{IBZ(\underline{q}_1)} [R(\Omega)/(\omega_2\omega_3)] \sum_{N(\underline{q}_1)} S_3 \qquad \text{(AIV-C9)}$$

with

$$S_3 = \left| \sum_{\alpha\beta\gamma} e_\alpha(1) e_\beta(2) e_\gamma(3) g_{\alpha\beta\gamma}(\underline{q}_1\underline{q}_2\underline{q}_3) \right|^2 . \qquad \text{(AIV-C10)}$$

The first summation is over the appropriate irreducible portion of the BZ, depending on $\underline{q}_1$, and the second summation is over the $N(\underline{q}_1)$ equivalent wave vectors $\underline{q}_2$ and $\underline{q}_3$.

The summation over α,β,γ is also considerably simplified for the major symmetry directions because $\underline{e}(1)$ is well defined.

As in the previous subsection, we first simplify the sums over κ in

$$g_{\alpha\beta\gamma}(\underline{q}_1\underline{q}_2\underline{q}_3) = \sum_i \sum_\kappa g^{(i)}_{\alpha\beta\gamma,\kappa}(\underline{q}_1\underline{q}_2\underline{q}_3).$$

There are two types of sum for i = 1, and one type for i = 2. They are

(a) $$I_1 = \sum_\kappa \sin(q_{\kappa x})\sin(q_{\kappa y})\sin(q_{\kappa z})$$

(b) $$I_{2(1)} = \sum_\kappa \sin(q_{\kappa x})\cos(q_{\kappa y})\cos(q_{\kappa z}), \text{ etc.}$$

(c) $$I_{3(1)} = \sum_\kappa \sin(2q_{\kappa x}), \text{ etc.} \qquad \text{(AIV-C11)}$$

For $\underline{q}_1$ along the three principal symmetry directions, the above sums take the special forms given in Table AIV-8.

We shall now demonstrate the summations over α,β,γ and over the equivalent wave vectors $\underline{q}_2$, for the case of the $[00\zeta]$T branch. The eigenvector $\underline{e}(1)$ is, in general,

$$\underline{e}(1) = (\ell,m,0), \text{ with } \ell^2 + m^2 = 1.$$

The eigenvectors $\underline{e}(2)$ and $\underline{e}(3)$ corresponding to $\underline{q}_2 = (r,s,t)$, are given by

$$\underline{e}(2) = (u,v,w)$$

$$\underline{e}(3) = (u',v',w').$$

We then have

$$S_3=[\ell\{uu'I_{2(1)}A_{31}'+(vv'+ww')I_{2(1)}A_{21}'+(uv'+vu')I_{2(2)}A_{21}'$$

$$+(uw'+wu')(I_{2(3)}A_{21}'+I_{3(3)}A_{12})-(vw'+wv')I_1A_{11}'\}$$

$$+m\{vv'I_{2(2)}A_{31}'+(uu'+ww')I_{2(2)}A_{21}'$$

$$+(uv'+vu')I_{2(1)}A_{21}'+(vw'+wv')(I_{2(3)}A_{21}'+I_{3(3)}A_{12})-(uw'+wu')I_1A_{11}'\}]^2$$

$$= [\ell U_1+mU_2]^2.$$

We now note that changing the sign of q_{2x} or q_{2y} changes the sign of U_1 or U_2 respectively; furthermore swapping q_{2x} and q_{2y} has the effect of swapping U_1 and U_2. Therefore

$$\sum_N S_3 = 2(\ell U_1+mU_2)^2 + 2(\ell U_1-mU_2)^2 + 2(\ell U_2+mU_1)^2 + 2(\ell U_2-mU_1)^2$$

$$=4(U_1{}^2 + U_2{}^2).$$

Complete results, for the seven branches, are given in Table AIV-9.

D. Alternative Formulation Using Scalar Products

The cubic and quartic terms have been considerably simplified in the previous section. Several steps are involved in this reduction, and there is always the possibility that a mistake has been made at some stage. To minimize this possibility, the expressions have been partially reduced in a somewhat different way. The two methods have then been compared by doing sample calculations on the computer using both methods.

(i) The Quartic Term

The quartic shift may be written as

$$\Delta_4(\lambda_1) = \frac{\hbar}{Nm^2\omega_1} \sum_{\underline{q}_2 j_2}^{IBZ} \left(\frac{n_2+\frac{1}{2}}{\omega_2}\right) W_4 \qquad \text{(AIV-D1)}$$

where

$$W_4 = 2 \sum_{48} \sum_{i} 2 \sum_{\ell_i > 0} \sin^2\left(\frac{\underline{q}_1 \cdot \underline{r}_{\ell i}}{2}\right) \sin^2\left(\frac{\underline{q}_2 \cdot \underline{r}_{\ell i}}{2}\right) J_i \qquad \text{(AIV-D2)}$$

and

$$J_i = -\sum_{\alpha\beta\gamma\sigma} \phi_{\alpha\beta\gamma\sigma}(000\ell_i) e_\alpha(1) e_\beta(1) e_\gamma(2) e_\sigma(2)$$

Using Equation (AIV-A1) we may largely separate the summations over $\alpha,\beta,\gamma,\sigma$, to obtain

$$\begin{aligned} J_i = {} & C_{4i}[\underline{s}\cdot\underline{e}(1)]^2[\underline{s}\cdot\underline{e}(2)]^2 \\ & + C'_{3i}\{[\underline{s}\cdot\underline{e}(1)]^2+[\underline{s}\cdot\underline{e}(2)]^2+4[\underline{s}\cdot\underline{e}(1)][\underline{s}\cdot\underline{e}(2)]\underline{e}(1)\cdot\underline{e}(2)]\} \\ & + C''_{2i}\{1 + 2[\underline{e}(1)\cdot\underline{e}(2)]^2\} \end{aligned} \qquad \text{(AIV-D3)}$$

The quantity W_4 has been calculated for a set of random values of $(\underline{q}_2 j_2)$, with an arbitrary set of coefficients C_{41}, C_{42}, etc., out to second neighbours. It was compared with the quantity (S_1+S_2) (Eq. AIV-C7), calculated with the same input parameters. In every case the agreement was exact. The second method of evaluating the matrix element is more than 100 times faster.

(ii) The Cubic Term

This may be expressed as

$$\Delta_3(\lambda_1,\Omega) = \left(\frac{\hbar}{4Nm^3\omega_1}\right) \sum_{\underline{q}_2 j_2 j_3}^{IBZ(\underline{q}_1)} [R(\Omega)/(\omega_2\omega_3)]W_3 \qquad \text{(AIV-D4)}$$

where

$$W_3 = \sum_{N(\underline{q}_1)} \left| \sum_i \sum_{\ell_i>0} \{\sum_\kappa \sin[\underline{q}_\kappa \cdot \underline{r}(\ell_i)]\}J \right|^2 \qquad \text{(AIV-D5)}$$

and

$$J = \sum_{\alpha\beta\gamma} \phi_{\alpha\beta\gamma}(00\ell_i)e_\alpha(1)e_\beta(2)e_\gamma(3)$$

Using Eq. (AIV-A1) this reduces to

$$J = C_{3i}[\underline{s}\cdot\underline{e}(1)][\underline{s}\cdot\underline{e}(2)][\underline{s}\cdot\underline{e}(3)]$$
$$+ C'_{2i}\{[\underline{s}\cdot\underline{e}(1)][\underline{e}(2)\cdot\underline{e}(3)]+[\underline{s}\cdot\underline{e}(2)][\underline{e}(3)\cdot\underline{e}(1)]+[\underline{s}\cdot\underline{e}(3)][\underline{e}(1)\cdot\underline{e}(2)]\}$$
$$\text{(AIV-D6)}$$

The quantity W_3 has been calculated by the above method and then compared with $\sum_{N(\underline{q}_1)} S_3$ (Eq. AIV-C10). Agreement is obtained for all seven branches, and the latter method is about 15, 12, and 8 times faster for the $[00\zeta]$, $[\zeta\zeta\zeta]$, and $[\zeta\zeta0]$ branches respectively.

E. Irreducible Volumes in the First Brillouin Zone

The various sums over $\underline{q}$, which appear in the expressions for the thermal expansion, and for Δ_3, Γ, and Δ_4 are performed over portions of the BZ. In this section we shall consider the conditions for $\underline{q}$ to lie within the various "irreducible" zones (IBZ's), and the method of weighting wave vectors which end on the surface of the zone.

First we consider the whole BZ (Fig.AIV-1(a)). This is defined by the equations

$$\begin{aligned} |x| + |y| &\leq 1 \\ |y| + |z| &\leq 1 \\ |z| + |x| &\leq 1 \end{aligned} \qquad \text{(AIV-E1)}$$

where x, y and z are the components of $\underset{\sim}{q}$ in units of $(2\pi/a)$. A general point has weight 1: a point lying on a surface has weight 1/2, and a point lying on an edge (H-P) has weight 1/3. The points P and H have weights of 1/4 and 1/6 respectively.

The sums over $\underset{\sim}{q}$ are generally performed using a "shifted" mesh of points (cf. Gilat and Dolling 1964, Gilat and Raubenheimer 1966). This mesh is defined by

$$q_\alpha = (m_\alpha - \frac{1}{2})\Delta q \ , \ (\alpha = x,y,z)$$

where the m_α are running integer indices, and Δ_q is the mesh size, which is such that $M_n\Delta_q = (\pi/a)$, where M_n is an integer known as the mesh number. With this arrangement the weighting scheme is simplified, since we need only consider what happens at surfaces which do not contain the origin. For each irreducible zone, the above conditions on $\underset{\sim}{q}$ (Eq. AIV-E1) must be satisfied, and the weight of a point is the product of its weight in the complete BZ and its "multiplicity" M within the irreducible zone. These multiplicities are defined below.

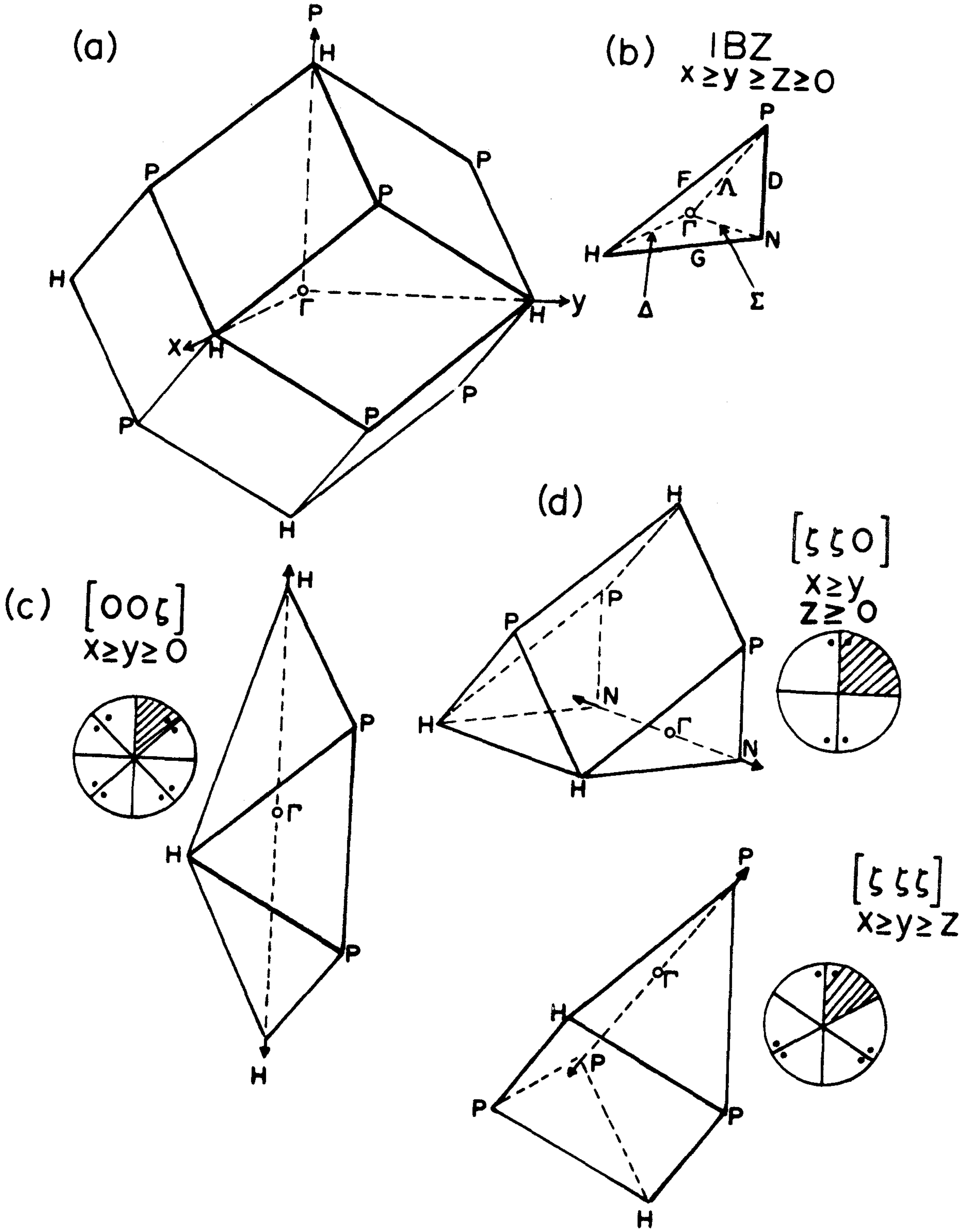

Fig. AIV-1. (a) The first Brillouin zone, corresponding to the body centred cubic direct lattice;

(b)-(e) Various "irreducible" Brillouin zones.

The normal IBZ (Fig. AIV-1(b)) may be defined by the further condition

$$x \geq y \geq z \geq 0 \qquad \text{(AIV-E2)}$$

A general point has $M = 48$: if $x = y$ or $y = z$, $M = 24$, whereas if $x = y = z$, $M = 8$. Thus the point (0.1,0.1,0.1) has weight 8, and the point (0.7,0.3,0.3) also has weight 8 since $y = z$ and the point lies on the edge denoted by F in Fig. AIV-1(b).

Finally we consider the three special IBZ's used in calculations of the cubic shift and width of certain modes. These zones are shown in Fig. AIV-1 (c), (d) and (e).

(i) If $\underline{q} = (0,0,\zeta)$, we define an IBZ by the further condition

$$x \geq y \geq 0$$

The weight of a point is its weight in the IBZ divided by 6.

(ii) For $\underline{q}_1 = (\zeta,\zeta,0)$ we have the extra conditions

$$x \geq y \ , \ z \geq 0.$$

The weight of a point is its weight in the IBZ, divided by 12.

(iii) For $\underline{q}_1 = (\zeta,\zeta,\zeta)$, the extra condition is

$$x \geq y \geq z.$$

The weight of a point is its weight in the IBZ, divided by 8.

TABLE AIV-1 Symbols used in this appendix.

$$C_{2i} = (\phi'' - \phi'/R)_i$$

$$C_{3i} = (\phi''' - 3\phi''/R + 3\phi'/R^2)_i$$

$$C_{4i} = (\phi'''' - 6\phi'''/R + 15\phi''/R^2 - 15\phi'/R^3)_i$$

$$C'_{2i} = C_{2i}/R_i$$

$$C'_{3i} = C_{3i}/R_i$$

$$C''_{2i} = C_{2i}/R_i^{\,2}$$

The subscript i indicates that the quantity is evaluated for $r = R_i$ where R_i is the separation between i'th nearest neighbours.

$c(j) = \cos(q_j)$; $s(j) = \sin(q_j)$ j = x, y or z

$c(2j) = \cos(2q_j)$; $s(2j) = \sin(2q_j)$ j = x, y or z

ccc = c(x)c(y)c(z); ccs = c(x)c(y)s(z), etc.

sss = s(x)s(y)s(z); ssc = s(x)s(y)c(z), etc.

d(2x) = c(2y) + c(2z), etc.

f(2x) = 1 - c(2y)c(2z), etc.

h(2x) = 1 + s(2y)s(2z), etc.

(continued)

TABLE AIV-1 Symbols used in this appendix (cont'd)

$A_{11} = 2C_{31}/3\sqrt{3}$; $A_{11}' = 2A_{11}$
$A_{21} = 2(C_{31}/3\sqrt{3} + C_{21}'/\sqrt{3})$; $A_{21}' = 2A_{21}$
$A_{31} = 2(C_{31}/3\sqrt{3} + \sqrt{3}C_{21}')$; $A_{31}' = 2A_{31}$
$A_{41} = 4(C_{41}/9 + 2C_{31}' + 3C_{21}'')$
$A_{51} = -4(C_{41}/9 + C_{31}')$
$A_{61} = 4(C_{41}/9 + 2C_{31}'/3 + C_{21}'')$
$A_{71} = -4(C_{41}/9 + C_{31}'/3)$

$A_{12} = C_{22}'$
$A_{22} = C_{32} + 3C_{22}'$
$A_{32} = C_{42} + 6C_{32}' + 3C_{22}''$
$A_{42} = 3C_{22}''$
$A_{52} = C_{32}' + C_{22}''$
$A_{62} = C_{22}''$

$A_{13} = C_{33} + 6C_{23}'$; $A_{13}' = A_{13}/\sqrt{2}$
$A_{23} = 4C_{23}'$; $A_{23}' = A_{23}/2\sqrt{2}$
$A_{33} = C_{33} + 2C_{23}'$; $A_{33}' = A_{33}/\sqrt{2}$
$A_{43} = C_{43}/2 + 6(C_{33}' + C_{23}'')$
$A_{53} = 6C_{23}''$
$A_{63} = -(C_{43}/2 + 3C_{33}')$
$A_{73} = C_{43}/2 + 2(C_{33}' + C_{23}'')$
$A_{83} = C_{33}' + 2C_{23}''$
$A_{93} = -C_{33}'$

TABLE AIV-2 Values of $(a^{-1})f^{(i)}_{\alpha\beta\gamma}(\underline{q})$, for all combinations of α, β, γ and for i = 1,2, and 3. The symbols are defined in Table AIV-1.

$\alpha\beta\gamma$	i=1	i=2	i=3
xxx	$A_{31}(1-ccc)$	$A_{22}[1-c(2x)]$	$A_{13}[2-c(2x)d(2x)]$
xxy	$A_{21}(1-ccc)$	$A_{12}[1-c(2y)]$	$A_{23}f(2x)+A_{33}f(2z)$
xxz	$A_{21}(1-ccc)$	$A_{12}[1-c(2z)]]$	$A_{23}f(2x)+A_{33}f(2y)$
xyx	A_{21} ssc	0	$A_{33}h(2z)$
xyy	A_{21} ssc	0	$A_{33}h(2z)$
xyz	A_{11} ssc	0	0
xzx	A_{21} scs	0	$A_{33}h(2y)$
xzy	A_{11} scs	0	0
xzz	A_{21} scs	0	$A_{33}h(2y)$
yxx	A_{21} ssc	0	$A_{33}h(2z)$
yxy	A_{21} ssc	0	$A_{33}h(2z)$
yxz	A_{11} ssc	0	
yyx	$A_{21}(1-ccc)$	$A_{12}[1-c(2x)]$	$A_{23}f(2y)+A_{33}f(2z)$
yyy	$A_{31}(1-ccc)$	$A_{22}[1-c(2y)]$	$A_{13}[2-c(2y)d(2y)]$
yyz	$A_{21}(1-ccc)$	$A_{12}[1-c(2z)]$	$A_{23}f(2y)+A_{33}f(2x)$
yzx	A_{11} css	0	
yzy	A_{21} css	0	$A_{33}h(2x)$
yzz	A_{21} css	0	$A_{33}h(2x)$
zxx	A_{21} scs	0	$A_{33}h(2y)$
zxy	A_{11} scs	0	0
zxz	A_{21} scs	0	$A_{33}h(2y)$

(continued)

TABLE AIV-2 Values of $(a^{-1})f^{(i)}_{\alpha\beta\gamma}(\underset{\sim}{q})$, for all combinations of α, β, γ and for i = 1, 2 and 3. The symbols are defined in Table AIV-1 (cont'd)

$\alpha\beta\gamma$	i=1	i=2	i=3
zyx	A_{11} css	0	0
zyy	A_{21} css	0	$A_{33}h(2x)$
zyz	A_{21} css	0	$A_{33}h(2x)$
zzx	$A_{21}(1-ccc)$	$A_{12}[1-c(2x)]$	$A_{23}f(2z)+A_{33}f(2y)$
zzy	$A_{21}(1-ccc)$	$A_{12}[1-c(2y)]$	$A_{23}f(2z)+A_{33}f(2x)$
zzz	$A_{31}(1-ccc)$	$A_{22}[1-c(2z)]$	$A_{13}[2-c(2z)d(2z)]$

TABLE AIV-3 Values of $(\mu_\kappa^{-1})h^{(i)}_{\alpha\beta\gamma\sigma,\kappa}(12)$, for i=1,2 and 3. Only one permutation of each set of indices $\alpha,\beta,\gamma,\sigma$ is given. The function does not change on permutation of the indices. The subscript κ is understood. Symbols are defined in Table AIV-1.

	i=1	i=2	i=3
xxxx	A_{41} ccc	$A_{32}c(2x)+A_{42}d(2x)$	$A_{43}c(2x)d(2x)+A_{53}c(2y)c(2z)$
xxxy	A_{51} ssc	0	$A_{63}s(2x)s(2y)$
xxxz	A_{51} scs	0	$A_{63}s(2x)s(2z)$
xxyy	A_{61} ccc	$A_{52}d(2z)+A_{62}c(2z)$	$A_{73}c(2x)c(2y)+A_{83}c(2z)d(2z)$
xxyz	A_{71} css	0	$A_{93}s(2y)s(2z)$
xxzz	A_{61} ccc	$A_{52}d(2y)+A_{62}c(2y)$	$A_{73}c(2x)c(2z)+A_{83}c(2y)d(2y)$
xyyy	A_{51} ssc	0	$A_{63}s(2x)s(2y)$
xyyz	A_{71} scs	0	$A_{93}s(2x)s(2z)$
xyzz	A_{71} ssc	0	$A_{93}s(2x)s(2y)$
xzzz	A_{51} scs	0	$A_{63}s(2x)s(2z)$
yyyy	A_{41} ccc	$A_{32}c(2y)+A_{42}d(2y)$	$A_{43}c(2x)d(2x)+A_{53}c(2x)c(2z)$
yyyz	A_{51} css	0	$A_{63}s(2y)s(2z)$
yyzz	A_{61} ccc	$A_{52}d(2x)+A_{62}c(2y)$	$A_{73}c(2y)c(2z)+A_{83}c(2x)d(2x)$
yzzz	A_{51} css	0	$A_{63}s(2y)s(2z)$
zzzz	A_{41} ccc	$A_{32}c(2z)+A_{42}d(2z)$	$A_{43}c(2x)d(2x)+A_{53}c(2x)c(2y)$

TABLE AIV-4 Values of $g^{(i)}_{\alpha\beta\gamma,\kappa}(\underline{q}_1\underline{q}_2\underline{q}_3)$, for i = 1, 2 and 3. Only one permutation of each set of indices α, β, γ is given. The function does not change on permutation of the indices. The subscript κ is understood. Symbols are defined in Table AIV-1.

$\alpha\beta\gamma$	i=1	i=2	i=3
xxx	A'_{31} scc	$A_{22}s(2x)$	$A'_{13}s(2x)d2x)$
xxy	A'_{21} csc	$A_{12}s(2y)$	$A'_{23}s(2y)c(2z)+A'_{33}c(2x)s(2y)$
xxz	A'_{21} ccs	$A_{12}s(2z)$	$A'_{23}c(2y)s(2z)+A'_{33}c(2x)s(2z)$
xyy	A'_{21} scc	$A_{12}s(2x)$	$A'_{23}s(2x)c(2z)+A'_{33}s(2x)c(2y)$
xyz	$-A'_{11}$ sss	0	0
xzz	A'_{21} scc	$A_{12}s(2x)$	$A'_{23}s(2x)c(2y)+A'_{33}s(2x)c(2z)$
yyy	A'_{31} csc	$A_{22}s(2y)$	$A'_{13}s(2y)d(2y)$
yyz	A'_{21} ccs	$A_{12}s(2z)$	$A'_{23}c(2x)s(2z)+A'_{33}c(2y)s(2z)$
yzz	A'_{21} csc	$A_{12}s(2y)$	$A'_{23}c(2x)s(2y)+A'_{33}s(2y)c(2z)$
zzz	A'_{31} ccs	$A_{22}s(2z)$	$A'_{13}s(2z)d(2z)$

TABLE AIV-5 Further symbols used in this Appendix.

$D_1 = c_{1x}c_{1y}c_{1z} - 1$

$D_2 = \cos(r)\cos(s)\cos(t) - 1$

$P_1 = e_x(1)e_y(1)s_{1x}s_{1y}c_{1z}+e_y(1)e_z(1)s_{1y}s_{1z}c_{1x}+e_z(1)e_x(1)s_{1z}s_{1x}c_{1y}$

$P_2 = uv\sin(r)\sin(s)\cos(t)+vw\sin(s)\sin(t)\cos(r)+wu\sin(t)\sin(r)\cos(s)$

$P_3 = 1-[e_x^2(1)\cos(2q_{1x}) + e_y^2(1)\cos(2q_{1y}) + e_z^2(1)\cos(2q_{1z})]$

$P_4 = 1 - [u^2\cos(2r) + v^2\cos(2s) + w^2\cos(2t)]$

$$P_5 = 2-\{e_x^2(1)[\cos(2q_{1y})+\cos(2q_{1z})] + e_y^2(1)[\cos(2q_{1z})+\cos(2q_{1x})] + e_z^2(1)[\cos(2q_{1x}) + \cos(2q_{1y})]\}$$

$$P_6 = 2-\{u^2[\cos(2s) + \cos(2t)] + v^2[\cos(2t) + \cos(2r)] + w^2[\cos(2r) + \cos(2s)]\}$$

TABLE AIV-6 Contributions to the quantity S_i, defined in Section C(ii) of this Appendix, for a particular choice of α, β, γ, σ .

Case	Example	i	Contribution to S_i
(i)	xxxx	1	$16A_{41}e_x^2(1)D_1D_2$
		2	$16A_{32}e_x{}^2(1)[1-\cos(2q_{1x})]P_4$ $+8A_{42}e_x^2(1)[2-\cos(2q_{1y})-\cos(2q_{1z})]P_6$
(ii)	xxyy	1	$16A_{61}e_x^2(1)D_1D_2$
		2	$8A_{62}e_x^2(1)[1-\cos(2q_{1z})]P_6$ $+8A_{52}e_x^2(1)[1-\cos(2q_{1x})]P_6$ $+16A_{52}e_x^2(1)[1-\cos(2q_{1y})]P_4$
(iii)	xxxy	1	$16A_{51}e_x^2(1)D_1P_2$
(iv)	xxyz	1	$16A_{71}e_x^2(1)D_1P_2$
(v)	xyxx	1	$16A_{51}e_x(1)e_y(1)s_{1x}s_{1y}c_{1z}D_2$
(vi)	xyxy	1	$16A_{61}e_x(1)e_y(1)s_{1x}s_{1y}c_{1z}P_2$
(vii)	xyxz	1	$-16A_{71}e_x(1)e_y(1)s_{1x}s_{1y}c_{1z}P_2$
(viii)	xyzz	1	$16A_{71}e_x(1)e_y(1)s_{1x}s_{1y}c_{1z}D_2$

TABLE AIV-7 Contributions to the quantity S_i, defined in Section C(ii), summed over all permutations for each of the eight cases.

Case	Example	N	i	Contributions to S_i
(i)	xxxx	3	1	$16A_{41}D_1D_2$
			2	$16A_{32}P_4P_5 + 8A_{42}P_6P_7$
(ii)	xxyy	6	1	$32A_{61}D_1D_2$
			2	$8A_{62}P_6P_7 + 8A_{52}P_4P_7 + 16A_{52}P_6P_5$
(iii)	xxxy	12	1	$64A_{51}D_1P_2$
(iv)	xxyz	6	1	$32A_{71}D_1P_2$
(v)	xyxx	12	1	$64A_{51}P_1D_2$
(vi)	xyxy	12	1	$64A_{61}P_1P_2$
(vii)	xyxz	24	1	$-128A_{71}P_3P_2$
(viii)	xyzz	6	1	$32A_{71}P_1D_2$

TABLE AIV-8 The sums defined by Eq. (AIV-C11), for the three major symmetry directions.

For $\underset{\sim}{q}_1 = (0,0,\zeta)$:

$I_1 = \sin(r)\sin(s)\ [\sin(t)-\sin(t+\zeta)]$

$I_{2(1)} = \sin(r)\cos(s)[\cos(t)-\cos(t+\zeta)]$

$I_{2(2)} = \cos(r)\sin(s)[\cos(t)-\cos(t+\zeta)]$

$I_2(3) = \sin(\zeta)+\cos(r)\cos(s)[\sin(t)-\sin(t+\zeta)]$

$I_{3(1)} = I_{3(2)} = 0$

$I_3(3) = \sin(2\zeta)+\sin(2t)-\sin(2(t+\zeta))$

For $\underset{\sim}{q}_1 = (\zeta,\zeta,\zeta)$:

$I_1 = \sin^3(\zeta)+\sin(r)\sin(s)\sin(t)-\sin(r+\zeta)\sin(s+\zeta)\sin(t+\zeta)$

$I_{2(1)} = \sin(\zeta)\cos^2(\zeta)+\sin(r)\cos(s)\cos(t)-\sin(r+\zeta)\cos(s+\zeta)\cos\ (t+\zeta)$, etc.

$I_{3(1)} = \sin(2\zeta)+\sin(2r)-\sin(2(r+\zeta))$, etc.

For $\underset{\sim}{q}_1 = (\zeta,\zeta,0)$:

$I_1 = [\sin(r)\sin(s)-\sin(r+\zeta)\sin(s+\zeta)]\sin(t)$

$I_{2(1)} = \sin(\zeta)\cos(\zeta)+[\sin(r)\cos(s)-\sin(r+\zeta)\cos(s+\zeta)]\cos(t)$

$I_{2(2)} = \sin(\zeta)\cos(\zeta)+[\cos(r)\sin(s)-\cos(r+\zeta)\sin(s+\zeta)]\cos(t)$

$I_{2(3)} = [\cos(r)\cos(s)-\cos(r+\zeta)\cos(s+\zeta)]\sin(t)$

$I_{3(1)} = \sin(2\zeta)+\sin(2r)-\sin(2(r+\zeta))$

$I_{3(2)} = \sin(2\zeta)+\sin(2s)-\sin(2(s+\zeta))$

$I_{3(3)} = \sin(2t)$

[Note that $I_{2(1)} = I_{2(2)}$]

TABLE AIV-9 The sums $\sum_{N(\underline{q}_i)} S_3$, defined in Section AIV-C(iii), for the seven major branches.

$\underline{q}_1$	Pol.	$N(\underline{q}_1)$	Sum
$(0,0,\zeta)$	T	8	$4\{[uu'I_{2(1)}A'_{31}+(vv'+ww')I_{2(1)}A'_{21}$ $+(uv'+vu')I_{2(2)}A'_{21}+(uw'+wu')H_3$ $-(vw'+wv')I_1A'_{11}]^2 +$ $[vv'I_{2(2)}A'_{31}+(uu'+ww')I_{2(2)}A'_{21}$ $+(uv'+vu')I_{2(1)}A'_{21}+(vw'+wv')H_3$ $-(uw'+wu')I_1A'_{11}]^2\}$
$(0,0,\zeta)$	L	8	$8[(uu'+vv')H_3+ww'G_3$ $-(uv'+vu')I_1A'_{11}+(uw'+wu')I_{2(1)}A'_{21}$ $+(vw'+wv')I_{2(2)}A'_{21}]$
(ζ,ζ,ζ)	T	6	$2[X_1^2+X_2^2+X_3^2-X_1X_2-X_2X_3-X_3X_1]$ where $X_1 = uu'G_1 + (vv'+ww')H_1$ $+ (uv'+vu')H_2+(uw'+wu')H_3$ $- (vw'+wv')I_1A'_{11}$ $X_2 = vv'G_2+(uv'+vu')H_1$ $+(uu'+ww')H_2+(vw'+wv')H_3$ $-(uw'+wu')I_1A'_{11}$ $X_3 = ww'G_3+(uw'+wu')H_1$ $+(vw'+wv')H_2+(uu'+vv')H_3$ $-(uv'+vu')I_1A'_{11}$

(continued)

TABLE AIV-9 The sums $\sum_{N(\underline{q}_1)} S_3$, defined in Section AIV-C(iii), for the seven major branches (cont'd)

$\underline{q}_1$	Pol.	$N(\underline{q}_1)$	Sum
(ζ,ζ,ζ)	L	6	$2[X_1+X_2+X_3]^2$ (X_1,X_2,X_3 are given above)
$(\zeta,\zeta,0)$	T2	4	$4[(uu'+vv')H_3+ww'G_3$ $-(uv'+vu')A'_{11}I_1$ $+(uw'+wu')H_1+(vw'+wv')H_2]^2$
$(\zeta,\zeta,0)$	L,T1	4	$2[uu'G_1\pm vv'G_2$ $+\{(vv'+ww')\pm(uv'+vu')\}H_1$ $+\{(uv'+vu')\pm(uu'+vv')\}H_2$ $+\{(uw'+wu')\pm(vw'+wv')\}$ $\times(H_3-I_1A'_{11})]^2$

Note (1) $G_i = I_{2(i)}A'_{31}+I_{3(i)}A_{22}$ for $i = 1,2,3$

$H_i = I_{2(i)}A'_{21}+I_{3(i)}A_{12}$ for $i = 1,2,3$

(2) The +(−) signs apply in the expression for the direction $(\zeta,\zeta,0)$ for L(T1) polarizations respectively.

APPENDIX V

FREE3, A PROGRAMME TO CALCULATE CUBIC ANHARMONIC CONTRIBUTIONS TO THERMODYNAMIC FUNCTIONS

The expression to be evaluated is (Eq. III-A32):

$$\Delta F_3 = -\frac{6}{\hbar} \sum_{\lambda_1\lambda_2\lambda_3} |V(\lambda_1\lambda_2\lambda_3)|^2 N_3(\omega_1\omega_2\omega_3) \qquad \text{(AV-1)}$$

with N_3 given by Eq. (III-A34). The quantities ΔS_3 and ΔC_3 are also calculated.

Comparing Eqs. (AIV-B4) and (AIV-D4) for the shift $\Delta_3(\lambda_1,\Omega)$, and noting that $V(\lambda_1\lambda_2\lambda_3)$ contains the restriction that

$$\underline{q}_1 + \underline{q}_2 + \underline{q}_3 = \underline{G},$$

we find that

$$|V(\lambda_1\lambda_2\lambda_3)|^2 = \frac{\hbar^3}{72Nm^3\omega_1\omega_2\omega_3} Y(\lambda_1\lambda_2\lambda_3) \qquad \text{(AV-2)}$$

where

$$Y(\lambda_1\lambda_2\lambda_3) = \left| \sum_{i} \sum_{\ell_i>0} \{\sum_{\kappa} \sin[\underline{q}_\kappa \cdot \underline{r}(\ell_i)]\} J \right|^2 \qquad \text{(AV-3)}$$

and J is given by Eq. (AIV-D6).

We may immediately drop the sum over $\underline{q}_3$ in Eq. (AV-1) because of the restriction noted above. In addition the sum over $\underline{q}_1$ need only be performed over the irreducible 1/48th of the first BZ (i.e. the IBZ). The sum over $\underline{q}_2$ must however be performed over the whole zone. The wave vector $\underline{q}_1$ is chosen to lie on an even mesh, and $\underline{q}_2$ (and therefore $\underline{q}_3$) lie on an odd mesh. That is,

$$q_{1\alpha} = m_{1\alpha}\Delta q \qquad , \quad (\alpha = x,y,z)$$
$$q_{2\alpha} = (m_{2\alpha} - \tfrac{1}{2})\Delta q, \quad (\alpha = x,y,z).$$

As before, $M_n \Delta q = (\pi/a)$, where M_n is an integer known as the mesh number.

In the first section of the programme the following quantities are calculated and stored, for each value of $\underline{q}$ on an odd mesh in the IBZ:

q_α	$\alpha = 1$ to 3
$\nu(\underline{q}j)$	$j = 1$ to 3
$e_\alpha(\underline{q}j)$	$j = 1$ to 3; $\alpha = 1$ to 3
$W(\underline{q})$	
$d_i(\underline{q}j)$	$j = 1$ to 3 ; $i = 1$ to 4
$s_i'(\underline{q})$	$i = 1$ to 4
$s_\alpha''(\underline{q})$	$\alpha = 1$ to 3

$W(\underline{q})$ is the weight of the vector $\underline{q}$ in the whole zone. This is given in Section E of Appendix IV. In order to avoid overcounting when $\underline{q}_2$ is transformed into the whole zone, we must introduce extra conditions. If $q_x = q_y$ or $q_y = q_z$, the weight is halved, and if $q_x = q_y = q_z$, the weight is further divided by 3. The remaining quantities are defined as follows:

$$\left.\begin{aligned} d_1 &= e_x + e_y + e_z \\ d_2 &= e_x + e_y - e_z \\ d_3 &= e_x - e_y + e_z \\ d_4 &= e_x - e_y - e_z \end{aligned}\right\} \quad (\underline{q}j) \text{ understood.}$$

$$\begin{aligned} s_1'(\underline{q}) &= \sin(q_x + q_y + q_z) \\ s_2'(\underline{q}) &= \sin(q_x + q_y - q_z) \\ s_3'(\underline{q}) &= \sin(q_x - q_y + q_z) \\ s_4'(\underline{q}) &= \sin(q_x - q_y - q_z) \end{aligned}$$

$$s_\alpha''(\underline{q}) = \sin(2q_\alpha) \qquad \alpha = 1 \text{ to } 3$$

These quantities are required in order to evaluate $Y(\lambda_1\lambda_2\lambda_3)$.

For each temperature, and for each $(\underline{q}j)$, the quantities n, (dn/dT), and (d^2n/dT^2) are also stored.

We now come to the main section of the programme. First the vector $\underline{q}_1$ is generated on an even mesh in the IBZ. Values of $\nu(\underline{q},j)$ and $\underline{e}(\underline{q},j)$ are obtained, and so is the weight $W'(\underline{q}_1)$. Since $\underline{q}_1$ is on an even mesh, this weight is given by the prescription of Section E, Appendix V, with several additional conditions. If $x \neq y \neq z = 0$, $M = 24$. If $x = y \neq z = 0$, $M = 12$, and if $x \neq y = z = 0$, then $M = 6$. Here x, y and z are the components of $\underline{q}_1$.

A value of $\underline{q}_2$ is now selected. A wave vector in the IBZ is read from the table of values, together with the other stored quantities. Since $\underline{q}_2$ must be summed over the whole zone, the wave vector must be transformed using each of the 48 operations of the cubic group in turn. In addition the quantities $\underline{e}(\underline{q}j)$, $d(\underline{q}j)$, $s_i'(\underline{q})$ and $s_\alpha''(\underline{q})$ must be transformed . These transformations are listed in Table AV-1. The vector $\underline{q}_3$ is now obtained, by writing $\underline{q}_3 = -\underline{q}_1 - \underline{q}_2$. It is translated back to the first zone, and the transformation necessary to bring it into the IBZ is then found. The values of ν, $\underline{e}$, etc. are obtained from the table, and appropriately transformed because $\underline{q}_3$ is not necessarily in the IBZ.

The complete expression for ΔF_3 may be written as

$$\frac{\Delta F_3}{N} = \frac{4\hbar^2}{m^3 C} \sum_{\underline{q}_1}^{IBZ} W'(\underline{q}_1) \sum_{\underline{q}_2}^{IBZ} W(\underline{q}_2) \sum_{48} \sum_{j_1 j_2 j_3} \frac{Y(\lambda_1\lambda_2\lambda_3) N_3(\omega_1\omega_2\omega_3)}{\omega_1\omega_2\omega_3} \tag{AV-4}$$

where

$$C = (48)^2 \times \sum_{\underline{q}_1}^{IBZ} W'(\underline{q}_1) \sum_{\underline{q}_2}^{IBZ} W(\underline{q}_2) \; . \tag{AV-5}$$

The above equation summarizes the order in which the various summations are performed in the programme. Typical timings are as follows (for calculations at one temperature only):-

$M_n = 2$, 12 secs.
$M_n = 3$, 54 secs.
$M_n = 4$, 165 secs.

In practice it is found that the sum has converged to within ± 1% when $M_n = 4$ is used. This value of M_n corresponds to 128 wave vectors $\underline{q}_2$ in the whole zone, and 14 wave vectors $\underline{q}_1$

in the IBZ.

The sum over $\underline{q}_1$ includes the origin, for which $\omega_1 = 0$, and the eigenvectors are not well defined. To avoid this complication, we have excluded the origin from the sum over $\underline{q}_1$. The normalization factor C is calculated both including and excluding the origin. The results obtained when C includes the origin are appropriate to very low temperatures, since the origin does not contribute at these temperatures; conversely the results obtained when the origin is excluded are appropriate to high temperatures, since the contribution of the origin is then similar in size to other contributions. In practice the difference between the two results, being equal to $1/2M_n^3$, is small.

TABLE AV-1 The 48 equivalent wave vectors $\underline{q}$ are listed. For each value of $\underline{q}$, the quantities d_1, d_2, d_3 and d_4 are given in terms of $U1 = E_x+E_y+E_z$, $U2 = E_x+E_y-E_z$, $U3 = E_x-E_y+E_z$, and $U4 = E_x-E_y-E_z$. Here $\underline{E}$ is an eigenvector corresponding to the wave vector $\underline{q}$ = (X,Y,Z). The eigenvector $\underline{e}(\underline{q})$ transforms in the same way as $\underline{q}$, and $s''_\alpha(\underline{q})$ transforms in the same way as q_α. The quantities $s'_i(\underline{q})$ transform in the same way as the d_i. For example, if $\underline{q}$ = (Y,Z,-X) [no. 13], d_1 = sin(-[X-Y-Z]), d_2 = sin(X+Y+Z), d_3 = sin(-[X-Y+Z]), d_4 = sin(X+Y-Z).

n	q_x	q_y	q_z	d_1	d_2	d_3	d_4	n	q_x	q_y	q_z	d_1	d_2	d_3	d_4
1	X	Y	Z	U1	U2	U3	U4	25	Z	Y	X	U1	-U4	U3	-U2
2	-X	Y	Z	-U4	-U3	-U2	-U1	26	-Z	Y	X	U2	-U3	U4	-U1
3	X	-Y	Z	U3	U4	U1	U2	27	Z	-Y	X	U3	-U2	U1	-U4
4	-X	-Y	Z	-U2	-U1	-U4	-U3	28	-Z	-Y	X	U4	-U1	U2	-U3
5	X	Y	-Z	U2	U1	U4	U3	29	Z	Y	-X	-U4	U1	-U2	U3
6	-X	Y	-Z	-U3	-U4	-U1	-U2	30	-Z	Y	-X	-U3	U2	-U1	U4
7	X	-Y	-Z	U4	U3	U2	U1	31	Z	-Y	-X	-U2	U3	-U4	U1
8	-X	-Y	-Z	-U1	-U2	-U3	-U4	32	-Z	-Y	-X	-U1	U4	-U3	U2
9	Y	Z	X	U1	-U4	U2	-U3	33	Y	X	Z	U1	U2	-U4	-U3
10	-Y	Z	X	U3	-U2	U4	-U1	34	-Y	X	Z	U3	U4	-U2	-U1
11	Y	-Z	X	U2	-U3	U1	-U4	35	Y	-X	Z	-U4	-U3	U1	U2
12	-Y	-Z	X	U4	-U1	U3	-U2	36	-Y	-X	Z	-U2	-U1	U3	U4
13	Y	Z	-X	-U4	U1	-U3	U2	37	Y	X	-Z	U2	U1	-U3	-U4
14	-Y	Z	-X	-U2	U3	-U1	U4	38	-Y	X	-Z	U4	U3	-U1	-U2
15	Y	-Z	-X	-U3	U2	-U4	U1	39	Y	-X	-Z	-U3	-U4	U2	U1
16	-Y	-Z	-X	-U1	U4	-U2	U3	40	-Y	-X	-Z	-U1	-U2	U4	U3
17	Z	X	Y	U1	U3	-U4	-U2	41	X	Z	Y	U1	U3	U2	U4
18	-Z	X	Y	U2	U4	-U3	-U1	42	-X	Z	Y	-U4	-U2	-U3	-U1
19	Z	-X	Y	-U4	-U2	U1	U3	43	X	-Z	Y	U2	U4	U1	U3
20	-Z	-X	Y	-U3	-U1	U2	U4	44	-X	-Z	Y	-U3	-U1	-U4	-U2
21	Z	X	-Y	U3	U1	-U2	-U4	45	X	Z	-Y	U3	U1	U4	U2
22	-Z	X	-Y	U4	U2	-U1	-U3	46	-X	Z	-Y	-U2	-U4	-U1	-U3
23	Z	-X	-Y	-U2	-U4	U3	U1	47	X	-Z	-Y	U4	U2	U3	U1
24	-Z	-X	-Y	-U1	-U3	U4	U2	48	-X	-Z	-Y	-U1	-U3	-U2	-U4

APPENDIX VI

THE COHERENT NEUTRON SCATTERING AMPLITUDE OF RUBIDIUM

Shull and Wollan (1951) first measured the coherent neutron scattering amplitude of rubidium (b_{Rb}) as 0.55×10^{-12} cm., using a powder sample of RbCl. More recently Mueller et al (1963) obtained a value of 0.85×10^{-12} cm., again using a RbCl powder specimen. In view of this discrepancy it was felt worthwhile to redetermine this quantity using powders of RbCl, RbBr, and RbI. This work is described in a reprint at the end of this thesis (Copley 1970). We obtained

$$b_{Rb} = (0.68_5 \pm 0.01) \times 10^{-12} \text{ cm.}$$

The observed powder peaks are shown in Figure AVI-1. For each compound the left and right hand peaks are (111) and (200) reflections respectively. In the case of the bromide, the experimental points for the (111) scan are shown instead, since no peak as such was discernible. The upward arrow indicates the expected position of this reflection. The numbers in brackets are proportional to the number of incident neutrons for each point on the appropriate scan (i.e. the monitor count).

It will be observed that the ratio of the (111) intensity to the (200) intensity can be determined to within a few per cent in the cases of RbCl and RbI. The calculated scattering amplitude is insensitive to small changes in these

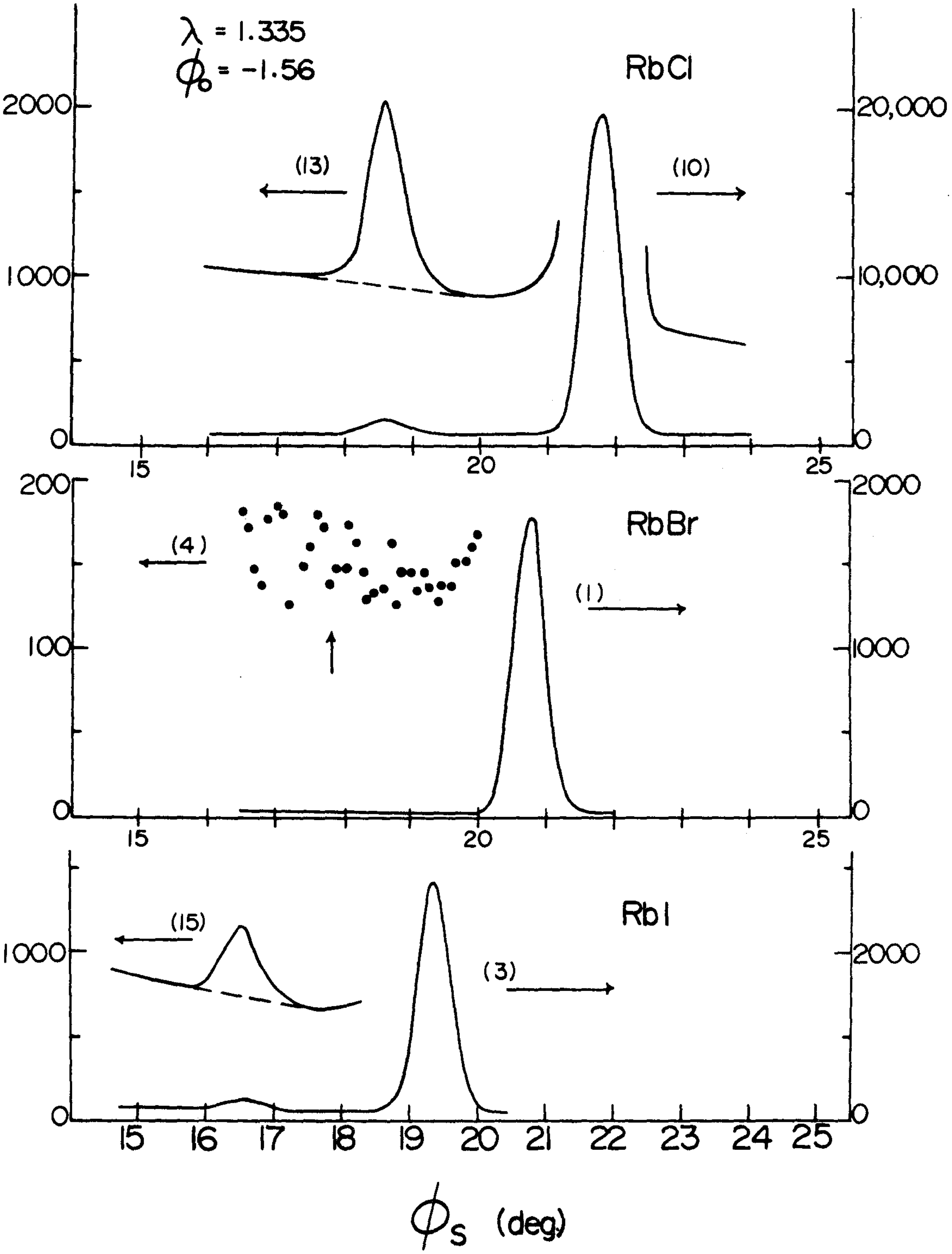

Fig. AVI-1. The observed (111) and (200) powder peaks in three rubidium halides. The scattering angle, ϕ, is given by $\phi = \phi_s - \phi_o$. The small numbers in brackets indicate counting times.

ratios, as can be seen in Fig. AVI-2, where the ordinate is proportional to the intensity ratio. Furthermore a systematic source of error in determining the intensity ratios would lead to inconsistent results. This is illustrated in Fig. AVI-2. The solid arrows indicate the values of b_{Rb} deduced from the measured intensities. The dashed arrows point to values of b_{Rb} which would be obtained if the intensity ratios were smaller by 1/3 : clearly they are no longer compatible. Thus a systematic discrepancy of this type may be safely discounted.

Since this work was completed, two other determinations of b_{Rb} have been reported. Wang and Cox (1970) obtained a value of $(0.70_5 \pm 0.02_5) \times 10^{-12}$ cm., and Meriel (1970) reported $b_{Rb} = (0.704 \pm 0.008) \times 10^{-12}$ cm. Both of these measurements were made using RbCl powder specimens. It is satisfactory to note that the value we obtain from measurements on RbCl alone, $(0.69 \pm 0.01) \times 10^{-12}$ cm., is in agreement with these other values.

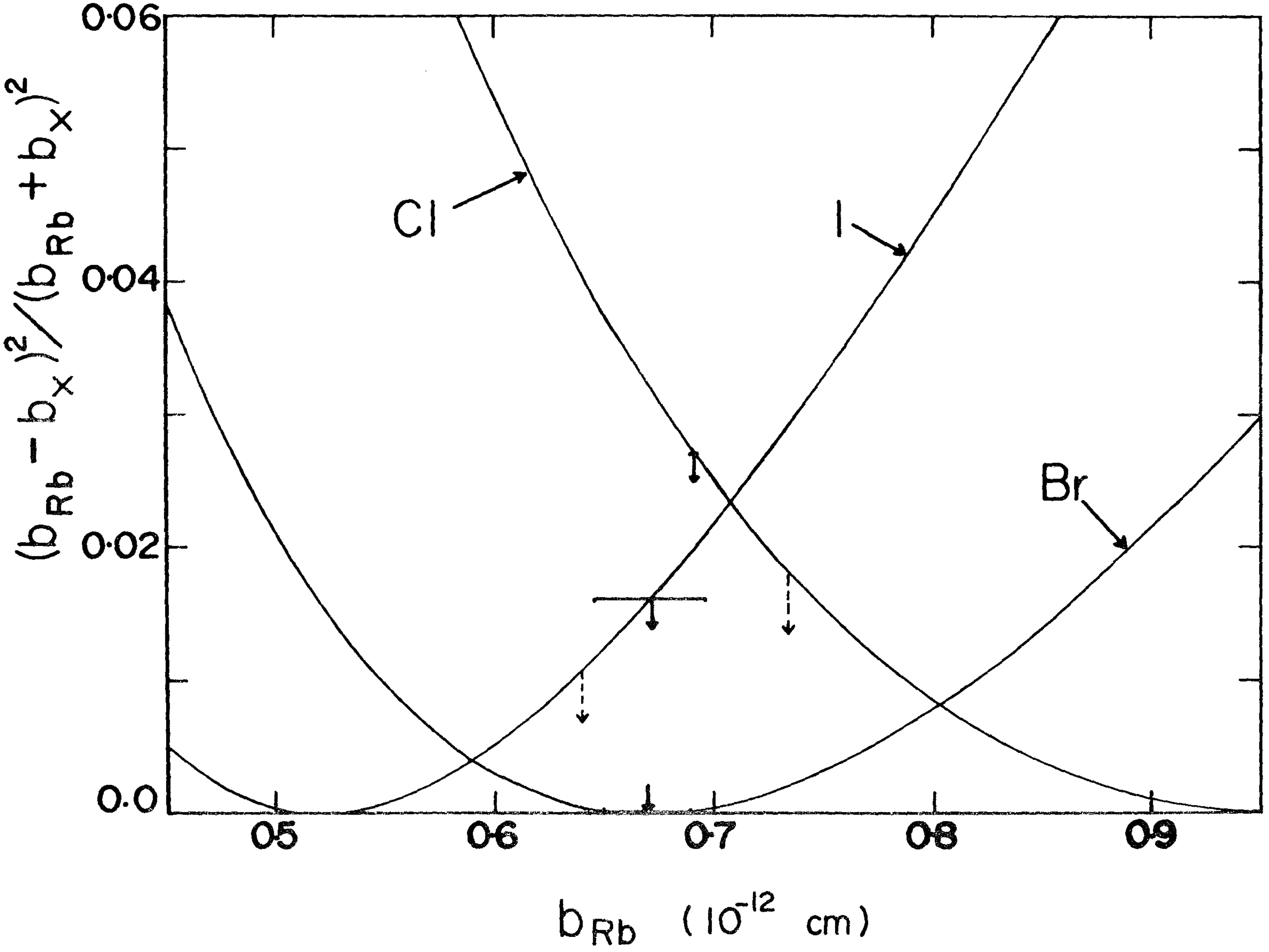

Fig. AVI-2. The ratio of the structure factors for odd and even peaks, as a function of the scattering amplitude of rubidium.

APPENDIX VII

LATTICE DYNAMICS OF POTASSIUM CHLORIDE

Because of the relatively high neutron absorption cross section of chlorine, the first measurements of phonons in alkali halides were made on NaI (Woods et al. 1960) and on KBr (Woods et al. 1963). More recently several other common alkali halides have been examined, with the notable exception of KCl. In this appendix we consider a neutron scattering investigation of phonons in KCl.

This work was motivated by the need for shell model parameters for KCl, from which optical properties may be calculated, for comparison with experiment. The experiments were carried out by the author, in collaboration with Dr. G. A. deWit in the early stages, and the subsequent shell model fits and calculations of the frequency distribution were performed by Dr. R. W. MacPherson and Dr. T. Timusk. The work is described in a reprint at the end of this thesis (Copley et al. 1969). The dispersion curves are also shown in Fig. AVII-1.

Raunio and Almqvist (1969) have also measured the dispersion curves of KCl. In a later publication, Raunio (1969) described measurements of phonon widths in three alkali chlorides. The Swedish work was recently analysed by Raunio and Rolandson (1970), who give shell model parameters for KCl and three other alkali halides. Their fits to the KCl data have somewhat smaller standard errors than those of Copley et al. (1969).

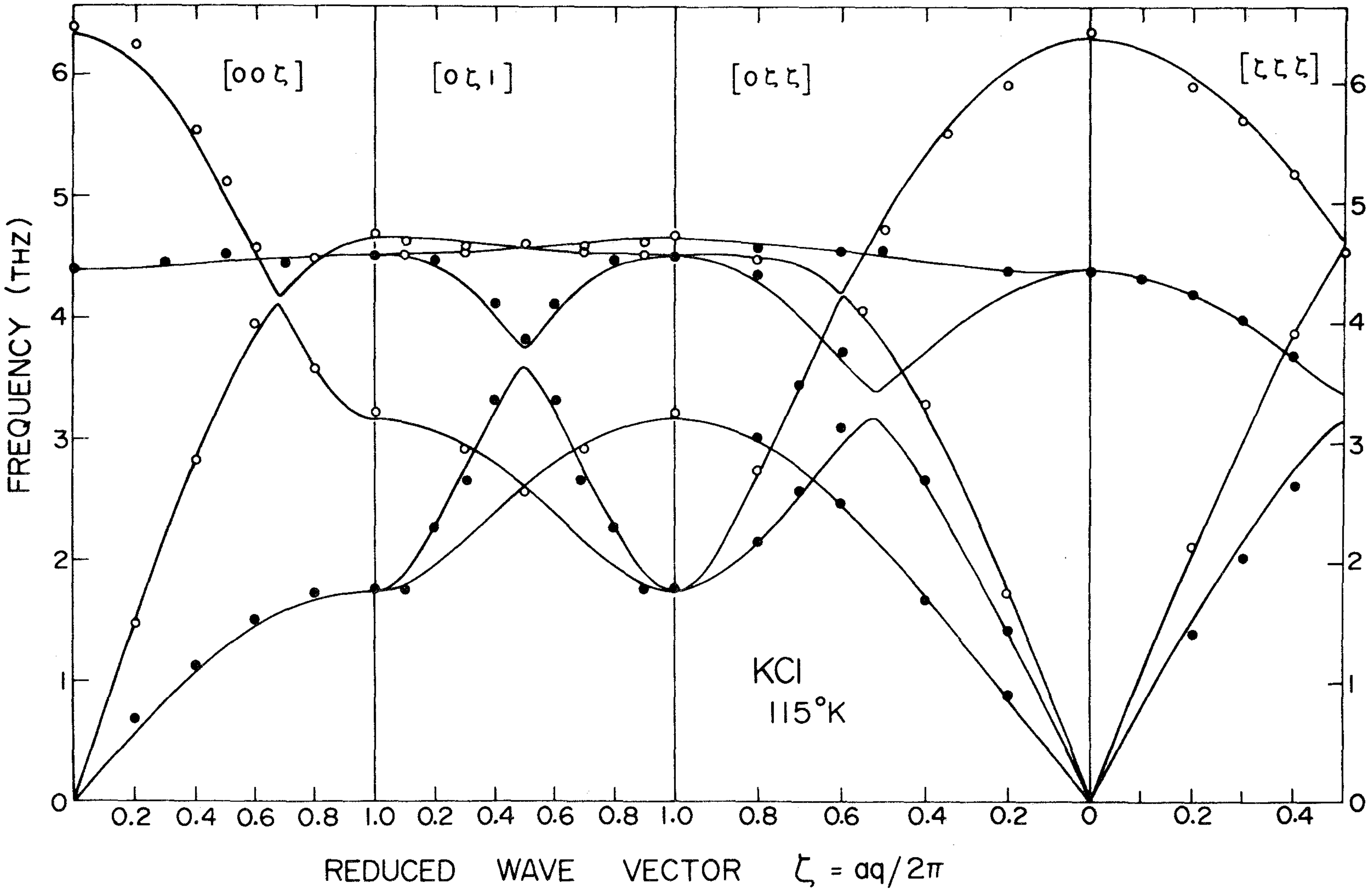

Figure AVII-1. The dispersion curves of KCl at 115°K. The points denote the measured phonons, and the lines show a shell model calculation (Model VI of Copley et al. 1969).

The Debye-Waller factors (B_i) of KCl were incorrectly calculated in the paper by Copley et al. (1969). An erratum was subsequently published. The calculated values of B_i have been corrected for thermal expansion using the formula (Willis 1969):

$$B_i^{qh} = B_i^{h}(1 + 2\gamma\chi T) \qquad \text{(AVII-1)}$$

where qh and h denote the quasiharmonic and the harmonic values, γ is the Gruneisen constant, and χ is the volume expansion coefficient. Values of γ and χ were taken from White (1965), Rubin et al. (1962), and Leadbetter and Newsham (1969). Since the "harmonic" values, B_i^h, were calculated using a frequency distribution appropriate to 115°K, the quantity T was replaced by (T - 115), in Eq. (AVII-1).

The results of this calculation are shown in Fig. AVII-2. The quasiharmonic values of the Debye-Waller factor are seen to deviate from the harmonic values above room temperature. It is satisfactory to note that the quasiharmonic values are in reasonable agreement with the measurements of Willis (1970) up to 600°K. The discrepancy at 900°K indicates that "true" anharmonic contributions have become important at this temperature. The measurements of Patomäki and Linkoaho (1969) and of Jayalakshmi and Viswamitra (1970) are also in reasonable agreement with the present calculations.

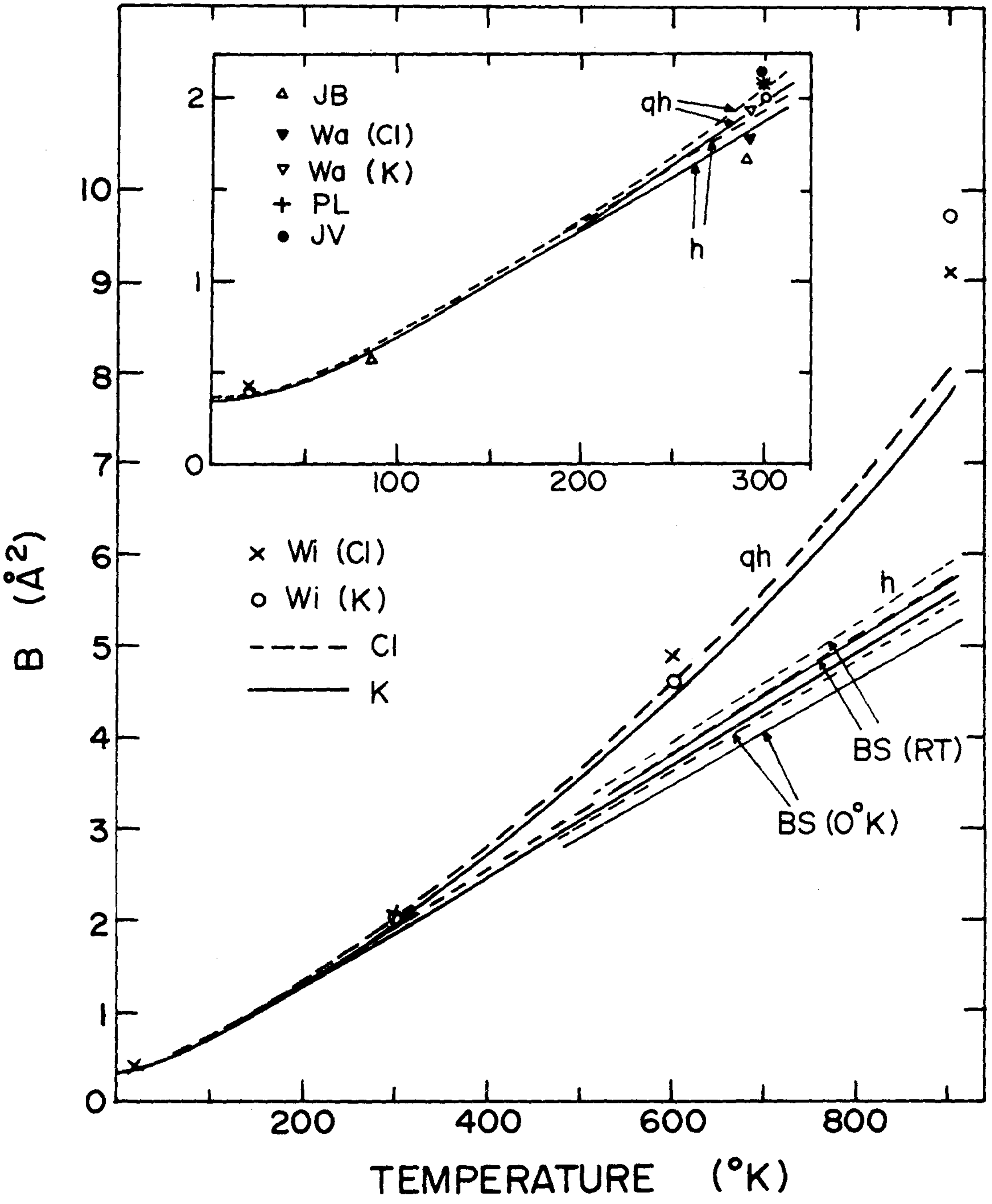

Figure AVII-2. Debye-Waller factors in KCl. The measurements of James and Brindley (1928) (JB), Wasastjerna (1946) (Wa), Patomäki and Linkoaho (1969) (PL), Jayalakshmi and Viswamitra (1970) (JV), and Willis (1970) (Wi) are also shown. The calculations of Buyers and Smith (1968) (BS) are indicated.

BIBLIOGRAPHY

A. GENERAL REFERENCES

1. Inelastic Scattering of Neutrons in Solids and Liquids. International Atomic Energy Agency, Vienna (1961).

2. Inelastic Scattering of Neutrons in Solids and Liquids. (Two volumes). International Atomic Energy Agency, Vienna (1963).

3. Inelastic Scattering of Neutrons (Two volumes). International Atomic Energy Agency, Vienna (1965).

4. Neutron Inelastic Scattering (Two volumes). International Atomic Energy Agency, Vienna (1968).

5. Phonons and Phonon Interactions, edited by T. A. Bak, W. A. Benjamin Inc., New York (1964).

6. Lattice Dynamics, edited by R. F. Wallis, Pergamon Press, London (1965).

7. Thermal Neutron Scattering, edited by P. A. Egelstaff. Academic Press, New York (1965).

8. Phonons in Perfect Lattices and in Lattices with Point Imperfections, edited by R.W.H. Stevenson. Oliver and Boyd, Edinburgh (1966).

B. SPECIFIC REFERENCES

A. O. E. Animalu, F. Bonsignori, and V. Bortolani, Nuovo Cimento 44, 159 (1966).

N. W. Ashcroft, Phys. Lett. 23, 48 (1966).

N. W. Ashcroft, J. Phys. C 1, 232 (1968).

G. E. Bacon, Neutron Diffraction, Second Ed., Clarendon Press, Oxford (1962).

J. Bardeen, Phys. Rev. 52, 688 (1937).

C. S. Barrett, J. Inst. Metals, 84, 43 (1955).

C. S. Barrett, Acta Cryst. 9, 671 (1956).

T. H. K. Barron, Discussions of the Faraday Society 40, 69 (1965a).

T. H. K. Barron, in General Reference 6, p. 247 (1965b).

T. H. K. Barron, A. J. Leadbetter and J. A. Morrison, Proc. Roy. Soc. (London) A279, 62 (1964).

T. H. K. Barron, A. J. Leadbetter, J. A. Morrison, and L. S. Salter, Acta Cryst. 20, 125 (1966).

J. Bergsma and C. van Dijk, Reactor Centrum Nederland Report RCN-34 (1965).

R. Blanchard, Ph.D. Thesis, University of Ottawa (unpublished) (1969).

R. Blanchard and Y. P. Varshni, (to be published) (1970).

L. Bohlin and T. Högberg, J. Phys. Chem. Solids 29, 1805 (1968).

B.Böhm and W. Klemm, Z. anorg. u. allgem. Chem. 243, 69 (1939).

G. Borelius, In Solid State Physics, edited by F. Seitz and D. Turnbull, Vol. 15, p. 1. Academic Press, New York (1963).

M. Born, in General Reference 6, p. 1 (1965).

M. Born and K. Huang, Dynamical Theory of Crystal Lattices, Clarendon Press, Oxford (1954).

M. Born and T. von Kármán, Phys. Zeit. 13, 297 (1912).

W. L. Bragg, Proc. Roy. Soc. (London) A89, 248 (1913).

P. W. Bridgman , Proc. Amer. Acad. Arts and Sci. 74, 425 (1942).

P. W. Bridgman, Proc. Amer. Acad. Arts and Sci. 76, 55 (1948); 76, 71 (1948).

B. N. Brockhouse, Phys. Rev. Letters 2, 256 (1959).

B. N. Brockhouse, in General Reference 1, p. 113 (1961).

B. N. Brockhouse, in General Reference 8, p. 110 (1966).

B. N. Brockhouse, in General Reference 4, Vol. I, p. 163 (1968).

B. N. Brockhouse, T. Arase, G. Caglioti, M. Sakamoto, R. N. Sinclair, and A.D.B. Woods, in General Reference 1, p. 531 (1961).

B. N. Brockhouse, T. Arase, G. Caglioti, K. R. Rao, and A. D. B. Woods, Phys. Rev. 128, 1099 (1962).

B. N. Brockhouse, G. A. deWit, E. D. Hallman and J. M. Rowe, in General Reference 4, Vol. II, p. 259 (1968a).

B. N. Brockhouse, E. D. Hallman, and S. C. Ng , in Magnetic and Inelastic Scattering of Neutrons by Metals, edited by T. J. Rowland and P. A. Beck, Gordon and Breach Inc., N. Y. (1968b).

B. N. Brockhouse and A. T. Stewart, Phys. Rev. 100, 756 (1955); see also B. N. Brockhouse and A. T. Stewart, Revs. Modern Phys. 30, 236 (1958).

T. D. Brotherton, O. N. Cole and R. E. Davis, Trans. Met. Soc. AIME, 224, 287 (1962).

R. J. Bruno. Private Communication (1970).

W. J. L. Buyers and R. A. Cowley, Phys. Rev. 180, 755 (1969).

W. J. L. Buyers and T. Smith, J. Phys. Chem. Solids 29, 1051 (1968).

R. S. Carter, H. Palevsky, and D. J. Hughes, Phys. Rev. 106, 1168 (1957).

W. Cochran, Proc. Roy. Soc. (London) A276, 308 (1963).

W. Cochran, in General Reference 8, p. 53 (1966).

M. F. Collins, Brit. J. Appl. Phys. 14, 805 (1963).

M. F. Collins, V. J. Minkiewicz, R. Nathans, L. Passell and G. Shirane, Phys. Rev. 179, 417 (1969).

M. J. Cooper and R. Nathans, Acta Cryst. 23, 357 (1967).

J. R. D. Copley, Acta Cryst. A26, 376 (1970).

J. R. D. Copley, B. N. Brockhouse and S. H. Chen, in General Reference 4, Vol. I, p. 209 (1968).

J. R. D. Copley, R. W. MacPherson and T. Timusk, Phys. Rev. 182, 965 (1969); B 1, 4193 (1970)(Erratum).

M. A. Coulthard, J. Phys. C3, 820 (1970).

R. A. Cowley, Adv. Phys. 12, 421 (1963).

R. A. Cowley, Rep. Prog. Phys. 31, 123 (1968).

E. R. Cowley. Private Communication (1970).

R. A. Cowley, W.J.L. Buyers, E. C. Svensson and G. L. Paul, in General Reference 4, Vol. I, p. 281 (1968).

R. A. Cowley, W. Cochran, B. N. Brockhouse and A.D.B. Woods, Phys. Rev. 131, 1030 (1963).

E. R. Cowley and R. A. Cowley, Proc. Roy. Soc. (London) A287, 259 (1965).

E. R. Cowley and R. A. Cowley, Proc. Roy. Soc. (London) A292, 209 (1966).

E. R. Cowley and A. K. Pant, Acta Cryst. (to be published) (1970).

R. A. Cowley, A. D. B. Woods and G. Dolling, Phys. Rev. 150, 487 (1966).

P. Debye, Ann. Physik 39, 789 (1912). An English translation of this paper is contained in "The Collected Papers of Peter J. W. Debye", Interscience, New York (1954).

E. Deuss, Vierteljahrsschr. naturforsch. Ges.Zürich 56, 15 (1911).

M. E. Diederich and J. Trivisonno, J. Phys. Chem. Solids 27, 637 (1966).

A. E. Dixon, A. D. B. Woods and B. N. Brockhouse, Proc. Phys. Soc. (London) 81, 973 (1963).

G. Dolling. Private Communication (1970).

G. Dolling, H. G. Smith, R. M. Nicklow, P.R. Vijayaraghavan, and M. K. Wilkinson, Phys. Rev. 168, 970 (1968).

P. L. Dulong and A. T. Petit, Ann. chim. et. phys. [2], 10, 395 (1819).

A. Einstein, Ann. Physik. 22, 180 (1907).

R. J. Elliott, in General Reference 8, p. 377 (1966).

E. Fermi, Ricerca Sci. 7, 13 (1936) [English translation: U.S.A.E.C. report NP-2385].

J. D. Filby and D. L. Martin, Proc. Roy. Soc. (London) A284, 83 (1965).

M. A. Filyand and E. I. Semenova, Handbook of the Rare Elements, Vol. I, Trace Elements and Light Elements, translated and edited by M. E. Alferieff, Boston Technical Publishers Inc., Cambridge, Mass. (1968).

J. Frenkel, Wave Mechanics, Elementary Theory, 1st Ed., p. 265. Oxford (1932).

C.-E. Fröberg, Introduction to Numerical Analysis, p. 181. Addison-Wesley Publishing Co., Reading, Mass. (1965).

K. Fuchs, Proc. Roy. Soc. (London) A151, 585 (1935).

K. Fuchs, Proc. Roy. Soc. (London) A157, 444 (1936).

D. J. W. Geldart and S. H. Vosko, Can. J. Phys. 44, 2137 (1966); 45, 2229 (1967) (Erratum).

G. Gilat and L. Bohlin, Solid State Commun. 7, 1727 (1969).

G. Gilat and G. Dolling, Phys. Lett. 8, 304 (1964).

G. Gilat and Z. Kam, Phys. Rev. Lett. 22, 715 (1969); 22, 1028 (1969) (Erratum).

G. Gilat and L. J. Raubenheimer, Phys. Rev. 144, 390 (1966).

R. Ginell and T. J. Quigley, J. Phys. Chem. Solids 26, 1157 (1965).

L. A. Girifalco and V. G. Weizer, Phys. Rev. 114, 687 (1959).

H. R. Glyde and R. A. Cowley, Solid State Commun. 8, 923 (1970).

M. D. Goldberg, S. F. Mughabghab, B. A. Magurno, and V. M. May, Neutron Cross Sections, Brookhaven National Laboratory report BNL-325, 2nd Ed., Suppl. no. 2, Vol. IIA (1966).

E. J. Gutman and J. Trivisonno, J. Phys. Chem. Solids 28, 805 (1967).

L. Hackspill, Compt. rend. 152, 259 (1911).

E. D. Hallman, Ph.D. Thesis, McMaster University, Hamilton (unpublished) (1969).

E. D. Hallman and B. N. Brockhouse, Can. J. Phys. 47, 1117 (1969).

W. A. Harrison, Pseudopotentials in the Theory of Metals, W. A. Benjamin, Inc., New York (1966).

P. S. Ho, Phys. Rev. 169, 523 (1968).

T. Högberg and R. Sandström, phys. stat. sol. 33, 169 (1969).

E. J. Holmyard and W. G. Palmer, A Higher School Inorganic Chemistry, p. 196, J. M. Dent and Sons, London (1939).

H. Horner, Phys. Rev. Lett. 25, 147 (1970).

D. J. Hughes and R. B. Schwartz, Neutron Cross Sections, Brookhaven National Laboratory report BNL-325, 2nd Ed. (1958).

W. Hume-Rothery and K. Lonsdale, Phil.Mag. 36, 842 (1945).

R. W. James and G. W. Brindley, Proc. Roy. Soc. (London) A121, 162 (1928).

K. Jayalakshmi and M. A. Viswamitra, Phys. Lett. 31A, 70 (1970).

S. K. Joshi and A. K. Rajagopal. In Solid State Physics, edited by F. Seitz and D. Turnbull, Vol. 22, p. 160. Academic Press, New York (1968).

J. M. Keller and D. C. Wallace, Phys. Rev. 126, 1275 (1962).

E. W. Kellermann,Phil. Trans. Roy. Soc. (London) 238, 513 (1940).

F. M. Kelly and W. B. Pearson, Can. J. Phys. 33, 17 (1955).

C. Kittel, Quantum Theory of Solids, John Wiley, New York (1963).

M. L. Klein, G. K. Horton, and J. L. Feldman, Phys. Rev. 184, 968 (1969).

T. R. Koehler, N. S. Gillis, and D. C. Wallace, Phys. Rev. B1, 4521 (1970).

W. Kohn, Phys. Rev. Lett. 2, 393 (1959).

F. J. Kollarits and J. Trivisonno, J. Phys. Chem. Solids 29, 2133 (1968).

G. F. Koster. In Solid State Physics, edited by F. Seitz and D. Turnbull, Vol. 5, p. 174. Academic Press, New York (1957).

K. E. Larsson, S. Holmryd, and U. Dahlborg, in General Reference 1, p. 587 (1961).

D. Lazarus, Phys. Rev. 76, 545 (1949).

A. J. Leadbetter and D. M. T. Newsham, J. Phys. C. 2, 210 (1969).

G. Leibfried, in General Reference 6, p. 237 (1965).

G. Leibfried and W. Ludwig. In Solid State Physics, edited by F. Seitz and D. Turnbull, Vol. 12, p. 275. Academic Press, New York (1961).

W. Ludwig, Recent Developments in Lattice Theory, Springer Tracts in Modern Physics, Vol. 43 (1967).

A. A. Maradudin, phys. stat. sol. 2, 1493 (1962).

A. A. Maradudin and A. E. Fein, Phys. Rev. 128, 2589 (1962).

A. A. Maradudin, A. E. Fein, and G. H. Vineyard, phys. stat. sol. 2, 1479 (1962).

A. A. Maradudin and P. A. Flinn, Phys. Rev. 129, 2529 (1963).

W. R. Marquardt and J. Trivisonno, J. Phys. Chem. Solids 26, 273 (1965).

D. L. Martin, Phys. Rev. 139, A150 (1965).

D. L. Martin, Can. J. Phys. 48, 1327 (1970).

P. Meriel, Compt. rend. 270 (série B), 560 (1970).

A. Messiah, Quantum Mechanics, John Wiley, New York (1962).

A. P. Miiller, Ph.D. Thesis, McMaster University, Hamilton (unpublished) (1969).

A. P. Miiller and B. N. Brockhouse, Can. J. Phys. (to be published) (1970).

A. Millington. Private Communication (1969).

H. B. Møller and M. Nielsen , "Resolution of Neutron Spectrometers for Inelastic Neutron Scattering", to be published in the Proceedings of the IAEA Panel Meeting on Instrumentation for Neutron Inelastic Scattering Research. International Atomic Energy Agency, Vienna (1970).

N. F. Mott and H. Jones, The Theory of the Properties of Metals and Alloys, Clarendon Press, Oxford (1936).

M. H.Mueller, S. S. Sidhu, L. Heaton, R. L. Hitterman and H. W. Knott, Argonne National Laboratory report ANL-6797, 393 (1963).

Neutron Diffraction Commission, Acta Cryst. A25, 391 (1969).

D. M. T. Newsham, Phys. Rev. 152, 841 (1966).

S. C. Ng, E. D. Hallman, and B. N. Brockhouse, Mater. Res. Bull. 2, 69 (1967).

Ph. Olmer, Acta Cryst. 1, 57 (1948); Bull. soc. franc. mineral. 71, 144 (1948).

A. W. Overhauser, Phys. Rev. 167, 691 (1968).

A. W. Overhauser. Private Communication (1970).

W. C. Overton, J. Phys. Chem. Solids 29, 711 (1968).

D. J.Page, Proc. Phys. Soc. 91, 76 (1967).

L. K. Patomäki and M. V. Linkoaho,Acta Cryst. A25, 304 (1969).

L. A. Pauer, Office of Naval Research, Technical Report No. 11, Contract Nonr. 1141 (05),Project NR 017-309 (1968).

W. B. Pearson, Handbook of Lattice Spacings and Structures of Metals and Alloys, Pergamon Press, New York (1958).

G. E. Peckham, United Kingdom Atomic Energy Authority Report, AERE-R 4380 (1964).

G. E. Peckham, D. H. Saunderson, and R. I. Sharp, Brit. J. Appl. Phys. 18, 473 (1967).

R. E. Peierls, Quantum Theory of Solids, Clarendon Press, Oxford (1955).

F. M. Perel'man, Rubidium and Caesium, translated by R.G.P. Towndrow. 1st English Ed. MacMillan, New York (1965).

D. Pines and P. Nozières, The Theory of Quantum Liquids, Vol. I, p. 104. Benjamin, New York (1966).

S. Prakash and S. K.Joshi, Phys. Rev. 187, 808 (1969).

D. L. Price, K. S. Singwi, and M. P. Tosi, Phys. Rev. (to be published)(1970).

G. Raunio, phys. stat. sol. 35, 299 (1969).

G. Raunio and L. Almqvist, phys. stat. sol. 33, 209 (1969).

G. Raunio and S. Rolandson, Phys. Rev. B (to be published) (1970).

M. H. Rice, J. Phys. Chem. Solids 26, 483 (1965).

F. Richarz, Ann. Physik 48, 708 (1893); 67, 702 (1899).

C. A. Roberts and R. Meister, J. Phys. Chem. Solids 27, 1401 (1966).

J. M. Rowe, Ph.D. Thesis, McMaster University, Hamilton (unpublished) (1966).

T. Rubin, H. L. Johnston, and H. W. Altman, J. Phys. Chem. 66, 948 (1962).

T. Schneider and E. Stoll, Phys. kondens Materie 5, 331 (1966a).

T. Schneider and E. Stoll, Phys. kondens Materie 5, 364 (1966b).

F. Seitz, Imperfections in Nearly Perfect Crystals, p. 15. John Wiley, New York (1952).

C. G. Shull, Transactions of the American Crystallographic Association, 3, 1 (1967).

C. G. Shull and E. O. Wollan, Phys. Rev. 81, 527 (1951).

F. Simon and E. Vohsen, Z. physik. Chem. A, 133, 165 (1928).

A. Sjölander, Arkiv Fysik 14, 315 (1958).

T. Slotwinski and J. Trivisonno, J. Phys. Chem. Solids 30, 1276 (1969).

H. G. Smith, G. Dolling, R. M. Nicklow, P. R. Vijayaraghavan and M. K. Wilkinson, in General Reference 4, Vol. I, p. 149 (1968).

C. J. Smithells, Metals Reference Book, (3rd Ed.) Vol. II. Butterworths, London (1958).

R. Stedman and G. Nilsson, Phys. Rev. 145, 492 (1966).

A. T. Stewart and B. N. Brockhouse, Rev. Mod. Phys. 30, 250 (1958).

E. C. Svensson, B. N. Brockhouse and J. M. Rowe, Phys. Rev. 155, 619 (1967).

C. A. Swenson, Phys. Rev. 99, 423 (1955).

T. Toya, J. Res. Inst. Catalysis, Hokkaido Univ. 6, 183 (1958).

T. Toya, J. Res. Inst. Catalysis, Hokkaido Univ., 7, 60 (1959).

L. Van Hove, Phys. Rev. 95, 249 (1954).

S. H. Vosko, R. Taylor, and G. H. Keech, Can. J. Phys. 43, 1187 (1965).

D. C. Wallace, Phys. Rev. 176, 832 (1968).

D. C. Wallace, Phys. Rev. 178, 900 (1969).

R. F. Wallis and D. C. Gazis, in General Reference 6, p. 537 (1965).

F. F. Y. Wang and D. E. Cox, Acta Cryst. A26, 377 (1970).

J. A. Wasastjerna, Soc. Sci. Fennica Commentationes Phys. Math., 13, 1 (1946). Quoted in International Tables for X-ray Crystallography, ed. Kathleen Lonsdale, (Kynoch Press, Birmingham, England, 1962), Vol. III, p. 240.

R. C. Weast (Editor), Handbook of Chemistry and Physics, 49th Ed., p. F-18, The Chemical Rubber Company, Cleveland, Ohio (1968).

G. K. White, Proc. Roy. Soc. (London) A286, 204 (1965).

B. T. M. Willis, Acta Cryst. A25, 277 (1969).

B. T. M. Willis, Private Communication (1970).

A. D. B. Woods, B. N. Brockhouse, R. A. Cowley, and W. Cochran, Phys. Rev. 131, 1025 (1963).

A. D. B. Woods, B. N. Brockhouse, R. H. March, A. T. Stewart and R. Bowers, Phys. Rev. 128, 1112 (1962). See also A.D.B. Woods, B.N. Brockhouse, R. H. March and R. Bowers, Proc. Phys. Soc. 79, 440 (1962) and Bull. Am. Phys. Soc. 6, 261 (1961).

A. D. B. Woods, W. Cochran, and B. N. Brockhouse, Phys. Rev. 119, 980 (1960).

M. W. Zemansky, Heat and Thermodynamics, 4th Ed., p. 251. McGraw Hill, New York (1957).

J. M. Ziman, Electrons and Phonons, p. 16. Oxford (1960).

J. M.Ziman, Adv. Phys. (Phil. Mag. Suppl.) 13, 89 (1964).

Reprinted from *Acta Crystallographica*, Vol. A 26, Part 3, May 1970

PRINTED IN DENMARK

Acta Cryst. (1970). A**26**, 376

A redetermination of the coherent neutron scattering amplitude of rubidium.

By J. R. D. Copley, *Department of Physics, McMaster University, Hamilton, Ontario, Canada*

(*Received* 25 *June* 1969)

The coherent neutron scattering amplitude of rubidium has been remeasured using powders of RbCl, RbBr, and RbI. A consistent value, $(0{\cdot}68_5 \pm 0{\cdot}01) \times 10^{-12}$ cm, was obtained, differing significantly from earlier measurements. The new value is believed to be more reliable. The bound coherent scattering cross-section is $5{\cdot}9 \pm 0{\cdot}2$ barns.

The coherent neutron scattering amplitude of rubidium (b_{Rb}) was first measured by Shull & Wollan (1951) who obtained $b_{\mathrm{Rb}} = 0{\cdot}55$ (scattering amplitudes are given throughout in units of 10^{-12} cm). In their structure study of $\mathrm{RbMnF_3}$, Pickart, Alperin & Nathans (1964) found this value low, and favoured a value of about 0·63. Mueller, Sidhu, Heaton, Hitterman & Knott (1963) reported a value of 0·85. In view of the considerable discrepancy between these measurements, a further investigation has been undertaken in order to obtain a better value of b_{Rb}.

The previously published values were both obtained by the powder diffraction technique (Bacon, 1962) using samples of RbCl and an external standard. The present measurements were made by the powder method using cylindrical samples of RbCl, RbBr, and RbI (which have the NaCl structure) using the halogens as internal standards. For cylindrical geometry and the NaCl structure, the integrated intensity, P, of the reflexion from a set of planes (hkl) is $P = KjI/(\sin\theta \sin 2\theta)$ where

$$I = |b_{\mathrm{Rb}} \exp(-W_{\mathrm{Rb}}) \pm b_{\mathrm{X}} \exp(-W_{\mathrm{X}})|^2 A\,.$$

Here j is the multiplicity of the (hkl) planes, θ is the Bragg scattering angle, b_{X} is the coherent scattering amplitude of the halogen, the exponential terms are Debye–Waller temperature factors, and A is the absorption factor: $P, I, j, \theta, W_{\mathrm{Rb}}, W_{\mathrm{X}}$, and A depend on the indices hkl. K is a constant depending on details of the spectrometer and on the size of the sample. The plus (minus) sign is used when h, k, l are all even (all odd). In this work, the intensities of the 111 and 200 reflexions from each halide were measured and a consistent value of b_{Rb} was obtained from the intensity ratios P_{111}/P_{200}.

Measurements were made at room temperature using the McMaster University triple-axis spectrometer at Chalk River (Brockhouse, de Wit, Hallman & Rowe, 1968) with $\lambda = 1{\cdot}335$ Å. The analyser was set to count neutrons elastically scattered by the specimen. Use of a double monochromator and an analyser significantly reduces second order contributions to the measured intensities. The specimens (obtained from K & K Laboratories, Plainsview, New York, 99·9% pure), were contained in a half inch diameter aluminum can having 0·012 inch walls.

The ratios $R_{\mathrm{X}} = I_{111}/I_{200}$, are given in Table 1. The 111 peak in RbBr was too weak to be seen. The errors assigned to the ratios R_{X} arise from counting statistics. Neglecting the absorption and temperature factors we may write $R_{\mathrm{X}} = (b_{\mathrm{Rb}} - b_{\mathrm{X}})^2/(b_{\mathrm{Rb}} + b_{\mathrm{X}})^2$. Since R_{Br} is very small, $b_{\mathrm{Rb}} \simeq b_{\mathrm{Br}}$. The values of b_{Rb} listed in Table 1 were obtained

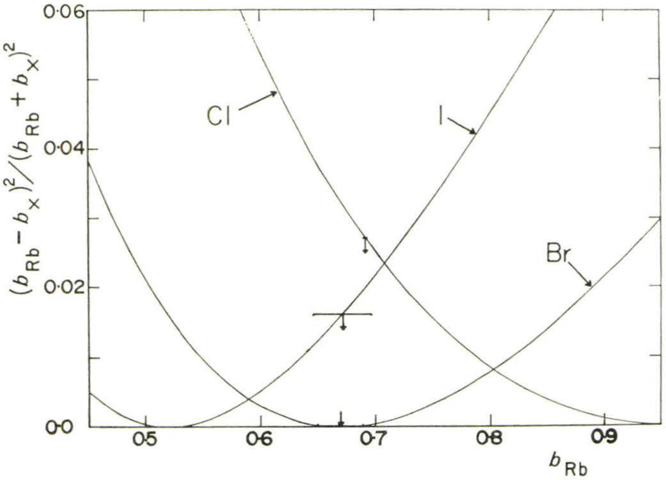

Fig. 1. The ratio $(b_{\mathrm{Rb}} - b_{\mathrm{X}})^2/(b_{\mathrm{Rb}} + b_{\mathrm{X}})^2$ as a function of b_{Rb}, for the three halogens. The arrows indicate the values of b_{Rb} deduced from each intensity ratio, neglecting temperature corrections. The short horizontal lines represent uncertainties in b_{Rb} arising from uncertainties in the values of b_{X}.

from the ratios R_X, corrected for the temperature factors as described below. The values of b_X are also given in Table 1. Fig. 1 illustrates the dependence of b_{Rb} on the ratios R_X.

Table 1. *Powder diffraction results from several* Rb *halides*

$R_X = I_{111}/I_{200}$ is calculated from the observed intensities; b_X is the assumed halogen scattering amplitude, and b_{Rb} is the calculated scattering amplitude for Rb. Scattering amplitudes in units of 10^{-12} cm.

X	Cl	Br	I
R_X	$0{\cdot}027_2 \pm 0{\cdot}001$	$0{\cdot}0 \pm 0{\cdot}0002$	$0{\cdot}016_4 \pm 0{\cdot}001$
b_X	$0{\cdot}963 \pm 0{\cdot}001$*	$0{\cdot}67 \pm 0{\cdot}02$†	$0{\cdot}52 \pm 0{\cdot}02$†
b_{Rb}	$0{\cdot}69 \pm 0{\cdot}01$	$0{\cdot}67 \pm 0{\cdot}02_5$	$0{\cdot}67 \pm 0{\cdot}03$

* Koester (1967).
† Shull & Wollan (1951).

Individual room temperature Debye–Waller parameters, $B_i = W_{i,hkl}(\lambda/\sin\theta_{hkl})^2$ were calculated (Dolling, Smith, Nicklow, Vijayaraghavan & Wilkinson, 1968) using the breathing shell model (Schröder, 1966) with the elastic and optical constants as input parameters. In the worst case, that of RbI, inclusion of the temperature factors reduces the calculated value of b_{Rb} by $(0{\cdot}7 \pm 0{\cdot}7)\%$ to the value given. The average Debye–Waller parameter for RbI, obtained from the relative intensities of 8 even *hkl* reflexions, was 3·6 Å^2, in substantial agreement with calculated values of 3·4 and 3·6 (5) Å^2, for the Rb^+ and I^- ions respectively. The degree of contamination of the monochromatic beam is best estimated from the ratio R_{Br}, since the 1st order 111 reflexion also contains a 2nd order 222 contribution. On this basis, corrections to b_{Rb} are estimated to be $< 0{\cdot}1\%$. Absorption corrections are $< 0{\cdot}01\%$.

From the 3 independent measurements of b_{Rb}, we obtain a best value, $b_{Rb} = 0{\cdot}68_5 \pm 0{\cdot}01$. The bound coherent scattering cross-section, $4\pi b_{Rb}^2$, is $5{\cdot}9 \pm 0.2$ barns. This work is in agreement with recent measurements of Wang & Cox (1970), who obtain $b_{Rb} = 0{\cdot}70_5 \pm 0{\cdot}02_5$ from the intensities of 18 reflexions in a powder sample of RbCl. Mueller *et al.* (1963) obtained $b_{Rb} = 0{\cdot}85$ using an external nickel standard. In that experiment an intensity ratio $I_{111}/I_{200} = 0{\cdot}030$ was obtained (Mueller, 1969), which gives $b_{Rb} \simeq 0{\cdot}68$. However the 111 and 200 reflexions were not fully resolved. These considerations indicate that the present measurements are more reliable than the earlier work.

The author is grateful to Professor B. N. Brockhouse for his advice and encouragement, and to Drs M. H. Mueller and D. E. Cox for useful discussions relating to this work. R. W. MacPherson assisted with the shell model calculations. This work was supported by a grant from the National Research Council; I am pleased to acknowledge an N.R.C. Studentship, and the support and encouragement of Atomic Energy of Canada, Ltd.

References

Bacon, G. E. (1962). *Neutron Diffraction*, 2nd ed. p. 95. Oxford: Clarendon Press.

Brockhouse, B. N., de Wit, G. A., Hallman, E. D. & Rowe, J. M. (1968). *Neutron Inelastic Scattering*, Vol. II, p. 259. Vienna: International Atomic Energy Agency.

Dolling, G., Smith, H. G., Nicklow, R. M., Vijayaraghavan, P. R. & Wilkinson, M. K. (1968). *Phys. Rev.* **168**, 970.

Koester, L. (1967). *Z. Phys.* **198**, 187.

Mueller, M. H. (1969). Private communication.

Mueller, M. H., Sidhu, S. S., Heaton, L., Hitterman, R. L. & Knott, H. W. (1963). Argonne National Laboratory Report ANL-6797, 393.

Pickart, S. J., Alperin, H. A. & Nathans, R. (1964). *J. Phys. Radium*, **25**, 565.

Schröder, U. (1966). *Solid State Comm.* **4**, 347.

Shull, C. G. & Wollan, E. O. (1951). *Phys. Rev.* **81**, 527.

Wang, F. F. Y. & Cox, D. E. (1970). *Acta Cryst.* A**26**, 377.

Printed in Denmark by P. J. Schmidts Bogtrykkeri, Vojens

Reprinted from THE PHYSICAL REVIEW, Vol. 182, No. 3, 965–972, 15 June 1969
Printed in U. S. A.

Lattice Dynamics of Potassium Chloride*

J. R. D. COPLEY,† R. W. MACPHERSON,† AND T. TIMUSK
Department of Physics and Institute for Materials Research, McMaster University, Hamilton, Ontario, Canada

(Received 6 January 1969)

Phonon dispersion curves along the $[00\zeta]$, $[0\zeta1]$, $[0\zeta\zeta]$, and $[\zeta\zeta\zeta]$ directions in KCl at 115°K have been measured by inelastic scattering of slow neutrons using the McMaster University triple-axis spectrometer at Chalk River. Various versions of the shell model have been fitted to the measurements. They are also compared with Kucher's predictions and with the results of Schröder's breathing-shell model. Several quantities are calculated using the best-fit shell model. The main features of the frequency distribution function do not, in general, occur at the frequencies of the symmetry points X and L. The most prominent peak in the frequency distribution is at 155 cm^{-1}. It agrees with the strongest peak in the Raman spectrum of KCl. The Debye temperature, the Debye-Waller factor, and the inelastic structure factor are also calculated.

I. INTRODUCTION

THE lattice vibrations of most of the common alkali-halide crystals have been investigated by slow neutron spectroscopy and by diffuse x-ray scattering. The most complete measurements to date have been made on LiF,[1] NaF,[2] NaCl,[3] NaI,[4] KBr,[5] and KI [6] by neutron spectroscopy and on NaF [7] and NaCl [8] by x-ray scattering. Potassium chloride is perhaps the most obvious crystal still missing from this list and although some diffuse x-ray measurements exist for KCl [9,10] there are several reasons why a more complete investigation of the lattice vibrations should be undertaken.

Work on the optical properties[11] of both pure and defect-containing crystals has demonstrated that for a full understanding of the influence of the lattice vibrations, detailed dynamic models based on neutron spectroscopy are essential. KCl is a good material for optical studies of all kinds because it can be prepared more easily in highly pure form than some of the other alkali halides. For this reason a large amount of experimental work has been done on this substance. KCl has long been a favorite in color-center research.

From a lattice dynamics point of view, KCl is also of special interest. A number of good measurements of its macroscopic properties have been made, and it has been possible to calculate dispersion curves from these data using several theoretical models. Noteworthy among these calculations are those of Tolpygo and co-workers,[12,13] of Hardy,[14] and more recently of Schröder.[15] It is of interest to compare these predictions of the phonon frequencies with actual measurements. A survey of models of this type may help us towards a better understanding of lattice dynamics from a microscopic point of view.

In Sec. II we review briefly the experimental techniques. The measured frequencies at various points along symmetry directions are given in Sec. III. The predictions of models based on macroscopic parameters are compared with experiment in Sec. IV. The shell model used by Woods *et al.*[4] and by Cowley *et al.*[16] is introduced and least-squares fits of this model to the measurements are given. In Sec. V the results of several calculations using the best least-squares-fit model are presented and compared with results of other experiments.

II. MEASUREMENTS

The phonon dispersion curves of KCl were measured by slow neutron inelastic scattering using the McMaster University triple-axis spectrometer at Chalk River.[17] This instrument uses twin monochromating crystals which produce a beam of neutrons of energy E_0 and wave vector $\mathbf{k}_0$ normal to the reactor face. Neutrons of energy E' and wave vector $\mathbf{k}'$, scattered from the speci-

---

* Work supported in part by the National Research Council of Canada and in part by the Alfred P. Sloan Foundation.

† National Research Council of Canada Studentship holder.

[1] G. Dolling, H. G. Smith, R. M. Nicklow, P. R. Vijayaraghavan, and M. K. Wilkinson, Phys. Rev. **168**, 970 (1968).

[2] W. J. L. Buyers, Phys. Rev. **153**, 923 (1967).

[3] L. Almqvist, G. Raunio, and R. Stedman, in *Neutron Inelastic Scattering* (International Atomic Energy Agency, Vienna, 1968), Vol. I, p. 295; G. Raunio, L. Almqvist, and R. Stedman, Phys. Rev. **178**, 1496 (1969).

[4] A. D. B. Woods, W. Cochran, and B. N. Brockhouse, Phys. Rev. **119**, 980 (1960).

[5] A. D. B. Woods, B. N. Brockhouse, R. A. Cowley, and W. Cochran, Phys. Rev. **131**, 1025 (1963).

[6] G. Dolling, R. A. Cowley, C. Schittenhelm, and I. M. Thorson, Phys. Rev. **147**, 577 (1966).

[7] J. D. Pirie and T. Smith, J. Phys. **C1**, 648 (1968).

[8] W. J. L. Buyers and T. Smith, Phys. Rev. **150**, 758 (1966).

[9] N. Boccara, Compt. Rend. **250**, 1025 (1960).

[10] V. I. Iveronova, Parangtopo, and A. P. Zvyagina, Fiz. Tverd. Tela **9**, 1609 (1967) [English transl.: Soviet Physics—Solid State **9**, 1265 (1967)].

[11] For recent reviews on localized vibrations see A. A. Maradudin, in *Solid State Physics*, edited by F. Seitz and D. Turnbull (Academic Press Inc., New York, 1966), Vols. 18 and 19; see also M. V. Klein, in *Physics of Color Centres*, edited by W. B. Fowler (Academic Press Inc., New York, 1968).

[12] K. B. Tolpygo and I. G. Zaslavskaya, Trudy Inst. Fiz. Acad. Nauk Ukr., SSR, No. 4, 71 (1953) [English transl.: United Kingdom Atomic Energy Authority, Harwell Report AERE-transl. 972 (1963) (unpublished)].

[13] T. I. Kucher, Zh. Eksperim. i Teor. Fiz. **32**, 498 (1957) [English transl.: Soviet Phys.—JETP **5**, 418 (1957)].

[14] J. R. Hardy, Phil. Mag. **7**, 315 (1962).

[15] U. Schröder, Solid State Commun. **4**, 347 (1966).

[16] R. A. Cowley, W. Cochran, B. N. Brockhouse, and A. D. B. Woods, Phys. Rev. **131**, 1030 (1963).

[17] B. N. Brockhouse, G. A. de Wit, E. D. Hallman, and J. M. Rowe, in *Neutron Inelastic Scattering* (International Atomic Energy Agency, Vienna, 1968), Vol. II, p. 259.

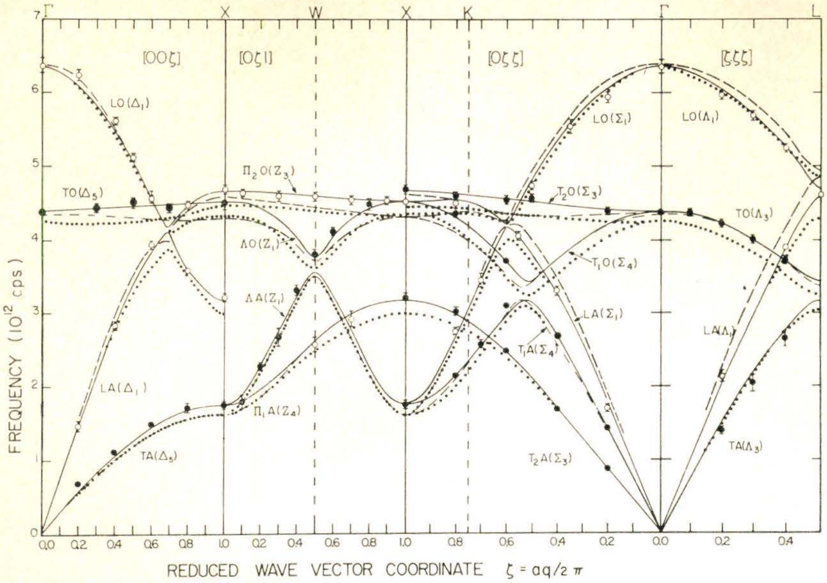

FIG. 1. Dispersion curves along major symmetry directions in KCl at 115°K. The open and filled circles denote the measured phonons. The solid line shows the model-VI fit. The dashed lines represent the breathing-shell-model calculation using parameters deduced from macroscopic data (model III). The dotted lines are the predictions of Kucher. The notation is explained in the text. The $\Pi_2A(Z_3)$ and $\Pi_1O(Z_4)$ branches are omitted for clarity.

men and selected by the analyzing crystal, are counted using a He^3 neutron detector.

In a one-phonon coherent scattering process, energy and wave vector are conserved[18]:

$$E_0-E'=(\hbar^2/2m_N)(k_0^2-k'^2)=\pm h\nu\,, \tag{1}$$

$$\mathbf{k}_0-\mathbf{k}'=\mathbf{Q}=2\pi\boldsymbol{\tau}+\mathbf{q}\,, \tag{2}$$

where m_N is the mass of the neutron, $\mathbf{Q}$ is the wave-vector transfer, and $\boldsymbol{\tau}$ is a reciprocal-lattice vector. The upper (lower) sign in Eq. (1) refers to phonon creation (annihilation). In this approximation the frequency ν and wave vector $\mathbf{q}$ of the phonon obey the dispersion relation $\nu=\nu_j(\mathbf{q})$, where j is the branch index; for a crystal having n atoms per (primitive) unit cell, the dispersion relation has $3n$ branches. The constant-$\mathbf{Q}$ method[19] was used throughout this experiment. Fixed incident neutron wavelengths, $2\pi/k_0$, between 1.425 and 1.335 Å, were employed, corresponding to frequencies between 9.75×10^{12} cps (325 cm^{-1}) and 11.09×10^{12} cps (370 cm^{-1}), and only neutron energy-loss (i.e., phonon creation) processes were examined.

The specimen, obtained from the Harshaw Chemical Co., was a cleaved single crystal of potassium chloride, $2\frac{1}{2}\times2\frac{1}{2}\times\frac{3}{4}$ in. with faces parallel to $\{200\}$ planes. Measurements were made in the (100) and $(1\bar{1}0)$ scattering planes. Where possible, measurements were made so that the path of the beam through the crystal was not too long, owing to the appreciable (34 b) absorption cross section[20] of chlorine.

The crystal was mounted in a metal cryostat and cooled from above to 115±5°K.

III. RESULTS

The measured phonons are shown in Fig. 1 and listed in Table I. The branches are labelled according to their polarization relative to $\mathbf{q}$. The $[0\zeta\zeta]$ T_1 and T_2 branches are polarized parallel to $[01\bar{1}]$ and $[100]$, respectively, and the $[0\zeta1]$ Λ, Π_1, and Π_2 branches have polarization vectors parallel to $[010]$, $[100]$, and $[001]$, respectively. The $[0\zeta1]$ branches are symmetrical about the point W, and, to avoid confusion, two of the Π branches have been omitted from the figure. The components of $\mathbf{q}$ are given in units of $2\pi/a$.

For any wave vector $\mathbf{q}$, along these symmetry directions, there are two branches of each polarization. The lower branch is labelled A (acoustic) and the upper branch is labelled O (optic).

The dispersion curves in Fig. 1 are also labelled according to the irreducible representations of the wave vector, using the notation of Bouckaert *et al.*[21]

From a consideration of the inelastic structure factor (see Sec. V) each group has been unambiguously assigned to a branch of the dispersion curves. Where two branches of the same polarization come close to each other, no difficulty was encountered in branch assignment, since the structure factors for A and O branches differ markedly at these points. The point $(\frac{1}{2},\frac{1}{2},\frac{1}{2})$ is not as well determined as some of the other symmetry points, since it was difficult to obtain good neutron groups at this point.

The errors assigned to the measured frequencies are normally $\pm0.1\Gamma$, where Γ is the width (full width at

---

[18] G. Placzek and L. Van Hove, Phys. Rev. **93**, 1207 (1954).

[19] B. N. Brockhouse, in *Inelastic Scattering of Neutrons in Solids and Liquids* (International Atomic Energy Agency, Vienna, 1961), p. 113.

[20] *Neutron Cross Sections, Brookhaven National Laboratory Report No. 325* compiled by D. J. Hughes and R. B. Schwartz (U. S. Government Printing Office, Washington, D. C., 1958), 2nd ed.

[21] L. P. Bouckaert, R. Smoluchowski, and E. Wigner, Phys. Rev. **50**, 58 (1936).

TABLE I. Normal-mode frequencies of KCl measured at 115°K. The branch index j is shown. The frequencies are in units of 10^{12} cps.

$\zeta = aq/2\pi$	ν (Acoustic)	j	ν (Optic)	j
[00ζ] T				
0.0			4.39 ±0.03	4,5
0.2	0.69 ±0.03	1,2		
0.3			$4.44_5 \pm 0.05$	4,5
0.4	$1.12_5 \pm 0.03$	1,2		
0.5			4.53 ±0.1	4,5
0.6	1.50 ±0.03	1,2		
0.7			4.45 ±0.05	5,6
0.8	1.72 ±0.05	1,2		
1.0	1.76 ±0.05	1,2	4.53 ±0.05	4,5
[00ζ] L				
0.0			6.39 ±0.1	6
0.2	1.47 ±0.08	3	6.25 ±0.08	6
0.4	2.83 ±0.08	3	5.55 ±0.04	6
0.5			5.13 ±0.03	6
0.6	3.95 ±0.06	3	4.58 ±0.05	6
0.8	3.59 ±0.04	3	4.49 ±0.05	6
1.0	3.23 ±0.05	3	4.70 ±0.05	6
[0ζζ] T_1				
0.2	1.43 ±0.02	2		
0.4	2.69 ±0.02	2		
0.6	3.10 ±0.1	2	3.73 ±0.03	3
0.7	2.57 ±0.04	1		
0.8	2.16 ±0.03	1	4.38 ±0.06	4
[0ζζ] T2				
0.2	0.89 ±0.03	1	4.41 ±0.05	5
0.4	$1.67 \pm 0.02_5$	1		
0.5			4.57 ±0.06	5
0.6	$2.47_5 \pm 0.02_5$	1	4.56 ±0.06	6
0.8	$3.02_5 \pm 0.04_5$	3	$4.60_5 \pm 0.04$	6
[0ζζ] L				
0.2	1.71 ±0.06	3	5.96 ±0.08	6
0.35			5.56 ±0.1	6
0.4	3.31 ±0.06	3		
0.5			4.75 ±0.06	6
0.55	4.08 ±0.06	4		
0.7	3.46 ±0.05	3		
0.8	2.75 ±0.06	2	4.51 ±0.05	5
[ζζζ] T				
0.1			4.37 ±0.04	4,5
0.2	1.41 ±0.05	1,2	4.23 ±0.06	4,5
0.3	2.04 ±0.15	1,2	4.02 ±0.04	4,5
0.4	2.64 ±0.13	1,2	3.72 ±0.04	3,4
[ζζζ] L				
0.2	2.12 ±0.04	3	5.97 ±0.04	6
0.3			5.70 ±0.07	6
0.4	3.91 ±0.03	5	5.25 ±0.05	6
0.5	4.60 ±0.02	5		
[0ζ1] Π_1				
0.5	2.57 ±0.1	1,2		
0.7	2.92 ±0.1	3		
[0ζ1] Π_2				
0.1			4.65 ±0.06	6
0.3			4.61 ±0.08	6
0.5			4.62 ±0.06	5,6
0.7			4.56 ±0.06	5
0.9			4.54 ±0.06	5
[0ζ1] Λ				
0.1	1.78 ±0.09	2		
0.2	2.27 ±0.06	2		
0.3	2.67 ±0.13	2		
0.4	3.33 ±0.07	3		
0.5			3.83 ±0.06	4
0.6			4.13 ±0.06	4
0.8			4.49 ±0.07	4

half-maximum) of the measured neutron group. In a few cases, where poor groups were obtained, the assigned errors are larger. (See note added in proof.)

IV. MODELS

The lattice vibrations of the alkali halides have been represented by three closely related formulations: the shell model used by Woods *et al.*,[4] extended by Cowley *et al.*,[16] and originally introduced by Dick and Overhauser[22]; Hardy's deformation dipole model,[14] and Tolpygo and Zaslavskaya's dipole model.[12] All the models are in the framework of the adiabatic and harmonic approximations. The Coulomb interactions and the short-range repulsive "overlap" forces are taken into account, and an attempt is made to account for the effect of the polarization of the ions on the lattice vibrations. The differences between the formulations have been discussed by Cowley *et al.*[16] We have fitted our data with the shell model, and compared the results with those due to Kucher[13] and to Tolpygo and Zaslavskaya, with Schröder's breathing-shell model,[15] and with Hardy's calculations.

The general shell model has a very large number of adjustable parameters. We have used the approximations due to Cowley *et al.* to reduce it to 11. These approximations assume that the overlap forces act only through the outer shells of valence electrons and that they extend only out to second-nearest neighbors. With axially symmetric forces, the parameters for the most general model under these assumptions are the radial and tangential short-range force constants A, B, A_{11}, B_{11}, A_{22}, and B_{22} between the K^+-Cl^-, K^+-K^+, and Cl^--Cl^- nearest-neighbor ions, respectively, the ionic charge Ze, and the electrical and mechanical polarizabilities α_1, α_2, d_1, and d_2 for the K^+ and Cl^- ions, respectively. The parameter B may be eliminated, since it is related to B_{11}, B_{12}, and Z by the stability condition $B+2B_{11}+2B_{22}=-\frac{2}{3}\alpha_M Z^2$, where $\alpha_M=1.74756$ is the Madelung constant. Noncentral forces are taken into account by introducing a parameter B'', so that B is replaced everywhere in the equations of motion by $B+B''$. The 11 independent parameters are therefore A, B'', A_{11}, B_{11}, A_{22}, B_{22}, Z, α_1, d_1, α_2, and d_2.

A modification of the model is Schröder's breathing-shell model, in which a new coordinate is introduced to express the compression (monopole) deformation of the shells. It is assumed that the spring constants between the cores and shells of the ions are the same for the compression as for the dipole deformations. This avoids the need for any new parameters.

We obtained the best-fitting values of the shell-model parameters by means of a nonlinear least-squares fit to the frequencies along certain symmetry directions using the program by Marquardt.[23] The calculation was performed on the CDC 6400 computer at the McMaster computing center. The parameters of the fits are given in Table II and the calculated frequencies are presented

---

[22] B. G. Dick and A. W Overhauser, Phys. Rev. **112**, 90 (1958).

[23] D. W. Marquardt, J. Soc. Indust. Appl. Math. **11**, 431 (1963). This program is available from Share General Program Library, Catalog No. SDA 3094 (unpublished).

TABLE II. Shell-model parameters for KCl at 115°K. Parameters for model III were estimated from the bulk properties of KCl (Table IV). The parameters for all other models were obtained from the results of least-squares fitting to neutron scattering data. Parameters A_{11} and B_{11} are zero for all these models. The short-range force constants are in units of $e^2/2v$, where v is the volume of the primitive unit cell.

Model parameters	Units	I	II	III	IV	V	VI
A	$e^2/2v$	9.91 ±0.19	11.48 ±0.36	12.58	12.24 ±0.80	12.07 ±0.16	12.12 ±0.53
B	$e^2/2v$	−1.53	−1.21	0.2782	−1.08	−0.96	−1.17
B''	$e^2/2v$	0.402±0.13	0.158±0.075	−0.5884	0.02 ±0.12	···	0.075±0.07
A_{22}	$e^2/2v$	−0.14 ±0.18	−0.095±0.12	0.7587	0.01 ±0.14	···	−0.10 ±0.20
B_{22}	$e^2/2v$	0.25 ±0.084	0.060±0.050	−0.3169	0.028±0.061	···	0.058±0.047
Z	e	0.735±0.015	0.895±0.029	0.900	0.928±0.057	0.910±0.014	0.918±0.049
α_1	$1/v$	···	···	0.01974	0.034±0.014	0.028±0.006	0.028±0.010
d_1	e	···	···	0.0753	−0.060±0.071	−0.014±0.024	−0.025±0.045
α_2	$1/v$	···	0.047±0.005	0.04888	0.036±0.016	0.035±0.007	0.035±0.010
d_2	e	···	0.123±0.028	0.1865	0.087±0.086	0.131±0.022	0.121±0.028
Std. error	10^{12} cps	0.126	0.077	0.141	0.071	0.065	0.065
χ^2		9.47	2.36	4.93	2.29	1.45	1.35

in Fig. 1 as the solid line for the model that best fits the data (model VI).

The standard errors given in Table II were calculated from

$$\text{S.E.}=\left(\sum_{i=1}^{N}\frac{(\nu_{\text{obs}}{}^{i}-\nu_{\text{model}}{}^{i})^2}{N-K}\right)^{1/2},$$

where N is the number of observations, K is the number of adjustable parameters, and the ν's are the phonon frequencies. The standard error represents an over-all average error in the fitted frequencies. We have also calculated the quantity

$$\chi^2=\frac{1}{N-K}\sum_{i=1}^{N}\left(\frac{\nu_{\text{obs}}{}^{i}-\nu_{\text{model}}{}^{i}}{\sigma_i}\right)^2,$$

where σ_i is the estimated experimental error for the ith phonon.

Table III gives some elastic and optical quantities calculated from the models and compares these with direct experiments. Table IV contains constants used in the calculations.

TABLE III. Calculated elastic constants, high-frequency dielectric constant, and small **q**-value optical frequencies for the various models of KCl. Values for the breathing-shell model, model III, are input parameters interpolated from experimental data to 115°K; ν_{LO} has been calculated using the LST relation.[a] The elastic constants are in units of 10^{11} dyn/cm^2 and the frequencies are in units of 10^{12} cps.

Model	I	II	III	IV	V	VI	Observed
C_{11}	3.15	4.46	4.60	3.53	4.76	4.72	4.60
C_{12}	0.095	0.53	0.58	0.71	0.70	0.63	0.58
C_{44}	0.583	0.73	0.653	0.73	0.70	0.72	0.653
ϵ_∞	1.0	1.73	2.15	2.22	2.08	2.08	2.15
ν_{TO}	4.39	4.42	4.36	4.41	4.43	4.41	4.36
ν_{LO}	6.36	6.35	6.36	6.39	6.33	6.34	···

[a] Reference 38.

Model I is a rigid-ion model with second-neighbor interactions between chlorine ions. The frequencies of the model are in error by up to 9%, especially along the $[0\zeta\zeta]$ direction. The elastic constants determined from the model are in wide disagreement with the ultrasonic values.

Model II has polarizable chlorine ions. The standard error has been reduced considerably, and the elastic constants obtained are closer to the experimental values than those of model I. The high-frequency dielectric constant is still in considerable error.

Model III is the breathing-shell model and was not fitted to the neutron-scattering data. Its parameters were estimated from the values of the bulk properties of KCl interpolated to 115°K, given in Table III. Dispersion curves for this model are plotted for comparison with the data as the dashed curve in Fig. 1. The over-all agreement with experiment of the calculated dispersion curves is quite good. The value of ν_{LO} at small **q** values is in excellent agreement, but there are discrepancies in the initial slopes of the longitudinal branches and the agreement around point X is not very good. The parameters of model III were used as the initial guess in all the least-squares fits.

Model IV is a fitted breathing-shell model. The fit is slightly improved over model II, and the high-frequency dielectric constant is in good agreement with experiment. However, the elastic constants now show discrepancies.

Note that the change in going from a breathing-shell model fitted to macroscopic parameters to one fitted to neutron measurements is not large, particularly in the case of the short- and long-range polarizabilities. This implies that within the breathing-shell-model framework the neutron measurements are in agreement with the macroscopic constants.

Model V is a six-parameter shell model with both ions polarizable and no second-neighbor repulsive forces. Model VI includes second-neighbor repulsive forces between chlorine ions and has a parameter to allow for noncentral forces. The errors of these last two models are essentially the same. Model VI gives a slightly better fit than model V to ν_{TO} at small $\mathbf{q}$. The mechanical polarizability of the K^+ ion in models IV–VI, while negative, is smaller than the error associated with it, so that no significance should be attached to its sign.

Another model with the full 11 parameters adjustable gave no significant improvement in fit and is not included in Table II. Model VI was therefore selected as the best model for the purpose of reproducing the frequencies and was used in all the subsequent calculations.

Figure 1 also shows Kucher's[13] calculated values as the dotted curve. The agreement with the neutron measurements is generally good. Similarly the calculations of Hardy are in qualitative agreement with experiment, although discrepancies of the order of 10% are common in both cases. Some of these variations might be due to the use of room-temperature macroscopic constants in the fitting. It can be seen, however, that even when parameters interpolated to 115°K (model III) are used, the standard error is more than twice as large as for model VI, fitted directly to neutron data.

V. CALCULATIONS FROM MODEL VI

A. Frequency Distributions

The frequency distribution function $g(\nu)d\nu$ is shown in Fig. 2. It was obtained by solving the shell-model dynamical matrix in the octant $0<q_x<2\pi/a$, $0<q_y<2\pi/a$, and $0<q_z<2\pi/a$ at 10 000 randomly chosen points. The frequencies were sorted into a histogram containing 127 bins. Figure 3 shows the frequency spectrum ordered according to the branch index j: at each $\mathbf{q}$, the six frequencies are numbered $j=1, \cdots, 6$ in order of increasing size. Figure 3 also shows the location of some of the symmetry points as given by model VI. For the phonons at Γ and X, the model differs from experiment by less than 2%. The whole $[\zeta\zeta\zeta]$ TA branch, however, is predicted high by the model and the zone-boundary frequency could be as much as 7 cm^{-1} lower than the value predicted by the model (106.2 cm^{-1}).

TABLE IV. Values of constants used in the KCl calculations.

$\frac{1}{2}a=r_0=3.12$ Å	$\nu_{\mathrm{TO}}=4.36\times10^{12}$ cps[a]
$v=2r_0^3=60.8$ Å^3	$\alpha_1=1.201$ Å^3 [b]
$e^2/2v=1896$ dyn/cm^2	$\alpha_2=2.974$ Å^3 [b]
$M_+=39.102$ amu	$C_{11}=4.60\times10^{11}$ dyn/cm^2 [c]
$M_-=35.457$ amu	$C_{12}=0.58\times10^{11}$ dyn/cm^2 [c]
$\epsilon_\infty=2.15$[b]	$C_{44}=0.653\times10^{11}$ dyn/cm^2 [c]
$\epsilon_0=4.57$[e]	

[a] See the Appendix.

[b] J. R. Tessman, A. H. Kahn, and W. Shockley, Phys. Rev. **92**, 890 (1953).

[c] Interpolated to 115°K from M. H. Norwood and C. V. Briscoe, Phys. Rev. **112**, 45 (1958).

[d] Interpolated to 115°K from M. Born and K. Huang, *Dynamical Theory of Crystal Lattices* (Oxford University Press, Oxford, 1954), Table 17, p. 85; and from D. H. Martin, Advan. Phys. **159**, 223 (1960).

[e] Interpolated to 115°K from M. C. Robinson and A. C. H. Hallett, Can. J. Phys. **44**, 2211 (1966).

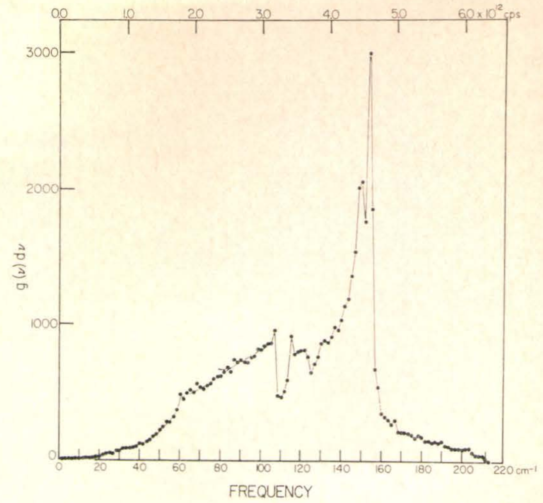

FIG. 2. Total frequency distribution calculated from model VI using 10 000 randomly selected wave vectors sorted into 127 bins.

It can be seen that the zone-boundary symmetry points do not, in general, correspond to very distinct features in the total $g(\nu)$ curve. It has been customary to use points X and L to explain peaks in the second-order Raman spectra.[24] With the exception of the lowest X frequency there seems to be little justification for this procedure at present.

The very strong peak at 155 cm^{-1} arises from a saddle-point in the sixth branch, which does not correspond to any of the symmetry points. This peak has been seen by

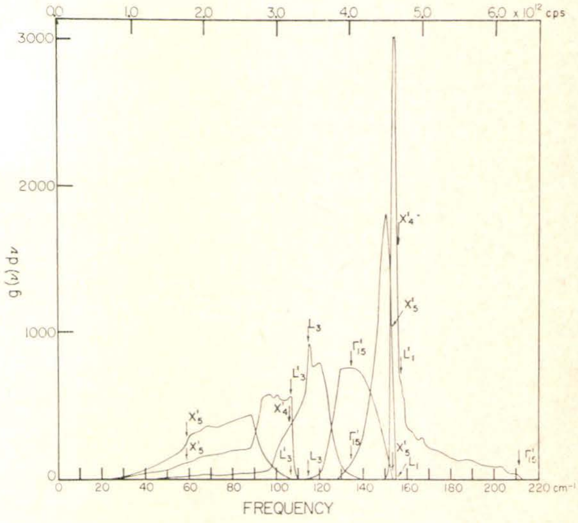

FIG. 3. Individual frequency distributions for the six branches, for the 10 000 wave vectors of Fig. 2. The points have been omitted for clarity. The frequencies of the symmetry points Γ, X, and L are shown for each branch.

---

[24] E. Burstein, F. A. Johnson, and R. Loudon, Phys. Rev. **139**, 1239 (1965).

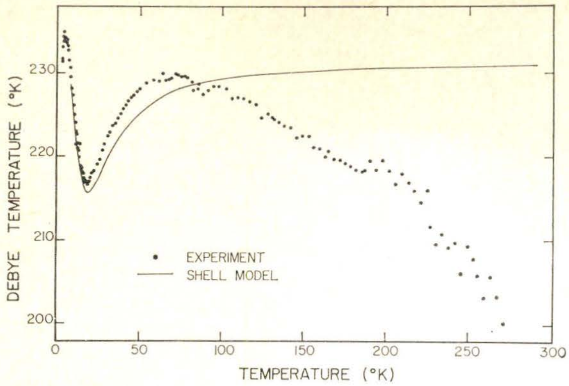

FIG. 4. Debye characteristic temperature Θ_D obtained from the heat capacity. The theoretical curve was calculated from model VI. The experimental points were derived from C_p measurements (Ref. 29), which were first corrected to give C_v.

Callender and Pershan[25] in the second-order helium-temperature Raman spectrum of KCl at 2×155 cm^{-1} and in the fluorescence sideband of KCl:Sm^{++} by Bron.[26] The half-width of this peak in the samarium fluorescence is only 2.5 cm^{-1} and its position is 156 cm^{-1}.[27]

The peak at 107 cm^{-1} is related to a near-degeneracy of a saddlepoint at (0.51, 0.51, 0) and a maximum near (0.5,0.5,0.5). This singularity is of some interest since it occurs in all alkali-halide crystals for Σ_4 symmetry branches at this point in the zone. Measurements of the impurity-induced far-infrared absorption in KBr show that the rise in the second branch from the saddle point to the maximum occurs in a 0.3-cm^{-1} interval. A similar effect should be observable in KCl near 107 cm^{-1}.

B. Heat Capacity, Debye Temperature, and Debye-Waller Factor

Using Eqs. (14.1) and (2.3) of Blackman,[28] the heat capacity C_v and Debye temperature Θ_D have been calculated from the frequency distribution function $g(\nu)$. The calculation is compared with the experimental measurements of Berg and Morrison[29] in Fig. 4. At very low temperatures Θ_D is sensitive to the low-frequency part of $g(\nu)$; the calculated values depend on the method of calculating $g(\nu)$ and have been omitted from the figure. Using de Launay's[30] procedure, and the elastic constants predicted by model VI, we obtain $\Theta_D(0)=241$°K. Estimating the initial slopes of the dispersion curves (and hence the elastic constants) gives $\Theta_D=238$°K.

In the low-temperature region, the calculated curve lies a few degrees below the experimental points. Better agreement would be expected if a frequency distribution appropriate to the temperature T were used to obtain $\Theta_D(T)$. At high temperatures, the experimental values fall off rapidly. This is interpreted as an anharmonic effect, since the harmonic approximation predicts that Θ_D becomes constant at high temperatures.

For a cubic crystal, the Debye-Waller factor W_i is related to the total mean-square displacement $\langle u_i^2\rangle$ of ion i by

$$2W_i=\tfrac{1}{3}Q^2\langle u_i^2\rangle,$$

where[31]

$$\langle u_i^2\rangle=\frac{h}{4\pi^2NM_i}\sum_{\mathbf{q}j}\frac{|\mathbf{e}_{ij}(\mathbf{q})|^2}{\nu_j(\mathbf{q})}[n_j(\mathbf{q})+\tfrac{1}{2}].$$

Here $\mathbf{e}_{ij}(\mathbf{q})$ is the eigenvector of the ith ion in the $(\mathbf{q},j)$ normal mode and $n_j(\mathbf{q})=(e^{h\nu_j(\mathbf{q})/k_BT}-1)^{-1}$.

The quantity $B_i=\tfrac{1}{3}8\pi^2\langle u_i^2\rangle$ has been calculated using individual frequency distribution functions[1] for the two ions, and is shown in Fig. 5.

The experimental measurements[32,33] of B_i are in poor agreement with the calculation. The experimental difficulties have been pointed out by Buyers and Smith,[34] and in view of this the disagreement is not surprising.

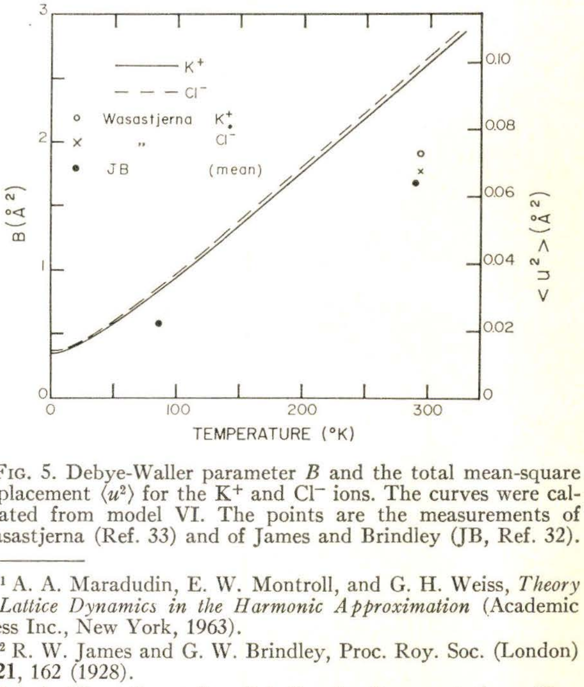

FIG. 5. Debye-Waller parameter B and the total mean-square displacement $\langle u^2\rangle$ for the K$^+$ and Cl$^-$ ions. The curves were calculated from model VI. The points are the measurements of Wasastjerna (Ref. 33) and of James and Brindley (JB, Ref. 32).

---

[25] R. H. Callender and P. S. Pershan, in Proceedings of International Conference on Light Scattering Spectra of Solids, New York University, 1968 (unpublished).

[26] W. E. Bron, Phys. Rev. **140**, A2005 (1965).

[27] M. Buchanan (private communication).

[28] M. Blackman, in *Handbuch der Physik*, edited by S. Flügge (Springer-Verlag, Berlin, 1955), Vol. VII, Pt. 1.

[29] W. T. Berg and J. A. Morrison, Proc. Roy. Soc. (London) **A242**, 467 (1967).

[30] J. de Launay, J. Chem. Phys. **30**, 91 (1959).

[31] A. A. Maradudin, E. W. Montroll, and G. H. Weiss, *Theory of Lattice Dynamics in the Harmonic Approximation* (Academic Press Inc., New York, 1963).

[32] R. W. James and G. W. Brindley, Proc. Roy. Soc. (London) **A121**, 162 (1928).

[33] J. A. Wasastjerna, Soc. Sci. Fennica Commentationes Phy. Math., **13**, 1 (1946); quoted in *International Tables for X-Ray Crystallography*, edited by K. Lonsdale (Kynoch Press, Birmingham, England, 1962), Vol. III, p. 240.

[34] W. J. L. Buyers and T. Smith, J. Phys. Chem. Solids **25**, 483 (1964).

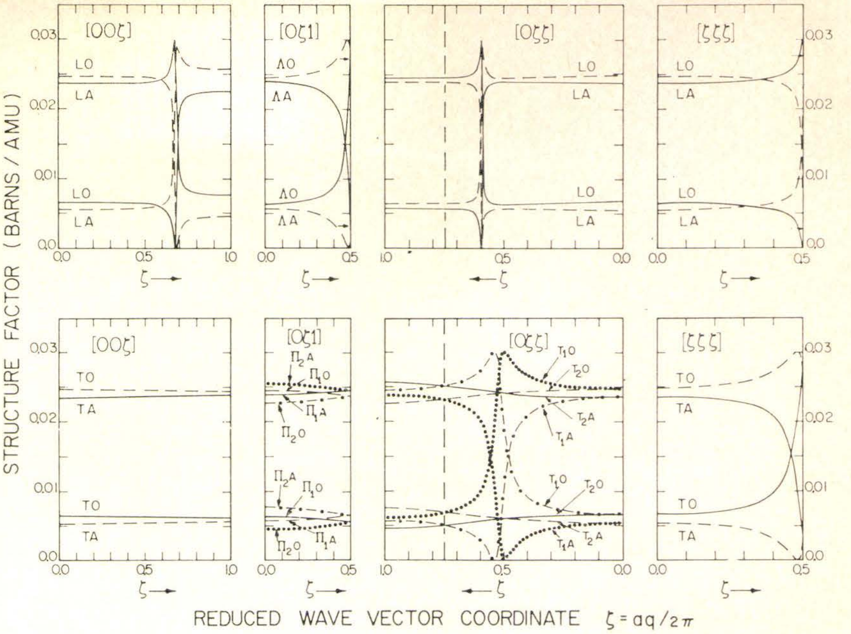

FIG. 6. Reduced inelastic structure factor $|f|^2$ for the major symmetry directions in KCl, calculated from model VI. The labelling of the branches is as in Fig. 1. The solid and dot-dash lines are calculated for a reciprocal-lattice vector $\boldsymbol{\tau}$ having even indices. The dashed and dotted lines are for $\boldsymbol{\tau}$ with odd indices. The arrows in the upper diagrams indicate the value of $|f|^2$ at $(0,\frac{1}{2},1)$ and $(\frac{1}{2},\frac{1}{2},\frac{1}{2})$.

C. Inelastic Structure Factor

The intensity of a (one-phonon) neutron group $(\mathbf{q},j)$ observed in a constant-$\mathbf{Q}$ scan is[35,36]

$$I=N\left(\frac{k'}{k_0}\right)\frac{\hbar[n_j(\mathbf{q})+\frac{1}{2}\pm\frac{1}{2}]}{4\pi\nu_j(\mathbf{q})}|F|^2,$$

where N is the number of primitive cells in the crystal, and the upper (lower) sign refers to phonon creation (annihilation). The structure factor $|F|^2$ is given by

$$|F|^2=|\sum_i b_i e^{i2\pi\boldsymbol{\tau}\cdot\mathbf{r}_i}\mathbf{Q}\cdot\mathbf{e}_{ij}(\mathbf{q})M_i^{-1/2}e^{-W_i(\mathbf{Q})}|^2,$$

where b_i, $\mathbf{r}_i$, M_i, and W_i are the coherent scattering length, position vector, mass, and Debye-Waller factor, respectively, for the ith atom or ion. For wave vectors along a symmetry direction in KCl, this reduces to

$$|F|^2=(\mathbf{Q}\cdot\hat{V})^2|b_1M_1^{-1/2}e^{-W_1(\mathbf{Q})}\xi_{1j}(\mathbf{q}) \pm b_2M_2^{-1/2}e^{-W_2(\mathbf{Q})}\xi_{2j}(\mathbf{q})|^2,$$

where $\hat{V}$ is a unit vector in the direction of the polarization vector of ion 1, and $\hat{V}\xi_i=\mathbf{e}_i$: The upper (lower) sign is used when the reciprocal-lattice vector $\boldsymbol{\tau}$ involved [see Eq. (2)] has even (odd) indices; subscripts 1 and 2 refer to the K^+ and Cl^- ions, respectively.

The Debye-Waller factors W_i, for $\mathbf{Q}=(0,0,6)\times 2\pi/a$ and $T=100°K$, are $W_1=0.211$, $W_2=0.216$, and $e^{-W_1}/e^{-W_2}=1.005$. We may therefore neglect the difference in the Debye-Waller factors and write

$$|F|^2=(\mathbf{Q}\cdot\hat{V})^2e^{-2W_{\mathrm{av}}(\mathbf{Q})}|f|^2,$$

where the "reduced inelastic structure factor"

$$|f|^2=|b_1M_1^{-1/2}\xi_{1j}(\mathbf{q})\pm b_2M_2^{-1/2}\xi_{2j}(\mathbf{q})|^2.$$

Using the values[20] $b_1=0.34_5$ and $b_2=0.98$, and eigenvectors calculated from model VI, $|f|^2$ has been calculated for the major symmetry directions and is shown in Fig. 6. The curves show important differences from the analogous curves for NaI [4] and LiF,[1] principally because of the similarity of the ionic masses and because of the large ratio of the scattering lengths.

Comparison with the dispersion curves (Fig. 1) indicates that rapid changes in $|f|^2$ occur whenever the separation of the acoustic and optic branches of the same polarization has a minimum value. At such points the two acoustic curves (for even and odd $\boldsymbol{\tau}$) intersect, indicating that one of the ions is stationary. Similarly the two optic curves cross, and for this mode the other ion is stationary. For phonons $(\mathbf{q},j)$ at (0,0,0.68) LA, (0,0.5,1) ΛO, (0,0.6,0.6) LO, (0.5,0.5,0.5) LA and TO, and (0,0.51,0.51) T_1O, only the Cl^- ions are moving and $|f|^2=b_{Cl}^2/M_{Cl}\simeq 0.027$ b/amu. At (0,0,0.68) LO, (0,0.5,1) ΛA, etc., the Cl^- ions are stationary and $|f|^2=b_K^2/M_K\simeq 0.003$. For all values of $\boldsymbol{\tau}$ the former modes are about nine times as intense as the latter modes and only the former modes can be observed. This effect is fortunately limited to very small regions in $\mathbf{q}$, particularly in the longitudinal cases.

VI. CONCLUSION

We have presented measurements of phonon frequencies along the major symmetry directions in KCl at 115°K. Neutron groups of well-defined frequency and polarization were observed at all $\mathbf{q}$ values except near $(\frac{1}{2},\frac{1}{2},\frac{1}{2})\times 2\pi/a$. The frequencies found agreed quite well

---

[35] I. Waller and P. O. Froman, Arkiv Fysik 4, 183 (1952).

[36] B. N. Brockhouse and P. K. Iyengar, Phys. Rev. 111, 747 (1958).

8746160

with a shell-model calculation based on macroscopic parameters; if the parameters are allowed to vary to give a best fit to the neutron measurements the agreement is further improved. The polarizabilities that are obtained in this way do not take on unphysically large negative values as was observed in KBr.

In the case of KCl at least, it seems that the shell model, in its various forms, offers a good description of the dynamical behavior of the lattice. KCl seems to behave very much like an ideal ionic crystal; even the rigid-ion model gives a fit that has only twice the standard error of the best shell model.

Using the best least-squares-fit shell model we have calculated some properties of KCl. The frequency distribution $g(\nu)$ shows the characteristic sharp peaks associated with saddle points in the frequency spectrum, the strongest of which can also be found in the Raman spectrum of KCl. Up to about 70°K the Debye temperature calculated from $g(\nu)$ is in good agreement with data from specific heats.

One of the main motivations for undertaking this work has been to provide good phonon frequencies for use in interpreting other experiments, in particular those optical effects where phonons play an important role.

Note added in proof. Recently G. Raunio and L. Almqvist have measured dispersion curves in KCl at 80 and 300°K, by neutron inelastic scattering. Their results are generally in good agreement with our own. Their measurements of the $[\zeta\zeta\zeta]$ *TA* branch, however, lie as much as 7% higher. Since the higher frequencies are in better agreement with our model VI (see Sec. IV), and since these workers took extra care to investigate the dispersion surfaces in the vicinity of this branch, we believe their results for this branch are more reliable than our own.

ACKNOWLEDGMENTS

We are grateful to Professor B. N. Brockhouse for his assistance and encouragement. Our thanks to our colleagues at McMaster for helpful discussions, in particular E. R. Cowley and M. Buchanan, and G. A. deWit (now at Rutgers University, New Brunswick, N. J.) for his assistance with some of the measurements. J. A. Morrison kindly sent his complete heat-capacity results and U. Schröder assisted us with the breathing-shell-model calculations. We are grateful to Atomic Energy of Canada, Ltd., for their support.

APPENDIX: TO FREQUENCY AT $q \rightarrow 0$

At the time of these measurements we were unable to find in the literature a recent measurement of the transverse ($\mathbf{q} \rightarrow 0$) optical frequency. We made a determination of $\nu_{\mathrm{TO}}(\mathbf{q} \rightarrow 0)$ ourselves with a far-infrared spectrometer on evaporated thin films of KCl. Such measurements are very difficult to interpret because of the importance of surface effects resulting from the very small penetration of the light. The observed peaks are generally very much broader than one would expect[37] for optical phonons. We also found an effect due to the differential expansion of the substrate which we attempted to correct for by extrapolating from quartz and lithium-fluoride substrates to a hypothetical KCl substrate. Our results are summarized in Table V, and it can be seen that they agree with the neutron measurements. Table V also gives a comparison of our measured frequencies at $\mathbf{q} \rightarrow 0$ with the prediction by Lyddane, Sachs, and Teller[38] (the LST relation). It will be seen that this relation, $\omega_{\mathrm{LO}} = (\epsilon_0/\epsilon_\infty)^{1/2}\omega_{\mathrm{TO}}$, holds for KCl. This is in agreement with results for the other alkali halides.

TABLE V. Lyddane-Sachs-Teller relation[a] and comparison with infrared absorption (reststrahlen) frequency.

T (°K)	$\nu_{\mathrm{LO}}(\mathbf{q} \rightarrow 0)$ Neutrons (10^{12} cps)	$\nu_{\mathrm{TO}}(\mathbf{q} \rightarrow 0)$ Neutrons (10^{12} cps)	$\nu_{\mathrm{TO}}(\mathbf{q} \rightarrow 0)$ Infrared (10^{12} cps)	$(\epsilon_0/\epsilon_\infty)^{1/2}$	$(\nu_{\mathrm{LO}}/\nu_{\mathrm{TO}})_{\mathbf{q}\rightarrow 0}$ Neutrons
4.2			4.50 ± 0.03		
115	6.39 ± 0.1	4.39 ± 0.03	4.36 ± 0.07	1.46	1.46
300		4.19 ± 0.05	4.19 ± 0.07		

[a] Reference 38.

---

[37] E. R. Cowley and R. A. Cowley, Proc. Roy. Soc. (London) **A287**, 259 (1965).

[38] R. H. Lyddane, R. G. Sachs, and E. Teller, Phys. Rev. **59**, 73 (1941).